Errata

Page vi, Line 14: The following line should be inserted:

"fs femtosecond".

Page vii, Line 4: The following line should be inserted:

"ns nanosecond".

Page vii, Line 8: The following line should be inserted:

"SCF self-consistent field".

Page vii, Line 20: The following line should be inserted:

"ZORA zero-order regular approximation".

Page ix. "C.E. Powell and M. G. Humphrey, *Coord. Chem. Rev.*, in press. *Nonlinear Optical Properties of Transition Metal Acetylides and Their Derivatives*" should read "C.E. Powell and M. G. Humphrey, *Coord. Chem. Rev.*, **248** (2004) 725-756. *Nonlinear Optical Properties of Transition Metal Acetylides and Their Derivatives*".

Page ix. "M.G. Humphrey, C.E. Powell, M.P. Cifuentes, J.P. Morrall and M. Samoc, *Polymer Preprints*, in press. *Synthesis and Nonlinear Optical Properties of Alkynylruthenium Dendrimers*" should read "M.G. Humphrey, C.E. Powell, M.P. Cifuentes, J.P. Morrall and M. Samoc, *Polymer Preprints*, **45** (2004) 367-368. *Synthesis and Nonlinear Optical Properties of Alkynylruthenium Dendrimers*"

Page ix. "C.E. Powell, J.P. Morrall, S. A. Ward, M. P. Cifuentes, E. G. A. Notaras, M. Samoc and M. G. Humphrey *J. Am. Chem. Soc.*, submitted. *Organometallic Complexes for Nonlinear Optics. 34. Z-scan Determination of the Dispersion of Third-order Nonlinear Optical Properties of an Organometallic Dendrimer*" should read "C.E. Powell, J.P. Morrall, S. A. Ward, M. P. Cifuentes, E. G. A. Notaras, M. Samoc and M. G. Humphrey, *J. Am. Chem. Soc.*, **126** (2004)

12234-12235. *Organometallic Complexes for Nonlinear Optics. 34. Z-scan Determination of the Dispersion of Third-order Nonlinear Optical Properties of an Organometallic Dendrimer*"

Page 24, Line 12: "...iodoanilinoacetylide..." should read "...indoanilinoacetylide...".

Page 74, Line 14: "*Angew. Chem. Int. Ed. Engl.*" should read "*Angew. Chem. Int. Ed.*"

Page 75, Line 10: "Nast, R. *Angew. Chem. Int. Ed.* **1960**, *72*, 26" should read "Nast, R. *Zeitschrift fuer Naturforschung.* **1953**, *8b*, 381.

Page 75, Line 31: "*J. Organmet. Chem.*" Should read "*J. Organomet. Chem.*"

Page 76, Line 18: "Powell, C.;..." should read "Powell, C.E.;..."

Page 78 Line 16: "*Synthetic Metals*" should read "*Synth. Met.*"

Page 78, Line 29: "*Angew. Chem. Int. Ed. Engl.*" should read "*Angew. Chem. Int. Ed.*"

Page 138, Line 17: "*Journal of Organometallic Chemistry*" should read "*J. Organomet. Chem.*"

Page 140, Line 12: "*Journal of Organometallic Chemistry*" should read "*J. Organomet. Chem.*"

Page 159, Line 4: "...bis(bidendatephosphine)ruthenium..." should read "...bis(bidentatephosphine)ruthenium..."

Page 179, Line 7: "*Inorganic Chemistry*" should read "*Inorg. Chem.*"

Page 179, Line 8: "Feringa, B. L. *Molecular Switches*; Wiley-VCH, 2001" should read "Feringa, B. L. *Molecular Switches*; Wiley-VCH, Weinheim, 2001".

Page 179, Line 23: "*Chem. Commun.*" should read "*J. Chem. Soc., Chem. Commun.*"

Page 179, Line 24: "*Synthetic Metals*" should read "*Synth. Met.*"

Transition Metal Acetylides for Nonlinear Optics

Clem Evans Powell
BSc(Hons)

A Thesis submitted for the degree of Doctor of Philosophy of the Australian National University

February, 2004

Contents

Summary iii

Statement iv

Acknowledgements v

Abbreviations vi

Published Results viii

Chapter 1
Transition Metal Acetylides for Nonlinear Optics 1

Chapter 2
Computational Investigation into the Optical and Nonlinear Optical Properties of Group 8 Metal Acetylide Complexes 79

Chapter 3
Electrochemical Switching of Third-order Nonlinear Optical Properties 142

Chapter 4
Ruthenium Acetylide Dendrimers and Related Complexes 182

Summary

Organometallic complexes are playing an increasing role in the field of nonlinear optics (NLO). This Thesis aims at extending the contribution of group 8 metal acetylides (primarily ruthenium) towards nonlinear optical properties.

Chapter 1 discusses NLO and the techniques used to measure it. A comprehensive literature review of the use of transition metal acetylides and vinylidenes in NLO is presented.

Chapter 2 covers density functional theory and its ability to calculate optical and nonlinear optical properties. The applicability of the program ADF to determine the quadratic hyperpolarizabilities of group 8 acetylide complexes was assessed. ADF was then used to characterize the absorption spectra of ruthenium acetylide complexes. The methodology used in the ruthenium acetylide complexes is then extended to cover osmium acetylide complexes.

Chapter 3 employs the results from Chapter 2 to demonstrate electrochemical switching of cubic hyperpolarizabilities. This is demonstrated at 800 and 1200 nm. This is the first demonstration of switching molecular third-order hyperpolarizabilities and of electrochemical switching of hyperpolarizabilities using an optically transparent thin-layer electrochemical cell. Additionally, the technique developed here has significant practical advantages over earlier examples.

Chapter 4 contains the synthesis of organometallic dendrimers and related complexes, and the measurement of their third-order nonlinearities. Novel dendrimers are synthesized and an improved synthetic route is developed. Additionally, molecular modelling is used to examine these large molecules.

Statement

I certify that the content of this Thesis has never been submitted for any degree and is not currently being submitted for any other degree or qualification, that all the work and results described are original unless due reference is made and that any help received has been acknowledged.

Clem Powell

Acknowledgements

My supervisor, Prof. Mark Humphrey, cannot be thanked enough. Through his ideas, support, and enthusiasm, his role in this thesis is impossible to overestimate.

Dr Marek Samoc is thanked for all of his ideas and assistance with the Z-scan, optical limiting and DFWM experiments. Mr Joseph Morrall is likewise thanked for his assistance with the NLO studies.

Dr Marie Cifuentes is thanked for the spectroelectrochemistry and TEM measurements, and for her help with the proofreading of this Thesis. Ms Eleni Notaras is also thanked for her role in the TEM study.

Dr Rob Stranger is thanked for the loan of his computers and ADF software package. Dr Chris Delfs is thanked for instructing me in how to use ADF.

Dr Graham Heath is thanked for the loan of the OTTLE cell and potentiostat.

Dr Tony Willis is thanked for the crystal structure determinations.

Thank you to the Molecular Materials group, for all of their ideas and friendship.

I would like to thank my friends and family for all of their support, and in particular, Maurice and Ina Powell for their encouragement and support.

Sylvia is thanked for just about everything.

Abbreviations

ADF	Amsterdam Density Functional
bR	bacteriorhodopsin
Bu^n	normal butyl
Bu^t	tertiary butyl
c.c.	complex conjugate
d	doublet
DFT	density functional theory
DFWM	degenerate four-wave mixing
dmso	dimethylsulfoxide
dppe	bis(diphenylphosphino)ethane
dppm	bis(diphenylphosphino)methane
EFISH	electric field-induced second harmonic generation
FMO	frontier molecular orbital
HOMO	highest occupied molecular orbital
HRMS	high resolution mass spectrometry
HRS	hyper-Rayleigh scattering
IDS	intensity dependent absorption
IR	infra-red
LMCT	ligand to metal charge transfer
LUMO	lowest unoccupied molecular orbital
m	multiplet
$[M]^+$	molecular ion
MALDI	matrix assisted laser desorption/ionization
Me	methyl
MECI	mono-excited configuration interaction
MLCT	metal to ligand charge transfer
MS	mass spectrometry

NLO	nonlinear optical
NMR	nuclear magnetic resonance
NIR	near infrared
OKG	Optical Kerr Gate
OTTLE	optically transparent thin-layer electrochemical
Ph	phenyl
s	singlet
SHG	second harmonic generation
t	triplet
TA	transient absorption
TD-DFT	time dependent-density functional theory
TEM	transmission electron microscopy
TBAF	tetrabutylammonium fluoride
thf	tetrahydrofuran
THG	third harmonic generation
TPA	two-photon absorption
UV	ultraviolet
vis	visible
ZINDO	Zerner's intermediate neglect of differential overlap

Published Results

Some of the results presented in this thesis have been published:

M. P. Cifuentes, C. E. Powell, M. G. Humphrey, G. A. Heath, M. Samoc and B. Luther-Davies, *J. Phys. Chem. A.*, **105** (2001) 9625-9627
Organometallic Complexes for Nonlinear Optics. 24. Reversible Electrochemical Switching of Nonlinear Absorption

C. E. Powell, M. P. Cifuentes, A. M. McDonagh, S. K. Hurst, N. T. Lucas, C. D. Delfs, R. Stranger, M. G. Humphrey, S. Houbrechts, I. Asselberghs, A. Persoons and D. C.R. Hockless, *Inorg. Chim. Acta*, **352** (2003) 9-18
Organometallic Complexes for Nonlinear Optics. Part 27. Syntheses and Optical Properties of Some Iron, Ruthenium and Osmium Alkynyl Complexes

C. E. Powell, M. P. Cifuentes, J. P. L. Morrall, R. Stranger, M. G. Humphrey, M. Samoc, B. Luther-Davies and G. A. Heath, *J. Am. Chem. Soc.*, **125** (2003) 602-610
Organometallic Complexes for Nonlinear Optics. Part 30. Electrochromic Linear and Nonlinear Optical Properties of Alkynylbis{bis(diphosphino)ethane}-ruthenium Complexes

M. Samoc, M. G. Humphrey, M. P. Cifuentes, A. M. McDonagh, C. E. Powell, G. A. Heath and B. Luther-Davies, *Proc. SPIE- Int. Soc. Opt. Eng.* **4461** (2001) 65-77.
Third-order optical nonlinearities of organometallics: influence of dendritic geometry on the nonlinear properties and electrochromic switching of nonlinear absorption.

A. M. McDonagh, C. E. Powell, J. P. Morrall, M. P. Cifuentes, and M. G. Humphrey, *Organometallics*, **22** (2003) 1402-1413.
Convergent Synthesis of Alkynylbis(bidentate phosphine)ruthenium Dendrimers

J. P. Morrall, C. E. Powell, R. Stranger, M. P. Cifuentes, M. G. Humphrey and G. A. Heath, *J. Organomet. Chem.*, **670** (2003) 248-255.
Organometallic Complexes for Nonlinear Optics. 32. Synthesis and Optical Properties of Some Osmium Alkynyl Complexes

C. E. Powell and M. G. Humphrey, *Coord. Chem. Rev.*, in press.
Nonlinear Optical Properties of Transition Metal Acetylides and Their Derivatives

C. E. Powell, M. G. Humphrey, M. P. Cifuentes, J. P. Morrall, M. Samoc and B. Luther-Davies *J. Phys Chem. A,* **107** (2003) 11264-11266.
Organometallic Complexes for Nonlinear Optics. 33. Electrochemical Switching of the Third-Order Nonlinearity Observed by Simultaneous Femtosecond Degenerate Four-Wave Mixing and Pump-probe Measurements

M. G. Humphrey, C. E. Powell, M. P. Cifuentes, J. P. Morrall and M. Samoc, *Polymer Preprints*, in press.
Synthesis and Nonlinear Optical Properties of Alkynylruthenium Dendrimers

C. E. Powell, J. P. Morrall, S. A. Ward, M. P. Cifuentes, E. G. A. Notaras, M. Samoc and M. G. Humphrey *J. Am. Chem. Soc.*, submitted.
Organometallic Complexes for Nonlinear Optics. 34. Z-scan Determination of the Dispersion of Third-order Nonlinear Optical Properties of an Organometallic Dendrimer

Chapter 1

Nonlinear Optical Properties of Transition Metal Acetylide and Vinylidene Complexes

Chapter 1

Nonlinear Optical Properties of Transition Metal Acetylide and Vinylidene Complexes

---

Contents

1.1. *Introduction*

1.2. *Theory and Processes*

1.3. *Experimental Techniques*

1.4. *Second-order Nonlinearities*

1.5. *Third-order Nonlinearities*

1.6. *Conclusions*

1.7. *References*

Chapter 1

Nonlinear Optical Properties of Transition Metal Acetylide and Vinylidene Complexes

1.1. *Introduction*

Over the last 17 years, organometallic complexes have been extensively investigated for their nonlinear optical (NLO) properties. A significant focus has been on two classes of organometallic complexes, ferrocenes and acetylides. This Chapter includes a comprehensive review of the NLO properties of transition metal acetylides and vinylidene complexes.

While an overview of the theory of nonlinear optics and experimental procedures to measure NLO responses is a necessary prerequisite to the survey of NLO properties of acetylide and vinylidene complexes that follows, excellent reviews of the field of nonlinear optics, and of the NLO properties of organic[1-6] and, particularly, organometallic molecules[7-21] are available elsewhere, so the present introduction to the field is abbreviated. When light interacts with materials possessing NLO properties the incident light can be changed and new electromagnetic field components produced (e.g. with differing phase, frequency, amplitude, polarization, path, etc). NLO materials have potential applications in optical signal processing, switching and frequency generation (making use of processes such as harmonic generation, frequency mixing, and optical parametric oscillation), and may also contribute to optical data storage, optical communication, and image processing.

Current NLO materials are mostly inorganic salts ($LiNbO_3$ and KH_2PO_4 (KDP) are used for frequency mixing and electrooptic modulation) or glasses such as silica (for applications involving third-order nonlinear processes). In inorganic salts the purely

electronic NLO effects are often accompanied by those arising from lattice distortions, with response times in the order of nanoseconds; the latter can be useful for relatively slow NLO processes (e.g. the electrooptic effect), but not for frequency conversions which require a purely electronic NLO response. Inorganic salts possess a large transparency range, are robust, are available as large single crystals, and suffer very low optical losses. The frequency doubling of lasers and optical parametric amplification require synchronization of the phases of the interacting optical fields (phase matching) which is not easy to satisfy, severely limiting the application of some materials. Semiconductors possess NLO effects originating from saturable absorption.[13] Their third-order NLO responses are amongst the largest known,[14] but NLO processes based on such resonant interactions may be relatively slow.

The limitations identified above spurred investigation of organic and, more recently, organometallic compounds. Many organic molecules have been examined for their NLO responses,[1-3,5,15-22] the main source of which is usually the electronic nonlinearities. Organic materials can possess a number of advantages, including a higher optical damage threshold than inorganic crystals, ease of synthesis and fabrication, structural diversity and architectural flexibility (permitting molecular design and engineering), and facile use in thin films for which electric field poling can introduce the asymmetry needed for the appearance of second-order NLO effects. Organics have several disadvantages: low energy transitions in the UV-visible region enhance the NLO efficiency, but result in a trade-off between nonlinear efficiency and optical transparency, they may have low thermal stability and (in poled guest-host systems) they may undergo a facile relaxation to random orientation.

Organometallic complexes are similar to organic molecules in that they can possess large NLO responses, fast response times, ease of fabrication and integration into composites. However, they possess the advantage of much greater design flexibility, e.g. by variation in metal, oxidation state, ligand environment and geometry, and can be strong oxidizing or reducing agents. The metal center may be an extremely strong donor or acceptor, a requirement for electron asymmetry and hence second-order nonlinearity. Unusual and/or unstable organic fragments (e.g. vinylidenes) may be stabilized on metals, allowing the NLO properties of these species to be assessed. The NLO properties of organometallic compounds have been reviewed previously together with those of some related coordination complexes.[8,12,23-26]

Metal acetylide complexes were first reported in the 1950s,[27] and have recently attracted significant interest because of possible materials applications.[28,29] This review focuses on the NLO properties of metal acetylide (alkynyl) and vinylidene complexes, the subject of this Thesis; this is an important subset of organometallic complexes for nonlinear optics, because these complexes can have high optical nonlinearities and have recently been shown to undergo facile NLO switching.

1.2. *Theory and Processes*

1.2.1. *Theory of Nonlinear Optics*

Optical nonlinearities can be explained by considering the interaction of strong electric fields with matter. A local electric field $\mathbf{E}_{loc}$ acting on a molecule will distort its electron density distribution $\rho(\mathbf{r})$, a result that can be described in terms of changes in the electron distribution moments. The first electron distribution moment, the dipole moment $\boldsymbol{\mu}$,is the most important moment from the perspective of optical properties. Changes in the dipole moment induced by a weak field are linear with the magnitude of the field. This is not the case when $\mathbf{E}_{loc}$ is comparable in strength to the internal electric fields within the molecule, at which point the distortion and the induced dipole moment should be treated as nonlinear functions of the field strength, usually being presented as a power series:

$$\boldsymbol{\mu} = \boldsymbol{\mu}_0 + \alpha\mathbf{E}_{loc} + \beta\mathbf{E}_{loc}\mathbf{E}_{loc} + \gamma\mathbf{E}_{loc}\mathbf{E}_{loc}\mathbf{E}_{loc} + \ldots \qquad (1)$$

The tensors α, β and γ defined by the above equation are the linear polarizability, the second-order or quadratic hyperpolarizability (the first hyperpolarizability) and the third-order or cubic hyperpolarizability (the second hyperpolarizability), respectively. Both $\boldsymbol{\mu}$ and $\mathbf{E}_{loc}$ are vectors, so the relation between the three cartesian components of $\boldsymbol{\mu}$ and the three cartesian components of $\mathbf{E}_{loc}$ needs nine proportionality factors, and hence α is a second-rank tensor (or a 3 x 3 matrix). Analogously, β is a third-rank tensor (or a 3 x 3 x 3 matrix) and γ is a fourth-rank tensor (or a 3 x 3 x 3 x 3 matrix). Fortunately, many of the tensor components of α, β, and γ are equivalent by various symmetry rules or equal to zero. The most straightforward simplification comes from permutation symmetry.[31] Additional simplification comes from polarizabilities being invariant with respect to all point group symmetry operations, this rule being especially important when considering β: all the components of β must vanish in centrosymmetric point groups.

The electric field of a light wave can be expressed as:

$$\mathbf{E}(t) = \mathbf{E}_0 \cos(\omega t) = \frac{\mathbf{E}_0}{2}[\exp(i\omega t) + \exp(-i\omega t)]$$

so Equation (1) can be written as:

$$\begin{aligned}\boldsymbol{\mu}(t) &= \boldsymbol{\mu}_0 + \alpha \mathbf{E}_0 \cos(\omega t) + \beta \mathbf{E}_0^2 \cos^2(\omega t) + \gamma \mathbf{E}_0^3 \cos^3(\omega t) + \ \ldots \\ &= \boldsymbol{\mu}_0 + \tfrac{1}{2}\alpha \mathbf{E}_0 \exp(i\omega t) + \tfrac{1}{2}\beta \mathbf{E}_0^2 \\ &\quad + \tfrac{1}{4}\beta \mathbf{E}_0^2 \exp(2i\omega t) + \tfrac{3}{8}\gamma \mathbf{E}_0^3 \exp(i\omega t) + \tfrac{1}{8}\gamma \mathbf{E}_0^3 \exp(3i\omega t) + \text{c.c.} + \ \ldots\end{aligned}$$

where c.c. stands for complex conjugate terms. It is readily apparent from the above expansions in terms of exponential factors or, equivalently, trigonometric relations such as $\cos^2(\omega t) = 1/2 + 1/2\cos(2\omega t)$ that the effect of the nonlinear terms in the dipole moment expansion has been to introduce contributions at different frequencies: the second-order (β) term has introduced a time-independent (d.c.) contribution as well as a term oscillating at the frequency of 2ω (the second-harmonic generation component). The quadratic term also provides a frequency mixing phenomenon if the input field is a sum of two components with different frequencies. It is also readily apparent that a constant (d.c.) field may influence an oscillating field if the two are combined in a medium containing second-order nonlinear molecules [this is known as the linear electrooptic (Pockels) effect]. The cubic term in Equation (1) leads to several nonlinear optical effects, one being oscillation of the induced dipoles at 3ω (third-harmonic generation).

Equation (1) is, strictly speaking, not suitable for optical fields, which are rapidly varying in time. For linear polarization, the oscillation of the induced dipole moment may be damped (by material resonances) and thereby phase shifted with respect to the oscillation of the external electric field. This is usually expressed by considering the relationship between the Fourier components of the induced effect (oscillation of the induced dipole) and the stimulus (the electric field), with the damping and phase shift conveniently expressed by treating the terms involved as complex. The linear polarizability can then be written as:

$$\Delta\mu^{(1)}(\omega) = \alpha(\omega)E(\omega)$$

where $\alpha(\omega)$ is complex, $E(\omega)$ is the Fourier amplitude of the field at frequency ω and $\Delta\mu^{(1)}(\omega)$ is the linear component of the oscillation of the dipole at the same frequency. The real part of α changes rapidly and the imaginary part of α increases in value near to the resonance frequencies of the molecule. Similarly, frequency dependent hyperpolarizabilities can be defined as complex quantities by considering the relationship between the nonlinear (quadratic and cubic) components of the induced dipole moment oscillations at particular frequencies, a complication being that more than a single field frequency is usually involved. The usual notation is:

$$\Delta\mu^{(2)}(\omega_3) = \beta(-\omega_3;\omega_1,\omega_2)E(\omega_1)E(\omega_2)$$

and:

$$\Delta\mu^{(3)}(\omega_4) = \gamma(-\omega_4;\omega_1,\omega_2,\omega_3)E(\omega_1)E(\omega_2)E(\omega_3)$$

for the quadratic and cubic NLO effects, respectively. The first frequency in the brackets describing the frequency dependence of the hyperpolarizability corresponds to the output frequency, the remaining frequencies being those of the input fields. Positive and negative signs of the frequencies can occur, depending on the type of interaction: for example, the β responsible for second-harmonic generation is represented as $\beta(-2\omega;\omega,\omega)$ whereas β for optical rectification is written as $\beta(0;-\omega,\omega)$. Resonant behavior of the hyperpolarizabilities (a rapidly changing real part and enhanced imaginary part) is expected not only when one of the frequencies in $\beta(-\omega_3;\omega_1,\omega_2)$ or $\gamma(-\omega_4;\omega_1,\omega_2,\omega_3)$ approaches a resonance but also for some combination of the input frequencies being close to a resonance.

Description of macroscopic NLO phenomena is analogous to the microscopic approach presented above. The macroscopic quantities of interest are the susceptibilities of various orders defined by:

$$\mathbf{P} = \chi^{(1)}\mathbf{E} + \chi^{(2)}\mathbf{E}^2 + \chi^{(3)}\mathbf{E}^3 + \ldots$$

$\chi^{(i)}$ are tensors of the same ranks as their molecular analogues and, similarly, the equation relating the polarization to the macroscopic optical field is rewritten in terms of the Fourier components of the polarization and of the input fields. The macroscopic

NLO properties are treated as the sum of molecular contributions, allowing for orientation of the molecules and for differences between the local field and the macroscopic electrical field. Tensor properties are usually transformed from one coordinate system to another using matrices of orientational cosines. Following this approach, the second-order susceptibility $\chi^{(2)}$ of a crystal composed of organic molecules with second-order hyperpolarizability β is equal to:[31]

$$\chi^{(2)}_{IJK}(-\omega_3;\omega_1,\omega_2) = L_I(\omega_3)L_J(\omega_1)L_K(\omega_2)\sum_{t=1}^{p} N_t b^t_{IJK}(-\omega_3;\omega_1,\omega_2)$$

where the L factors are the local field factors (usually approximated by the Lorenz-Lorentz expression $L = (n^2+2)/3$ where n = refractive index), and for which:

$$b^t_{IJK}(-\omega_3;\omega_1,\omega_2) = \frac{1}{N_g}\sum_{ijk}\sum_{s=1}^{N_g} \cos\theta^{(s)}_{Ii} \cos\theta^{(s)}_{Jj} \cos\theta^{(s)}_{Kk}\beta_{ijk}(-\omega_3;\omega_1,\omega_2)$$

where ijk denotes the cartesian coordinates of a molecule, IJK those of a crystal (a unit cell), N_t is the number of molecules in a unit volume occupying each particular inequivalent site in the unit cell, p is the number of inequivalent positions of a molecule in a unit cell and N_g is the number of equivalent positions in a unit cell. The directional cosines are used to transform each of the molecular β components to those of the new coordinate system (b_{IJK}) and the contributions are summed.

Due to statistical orientation of molecules, orientation averaging can be performed; for fourth-rank tensors, this leads to substantial simplification. From symmetry considerations, the $\chi^{(3)}$ tensor for an isotropic medium can only have two independent components, namely $\chi^{(3)}_{1111}$ and $\chi^{(3)}_{1122}$. The component $\chi^{(3)}_{1111}$ can be related to components of the molecular hyperpolarizability tensor as follows:

$$\chi^{(3)}_{1111}(-\omega_4;\omega_1,\omega_2,\omega_3) = L_{\omega_1}L_{\omega_2}L_{\omega_3}L_{\omega_4}N\langle\gamma(-\omega_4;\omega_1,\omega_2,\omega_3)\rangle$$

where L_{ω_i} is the local field factor at frequency ω_i (usually approximated by the Lorenz-Lorentz expression $L_\omega = [n_\omega{}^2 + 2]/3$) and:

$$\langle\gamma\rangle = \tfrac{1}{5}(\gamma_{1111} + \gamma_{2222} + \gamma_{3333} + 2\gamma_{1122} + 2\gamma_{1133} + 2\gamma_{2233})$$

The simplest case is that of an isotropic medium containing molecules with a single dominant component of γ, say γ_{1111} (a realistic approximation for linear π-conjugated

molecules, for which the hyperpolarizability component along the molecular axis is likely to be dominant); $\langle\gamma\rangle = \frac{1}{5}\gamma_{1111}$ is then a reasonable approximation.

The two common unit systems employed for the description of nonlinear optical properties are the SI (or MKS) and Gaussian (or cgs) systems. A detailed discussion on conversions between these systems of units is available elsewhere.[10,11] The Gaussian system (in which properties are described in terms of esu) has been used in almost all reports of metal acetylide or vinylidene complexes thus far.

1.2.2. *Nonlinear Optical Processes*

The major use of second-order nonlinearities is for a variety of frequency mixing schemes. Among the possible processes, there are several which have specific technological applications and are therefore of significant interest: (i) second-harmonic generation, i.e. the $\omega + \omega \rightarrow 2\omega$ mixing process which doubles the energy of photons (e.g. to convert infrared into visible light), (ii) the linear electrooptic (Pockels) effect, i.e. the $\omega + 0 \rightarrow \omega$ process which is often used to modulate the phase or amplitude of a light wave (to make it carry information), and (iii) parametric generation, i.e. the $\omega \rightarrow \omega_1 + \omega_2$ process which involves splitting an energetic photon into a sum of two less energetic ones (a popular way of generating laser beams at tunable wavelengths).

There are many possible third-order nonlinear processes, some of which are important as valuable tools for nonlinear spectroscopy, while others have technological significance. The presence of $\chi^{(3)}$ in any substance (even air) means that all materials exhibit third-harmonic generation of laser frequencies. The direct process of third-harmonic generation is, however, not usually exploited for generation of short wavelength laser beams, a cascade of two second-order mixing processes ($\omega + \omega \rightarrow 2\omega$ and $2\omega + \omega \rightarrow 3\omega$) being preferred for generation of 3ω from ω (one reason for this is that phase matching is virtually impossible to obtain for third-harmonic generation). From the technological point of view, the most interesting applications of $\chi^{(3)}$ are those which correspond to all-optical interactions of light beams. For interacting fields of the same frequency (the degenerate case), the frequency mixing scheme is $\omega - \omega + \omega \rightarrow \omega$, which

means that the interaction of three fields of the same frequency generates a fourth field of the same frequency.

Optical power limiting has attracted considerable interest with applications such as the protection of sensors from damage resulting from exposure to high energy laser pulses. In principle, the direct two-photon absorption process is suitable for optical limiting, but practical estimates show that power limiting properties of existing materials (even those with the largest two-photon absorption coefficients such as ruthenium acetylide dendrimers – see later discussion) are insufficient for the most important applications, namely, the protection of sensors from laser pulses of duration of the order of nanoseconds.

1.3. *Experimental Techniques*

A large number of techniques have been employed to measure quadratic and cubic nonlinearities of organic molecules, excellent descriptions of which can be found elsewhere.[32] The discussion that follows is restricted to techniques utilized with metal acetylide and vinylidene complexes.

1.3.1. *Kurtz Powder Technique*

In this procedure a laser beam is directed onto a powder sample and the emitted second-harmonic light is collected, filtered, detected and compared with a standard (usually urea). As the magnitude of the response depends on particle size, samples are commonly sieved to ensure a narrow particle size range. Materials can be classed as phase matchable or non-phase matchable (Figure 1.1.). For the latter, second-harmonic generation (SHG) is effective over distances smaller than the coherence length (the coherence length L_c for a second-harmonic process is given by $L_c = [\lambda_\omega/4(n_{2\omega}-n_\omega)]$ for fundamental wavelength λ_ω and the refractive indices of the material at the fundamental n_ω and second-harmonic $n_{2\omega}$). When the light path is smaller than the coherence length the second-harmonic intensity increases with the square of the interaction distance. However, when the crystal sizes are similar to the coherence length, there is no further increase of second-harmonic intensity with the propagation distance and the signal actually decreases, due to a decrease in the number of crystals being sampled. In contrast, there is a direction of propagation in phase matchable materials for which the second harmonic intensity increases quadratically without a limit. The SHG intensity does not decrease because the decrease in the number of crystallites as they become bigger is compensated by the contribution from phase-matched interactions. Figure 1.1. demonstrates the differing behaviour of non-phase matched and phase-matched materials.

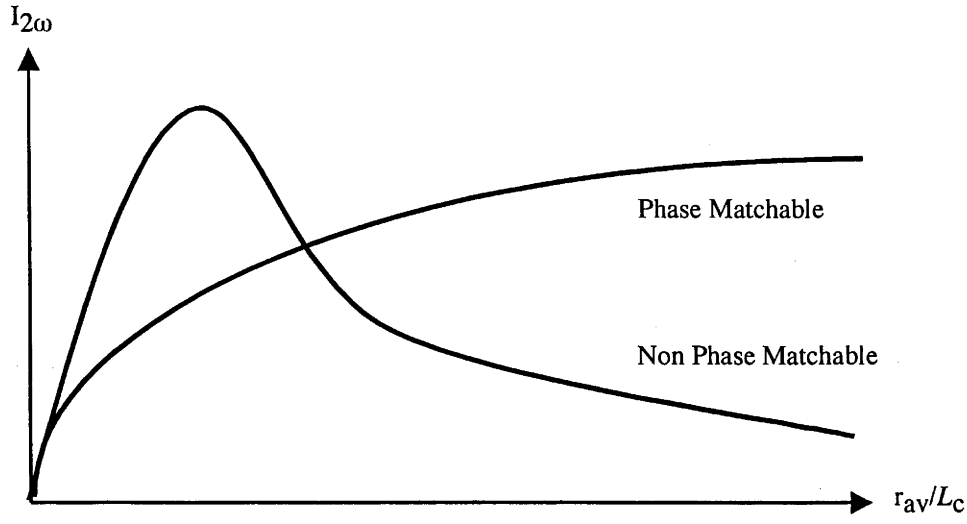

Figure 1.1. Particle size dependence of the second-harmonic intensity

Because the light intensities measured in the powder technique depend on several factors, results from Kurtz SHG studies should not be considered as quantitative. The magnitude of the tensor components of the molecular hyperpolarizability β is only one of these factors. A critical issue is the molecular packing in the unit cell of the crystal. The unit cell hyperpolarizability tensor components are all identically equal to zero in a centrosymmetric arrangement. In noncentrosymmetric arrangements, substantial differences in the nonlinear coefficients may result from packing nonlinear molecules in different ways. Unit cell hyperpolarizability is transformed into macroscopic second-order susceptibility with the contribution of local field factors; this can modify the properties also. SHG efficiency is critically dependent on the coherence lengths, which depend in turn on crystal optics. The measured second-harmonic intensities also depend on other factors: reflection coefficients at the crystal/air interfaces, absorption and scattering of fundamental and second-harmonic light, etc. All of the foregoing is consistent with the powder technique affording qualitative information at best about the molecular properties of molecules in the crystals being investigated. In particular, observation of high power SHG is consistent with large β for a compound, while its absence does not necessarily preclude high molecular nonlinearities.

A major shortcoming of the technique is that materials which crystallize in centrosymmetric space groups theoretically cannot exhibit SHG, so the Kurtz method is only applicable to the *ca* twenty percent of complexes that crystallize noncentrosymmetrically. However, despite the requirement for noncentrosymmetric

crystal packing and the lack of a quantitative significance of the results, the Kurtz technique has been widely used because one can rapidly screen a large number of samples, and because one can conveniently study SHG without access to large single crystals.

1.3.2. *Electric Field-induced Second-Harmonic Generation*

Electric field-induced second-harmonic generation (EFISH) was used to measure molecular quadratic nonlinearities of metal acetylide complexes in early studies, but it has been largely superceded by the more widely applicable hyper-Rayleigh scattering technique (see below). In the EFISH technique, the molecules in a solution of the complex are aligned using a high voltage d.c. pulse, which is synchronized with the laser beam pulse; this permits observation of $\chi^{(2)}$ in what was previously an isotropic medium. EFISH is formally a third-order nonlinear process described by the susceptibility $\chi^{(3)}(-2\omega;\omega,\omega,0)$, so all materials will produce an EFISH signal. There are two contributions to this susceptibility, one arising from the sum of the orientationally-averaged third-order hyperpolarizabilities $\gamma(-2\omega;\omega,\omega,0)$ of the medium, and another due to the vectorial sum of the components of the second-order hyperpolarizabilities. Molecules with a permanent dipole μ partially align with the d.c. field. The net second-order effect is dependent on the $\mu\cdot\beta_{vec}$ product where μ is the dipole moment of the molecule and β_{vec} is the vectorial component of the second-order hyperpolarizability (the hyperpolarizability β is a symmetric third-rank tensor that can be treated as being composed of a vector part and a septor part).[33] In general, the directions of β_{vec} and of μ are not coincident. The effective hyperpolarizability measured by the EFISH technique, β_{EFISH}, is given by $\mu\cdot\beta_{vec} = \mu\beta_{EFISH}$. For dipolar molecules containing strong electron donor and acceptor groups, β_{CT} (the hyperpolarizability along the charge-transfer axis) usually accounts for most of β_{EFISH}.

The solution of the sample is contained in a wedge shaped cell which is translated in a direction perpendicular to the incident laser beam. This creates Maker fringes whose periodicity is related to the wedge design and to the coherence length; the latter can therefore be determined. A measurement on a pure solvent is usually used to calibrate

the system. The EFISH-derived third-order susceptibility $\Gamma = 3\chi^{(3)}(-2\omega;\omega,\omega,0)$ is related to the molecular second hyperpolarizability γ' by local field factors and the molecule number density, and β can then be obtained from $\gamma' = \gamma + \mu\beta_{EFISH}/(5k_bT)$, where γ' is the effective second hyperpolarizability, γ is the intrinsic second hyperpolarizability (consisting of electronic and vibrational parts), k_b is Boltzmann's constant and T is the temperature in K. Comparison against a reference enables Γ values to be determined. EFISH measurements are usually performed as a function of concentration in a well-characterized solvent, a concentration dependence study being necessary to resolve ambiguities because the $\mu\beta_{EFISH}$ products for the solvent and the solute may be of the same or of opposite signs, and the SHG signal is proportional to the square of the EFISH susceptibility. Several other quantities may be required for the interpretation of the results: the dielectric constant, the permanent dipole moment, and the intrinsic second hyperpolarizability of the solute (found from a separate experiment or ignored).

EFISH has only been used to evaluate nonlinearities of neutral metal acetylide complexes, the presence of ionic species rendering it impossible to apply high electric fields to a solution. From the aforementioned description, it is clear that it is also not possible to utilize EFISH when the complex has no net dipole moment.

1.3.3. *Hyper-Rayleigh Scattering (HRS)*

Hyper-Rayleigh scattering (HRS) has been (by far) the most widely utilized technique that has been employed to measure molecular quadratic nonlinearities of metal acetylide and vinylidene complexes. The HRS technique involves detecting the incoherently scattered second-harmonic light generated from an isotropic solution in order to determine the first hyperpolarizability. HRS arises from orientational fluctuations of unsymmetrical molecules in solution, resulting in local asymmetry in an isotropic liquid.[34] The scattered light can have a second-harmonic component that depends only on the first hyperpolarizability of the solute molecules, and varies quadratically with the incident intensity. The solute concentration is proportional to the square of the nonlinearity of all species in solution, and so varying the concentration of solutes allow β^2 to be extracted.

A schematic diagram of the HRS experiment is shown in Figure 1.2. A seed injected, Q-switched laser pumps the HRS cell, the incident intensity and polarization being controlled by a half-wave plate polarizer combination and monitored by a photodiode or energy meter. The incident beam is focussed into the sample solution. A concave mirror, with its focus at the interaction focal volume, and a lens are used to collect the scattered light which is filtered to isolate the second-harmonic light, detected by a photomultiplier tube and averaged by a gated integrator.

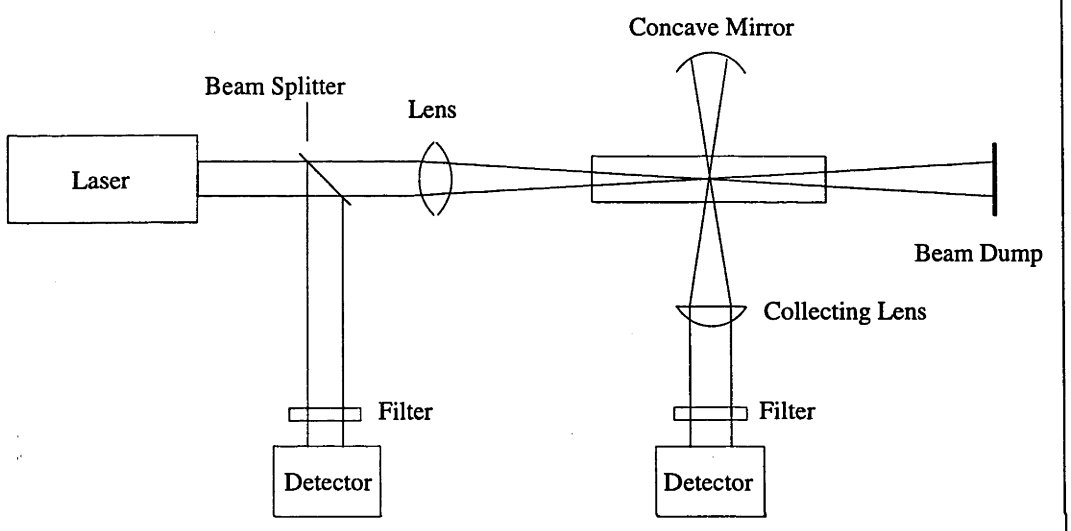

Figure 1.2. Schematic diagram of the HRS experiment

HRS has a number of advantages compared to EFISH: it is simpler (a d.c. field is not required, and neither are measurements of μ or γ), it is sensitive to non-vector components of the β tensor, and one can measure octupolar molecules and ionic species, the last-mentioned being particularly important for organometallics with more than one accessible oxidation state. However the need for sensitive detection and high intensity of the fundamental (due to the low intensity of the second-harmonic light) are disadvantages, the need for high intensity of the fundamental being particularly detrimental due to stimulated Raman or Brillouin scattering, self-focussing, or dielectric breakdown. Other disadvantages of HRS are that it is only possible to find the magnitude of β (this results from the quadratic dependence on the HRS signal) and that unreliable results are obtained when the complex fluoresces at the frequency-doubled wavelength.

1.3.4. *Degenerate Four-wave Mixing*

Degenerate four-wave mixing (DFWM) was used to measure molecular cubic nonlinearities of metal acetylide complexes in early studies, but it is now much less popular than the experimentally simpler Z-scan technique (see below). In DFWM, two coherent "pump" beams interact within a material creating an interference pattern of light intensity. Because the change in refractive index of a third-order material depends on the intensity of the applied field, a refractive index grating results, which, in the simplest case, can be described by the dependence $\Delta n(r) = n_2 I(r)$. When a third beam is incident on this grating, a fourth beam is generated, the intensity of which is proportional to the product of all the input intensities and to the square of the absolute value of the complex third-order susceptibility, i.e. $I_4 \sim |\chi^{(3)}|^2 I_1 I_2 I_3$. In practice, one laser is used and the beam is split to provide the pump beams and the probe beam. DFWM has several advantages: one can measure all of the independent $\chi^{(3)}$ tensor components of an isotropic medium by using various combinations of polarizations for the four beams employed in the experiment, absolute and relative measurements of $\chi^{(3)}$ are possible,[32] and the time dependence of the nonlinear response can be studied; the last-mentioned is significant because off-resonance electronic nonlinearities show a practically instantaneous response, and these can be separated from slower processes that also contribute to the nonlinear refractive index. One difficulty with DFWM is that, in order to distinguish between contributions from the real and imaginary part of the third-order susceptibility, one must perform a series of measurements on solutions of a compound with varying concentrations in a non-absorbing solvent. The concentration dependence of the DFWM signal is:

$$I_{DFWM} \propto \left|\chi^{(3)}\right|^2 \propto [N_{solvent}\gamma_{solvent} + N_{solute}\mathrm{Re}(\gamma_{solute})]^2 + [N_{solute}\mathrm{Im}(\gamma_{solute})]^2$$

it being assumed that the solvent contributes only to the real part of the solution susceptibility, whereas the solute can contribute to both the real (refractive) and imaginary (absorptive) components.

Despite its experimental complexity, DFWM forms a complementary technique to the technically less difficult Z-scan, in that it can be used to verify that the origin of the observed nonlinearity is electronic in nature.

1.3.5. *Z-scan*

Z-scan is the technique that has been used to measure the cubic NLO merit of the vast majority of metal acetylide complexes studied thus far. It involves examining self-focussing or self-defocussing phenomena in a nonlinear material, from which one can derive the nonlinear refractive index intensity coefficient n_2 and thereby $\chi^{(3)}$ and γ.[35] Using a single Gaussian laser beam in a tight focus geometry (Figure 1.3.), the transmittance of a nonlinear medium through a fixed aperture in the far field is measured as the position of the material is varied. At the start (A) (and finish (E)) of the scan the sample is far removed from the focal plane. As a consequence, the intensity of the beam is low and lensing is not observed. As the material approaches the focal plane (B), lensing results in the beam focussing earlier, and the measured transmittance is thereby reduced. At the focal plane (C), there is no change in transmittance, because a thin lens at the focus causes no change in the far-field. After the focal plane (D), focussing of the beam by the lensing of the material results in an increase in measured transmittance. The measured, normalized energy transmittance from a Z-scan experiment is numerically fitted to equations derived from theory, permitting the determination of n_2, $\chi^{(3)}$ and γ.

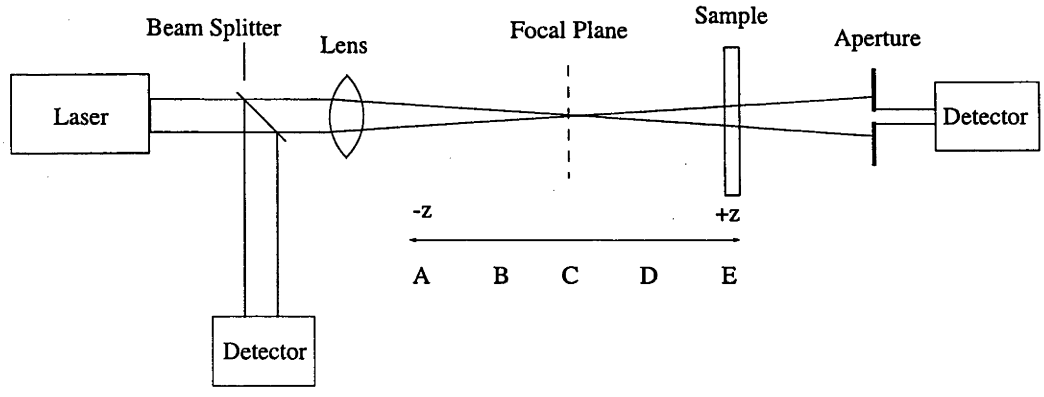

Figure 1.3. Schematic diagram of the Z-scan experiment

The shape of the Z-scan curve can be modified if nonlinear transmission (absorption bleaching) or nonlinear absorption occur, e.g. due to an imaginary component of $\chi^{(3)}$ of the material. The curves are then unsymmetrical because of increased transmission or

absorption close to the focal plane. The nonlinear absorption coefficient β_2 or the related imaginary part of $\chi^{(3)}$ can be determined by analyzing the shape of such a modified Z-scan curve. An alternative experiment (usually referred to as an "open aperture Z-scan") can be used to determine the nonlinear absorption properties of a sample. In this experiment, the total intensity of the transmitted beam is measured without an aperture, as a function of the sample position with respect to the focal plane. Materials with potential optical limiting properties are often investigated by this means. For solutions, the nonlinearity changes on varying the concentration are determined, and hence measurements performed in an absolute manner, or, alternatively, results can be referenced to a standard.

There are several advantages of the Z-scan technique: the sign and magnitude of the nonlinear refractive index can be determined, both the real and imaginary parts of $\chi^{(3)}$ can be determined, and the single beam configuration results in simplicity (compared to DFWM). Z-scan also has disadvantages: a high quality Gaussian beam and good optical quality of samples are necessary, and the experiment does not afford information about the temporal nature of the nonlinear response.

1.3.6. *Third-Harmonic Generation (THG)*

Third-harmonic generation is employed to measure the electronic molecular second hyperpolarizability of centrosymmetric materials, because no process other than nonresonant electron cloud distortion responds sufficiently rapidly to produce a nonlinear polarization oscillating at the third harmonic.[32] All materials exhibit THG, including any glass used for a sample cell, or even air, so this experiment is technically difficult. One can avoid some problems by placing the sample in a vacuum sealed cell inside a vacuum chamber, but a simpler method involves using thick glass windows, permitting the contribution from air to be ignored; in this procedure, though, the third-order susceptibility of the glass and solvent must be known. While THG has been used to study $\chi^{(3)}$ for several group 4 metal acetylides, it has not approached the popularity of the experimentally simpler Z-scan technique.

1.3.7. *Optical Kerr Gate*

Optical Kerr gate (OKG) has been used less frequently than Z-scan for studies of metal acetylide complexes. In this experiment (Figure 1.4.), the sample is subjected to a linearly polarized pump beam which induces optical birefringence.[32] A probe beam of known linear polarization which is almost collinear with the pump beam then passes through the material, and the resultant light intensity through a crossed polarizer is measured. The Kerr gate transmittance is proportional to the square of the nonlinear phase shift between the slow and fast axes of the induced birefringence, with the phase shift itself being proportional to $(\chi^{(3)}_{xxyy} + \chi^{(3)}_{xyyx})I_{pump}$. Both the real and imaginary parts of $\chi^{(3)}$ contribute to the signal in the Kerr gate experiment, but a slightly modified experiment, heterodyne Kerr gate, can be used to resolve these two contributions. For electronic nonlinearity, the measured sum of the tensor components is equal to $\frac{2}{3}\left(\chi^{(3)}_{xxxx}\right)$. An auxiliary experiment, polarization ellipse rotation, can be used to fully characterize the $\chi^{(3)}$ tensor. The Kerr gate experiments are slightly simpler than DFWM (although not as simple as Z-scan), both the real and imaginary parts of $\chi^{(3)}$ can be measured, and the temporal dependence of the nonlinear response can be studied, but the necessity to run two independent experiments to determine all the tensor components of $\chi^{(3)}$ has resulted in these techniques being significantly less popular because Z-scan and DFWM reveal more information from one experiment.

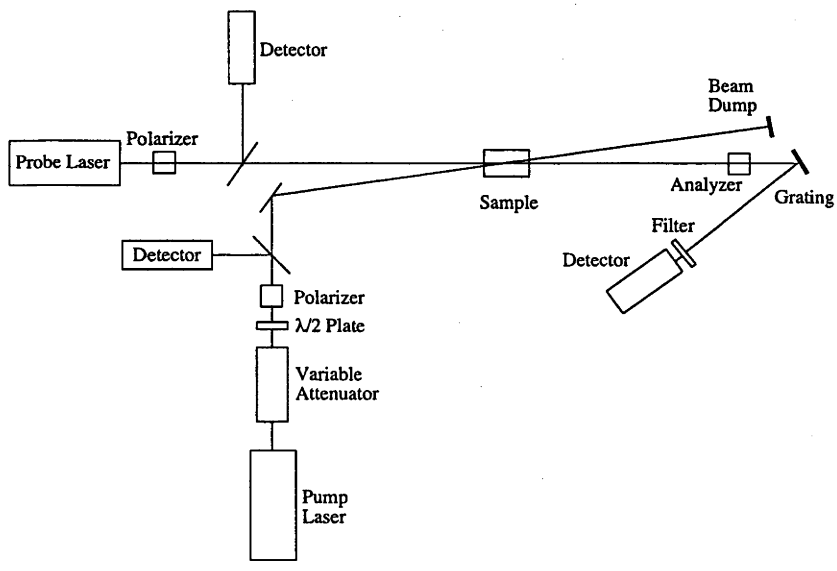

Figure 1.4. Schematic diagram of an optical Kerr gate experiment

1.3.8. *ZINDO (for Calculating Optical Nonlinearities)*

Computational techniques can afford insight into the structure-property relationships of molecules and materials, because the often time-consuming syntheses may be avoided by predicting responses computationally. Perhaps more importantly, otherwise inaccessible structural variations (such as bond length variation) may be probed. Unfortunately, though, modeling environmental interactions (intermolecular or solvent/molecule) is difficult,[26,36,37] and so all calculated NLO responses of acetylide complexes are of individual molecules in the gas phase rather than of bulk materials. The only calculations of acetylide complexes thus far have employed ZINDO, which is a semi-empirical intermediate neglect of differential overlap/spectroscopy (INDO/S) based routine. ZINDO utilizes a sum over excited particle hole states (SOS) method to calculate second-order nonlinear optical coefficients, and is parameterized to accommodate transition metal calculations. To achieve computational efficiency, some terms are replaced by empirical data or neglected. The SOS treatment is then used with the mono-excited state configuration interaction (MECI) approximation.[38,39] The values reported are β_{vec}, the value of β that lies along the dipolar axis (this is the value sampled by the EFISH technique), and β_{tot}, the total quadratic hyperpolarizability, which is defined as:

$$\beta_{tot} = \sqrt{\left(\beta_x^2 + \beta_y^2 + \beta_z^2\right)}$$

1.4. *Second-Order Nonlinearities*

1.4.1. *Group 8 Acetylide Complexes*

Complexes of the group 8 metals comprise the largest group of acetylide complexes to have been assessed for quadratic NLO merit, the results of these studies being collected in Table 1.1., and the structural formulas of some of the more efficient compounds being displayed in Figure 1.5.

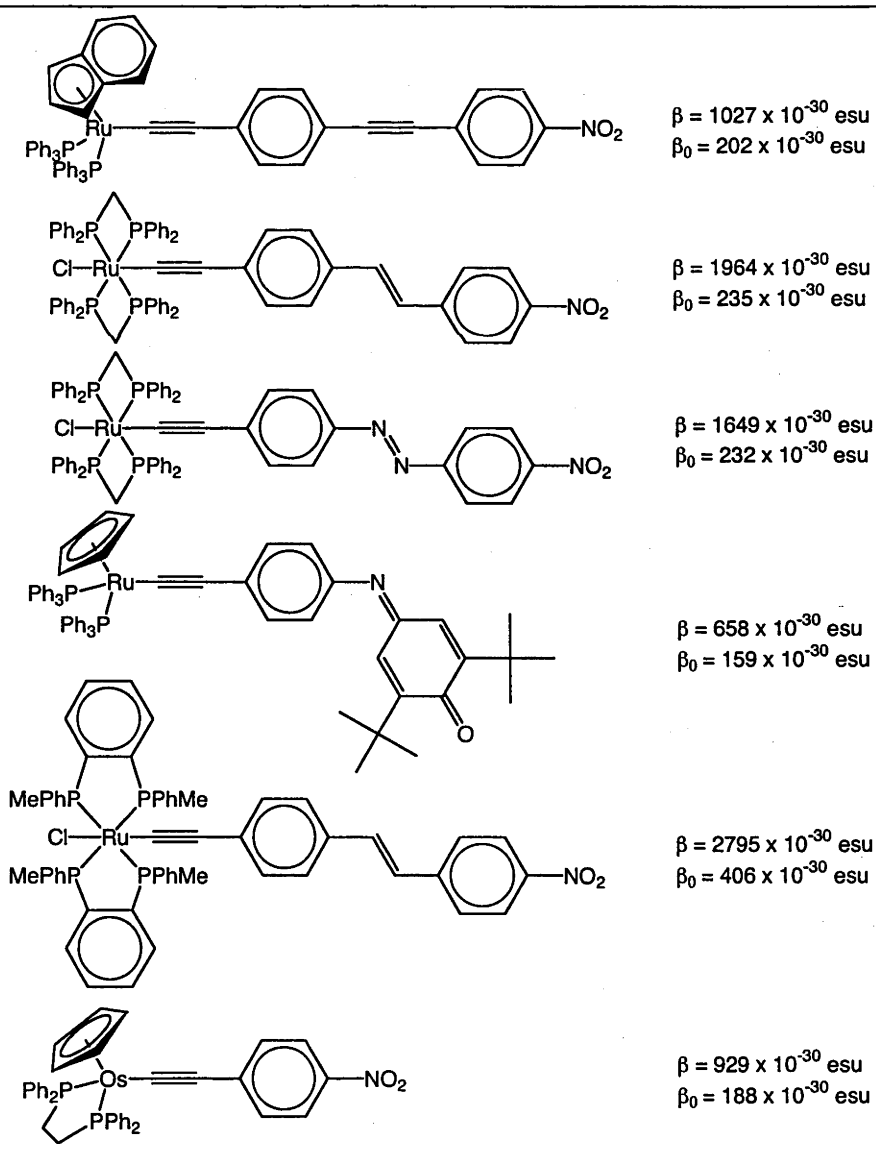

Figure 1.5. Selected Group 8 acetylides with high second-order nonlinearities

At this point it is apropos to mention that one must be very cautious in comparing results from different laboratories (perhaps obtained using different techniques and at different wavelengths). Dispersion is a serious concern: results are influenced by material resonances and the degree of this resonance enhancement is difficult to quantify. Dispersion of β for linear charge-transfer molecules can be described by a two state model, but such a model is probably not sufficient for metal acetylide complexes, and particularly octupolar examples. The two-level corrected β values (β_0) are available from:

$$\beta_0 = \beta(1-(\lambda_{max}/\lambda)^2)(1-(2\lambda_{max}/\lambda)^2)$$

The values (β_0) are listed in Table 1.1. and subsequent Tables, but these data should be treated cautiously: three complexes in Table 1.1. have been examined by HRS at two wavelengths, the varying β_0 values testifying to the lack of applicability of the two-level model. The other major concern is that the various experimental techniques can sample different tensorial components or combinations thereof. Two complexes in Table 1.1. have been examined by both HRS and EFISH, the equivalent β values (within the experimental error margins) suggesting that there is one dominant tensor component ($\beta_{vec} = \beta_{EFISH} = \beta_{HRS} = \beta_{zzz}$).

Structure-NLO activity trends revealed from the data in Table 1.1. and subsequent Tables in many cases mimic those found for organic molecules. Organic molecules containing conjugated π systems with unsymmetrical charge distribution have been shown to exhibit large second-order NLO properties; thus, donor-acceptor substituted azo dyes, Schiff bases, and stilbenes, which are all molecules with easily polarizable π-electrons, all show large second-order nonlinearities. Nonlinearities can be enhanced by either increasing the conjugation length (improving delocalization) or increasing the strength of donor or acceptor groups (improving electron asymmetry). These NLO chromophore improvements result in a red-shift in the important linear optical absorption band, which reduces optical transparency, so octupolar molecules have been investigated in a bid to overcome this NLO efficiency/transparency trade off – the lack of a molecular dipole also improves the prospects of noncentrosymmetric crystal packing, required to manifest bulk susceptibility.

The data in Table 1.1. are consistent with an increase in β value upon increasing acetylide ligand chain length (proceeding from one-ring to biphenyl-, imino- and yne-linked two-ring acetylide ligand, with the azo- and ene-linked acetylide complexes the most efficient, and, indeed, more efficient than the complex with the three-ring yne-linked ligand; not surprisingly, an increase in β and β_0 value is seen on increasing n from 0 to 2 for *trans*-[Ru(C≡C(C_6H_4-4-C≡C)$_n$$C_6H_4$-4-$NO_2$)Cl(dppm)$_2$], although the β value for n = 0 and 1 are the same within the error margins. Ease of delocalization is enhanced upon replacing phenyl rings with heterocycles; however, nonlinearities do not consistently increase on replacing phenyl by pyridyl[40,41] and in fact decrease on incorporation of furyl ring,[42] while the location of the thienyl ring and phenyl ring in two-ring acetylide ligands was found to be unimportant in influencing NLO merit.[43] The use of iodoanilinoacetylide ligands such as in [Ru{C≡CC_6H_4N=CCH=CBu^{t}C(O)C(Bu^t)=CH}(PPh_3)$_2$(η^5-C_5H_5)] has been examined, because in the charge-transfer excited state the ring closer to the metal center becomes quinoidal, but the ring remote from the metal center becomes aromatic (Figure 1.6.), eliminating loss of aromatic stabilization energy and thereby enhancing nonlinearities. While the quadratic nonlinearity for this complex is large,[44] it is not as large as similarly-sized two-ring azo- or ene- linked complexes.[45]

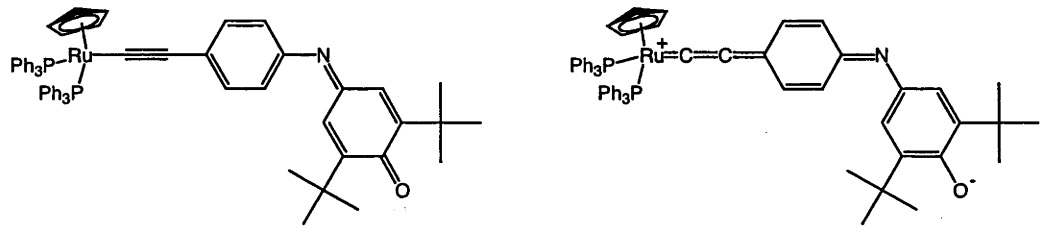

Figure 1.6. Ground state (left) and charge-transfer excited state (right) representations of an indoanilinoacetylide complex

Increasing the donor and/or acceptor strength generally results in an increase in nonlinearity. The 18 electron readily oxidizable ruthenium(II) centers in these complexes are very efficient donors – where direct comparison to related organic compounds is possible, it appears that the Ru(II) center is a stronger donor, resulting in large NLO coefficients. The efficient nitro group has been the most widely used acceptor across this series of complexes, replacement with other acceptor groups (CHO,

CN) generally resulting in a decrease in nonlinearity, while alkylation of the 4-pyridylacetylide ligand to afford a 4-methylpyridylinium acceptor afforded a complex with similar optical transparency to the 4-nitrophenylacetylide analogue, but greatly reduced nonlinearity. The 4-pyridyl group in [Ru{C≡C-(*E*)-CH=CH-4-C_5H_4N}$(PPh_3)_2(\eta^5$-indenyl)] has been metallated with $Cr(CO)_5$ and $W(CO)_5$ units, the products possessing considerably red-shifted linear absorption bands and significantly enhanced nonlinearities. Similarly, the nitrile group in [Ru{C≡C-(*E*)-CH=CH-4-C_6H_4CN}$(PPh_3)_2(\eta^5$-indenyl)] has been metallated with $Cr(CO)_5$, $W(CO)_5$ and $[Ru(NH_3)_5]^{3+}$ groups, with addition of the group 6 metals proving the more effective route to enhancing nonlinearities. In both cases, the tungsten-containing complexes are the more efficient.[42,46,47] It is also important to maintain conjugation pathway, replacement of C_6H_4-4-CHO with C_6H_4-3-CHO resulting in a decrease of the nonlinearity.[48,49]

One advantage of organometallic complexes over organic compounds is the possibility of tuning NLO response by co-ligand modification. For the group 8 metal acetylide complexes, varying co-ligand should modify donor strength or delocalization possibilities. Replacing two CO ligands by dppe results in a significant increase in nonlinearity,[50] while subtle variations (replacing dppe by dppm or two PPh_3 ligands) have no effect within the error margins. Interestingly, the nonlinearity for the triphenylphosphine complex is greater than that of the trimethylphosphine complex in the pair [Ru(C≡C C_6H_4-4-NO_2)$(L)_2(\eta^5$-C_5H_5)], suggesting that the greater delocalization possibilities of the former are more important for NLO merit than the greater basicity of the latter.[46,51] Replacing cyclopentadienyl by indenyl ligand generally results in increased quadratic nonlinearity, while for metal variation the limited data thus far suggest increasing nonlinearity as β(iron complex) ≤ β(ruthenium complex) ≤ β(osmium complex).[42,46,47,50]

Recently, several octupolar acetylide complexes have been examined; their nonlinearities are modest,[52-54] but none thus far incorporate acceptor groups at the core, introduction of which would be expected to enhance nonlinearity significantly. The "best" dipolar group 8 acetylide complexes represent the most efficient organometallic compounds with respect to quadratic NLO response, the β values being the same order of magnitude as the most efficient organic compounds.

Table 1.1. Molecular Quadratic NLO Measurements for Group 8 Acetylide Complexes

Complex	λ_{max} (nm)	β^a (10^{-30} esu)	$\beta_0{}^a$ (10^{-30} esu)	Technique	Solvent	Fund. (μm)	Ref.
[Fe(C≡CPh)(dppe)(η^5-C_5Me_5)]	348	52	24	HRS	CH_2Cl_2	1.064	52
1,3-C_6H_4[(C≡C)Fe(dppe)(η^5-C_5Me_5)]$_2$	349	210	98	HRS	CH_2Cl_2	1.064	52
1,3,5-C_6H_3[(C≡C)Fe(dppe)(η^5-C_5Me_5)]$_3$	351	175	87	HRS	CH_2Cl_2	1.064	52
1,4-C_6H_4[(C≡C)Fe(dppe)(η^5-C_5Me_5)]$_2$	413	180	60	HRS	CH_2Cl_2	1.064	52
(-)$_{436}$-*trans*-[Fe(C≡CC_6H_4-4-NO_2)Cl{(*R*,*R*)-diph}$_2$]	543	440	14	HRS	thf	1.064	55
[Fe(C≡CC_6H_4-4-NO_2)(CO)$_2$(η^5-C_5H_5)]	370	49	22	HRS	thf	1.064	50
[Fe(C≡CC_6H_4-4-NO_2)(dppe)(η^5-C_5H_5)]	498	665	64	HRS	thf	1.064	50
[Ru(C≡CPh)(PPh_3)$_2$(η^5-C_5H_5)]	310	89	45	HRS	thf	1.064	46,56
[Ru(C≡CC_6H_4-4-NO_2)(PPh_3)$_2$(η^5-C_5H_5)]	460	468	96	HRS	thf	1.064	46,51
[Ru(C≡CC_6H_4-4-NO_2)(PMe_3)$_2$(η^5-C_5H_5)]	477	248	39	HRS	thf	1.064	46,51
[Ru(C≡CC_6H_4-4-C≡CC_6H_4-4-NO_2)(PPh_3)$_2$(η^5-C_5H_5)]	448	560	134	HRS	thf	1.064	46,56
[Ru(C≡CC_6H_4-4-(*E*)-CH=CHC_6H_4-4-NO_2)(PPh_3)$_2$(η^5-C_5H_5)]	476	1455	232	HRS	thf	1.064	46,51
	476	1464	234	EFISH	thf	1.064	46,51
	478	186	105	HRS	CH_2Cl_2	1.560	43
[Ru(C≡C-2-C_5H_4N)(PPh_3)$_2$(η^5-C_5H_5)]	331	18	10	HRS	thf	1.064	40
[Ru(C≡C-2-C_5H_3N-5-NO_2)(PPh_3)$_2$(η^5-C_5H_5)]	468	622	113	HRS	thf	1.064	40
[Ru(C≡CC_6H_4-4-C≡CC_6H_4-4-NO_2)(PPh_3)$_2$(η^5-C_5H_5)]	446	865	212	HRS	thf	1.064	46,56
[Ru(C≡CC_6H_4-4-N=CHC_6H_4-4-NO_2)(PPh_3)$_2$(η^5-C_5H_5)]	496	840	86	HRS	thf	1.064	46,51
	496	760	78	EFISH	thf	1.064	46,51

Table 1.1. (continued) Molecular Quadratic NLO Measurements for Group 8 Acetylide Complexes

Complex	λ_{max} (nm)	β^a (10^{-30} esu)	$\beta_0{}^a$ (10^{-30} esu)	Technique	Solvent	Fund. (μm)	Ref.
[Ru(C≡CC$_6$H$_4$-4-(*E*)-CH=CH-2-C$_4$H$_2$S-5-NO$_2$)(PPh$_3$)$_2$(η^5-C$_5$H$_5$)]	533	294	138	HRS	CH_2Cl_2	1.560	43
[Ru(C≡C-2-C$_4$H$_2$S-5-(*E*)-CH=CHC$_6$H$_4$-4-NO$_2$)(PPh$_3$)$_2$(η^5-C$_5$H$_5$)]	522	333	163	HRS	CH_2Cl_2	1.560	43
[Ru(C≡CC$_6$H$_4$-4-C≡C-2-C$_4$H$_2$S-5-NO$_2$)(PPh$_3$)$_2$(η^5-C$_5$H$_5$)]	505	210	109	HRS	CH_2Cl_2	1.560	43
[Ru{C≡C-(2-C$_4$H$_2$S-5-(*E*)-CH=CH)$_2$C$_6$H$_4$-4-NO$_2$}(PPh$_3$)$_2$(η^5-C$_5$H$_5$)]	536	419	195	HRS	CH_2Cl_2	1.560	43
[Ru(C≡CC$_6$H$_4$-4-N=CH-2-C$_4$H$_2$S-5-NO$_2$)(PPh$_3$)$_2$(η^5-C$_5$H$_5$)]	562	308	129	HRS	CH_2Cl_2	1.560	43
[Ru(C≡C-4-C$_5$H$_4$NMe)(PPh$_3$)$_2$(η^5-C$_5$H$_5$)][PF$_6$]	460	80	16	HRS	CH_2Cl_2	1.064	57
[Ru(C≡CC$_6$H$_4$-4-(*E*)-CH=CH-4-C$_5$H$_4$NMe)(PPh$_3$)$_2$(η^5-C$_5$H$_5$)][PF$_6$]	582	1600	154	HRS	CH_2Cl_2	1.064	57
[Ru(C≡CC$_6$H$_4$-4-C≡C-4-C$_5$H$_4$NMe)(PPh$_3$)$_2$(η^5-C$_5$H$_5$)][PF$_6$]	558	1400	102	HRS	CH_2Cl_2	1.064	57
[Ru(C≡CC$_6$H$_4$-4-NO$_2$)(PPh$_3$)$_2$(η^5-indenyl)]	476	746	119	HRS	CH_2Cl_2	1.064	42.46,47
[Ru(C≡CC$_6$H$_4$-4-NO$_2$)(dppe)(η^5-indenyl)]	459	516	107	HRS	CH_2Cl_2	1.064	42
[Ru(C≡CC$_6$H$_4$-4-NO$_2$)(dppm)(η^5-indenyl)]	456	540	117	HRS	CH_2Cl_2	1.064	42
[Ru(C≡C-(*E*)-CH=CHC$_6$H$_4$-4-NO$_2$)(PPh$_3$)$_2$(η^5-indenyl)]	507	1257	89	HRS	CH_2Cl_2	1.064	42.46,47
[Ru(C≡C-(*E*)-CH=CHC$_6$H$_4$-4-CN)(PPh$_3$)$_2$(η^5-indenyl)]	427	238	71	HRS	CH_2Cl_2	1.064	42.46,47
[Ru(C≡C-(*E*)-CH=CH-(*E*)-CH=CHC$_6$H$_4$-4-NO$_2$)(PPh$_3$)$_2$(η^5-indenyl)]	523	1320	34	HRS	CH_2Cl_2	1.064	42.46,47

Table 1.1. (continued) Molecular Quadratic NLO Measurements for Group 8 Acetylide Complexes

Complex	λ_{max} (nm)	β^a (10^{-30} esu)	$\beta_0{}^a$ (10^{-30} esu)	Technique	Solvent	Fund. (μm)	Ref.
[Ru(C≡C-(*E*)-CH=CH-4-C_5H_4N)$(PPh_3)_2(\eta^5$-indenyl)]	399	100	37	HRS	CH_2Cl_2	1.064	46,47
[Ru(C≡CC_6H_4-4-C≡CC_6H_4-4-NO_2)$(PPh_3)_2(\eta^5$-indenyl)]	463	1027	202	HRS	CH_2Cl_2	1.064	42
[Ru(C≡CC_6H_4-4-N=CHC_6H_4-4-NO_2)$(PPh_3)_2(\eta^5$-indenyl)]	509	1295	85	HRS	CH_2Cl_2	1.064	42
[Ru(C≡C-(*E,Z*)-CH=CH-2-C_4H_2O-5-NO_2)$(PPh_3)_2(\eta^5$-indenyl)]	550	908	43	HRS	CH_2Cl_2	1.064	42
[Ru(C≡C-(*E*)-CH=CH-2-C_4H_2S-5-NO_2)$(PPh_3)_2(\eta^5$-indenyl)]	598	487	88	HRS	CH_2Cl_2	1.064	42
[Ru{C≡CCH=C$(C_6H_4$-3-$NO_2)_2$}$(PPh_3)_2(\eta^5$-indenyl)]	345	48	25	HRS	CH_2Cl_2	1.064	42
[Ru{C≡C-(*E*)-CH=CH-4-C_5H_4N-1-$Cr(CO)_5$}$(PPh_3)_2(\eta^5$-indenyl)]	451	260	60	HRS	CH_2Cl_2	1.064	42.46,47
[Ru{C≡C-(*E*)-CH=CH-4-C_5H_4N-1-$W(CO)_5$}$(PPh_3)_2(\eta^5$-indenyl)]	462	535	71	HRS	CH_2Cl_2	1.064	42.46,47
[Ru{C≡C-(*E*)-CH=CHC_6H_4-4-C≡N$Cr(CO)_5$}$(PPh_3)_2(\eta^5$-indenyl)]	442	465	119	HRS	CH_2Cl_2	1.064	42.46,47
[Ru{C≡C-(*E*)-CH=CHC_6H_4-4-C≡N$W(CO)_5$}$(PPh_3)_2(\eta^5$-indenyl)]	456	700	150	HRS	CH_2Cl_2	1.064	42.46,47
[Ru{C≡C-(*E*)-CH=CHC_6H_4-4-C≡N$Ru(NH_3)_5$}$(PPh_3)_2(\eta^5$-indenyl)][CF_3SO_3]$_3$	442	315	80	HRS	acetone	1.064	42.46,47
[Fe(η^5-C_5H_5){η^5-C_5H_4-(*E*)-CH=CHC≡C$Ru(PPh_3)_2(\eta^5$-indenyl)}]	345	273	141	HRS	CH_2Cl_2	1.064	42
trans-[Ru(C≡CPh)Cl$(dppm)_2$]	308	20	12	HRS	thf	1.064	41

Table 1.1. (continued) Molecular Quadratic NLO Measurements for Group 8 Acetylide Complexes

Complex	λ_{max} (nm)	β^a (10^{-30} esu)	$\beta_0{}^a$ (10^{-30} esu)	Technique	Solvent	Fund. (μm)	Ref.
trans-[Ru(C≡CC_6H_4-4-NO_2)Cl(dppm)$_2$]	473	767	129	HRS	thf	1.064	41
trans-[Ru(C≡CC_6H_4-4-C_6H_4-4-NO_2)Cl(dppm)$_2$]	465	933	178	HRS	thf	1.064	41
trans-[Ru(C≡CC_6H_4-4-(*E*)-CH=CHC_6H_4-4-NO_2)Cl(dppm)$_2$]	490	1964	235	HRS	thf	1.064	41
trans-[Ru(C≡C-2-C_5H_4N)Cl(dppm)$_2$]	351	35	19	HRS	thf	1.064	41
trans-[Ru(C≡C-2-C_5H_3N-5-NO_2)Cl(dppm)$_2$]	490	468	56	HRS	thf	1.064	41
trans-[Ru(C≡CC_6H_4-4-C≡CPh)Cl(dppm)$_2$]	381	101	43	HRS	thf	1.064	48
trans-[Ru(C≡CC_6H_4-4-CHO)Cl(dppm)$_2$]	405	106	38	HRS	thf	1.064	48
trans-[Ru(C≡CC_6H_4-4-C≡CC_6H_4-4-NO_2)Cl(dppm)$_2$]	464	833	161	HRS	thf	1.064	48
trans-[Ru(C≡CC_6H_4-4-C≡CC_6H_4-4-C≡CC_6H_4-4-NO_2)Cl(dppm)$_2$]	439	1379	365	HRS	thf	1.064	48
trans-[Ru(C≡CPh)Cl(dppe)$_2$]	319	6	3	HRS	thf	1.064	48
trans-[Ru(C≡CC_6H_4-4-CHO)Cl(dppe)$_2$]	413	120	40	HRS	thf	1.064	48
trans-[Ru(C≡CC_6H_4-4-NO_2)Cl(dppe)$_2$]	477	351	55	HRS	thf	1.064	48
trans-[Ru(C≡CC_6H_4-(*E*)-4-CH=CHC_6H_4-4-NO_2)Cl(dppe)$_2$]	489	2676	342	HRS	thf	1.064	48
[Ru{C≡CC_6H_4-(*E*)-4-N=NC_6H_4-4-NO_2}$(PPh_3)_2(\eta^5$-$C_5H_5)$]	565	1627	149	HRS	thf	1.064	45
trans-[Ru(C≡CC_6H_4-(*E*)-4-N=NC_6H_4-4-NO_2)Cl(dppm)$_2$]	583	1649	232	HRS	thf	1.064	45
[Ru{C≡CC_6H_4N=CCH=CBu^tC(O)C(Bu^t)=CH}$(PPh_3)_2(\eta^5$-$C_5H_5)$]	622	658	159	HRS	thf	1.064	44
[Ru{C≡CC_6H_4N=CCH=CBu^tC(O)C(Bu^t)=CH}Cl(dppm)$_2$]	645	417	124	HRS	thf	1.064	44

Table 1.1. (continued) Molecular Quadratic NLO Measurements for Group 8 Acetylide Complexes							
Complex	λ_{max} (nm)	β^a (10^{-30} esu)	$\beta_0{}^a$ (10^{-30} esu)	Technique	Solvent	Fund. (μm)	Ref.
1,3,5-{*trans*-[RuCl(dppe)$_2$(C≡C-4-C$_6$H$_4$C≡C)]}$_3$C$_6$H$_3$	414	94	18	HRS	thf	1.064	53
1,3,5-{*trans*-[Ru(C≡CPh)(dppe)$_2$(C≡C-4-C$_6$H$_4$C≡C)]}$_3$C$_6$H$_3$	411	93	18	HRS	thf	1.064	53
trans-[Ru(C≡CPh)(C≡CC$_6$H$_4$-4-C≡CPh)(dppe)$_2$]	383	34	8	HRS	thf	1.064	53
trans-[Ru(C≡CPh)Cl(dppe)$_2$]	319	6	2	HRS	thf	1.064	53
[1-(HC≡C)-3,5-C$_6$H$_3$*trans*-C≡CRuCl(dppm)$_2$}$_2$]	323	< 42	< 24	HRS	thf	1.064	58
trans-[Ru(C≡CC$_6$F$_4$-4-OMe)Cl(dppm)$_2$]	337	26	14	HRS	thf	1.064	59
trans-[Ru(C≡CC$_6$H$_4$-(*E*)-4-CH=CHPh)Cl(dppm)$_2$]	397	200 ± 40	44 ± 9	HRS	thf	1.064	54
	397	920[b]	5	HRS	thf	0.800	54
1,3,5-(*trans*-[RuCl(dppm)$_2$}{C≡CC$_6$H$_4$-(*E*)-4-CH=CH}$_3$C$_6$H$_3$	415	150 ± 92	28 ± 14	HRS	thf	1.064	54
	415	577 ± 19	16 ± 1	HRS	thf	0.800	54
(-)$_{578}$-*trans*-[Ru(C≡CPh)Cl{(*R*,*R*)-diph}$_2$]	292	too low	too low	HRS	thf	1.064	55
(-)$_{589}$-*trans*-[Ru(C≡CC$_6$H$_4$-4-NO$_2$)Cl{(*R*,*R*)-diph}$_2$]	467	530	97	HRS	thf	1.064	55
(-)$_{589}$-*trans*-[Ru(C≡CC$_6$H$_4$-(*E*)-4-CH=CHC$_6$H$_4$-4-NO$_2$)Cl{(*R*,*R*)-diph}$_2$]	481	2795	406	HRS	thf	1.064	55
[Ru(C≡CC$_6$H$_4$-4-NO$_2$)(CO)$_2$(η^5-C$_5$H$_5$)]	364	58	27	HRS	thf	1.064	50
[Ru(C≡CC$_6$H$_4$-4-NO$_2$)(dppe)(η^5-C$_5$H$_5$)]	447	664	161	HRS	thf	1.064	50
[Ru(C≡CC$_6$H$_4$-4-NO$_2$)(PPh$_3$)$_2$(η^5-C$_5$H$_5$)]	468	96	9	HRS	thf	1.064	50
[Ru(C≡CC$_6$H$_4$-4-CH{OC(O)Me}$_2$)(PPh$_3$)$_2$(η^5-C$_5$H$_5$)]	326	68	38	HRS	thf	1.064	49
[Ru(C≡CC$_6$H$_4$-4-CHO)(PPh$_3$)$_2$(η^5-C$_5$H$_5$)]	400	120	45	HRS	thf	1.064	49

Table 1.1. (continued) Molecular Quadratic NLO Measurements for Group 8 Acetylide Complexes							
Complex	λ_{max} (nm)	β^a (10^{-30} esu)	$\beta_0{}^a$ (10^{-30} esu)	Technique	Solvent	Fund. (μm)	Ref.
trans-[Ru{C≡C-4-C_6H_4CHO(CHO$(CH_2)_3$O}Cl$(dppm)_2$]	320	61	35	HRS	thf	1.064	49
trans-[Ru(C≡CC_6H_4-3-CHO)Cl$(dppm)_2$]	321	58	34	HRS	thf	1.064	49
$(-)_{365}$-*trans*-[Os(C≡CC_6H_4-4-NO_2)Cl{(*R*,*R*)-diph}$_2$]	326	68	38	HRS	thf	1.064	55
[Os(C≡CC_6H_4-4-NO_2)(dppe)(η^5-C_5H_5)]	461	929	188	HRS	thf	1.064	50
[Os(C≡CC_6H_4-4-NO_2)(PPh_3)$_2$(η^5-C_5H_5)]	474	1051	174	HRS	thf	1.064	50

[a] β values have uncertainty of 10% unless otherwise noted

[b] Upper bound only. No complete demodulation of the fluorescence contribution could be achieved

1.4.2. *Group 10 Acetylide Complexes*

The molecular quadratic nonlinearities of a systematically varied series of (cyclopentadienyl)(triphenylphosphine)nickel acetylide complexes have been determined by hyper-Rayleigh scattering at 1.064 μm, the results being given in Table 1.2. and the structural formulas of some of the more efficient compounds being shown in Figure 1.7. As with results for the ruthenium examples summarized above, dispersion-enhanced and two–level corrected nonlinearities increase upon introduction of acceptor substituent (nitro group), chain lengthening of acetylide ligand, and replacing *Z* by *E* stereochemistry at the acetylide ligand alkene linkage.[40,60] The nonlinearities for these 18-electron complexes are smaller than those for their 18-electron (cyclopentadienyl)bis(phosphine)ruthenium analogues, suggesting that the greater ease of oxidation of the latter is an important determinant of NLO merit in metal acetylide complexes.[60]

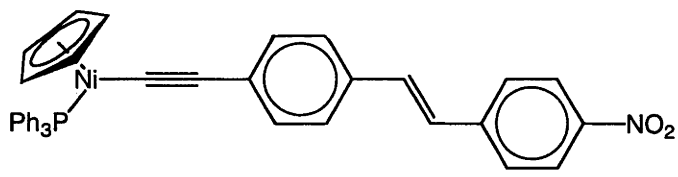

$\beta = 445 \times 10^{-30}$ esu
$\beta_0 = 120 \times 10^{-30}$ esu

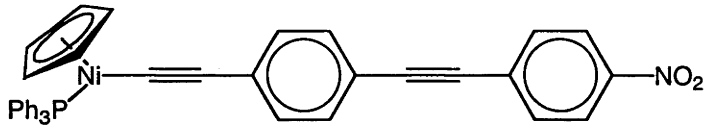

$\beta = 326 \times 10^{-30}$ esu
$\beta_0 = 106 \times 10^{-30}$ esu

Figure 1.7. Selected Group 10 acetylides with high second-order optical nonlinearities

Table 1.2. Molecular Quadratic NLO Measurements of Group 10 Acetylide Complexes[a]

Complex	λ_{max} (nm)	β[b] (10^{-30} esu)	β_0[b] (10^{-30} esu)	Ref.
$[Ni(C{\equiv}CPh)(PPh_3)(\eta^5\text{-}C_5H_5)]$	307	24[c]	15	60
$[Ni(C{\equiv}CC_6H_4\text{-}4\text{-}NO_2)(PPh_3)(\eta^5\text{-}C_5H_5)]$	439	221	59	60
$[Ni(C{\equiv}CC_6H_4\text{-}4\text{-}C_6H_4\text{-}4\text{-}NO_2)(PPh_3)(\eta^5\text{-}C_5H_5)]$	413	193	65	60
$[Ni(C{\equiv}CC_6H_4\text{-}4\text{-}(E)\text{-}CH{=}CHC_6H_4\text{-}4\text{-}NO_2)(PPh_3)(\eta^5\text{-}C_5H_5)]$	437	445	120	60
$[Ni(C{\equiv}CC_6H_4\text{-}4\text{-}(Z)\text{-}CH{=}CHC_6H_4\text{-}4\text{-}NO_2)(PPh_3)(\eta^5\text{-}C_5H_5)]$	417	145	47	60
$[Ni(C{\equiv}CC_6H_4\text{-}4\text{-}C{\equiv}CC_6H_4\text{-}4\text{-}NO_2)(PPh_3)(\eta^5\text{-}C_5H_5)]$	417	326	106	60
$[Ni(C{\equiv}CC_6H_4\text{-}4\text{-}N{=}CHC_6H_4\text{-}4\text{-}NO_2)(PPh_3)(\eta^5\text{-}C_5H_5)]$	448	387	93	60
$[Ni(C{\equiv}C\text{-}2\text{-}C_5H_4N)(PPh_3)(\eta^5\text{-}C_5H_5)]$	415	25	8	40
$[Ni(C{\equiv}C\text{-}2\text{-}C_5H_3N\text{-}5\text{-}NO_2)(PPh_3)(\eta^5\text{-}C_5H_5)]$	456	186	41	40
$[1\text{-}(HC{\equiv}C)\text{-}3,5\text{-}C_6H_3\{C{\equiv}CNi(PPh_3)(\eta^5\text{-}C_5H_5)\}_2]$	316	94	55	58

[a] HRS, thf solvent, 1.064 μm.

[b] β values have uncertainty of 10% unless otherwise noted.

[c] uncertainty of 20%.

1.4.3. *Group 11 Acetylide Complexes*

All group 11 acetylide complexes examined thus far are (phosphine)gold complexes by HRS at 1.064 μm, the results of which are summarized in Table 1.3., while structural formulas of some of the more efficient complexes are displayed in Figure 1.8. Unlike the other extensively investigated series (the ruthenium acetylide complexes), all of the gold complexes possess optical transitions in the UV and are optically transparent at the second-harmonic frequency. This is important as it permits a realistic evaluation of intrinsic off-resonance hyperpolarizabilities, and thereby reliable development of structure-NLO property relationships. The quadratic nonlinearities of these complexes show a similar dependence on the nature of the acetylide ligand as has been reported previously for organic chromophores. The efficiency sequence for acetylide ligand bridge variation C_6H_4 < $C_6H_4C_6H_4$ < $C_6H_4C{\equiv}CC_6H_4$ < *E*-$C_6H_4CH{=}CHC_6H_4$ was rationalized from π-bridge lengthening, torsion effects at the phenyl-phenyl linkage (of the biphenyl compound), and orbital energy mismatch of *p* orbitals of *sp*-hybridized acetylenic carbons with orbitals of sp^2 hybridized phenyl carbons (for the diphenylacetylene compound).[61] Bridge stereochemistry affects quadratic nonlinearities as β(*Z* isomer) < β(*E* isomer), explained from a combination of greater dipole moment and more intense optical transition for the latter.[61] Quadratic nonlinearities are also observed to increase with increasing acceptor strength, *viz.* β(H) < β(CHO) < β(NO_2) and for acceptor substitution site β(3-CHO) < β(4-CHO).[49] The most efficient complex [Au(C≡CC_6H_4-4-(*E*)-N=NC_6H_4-4-NO_2)(PPh_3)] possesses the same alkynyl ligand as one of the most efficient ruthenium acetylide complexes of similar size;[45] the efficiency of this ligand was predicted (before its synthesis) in earlier semi-empirical ZINDO studies.[51]

Table 1.3. Molecular Quadratic NLO Measurements of Group 11 Acetylide Complexes[a]

Complex	λ_{max} (nm)	β^b (10^{-30} esu)	$\beta_0{}^b$ (10^{-30} esu)	Ref.
[Au(C≡CPh)(PPh_3)]	296	6	4	46,61
[Au(C≡CC_6H_4-4-NO_2)(PPh_3)]	338	22	12	46,61
[Au(C≡CC_6H_4-4-C_6H_4-4-NO_2)(PPh_3)]	350	39	20	46,61
[Au(C≡CC_6H_4-4-(*E*)-CH=CHC_6H_4-4-NO_2)(PPh_3)]	386	120	49	46,61
[Au(C≡CC_6H_4-4-(*Z*)-CH=CHC_6H_4-4-NO_2)(PPh_3)]	362	58	28	46,61
[Au(C≡CC_6H_4-4-C≡CC_6H_4-4-NO_2)(PPh_3)]	362	59	28	46,61
[Au(C≡CC_6H_4-4-N=CHC_6H_4-4-NO_2)(PPh_3)]	392	85	34	46,61
[Au(C≡CC_6H_4-4-(*E*)-N=NC_6H_4-4-NO_2)(PPh_3)]	398	180	68	45
[Au(C≡C-2-C_5H_4N)(PPh_3)]	300	7	4	40
[Au(C≡C-2-C_5H_3N-5-NO_2)(PPh_3)]	339	38	20	40
[Au(C≡C-2-C_5H_3N-5-NO_2)(PMe_3)]	340	12	6	40
[1,3,5-C_6H_3(C≡C$AuPPh_3$)$_3$]	298	6	4	58
[Au(C≡CC_6H_4-4-CHO)(PPh_3)]	322	14	8	49
[Au(C≡CC_6H_4-4-CHO)(PMe_3)]	322	c		49
[Au(C≡CC_6H_4-4-CHO$(CH_2)_3$O)(PPh_3)]	296	15	10	49
[Au(C≡CC_6H_4-4-CHO$(CH_2)_3$O)(PMe_3)]	292	48	31	49
[Au(C≡CC_6H_4-3-CHO)(PPh_3)]	318	c		49
[Au(C≡CC_6H_4-3-CHO)(PMe_3)]	322	c		49
[Au(C≡CC_6H_4-4-NO_2)(PCy_3)]	342	31	16	62
[Au(C≡CC_6H_4-4-NO_2)(PMe_3)]	339	50	27	62
[Au(C≡CC_6H_4-4-OMe)(PMe_3)]	339	44	25	59

Table 1.3. (continued) Molecular Quadratic NLO Measurements of Group 11 Acetylide Complexes[a]				
Complex	λ_{max} (nm)	β^b (10^{-30} esu)	$\beta_0{}^b$ (10^{-30} esu)	Ref.
[Au(C≡CC_6H_4-4-OMe)(PPh_3)]	296	20	14	59

[a] HRS, thf, 1.064 μm

[b] β values have uncertainty of 10% unless otherwise noted

[c] too low to measure

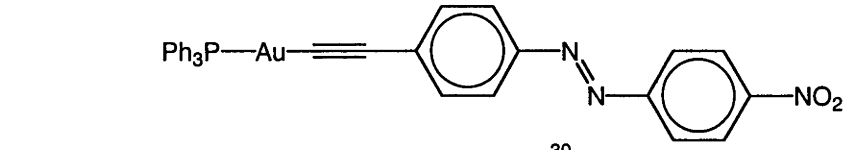

$\beta = 180 \times 10^{-30}$ esu
$\beta_0 = 68 \times 10^{-30}$ esu

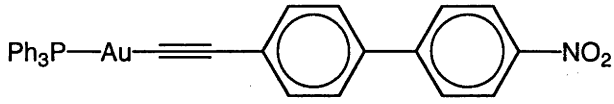

$\beta = 39 \times 10^{-30}$ esu
$\beta_0 = 20 \times 10^{-30}$ esu

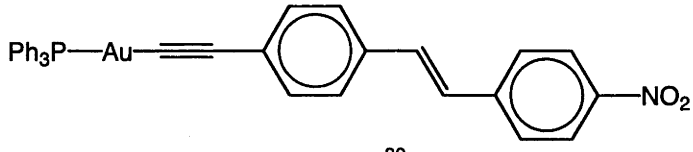

$\beta = 120 \times 10^{-30}$ esu
$\beta_0 = 49 \times 10^{-30}$ esu

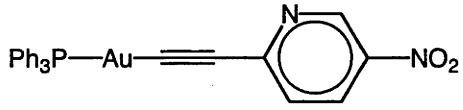

$\beta = 38 \times 10^{-30}$ esu
$\beta_0 = 20 \times 10^{-30}$ esu

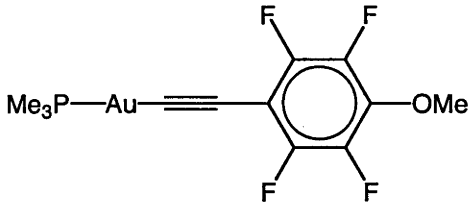

$\beta = 44 \times 10^{-30}$ esu
$\beta_0 = 25 \times 10^{-30}$ esu

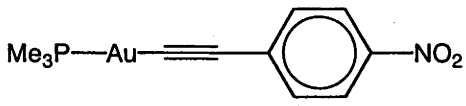

$\beta = 50 \times 10^{-30}$ esu
$\beta_0 = 27 \times 10^{-30}$ esu

Figure 1.8. Selected Group 11 acetylides with high second-order nonlinearities

1.4.4. *Vinylidene Complexes*

Study of the quadratic NLO merit of vinylidene complexes is comparatively recent, significant impetus to this development being given from the interest in switching NLO properties coupled to the facile interconvertibility of acetylide and vinylidene complex pairs via protonation/deprotonation sequences. Thus far, all reports are of ruthenium vinylidene complexes assessed by hyper-Rayleigh scattering at 1.064 μm, the results from which are collected in Table 1.4. The vinylidene complexes were not designed to have large quadratic NLO responses and, perhaps not surprisingly, nonlinearities for the monoruthenium vinylidene complexes are mostly low. Introduction of a nitro acceptor group affords larger β values, a somewhat surprising observation, as the cationic ruthenium center in these vinylidene complexes is not regarded as a strong donor group in a classical donor-bridge-acceptor NLO chromophore composition. The octupolar complex [1,3,5-(*trans*-[RuCl(dppm)$_2${C=CHC$_6$H$_4$-(*E*)-4-CH=CH}])$_3$C$_6$H$_3$](PF$_6$)$_3$ was examined by HRS with ns pulses at 1064 nm and fs pulses at 800 nm, the β values at the shorter wavelength being much greater, consistent with significant resonance enhancement resulting from close proximity of the optical absorption maximum to the second-harmonic wavelength of the latter (400 nm).[54]

The aryldiazovinylidene complexes are derivatives of [Ru(C≡CPh)(PPh$_3$)$_2$(η^5-C$_5$H$_5$)] for which β = 16 x 10^{-30} esu (β_0 = 10 x 10^{-30} esu); an increase in β is observed upon introduction of functionalized aryldiazo group, but not upon incorporation of phenyldiazo unit. Complex [Ru(C=CPhN=NC$_6$H$_4$-4-NO$_2$)(PPh$_3$)$_2$(η^5-C$_5$H$_5$)]I was examined in three different solvents, nonlinearities varying as β(acetone) ≥ β(CH$_2$Cl$_2$) > β(thf). The molecular variation across these vinylidene complex salts affords trends in β consistent with the introduction of polarizing substituents (NO$_2$, OMe) and location of nitro substituent (4-NO$_2$ cf 3,5-(NO$_2$)$_2$) making a significant contribution to the observed responses.[63]

Table 1.4. Molecular Quadratic NLO Measurements of Vinylidene Complexes[a]

Complex	λ_{max} (nm)	β[b] (10^{-30} esu)	β_0[b] (10^{-30} esu)	Solvent	Fund. (μm)	Ref.
trans-[Ru(C=CHC$_6$F$_4$-4-OMe)Cl(dppm)$_2$]PF$_6$	334	32	17	thf	1.064	59
trans-[Ru(C=CHC$_6$H$_4$-2-CHO)Cl(dppm)$_2$]PF$_6$	555	27	2	thf	1.064	49
trans-[Ru(C=CHC$_6$H$_4$-3-CHO)Cl(dppm)$_2$]PF$_6$	320	45	26	thf	1.064	49
trans-[Ru{C=CHC$_6$H$_4$-4-CHO(CH$_2$)$_3$O}Cl(dppm)$_2$]PF$_6$	317	64	38	thf	1.064	49
trans-[Ru(C=CHPh)Cl(dppm)$_2$]PF$_6$	320	24	16	thf	1.064	48
trans-[Ru(C=CHC$_6$H$_4$-4-C≡CPh)Cl(dppm)$_2$]PF$_6$	380	64	31	thf	1.064	48
trans-[Ru(C=CHC$_6$H$_4$-4-CHO)Cl(dppm)$_2$]PF$_6$	403	108	39	thf	1.064	48
trans-[Ru(C=CHC$_6$H$_4$-4-NO$_2$)Cl(dppm)$_2$]PF$_6$	470	721	127	thf	1.064	48
trans-[Ru(C=CHC$_6$H$_4$-4-C≡CC$_6$H$_4$-4-NO$_2$)Cl(dppm)$_2$]PF$_6$	326	424	122	thf	1.064	48
trans-[Ru(C=CHC$_6$H$_4$-4-(*E*)-CH=CHC$_6$H$_4$-4-NO$_2$)Cl(dppm)$_2$]PF$_6$	369	1899	314	thf	1.064	48
trans-[Ru(C=CHC$_6$H$_4$-4-CHO)Cl(dppe)$_2$]PF$_6$	412	181	61	thf	1.064	48
trans-[Ru(C=CHC$_6$H$_4$-4-NO$_2$)Cl(dppe)$_2$]PF$_6$	470	1130	180	thf	1.064	48
trans-[Ru(C=CHC$_6$H$_4$-4-(*E*)-CH=CHC$_6$H$_4$-4-NO$_2$)Cl(dppm)$_2$]PF$_6$	473	441	74	thf	1.064	48
[Ru(C=CHC$_6$H$_4$-4-NO$_2$)(PPh$_3$)$_2$(η^5-indenyl)]PF$_6$	379	116	50	CH_2Cl_2	1.064	42,46,47
[1,3,5-(*trans*-[RuCl(dppm)$_2${C=CHC$_6$H$_4$-(*E*)-4-CH=CH}])$_3$C$_6$H$_3$](PF$_6$)$_3$	396	165 ± 33	36 ± 7	thf	1.064	54
	396	101 ± 62[c]	22 ± 14	thf	1.064	54
	396	483 ± 100	4 ± 1	thf	0.800	54
	396	298 ± 62[c]	2 ± 1	thf	0.800	54
[Ru(C=CPhN=NPh)(PPh$_3$)$_2$(η^5-C$_5$H$_5$)]BF$_4$	363	14	6.6	acetone	1.064	63

Table 1.4. (continued) Molecular Quadratic NLO Measurements of Vinylidene Complexes[a]

Complex	λ_{max} (nm)	β^b (10^{-30} esu)	$\beta_0{}^b$ (10^{-30} esu)	Solvent	Fund. (μm)	Ref.
$[Ru(C{=}CPhN{=}NC_6H_4\text{-}2\text{-}OMe)(PPh_3)_2(\eta^5\text{-}C_5H_5)]Cl$	373	22	10	acetone	1.064	63
$[Ru(C{=}CPhN{=}NC_6H_4\text{-}3\text{-}OMe)(PPh_3)_2(\eta^5\text{-}C_5H_5)]BF_4$	382	23	10	acetone	1.064	63
$[Ru(C{=}CPhN{=}NC_6H_4\text{-}4\text{-}OMe)(PPh_3)_2(\eta^5\text{-}C_5H_5)]Cl$	370	26	12	acetone	1.064	63
$[Ru(C{=}CPhN{=}NC_6H_4\text{-}4\text{-}NO_2)(PPh_3)_2(\eta^5\text{-}C_5H_5)]BF_4$	413	184	62	CH_2Cl_2	1.064	63
$[Ru(C{=}CPhN{=}NC_6H_4\text{-}4\text{-}NO_2)(PPh_3)_2(\eta^5\text{-}C_5H_5)]Cl$	413	137	46	CH_2Cl_2	1.064	63
$[Ru(C{=}CPhN{=}NC_6H_4\text{-}4\text{-}NO_2)(PPh_3)_2(\eta^5\text{-}C_5H_5)]Br$	413	136	45	CH_2Cl_2	1.064	63
$[Ru(C{=}CPhN{=}NC_6H_4\text{-}4\text{-}NO_2)(PPh_3)_2(\eta^5\text{-}C_5H_5)]I$	417	150	48	acetone	1.064	63
	415	101	33	thf	1.064	63
	413	134	45	CH_2Cl_2	1.064	63
$[Ru(C{=}CPhN{=}NC_6H_4\text{-}4\text{-}NO_2)(PPh_3)_2(\eta^5\text{-}C_5H_5)](4\text{-}MeC_6H_4SO_3)$	413	164	55	CH_2Cl_2	1.064	63
$[Ru(C{=}CPhN{=}NC_6H_4\text{-}4\text{-}NO_2)(PPh_3)_2(\eta^5\text{-}C_5H_5)]NO_3$	413	181	61	CH_2Cl_2	1.064	63

[a] HRS.

[b] ± 10% unless otherwise stated

[c] $\sqrt{(\beta^2)}$

1.4.5. *Kurtz Powder Measurements*

The SHG efficiencies of more than forty acetylide or vinylidene complexes have been assessed using the Kurtz powder method, the results being listed in Table 1.5. and the structural formulas of the more efficient compounds being shown in Figure 1.9.

In general, the bulk second-order data for vinylidene and acetylide complexes are disappointingly modest in comparison with literature-extant data for ferrocenyl complexes, for example, despite the fact that molecular quadratic nonlinearities for the more efficient acetylide complexes are significantly larger than those for the more efficient ferrocenyl complexes. The majority of the gold acetylide complexes to have been examined by the Kurtz technique decomposed. Strategies to engineer sizable $\chi^{(2)}$ values have been developed. For example, Marder and co-workers have shown that variation of counterions is a highly successful and very straightforward method to rapidly sample different lattice arrangements and thereby obtain materials with large nonlinearities.[64] This idea was utilized with the vinylidene complex cations, and proved its utility, but data for these salts of varying anion are uniformly low.[65] This strategy is not applicable to neutral complexes, although alternative procedures for organizing favourable lattice alignment have been developed, namely formation of guest-host inclusion complexes, and incorporation of chiral ligands. The former idea has not been pursued with vinylidene or acetylide complexes. The latter approach has been utilized using diph [1,2-bis(methylphenylphosphino)benzene] as the chiral ligand. For a variation in group 8 metal across the series *trans*-[M(C≡CC_6H_4-4-NO_2)Cl{(*R*,*R*)-diph}$_2$], the iron-containing complex has the largest Kurtz powder SHG efficiency, but its molecular nonlinearity is the lowest of the three complexes,[55] emphasizing the fact that the usefulness of the Kurtz technique is to rapidly identify SHG activity; structure-NLO property correlations are not justified. The most SHG-efficient acetylide or vinylidene complex, [Ni(C≡C-2-C_5H_3N-5-NO_2)(PPh_3)(η^5-C_5H_5)], was shown to have a non-centrosymmetric crystal lattice, in a complementary X-ray diffraction study,[40] but the acetylide chromophores were not aligned favorably. Crystal engineering to convert large molecular nonlinearities into significant bulk nonlinearities remains a major challenge.

Table 1.5. Kurtz Powder Measurements of Acetylide or Vinylidene Complexes

Complex	SHG	Ref.
$(-)_{436}$-*trans*-[Fe(C≡CC_6H_4-4-NO_2)Cl{(*R*,*R*)-diph}$_2$]	~2	55
$(-)_{589}$-*trans*-[Ru(C≡CC_6H_4-4-NO_2)Cl{(*R*,*R*)-diph}$_2$]	None Detected	55
$(-)_{365}$-*trans*-[Os(C≡CC_6H_4-4-NO_2)Cl{(*R*,*R*)-diph}$_2$]	<<1	55
[Ru(C≡C-2-C_5H_3N)$(PPh_3)_2(\eta^5$-$C_5H_5)$]	<<1	40
[Ru(C≡C-2-C_5H_3N-5-NO_2)$(PPh_3)_2(\eta^5$-$C_5H_5)$]	<<1	40
[Ni(C≡C-2-C_5H_3N)$(PPh_3)(\eta^5$-$C_5H_5)$]	<<1	40
[Ni(C≡C-2-C_5H_3N-5-NO_2)$(PPh_3)(\eta^5$-$C_5H_5)$]	8	40
[Au(C≡C-2-C_5H_3N-5-NO_2)(PPh_3)]	<<1	40
[Au(C≡C-2-C_5H_3N-5-NO_2)(PMe_3)]	<<1	40
[Au(C≡CPh)(nmdpp)]	0	66
[Au(C≡CC_6H_4-4-NO_2)(nmdpp)]	2	66
[Au(C≡CC_6H_4-4-C_6H_4-4-NO_2)(nmdpp)]	<1, fluoresced, decomposed	66
[Au(C≡CC_6H_4-(*E*)-4-CH=CHC_6H_4-4-NO_2)(nmdpp)]	<1, fluoresced, decomposed	66
[Au(C≡CC_6H_4-(*Z*)-4-CH=CHC_6H_4-4-NO_2)(nmdpp)]	<1, fluoresced, decomposed	66
[Au(C≡CC_6H_4-4-C≡CC_6H_4-4-NO_2)(nmdpp)]	<1, fluoresced, decomposed	66
[Au(C≡CC_6H_4-4-N=CHC_6H_4-4-NO_2)(nmdpp)]	<1, fluoresced, decomposed	66
[Au(C≡CPh)(PPh_3)]	0	66
[Au(C≡CC_6H_4-4-NO_2)(PPh_3)]	0	66
[Au(C≡CC_6H_4-4-C_6H_4-4-NO_2)(PPh_3)]	fluoresced, decomposed	66
[Au(C≡CC_6H_4-(*E*)-4-CH=CHC_6H_4-4-NO_2)(PPh_3)]	fluoresced, decomposed	66
[Au(C≡CC_6H_4-(*Z*)-4-CH=CHC_6H_4-4-NO_2)(PPh_3)]	fluoresced, decomposed	66
[Au(C≡CC_6H_4-4-C≡CC_6H_4-4-NO_2)(PPh_3)]	fluoresced, decomposed	66
[Au(C≡CC_6H_4-4-N=CHC_6H_4-4-NO_2)(PPh_3)]	fluoresced, decomposed	66

Table 1.5. (continued) Kurtz Powder Measurements of Acetylide or Vinylidene Complexes		
Complex	SHG	Ref.
$[Ru(C{=}CPhN{=}NPh)(PPh_3)_2(\eta^5\text{-}C_5H_5)]BF_4$	0.48	65
$[Ru(C{=}CPhN{=}NPh)(PPh_3)_2(\eta^5\text{-}C_5H_5)](4\text{-}MeC_6H_4SO_3)$	0.50	65
$[Ru(C{=}CPhN{=}NPh)(PPh_3)_2(\eta^5\text{-}C_5H_5)]NO_3$	0.57	65
$[Ru(C{=}CPhN{=}NPh)(PPh_3)_2(\eta^5\text{-}C_5H_5)]Cl$	0.50	65
$[Ru(C{=}CPhN{=}NPh)(PPh_3)_2(\eta^5\text{-}C_5H_5)]I$	0.53	65
$[Ru(C{=}CPhN{=}NC_6H_4\text{-}4\text{-}OMe)(PPh_3)_2(\eta^5\text{-}C_5H_5)]BF_4$	1.05	65
$[Ru(C{=}CPhN{=}NC_6H_4\text{-}4\text{-}OMe)(PPh_3)_2(\eta^5\text{-}C_5H_5)](4\text{-}MeC_6H_4SO_3)$	<0.05	65
$[Ru(C{=}CPhN{=}NC_6H_4\text{-}4\text{-}OMe)(PPh_3)_2(\eta^5\text{-}C_5H_5)]NO_3$	<0.05	65
$[Ru(C{=}CPhN{=}NC_6H_4\text{-}4\text{-}OMe)(PPh_3)_2(\eta^5\text{-}C_5H_5)]Cl$	<0.05	65
$[Ru(C{=}CPhN{=}NC_6H_4\text{-}4\text{-}OMe)(PPh_3)_2(\eta^5\text{-}C_5H_5)]I$	<0.05	65
$[Ru(C{=}CPhN{=}NC_6H_4\text{-}2\text{-}OMe)(PPh_3)_2(\eta^5\text{-}C_5H_5)]BF_4$	0.63	65
$[Ru(C{=}CPhN{=}NC_6H_4\text{-}2\text{-}OMe)(PPh_3)_2(\eta^5\text{-}C_5H_5)](4\text{-}MeC_6H_4SO_3)$	<0.05	65
$[Ru(C{=}CPhN{=}NC_6H_4\text{-}2\text{-}OMe)(PPh_3)_2(\eta^5\text{-}C_5H_5)]NO_3$	<0.05	65
$[Ru(C{=}CPhN{=}NC_6H_4\text{-}2\text{-}OMe)(PPh_3)_2(\eta^5\text{-}C_5H_5)]Cl$	<0.05	65
$[Ru(C{=}CPhN{=}NC_6H_4\text{-}2\text{-}OMe)(PPh_3)_2(\eta^5\text{-}C_5H_5)]I$	<0.05	65
$[Ru(C{=}CPhN{=}NC_6H_4\text{-}4\text{-}NO_2)(PPh_3)_2(\eta^5\text{-}C_5H_5)]BF_4$	<0.05	65
$[Ru(C{=}CPhN{=}NC_6H_4\text{-}4\text{-}NO_2)(PPh_3)_2(\eta^5\text{-}C_5H_5)](4\text{-}MeC_6H_4SO_3)$	<0.05	65
$[Ru(C{=}CPhN{=}NC_6H_4\text{-}4\text{-}NO_2)(PPh_3)_2(\eta^5\text{-}C_5H_5)]NO_3$	<0.05	65
$[Ru(C{=}CPhN{=}NC_6H_4\text{-}4\text{-}NO_2)(PPh_3)_2(\eta^5\text{-}C_5H_5)]Cl$	<0.05	65
$[Ru(C{=}CPhN{=}NC_6H_4\text{-}4\text{-}NO_2)(PPh_3)_2(\eta^5\text{-}C_5H_5)]I$	<0.05	65
$[Ru(C{=}CPhN{=}NC_6H_4\text{-}3,5\text{-}(NO_2)_2)(PPh_3)_2(\eta^5\text{-}C_5H_5)]BF_4$	<0.05	65
$[Ru(C{=}CPhN{=}NC_6H_4\text{-}3,5\text{-}(NO_2)_2)(PPh_3)_2(\eta^5\text{-}C_5H_5)](4\text{-}MeC_6H_4SO_3)$	<0.05	65
$[Ru(C{=}CPhN{=}NC_6H_4\text{-}3,5\text{-}(NO_2)_2)(PPh_3)_2(\eta^5\text{-}C_5H_5)]NO_3$	<0.05	65
$[Ru(C{=}CPhN{=}NC_6H_4\text{-}3,5\text{-}(NO_2)_2)(PPh_3)_2(\eta^5\text{-}C_5H_5)]Cl$	<0.05	65
$[Ru(C{=}CPhN{=}NC_6H_4\text{-}3,5\text{-}(NO_2)_2)(PPh_3)_2(\eta^5\text{-}C_5H_5)]I$	<0.05	65

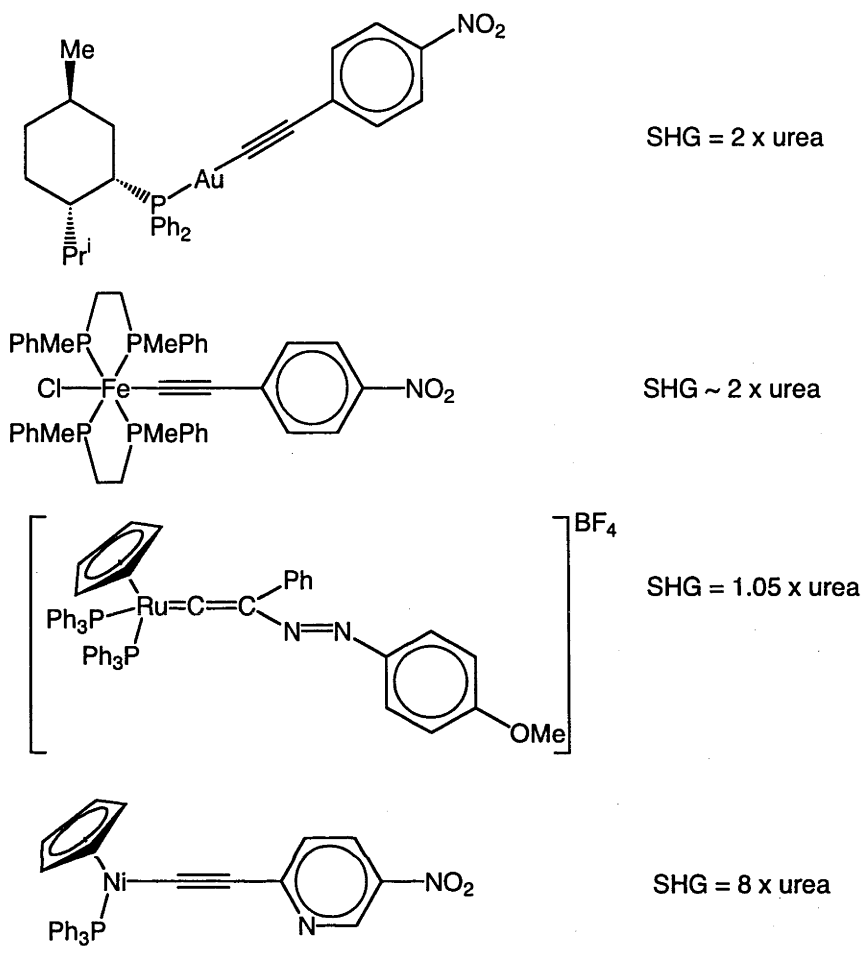

Figure 1.9. Acetylide or vinylidene complexes with the largest $\chi^{(2)}$ values measured by the Kurtz powder technique

1.4.6. *ZINDO–derived Computational Results*

Table 1.6. contains data for computationally-derived second-order nonlinearities, obtained using ZINDO. Although ZINDO has been unsuccessful in reproducing absolute values of nonlinearities for acetylide complexes, a not-unexpected result when comparing resonance-enhanced solution-phase measurements in dipolar solvents with computationally-derived gas phase measurements far from resonance, it generally reproduces experimental trends. For example, for the acetylide complexes studied thus far, incorporation of a strong acceptor group and acetylide ligand chain lengthening both serve to increase nonlinearity, as expected.[67,68] The greatest utility of computational methods is in probing the effect of structural modifications that are not easy to accomplish experimentally. For example, Figures 1.10. and 1.11. show the effect of Ru-C bond length variation and acetylide phenyl ring rotation upon ZINDO–derived β_{vec} values for [Ru(C≡C C_6H_4-4-NO_2)(PMe_3)$_2$(η^5-C_5H_5)], the calculations suggesting that one should minimize the Ru-C distance in order to maximize β_{vec}, and that the orientation of the phenylacetylide ligand with respect to the metal center is not an important concern for optimizing β_{vec} – the latter is a key result given difficulties in controlling ligand orientation in the crystal lattice.[67]

Table 1.6. Computationally-Derived Optical Nonlinearities by ZINDO for Acetylide Complexes[a]

Complex	β_{vec} (10^{-30} esu)	Reference
[Ru(C≡CPh)(PPh_3)$_2$(η^5-C_5H_5)]	2	67
[Ru(C≡CPh)(PMe_3)$_2$(η^5-C_5H_5)]	5	67
[Ru(C≡CC_6H_4-4-NO_2)(PPh_3)$_2$(η^5-C_5H_5)]	29	67
[Ru(C≡CC_6H_4-4-NO_2)(PMe_3)$_2$(η^5-C_5H_5)]	31	67
trans-[Ru(C≡CPh)Cl(dppm)$_2$]	-13	68
trans-[Ru(C≡CC_6H_4-4-NO_2)Cl(dppm)$_2$]	34	68
trans-[Ru(C≡CC_6H_4-4-C_6H_4-4-NO_2)Cl(dppm)$_2$]	45	68
trans-[Ru(C≡CC_6H_4-(*E*)-4-CH=CHC_6H_4-4-NO_2)Cl(dppm)$_2$]	60	68
trans-[Ru(C≡CC_6H_4-4-NO_2)$_2$(dppm)$_2$]	0	69
trans-[Ru(C≡CPh)(C≡CC_6H_4-4-NO_2)(dppm)$_2$]	32	69

[a] 1.91 μm

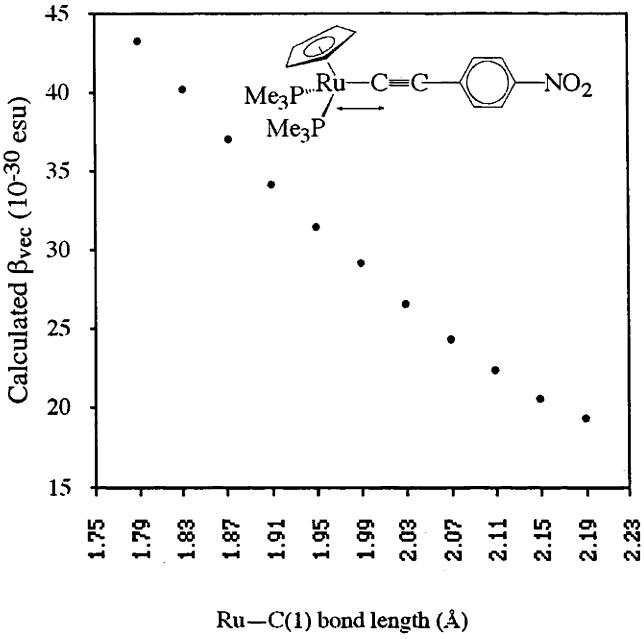

Figure 1.10. The effect of varying Ru–C bond length on ZINDO-derived quadratic nonlinearity for $[Ru(C{\equiv}CC_6H_4\text{-}4\text{-}NO_2)(PMe_3)_2(\eta^5\text{-}C_5H_5)]$[67]

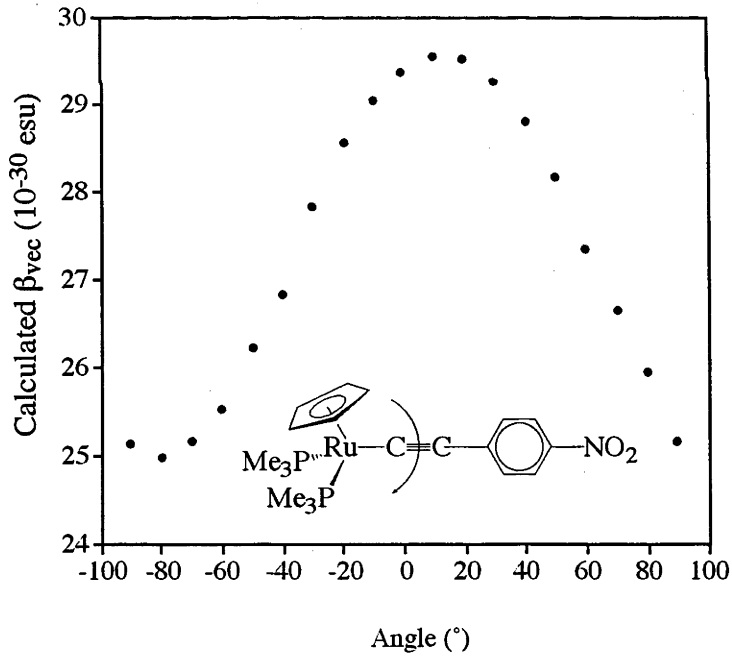

Figure 1.11. The effect of nitrophenylacetylide ligand rotation on ZINDO-derived quadratic nonlinearity for $[Ru(C{\equiv}CC_6H_4\text{-}4\text{-}NO_2)(PMe_3)_2(\eta^5\text{-}C_5H_5)]$[67]

1.5. *Third-Order Nonlinearities*

1.5.1. *Group 4 Acetylide Complexes*

The cubic nonlinearities of a series of group 4 metallocene acetylide complexes have been assessed by THG at 1.91 μm, results being displayed in Table 1.7. Although absolute values are low, some interesting trends in the data can be seen. Increasing nonlinearity is observed on replacing chloride by an acetylide ligand, butyl by phenyl substituent (acetylide variation), and in proceeding up the group upon metal replacement. The last-mentioned result was ascribed to two factors: the involvement of ligand-to-metal charge-transfer transition for these complexes, and increasing electron accepting ability of the metal.[70]

Table 1.7. Molecular Cubic NLO Measurements of Group 4 Acetylide Complexes[a]

Complex	λ (nm)	γ (10^{-36} esu)	Ref.
$[Ti(C{\equiv}CBu^n)_2(\eta^5\text{-}C_5H_4Me)_2]$	b	15 ± 2	71
$[Ti(C{\equiv}CBu^n)_2(\eta^5\text{-}C_5H_5)_2]$	390	12 ± 2	72
$[Ti(C{\equiv}CPh)_2(\eta^5\text{-}C_5H_5)_2]$	416	92 ± 14	70,72
$[Zr(C{\equiv}CPh)_2(\eta^5\text{-}C_5H_5)_2]$	390	58 ± 9	70,72
$[Hf(C{\equiv}CPh)_2(\eta^5\text{-}C_5H_5)_2]$	390	51 ± 8	70,72
$[Ti(C{\equiv}CPh)Cl(\eta^5\text{-}C_5H_5)_2]$	510	31 ± 5	70,72

[a] THG, 1.91 μm

[b] not reported

1.5.2. *Group 8 Acetylide Complexes*

The third-order NLO properties of group 8 acetylide complexes have been intensively examined; the studies were carried out at 800 nm, are exclusively on ruthenium acetylide compounds and all bar one by Z-scan at 0.80 μm, results are collected in Table 1.8., while

structural formulas of some of the more efficient examples are displayed in Figure 1.12. One complex, $[Ru(C{\equiv}CC_6H_4\text{-}4\text{-}NO_2)(PPh_3)_2(\eta^5\text{-}C_5H_5)]$, has been examined by both Z-scan and DFWM; the latter study revealed an equivalent γ value (within the error margins) to the Z-scan-derived response, and confirmed an electronic origin for cubic NLO response in this molecule.[73]

While less is known of molecular structure-NLO activity relationships for third-order properties than for second-order properties, it has been established with organic compounds that increase in π-delocalization possibilities (e.g. progressing from small molecules to π-conjugated polymers), the introduction of strong donor and acceptor functional groups, controlling chain orientation, packing density, and conformation, and increasing dimensionality can all result in increased cubic nonlinearity. Where applicable, similar trends are seen with the ruthenium acetylide complexes, although in many instances error margins are large (note that many of the small donor-acceptor acetylide complexes were designed for optimizing second-order rather than third-order NLO response). Negative real components of the nonlinearities (γ_{real}) are observed in many instances and significant imaginary components (γ_{imag}) are seen for almost all complexes, consistent with two-photon effects contributing to the observed molecular nonlinearities. Two-photon absorption (TPA) is a third-order NLO property that is of interest for applications in multiphoton microscopy, optical limiting, and optical data storage, and for which structure-activity trends are identical with those for γ_{imag}. Cubic nonlinearities for these acetylide complexes increase significantly on progression from monometallic linear ("one-dimensional") complex to bimetallic linear complex, trimetallic octupolar ("two-dimensional") complex,[53,54] and nonametallic dendritic complex[74] without significant loss of optical transparency. For these complexes, TPA similarly increases substantially on progression to larger π-delocalizable compounds, TPA cross-sections for the dendritic examples being of the same order of magnitude as the best organic compounds.

Table 1.8. Molecular Cubic NLO Measurements of Group 8 Acetylide Complexes

Complex	λ_{max} (nm)	γ_{real} (10^{-36} esu)	γ_{imag} (10^{-36} esu)	γ (10^{-36} esu)	Technique	Solvent	Fund. (μm)	Ref.
$[Ru(C{\equiv}CPh)(PPh_3)_2(\eta^5\text{-}C_5H_5)]$	311	≤ 150		≤ 150	Z-scan	thf	0.80	73
$[Ru(C{\equiv}CC_6H_4\text{-}4\text{-}Br)(PPh_3)_2(\eta^5\text{-}C_5H_5)]$	325	≤ 150		≤ 150	Z-scan	thf	0.80	73
$[Ru(C{\equiv}CC_6H_4\text{-}4\text{-}NO_2)(PPh_3)_2(\eta^5\text{-}C_5H_5)]$	461	-210 ± 50	≤ 10	-210 ± 50	Z-scan	thf	0.80	73
	461	-260 ± 60		-260 ± 60	DFWM	thf	0.80	73
$[Ru(C{\equiv}CC_6H_4\text{-}4\text{-}NO_2)(PMe_3)_2(\eta^5\text{-}C_5H_5)]$	480	-230 ± 70	74 ± 30	240 ± 76	Z-scan	thf	0.80	73
$[Ru(C{\equiv}CC_6H_4\text{-}4\text{-}C_6H_4\text{-}4\text{-}NO_2)(PPh_3)_2(\eta^5\text{-}C_5H_5)]$	448	-380 ± 200	320 ± 160	500 ± 260	Z-scan	thf	0.80	73
$[Ru(C{\equiv}CC_6H_4\text{-}4\text{-}(E)\text{-}CH{=}CHC_6H_4\text{-}4\text{-}NO_2)(PPh_3)_2(\eta^5\text{-}C_5H_5)]$	476	-450 ± 100	210 ± 100	500 ± 140	Z-scan	thf	0.80	73
$[Ru(C{\equiv}CC_6H_4\text{-}4\text{-}C{\equiv}CC_6H_4\text{-}4\text{-}NO_2)(PPh_3)_2(\eta^5\text{-}C_5H_5)]$	447	-450 ± 100	≤ 20	-450 ± 100	Z-scan	thf	0.80	73
$[Ru(C{\equiv}CC_6H_4\text{-}4\text{-}N{=}CHC_6H_4\text{-}4\text{-}NO_2)(PPh_3)_2(\eta^5\text{-}C_5H_5)]$	496	-850 ± 300	360 ± 200	920 ± 360	Z-scan	thf	0.80	56
trans-$[Ru(C{\equiv}CC_6H_4\text{-}4\text{-}NO_2)Cl(dppm)_2]$	466	170 ± 34	230 ± 46	290 ± 57	Z-scan	CH_2Cl_2	0.80	75
trans-$[Ru(C{\equiv}CC_6H_4\text{-}4\text{-}C_6H_4\text{-}4\text{-}NO_2)Cl(dppm)_2]$	448	140 ± 28	64 ± 13	150 ± 31	Z-scan	CH_2Cl_2	0.80	75
trans-$[Ru(C{\equiv}CC_6H_4\text{-}4\text{-}(E)\text{-}CH{=}CHC_6H_4\text{-}4\text{-}NO_2)Cl(dppm)_2]$	471	200 ± 40	1100 ± 220	1100 ± 220	Z-scan	CH_2Cl_2	0.80	75
trans-$[Ru(C{\equiv}CC_6H_4\text{-}4\text{-}NO_2)_2(dppm)_2]$	474	300 ± 60	490 ± 98	570 ± 110	Z-scan	CH_2Cl_2	0.80	75
trans-$[Ru(C{\equiv}CC_6H_4\text{-}4\text{-}C_6H_4\text{-}4\text{-}NO_2)_2(dppm)_2]$	453	≤ 800	2500 ± 500	2500 ± 500	Z-scan	CH_2Cl_2	0.80	75
trans-$[Ru(C{\equiv}CC_6H_4\text{-}4\text{-}(E)\text{-}CH{=}CHC_6H_4\text{-}4\text{-}NO_2)_2(dppm)_2]$	367	≤ 1100	3400 ± 680	3400 ± 680	Z-scan	CH_2Cl_2	0.80	75

Table 1.8. (continued) Molecular Cubic NLO Measurements of Group 8 Acetylide Complexes

Complex	λ_{max} (nm)	γ_{real} (10^{-36} esu)	γ_{imag} (10^{-36} esu)	γ (10^{-36} esu)	Technique	Solvent	Fund. (μm)	Ref.
1,3,5-{*trans*-[RuCl(dppe)$_2$(C≡CC$_6$H$_4$-4-C≡C)}$_3$C$_6$H$_3$	414	-330 ± 100	2200 ± 500	2200 ± 600	Z-scan	thf	0.80	53
1,3,5-{*trans*-[Ru(C≡CPh)(dppe)$_2$(C≡CC$_6$H$_4$-4-C≡C)}$_3$C$_6$H$_3$	411	-600 ± 200	2900 ± 500	3000 ± 600	Z-scan	thf	0.80	53
1-(Me$_3$SiC≡C)-C$_6$H$_3$-3,5-{C≡CC$_6$H$_4$-4-C≡C-*trans*-[RuCl(dppe)$_2$]}$_2$	411	-510 ± 500	4700 ± 1500	4700 ± 2000	Z-scan	thf	0.80	74
1-(Me$_3$SiC≡C)-C$_6$H$_3$-3,5-{C≡CC$_6$H$_4$-4-C≡C-*trans*-[Ru(C≡CPh)(dppe)$_2$]}$_2$	407	-700 ± 100	2270 ± 300	2400 ± 300	Z-scan	thf	0.80	74
1-(HC≡C)-C$_6$H$_3$-3,5-{C≡CC$_6$H$_4$-4-C≡C-*trans*-[Ru(C≡CPh)(dppe)$_2$]}$_2$	408	-830 ± 100	2200 ± 300	2400 ± 300	Z-scan	thf	0.80	74
1,3,5-C$_6$H$_3$-(C≡CC$_6$H$_4$-4-C≡C-*trans*-[Ru(dppe)$_2$]C≡C-3,5-C$_6$H$_3$-{C≡CC$_6$H$_4$-4-C≡C-*trans*-[Ru(C≡CPh)(dppe)$_2$]$_2$}$_3$	402	-5050 ± 500	20 100 ± 2000	20 700 ± 2000	Z-scan	thf	0.80	74
trans-[Ru(C≡CPh)(C≡CC$_6$H$_4$-4-C≡CPh)(dppe)$_2$]	383	-670 ± 300	1300 ± 300	1500 ± 500	Z-scan	CH_2Cl_2	0.80	53
trans-[Ru(C≡CPh)Cl(dppe)$_2$]	319	-170 ± 40	71 ± 20	200 ± 50	Z-scan	CH_2Cl_2	0.80	53
trans-[Ru{C≡CC$_6$H$_4$-(*E*)-4-CH=CHPh}Cl(dppm)$_2$]	397	-600 ± 400	700 ± 400	920 ± 600	Z-scan	thf	0.80	54,76
trans-[Ru{C≡CC$_6$H$_4$-(*E*)-4-CH=CHPh}Cl(dppe)$_2$]	404	300 ± 400	300 ± 100	420 ± 350	Z-scan	thf	0.80	54,76
1,3,5-(*trans*-[RuCl(dppm)$_2${4-C≡CC$_6$H$_4$-(*E*)-4-CH=CH}])$_3$C$_6$H$_3$	415	-640 ± 500	2000 ± 500	2100 ± 600	Z-scan	thf	0.80	54,76
1,3,5-(*trans*-[RuCl(dppe)$_2${C≡CC$_6$H$_4$-(*E*)-4-CH=CH}])$_3$C$_6$H$_3$	426	-4600 ± 2000	4200 ± 800	6200 ± 2000	Z-scan	thf	0.80	54,76

Table 1.8. (continued) Molecular Cubic NLO Measurements of Group 8 Acetylide Complexes

Complex	λ_{max} (nm)	γ_{real} (10^{-36} esu)	γ_{imag} (10^{-36} esu)	γ (10^{-36} esu)	Technique	Solvent	Fund. (μm)	Ref.
1,3,5-(*trans*-[Ru(C≡CPh)(dppe)$_2${C≡CC$_6$H$_4$-(*E*)-4-CH=CH}])$_3$C$_6$H$_3$	421	-11 200 ± 3000	8600 ± 2000	14 000 ± 4000	Z-scan	thf	0.80	54,76
[Fe{η^5-C$_5$H$_4$-(*E*)-CH=CHC$_6$H$_4$-4-C≡CRuCl(dppm)$_2$}$_2$]	396	-3000 ± 1200	2300 ± 800	3800 ± 1400	Z-scan	thf	0.80	77
[Fe{η^5-C$_5$H$_4$-(*E*)-CH=CHC$_6$H$_4$-4-C≡CRuCl(dppe)$_2$}$_2$]	388	-7100 ± 3000	10 600 ± 2000	13 000 ± 3000	Z-scan	thf	0.80	77
trans,*trans*-[RuCl(dppm)$_2$(-μ-C≡CC$_6$H$_4$-4-C≡C)RuCl(dppm)$_2$]	354	-3200 ± 500	1400 ± 300	3500 ± 600	Z-scan	thf	0.80	62
trans,*trans*-[RuCl(dppm)$_2$(-μ-C≡CC$_6$H$_4$-4-C$_6$H$_4$-4-C≡C)RuCl(dppm)$_2$]	360	-1100 ± 300	300 ± 60	1100 ± 300	Z-scan	thf	0.80	62
trans,*trans*-[Ru(C≡CPh)(dppe)$_2$(-μ-C≡CC$_6$H$_4$-4-C≡CC≡CC$_6$H$_4$-4-C≡C)Ru(C≡CPh)(dppe)$_2$]	438	-4000 ± 1500	12 000 ± 2000	13 000 ± 2400	Z-scan	thf	0.80	62
trans-[Ru(C≡CPh)Cl(dppm)$_2$]	308	<120	0	<120	Z-scan	thf	0.80	48
trans-[Ru(C≡CC$_6$H$_4$-4-C≡CPh)Cl(dppm)$_2$]	381	65 ± 40	520 ± 200	520 ± 200	Z-scan	thf	0.80	48
trans-[Ru(C≡CC$_6$H$_4$-4-CHO)Cl(dppm)$_2$]	405	<120	210 ± 60	210 ± 60	Z-scan	thf	0.80	48
trans-[Ru(C≡CC$_6$H$_4$-4-C≡CC$_6$H$_4$-4-NO$_2$)Cl(dppm)$_2$]	464	-160 ± 80	160 ± 60	230 ± 100	Z-scan	thf	0.80	48
trans-[Ru(C≡CC$_6$H$_4$-4-C≡CC$_6$H$_4$-4-C≡CC$_6$H$_4$-4-NO$_2$)Cl(dppm)$_2$]	439	-920 ± 200	970 ± 200	1300 ± 300	Z-scan	thf	0.80	48
trans-[Ru(C≡CC$_6$H$_4$-4-CHO)Cl(dppe)$_2$]	413	-300 ± 500	<200	-300 ± 500	Z-scan	thf	0.80	48
trans-[Ru(C≡CC$_6$H$_4$-4-NO$_2$)Cl(dppe)$_2$]	477	-320 ± 55	<50	-320 ± 55	Z-scan	thf	0.80	48

Table 1.8. (continued) Molecular Cubic NLO Measurements of Group 8 Acetylide Complexes

Complex	λ_{max} (nm)	γ_{real} (10^{-36} esu)	γ_{imag} (10^{-36} esu)	γ (10^{-36} esu)	Technique	Solvent	Fund. (μm)	Ref.
trans-[Ru{C≡CC_6H_4-4-(*E*)-CH=CHC_6H_4-4-NO_2}Cl$(dppe)_2$]	489	40 ± 200	<100	40 ± 200	Z-scan	thf	0.80	48
[Ru(C≡CC_6H_4-4-CH{OC(O)Me}$_2$)$(PPh_3)_2(\eta^5$-$C_5H_5)$]	326	100 ± 100	0	100 ± 100	Z-scan	thf	0.80	49
[Ru(C≡CC_6H_4-4-CHO)$(PPh_3)_2(\eta^5$-$C_5H_5)$]	400	-75 ± 50	210 ± 50	220 ± 60	Z-scan	thf	0.80	49
trans-[Ru{C≡CC_6H_4-4-CHO$(CH_2)_3$O}Cl$(dppm)_2$]	320	50 ± 50	0	50 ± 50	Z-scan	thf	0.80	49
trans-[Ru(C≡CC_6H_4-3-CHO)Cl$(dppm)_2$]	321	150 ± 150	0	150 ± 150	Z-scan	thf	0.80	49

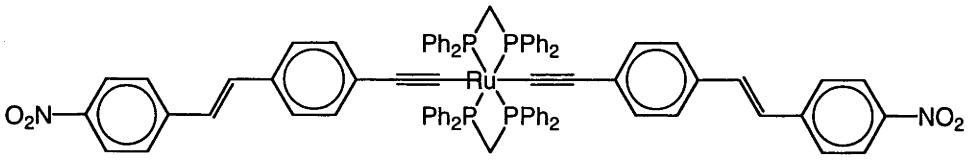

γ_{real} ≤ 1100 x 10^{-36} esu
γ_{imag} = 3400 ± 680 x 10^{-36} esu
$|\gamma|$ = 3400 ± 680 x 10^{-36} esu

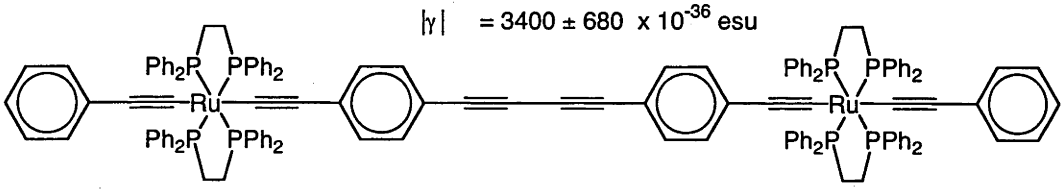

γ_{real} = -4000 ± 1500 x 10^{-36} esu
γ_{imag} = 12 000 ± 2000 x 10^{-36} esu
$|\gamma|$ = 13 000 ± 2400 x 10^{-36} esu

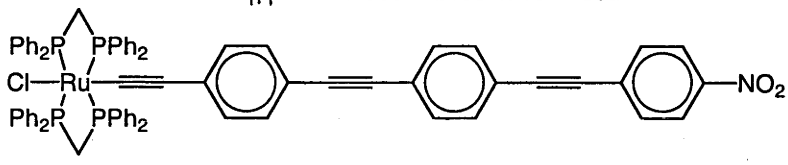

γ_{real} = -920 ± 200 x 10^{-36} esu
γ_{imag} = 970 ± 200 x 10^{-36} esu
$|\gamma|$ = 1300 ± 300 x 10^{-36} esu

Figure 1.12. Selected Group 8 acetylide complexes with large γ values.

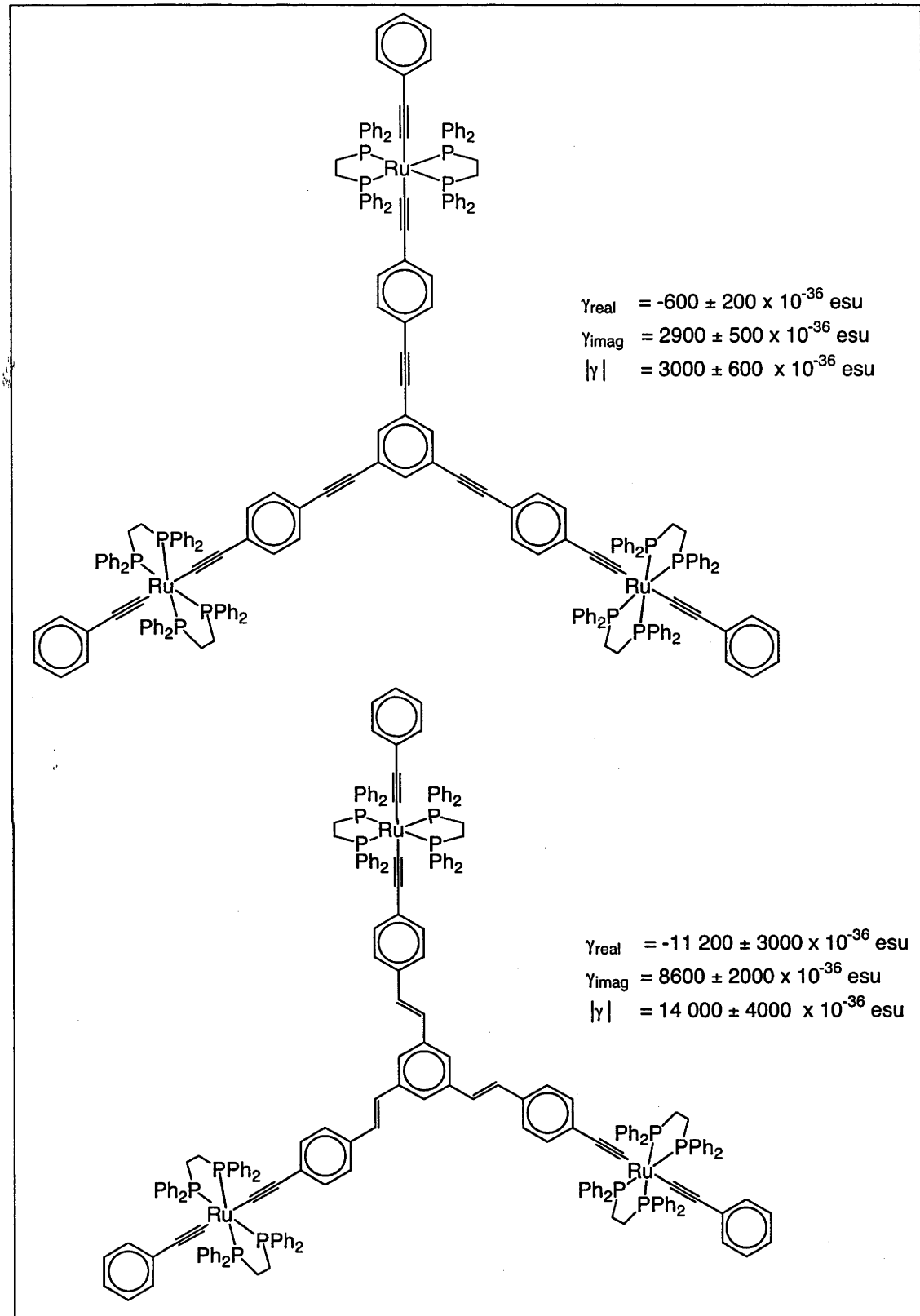

Figure 1.12. (continued). Group 8 acetylide complexes with large γ values

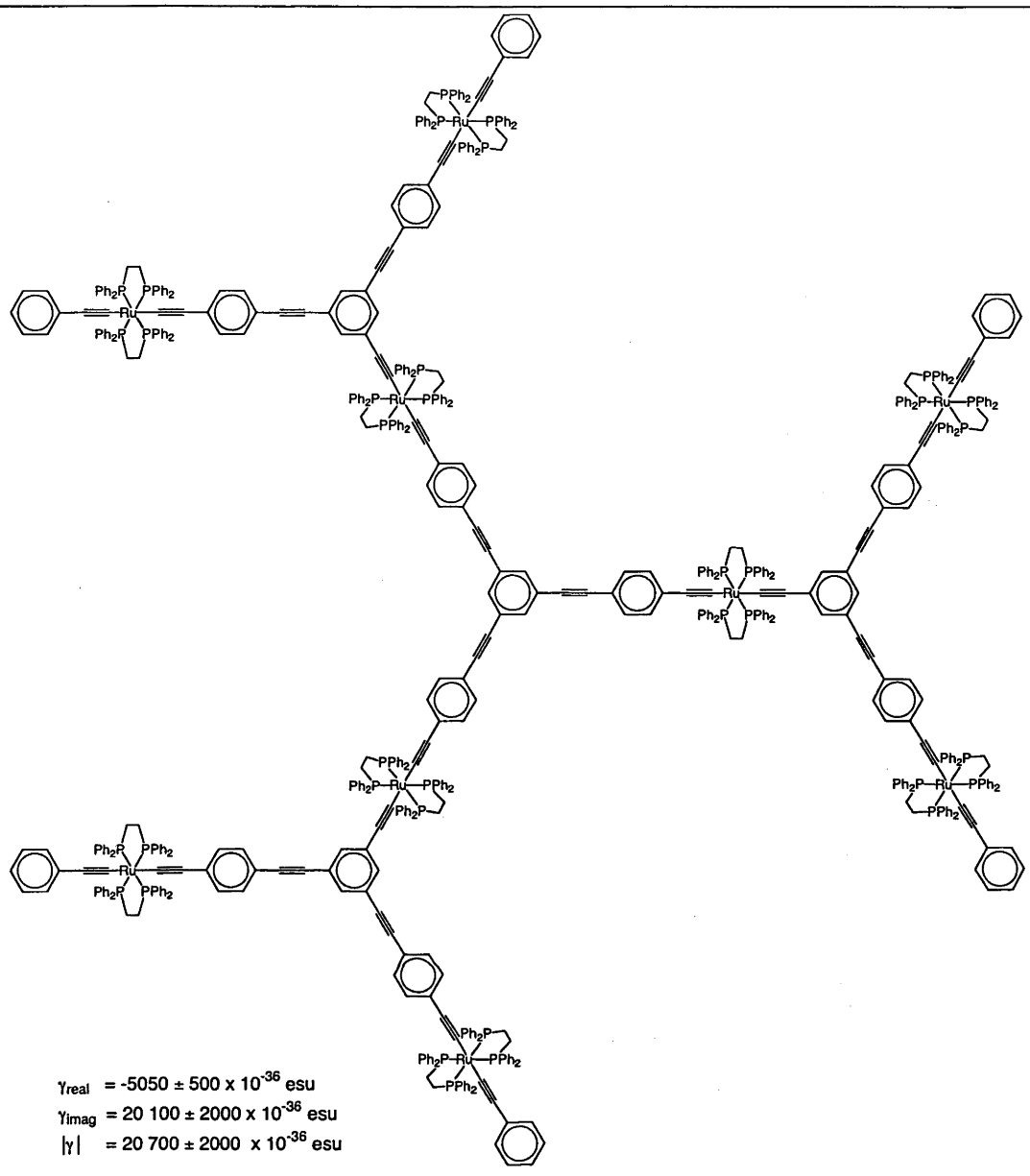

Figure 1.12. (continued). Group 8 acetylide complexes with large γ values

1.5.3 *Group 10 Acetylide Complexes*

The molecular cubic nonlinearities of group 10 acetylide complexes for which nonlinearities are reported in cgs units are listed in Table 1.9., structural formulas of some of the more efficient compounds being shown in Figure 1.13. (Cyclopentadienyl)(triphenylphosphine)nickel acetylide complexes were examined by Z-

scan at 0.80 μm, the negative γ_{real} and significant γ_{imag} data being suggestive of two-photon dispersion contributing to the observed responses; as noted with the related (cyclopentadienyl)bis(triphenylphosphine)ruthenium complexes, these two-photon states become important for an 800 nm irradiating wavelength when complexes contain λ_{max} > 400 nm.[60] The γ_{real} values for the nickel complexes are the same (within the error margins) as those of their ruthenium analogues, ease of oxidation and greater delocalization possibilities with the additional triphenylphosphine ligand making no significant difference to cubic NLO merit (in contrast to the situation with quadratic optical nonlinearities).

Cubic nonlinearities for palladium and platinum acetylides have been determined by four-wave mixing or optical Kerr gate techniques, with γ_{real} values uniformly small and γ_{imag} values significant – the data are similar in magnitude to the monoruthenium and nickel acetylide complexes discussed above.

Measurements made by DFWM on Group 10 bis(acetylide) complexes for which results have been reported in SI units are listed in Table 1.10. Although results cannot be directly compared to those mentioned earlier, internal comparisons within the series are valid. These reveal that hyperpolarizability decreases progressing down the group for phenylacetylide and butadiynide complexes. The complexes exhibit a high-order intensity dependence, characteristic of multiphoton resonant enhancement; for these complexes this is possibly due to three-photon resonant enhancement, as λ_{max} is, in all cases, close to 3ω.[80-82]

Table 1.9. Molecular Cubic NLO Results for Group 10 Acetylide Complexes

Complex	λ_{max} (nm)	γ_{real} (10^{-36} esu)	γ_{imag} (10^{-36} esu)	γ (10^{-36} esu)	Technique	Solvent	Fund. (μm)	Ref.
$[Ni(C{\equiv}CPh)(PPh_3)(\eta^5\text{-}C_5H_5)]$	307	15 ± 10	< 10	15 ± 10	Z-scan	thf	0.80	60
$[Ni(C{\equiv}CC_6H_4\text{-}4\text{-}NO_2)(PPh_3)(\eta^5\text{-}C_5H_5)]$	439	-270 ± 100	70 ± 50	280 ± 110	Z-scan	thf	0.80	60
$[Ni(C{\equiv}CC_6H_4\text{-}4\text{-}C_6H_4\text{-}4\text{-}NO_2)(PPh_3)(\eta^5\text{-}C_5H_5)]$	413	-580 ± 200	300 ± 60	650 ± 210	Z-scan	thf	0.80	60
$[Ni(C{\equiv}CC_6H_4\text{-}4\text{-}(E)\text{-}CH{=}CHC_6H_4\text{-}4\text{-}NO_2)(PPh_3)(\eta^5\text{-}C_5H_5)]$	437	-420 ± 100	480 ± 150	640 ± 180	Z-scan	thf	0.80	60
$[Ni(C{\equiv}CC_6H_4\text{-}4\text{-}(Z)\text{-}CH{=}CHC_6H_4\text{-}4\text{-}NO_2)(PPh_3)(\eta^5\text{-}C_5H_5)]$	417	-230 ± 50	160 ± 80	280 ± 94	Z-scan	thf	0.80	60
$[Ni(C{\equiv}CC_6H_4\text{-}4\text{-}C{\equiv}CC_6H_4\text{-}4\text{-}NO_2)(PPh_3)(\eta^5\text{-}C_5H_5)]$	417	-640 ± 300	720 ± 300	960 ± 420	Z-scan	thf	0.80	60
$[Ni(C{\equiv}CC_6H_4\text{-}4\text{-}N{=}CHC_6H_4\text{-}4\text{-}NO_2)(PPh_3)(\eta^5\text{-}C_5H_5)]$	448	< 120	360 ± 100	360 ± 100	Z-scan	thf	0.80	60
trans-$[Pd(C{\equiv}CPh)_2(PBu^n{}_3)_2]$	a			110[b]	FWM	a	0.63	78
cis,cis-$[PtCl(PBu^n{}_3)_2(\mu\text{-}C{\equiv}CC_6H_4\text{-}4\text{-}C{\equiv}C)PtCl(PBu^n{}_3)_2]$	a	11 ± 3	224 ± 56	224 ± 56	OKG/IDA[c]	thf	1.06/0.53	79
trans,trans-$[PtCl(PBu^n{}_3)_2(\mu\text{-}C{\equiv}CC_6H_4\text{-}4\text{-}C{\equiv}C)PtCl(PBu^n{}_3)_2]$	a	19 ± 5	827 ± 207	827 ± 207	OKG/IDA[c]	thf	1.06/0.53	79
trans,trans-$[PtCl(PBu^n{}_3)_2(\mu\text{-}C{\equiv}CC_6H_4\text{-}4\text{-}C{\equiv}C)Pt(PBu^n{}_3)_2(\mu\text{-}C{\equiv}CC_6H_4\text{-}4\text{-}C{\equiv}C)PtCl(PBu^n{}_3)_2]$	a	45 ± 11	1196 ± 299	1196 ± 299	OKG/IDA[c]	thf	1.06/0.53	79

Table 1.9. (continued) Molecular Cubic NLO Results for Group 10 Acetylide Complexes

Complex	λ_{max} (nm)	γ_{real} (10^{-36} esu)	γ_{imag} (10^{-36} esu)	γ (10^{-36} esu)	Technique	Solvent	Fund. (μm)	Ref.
trans,trans-[PtCl(PBu$^n_3$)$_2$(μ-C≡CC$_6$H$_4$-4-C≡CC≡CC$_6$H$_4$-4-C≡C)PtCl(PBu$^n_3$)$_2$]	[a]	88 ± 22	2167 ± 542	2167 ± 542	OKG/IDA[c]	thf	1.06/0.53	79
trans-[Pt(C≡CC$_6$H$_4$-4-C≡CH)$_2$(PBu$^n_3$)$_2$]	[a]	53 ± 13	759 ± 190	760 ± 190	OKG/IDA[c]	thf	1.06/0.53	79
trans,trans-[Pt(C≡CC$_6$H$_4$-4-C≡CH)(PBu$^n_3$)$_2$(μ-C≡CC$_6$H$_4$-4-C≡C)Pt(C≡CC$_6$H$_4$-4-C≡CH)(PBu$^n_3$)$_2$]	[a]	66 ± 17	1328 ± 332	1328 ± 332	OKG/IDA[c]	thf	1.06/0.53	79
trans,trans-[Pt(NCS)(PBu$^n_3$)$_2$(μ-C≡CC$_6$H$_4$-4-C≡C)Pt(NCS)(PBu$^n_3$)$_2$]	[a]	30 ± 8	1134 ± 284	1134 ± 284	OKG/IDA[c]	thf	1.06/0.53	79
trans,trans-[PtCl(PBu$^n_3$)$_2$(μ-C≡CC$_6$H$_4$-4-C≡C)PtCl(PBu$^n_3$)$_2$]	[a]			350[b]	FWM	[a]	0.63	78
cis-[Pt(C≡CC$_6$H$_4$-4-C≡CH)$_2$(PBu$^n_3$)$_2$]	[a]	230[b]	260[b]	290[b]	FWM	[a]	0.63	78

[a] Not Reported

[b] Error not reported

[c] IDA = Intensity dependent absorption

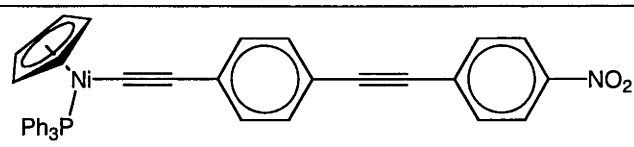

γ_{real} = -640 ± 300 x 10^{-36} esu

γ_{imag} = 720 ± 300 x 10^{-36} esu

$|\gamma|$ = 960 ± 420 x 10^{-36} esu

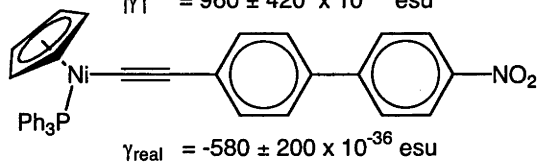

γ_{real} = -580 ± 200 x 10^{-36} esu

γ_{imag} = 300 ± 60 x 10^{-36} esu

$|\gamma|$ = 650 ± 210 x 10^{-36} esu

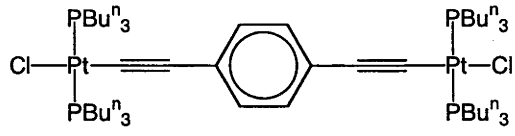

γ_{real} = 19 ± 5 x 10^{-36} esu

γ_{imag} = 830 ± 210 x 10^{-36} esu

$|\gamma|$ = 830 ± 210 x 10^{-36} esu

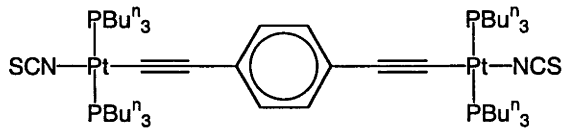

γ_{real} = 30 ± 8 x 10^{-36} esu

γ_{imag} = 1100 ± 280 x 10^{-36} esu

$|\gamma|$ = 1100 ± 280 x 10^{-36} esu

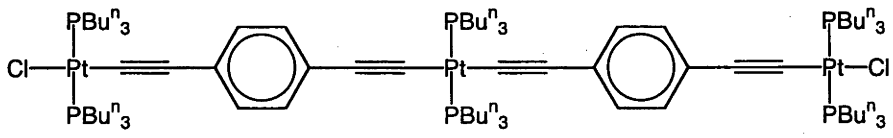

γ_{real} = 45 ± 11 x 10^{-36} esu

γ_{imag} = 1200 ± 300 x 10^{-36} esu

$|\gamma|$ = 1200 ± 300 x 10^{-36} esu

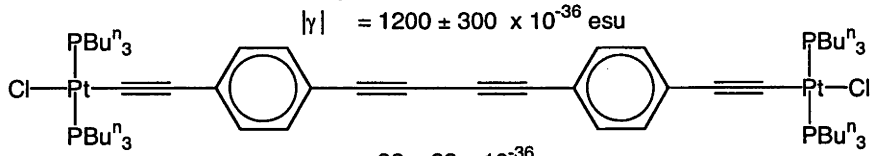

γ_{real} = 88 ± 22 x 10^{-36} esu

γ_{imag} = 2200 ± 540 x 10^{-36} esu

$|\gamma|$ = 2200 ± 540 x 10^{-36} esu

Figure 1.13. Selected Group 10 acetylide complexes with large γ values

Table 1.10. Molecular Cubic NLO Measurements of Group 10 Acetylide Complexes[a]

Complex	λ_{max} (nm)	γ_{real} (10^{-44} m^5 V^{-2})	γ_{imag} (10^{-44} m^5 V^{-2})	γ (10^{-44} m^5 V^{-2})	Ref.
trans-[Ni(C≡CPh)$_2$(PEt$_3$)$_2$]	370	-27.5	14.6	31.1	80,81
trans-[Ni(C≡CC≡CH)$_2$(PEt$_3$)$_2$]	336	-7.87	17.2	18.9	80,81
trans-[Pd(C≡CPh)$_2$(PEt$_3$)$_2$]	370	-21.0	3.39	21.3	80,81
trans-[Pd(C≡CC≡CH)$_2$(PEt$_3$)$_2$]	290	-3.85	0.919	3.96	80-82
trans-[Pt(C≡CPh)$_2$(PEt$_3$)$_2$]	332	-11.2	2.15	11.4	80,81
trans-[Pt(C≡CC≡CH)$_2$(PEt$_3$)$_2$]	318	-1.93	0.771	2.08	80-82

[a] DFWM, 1.064 μm, $CHCl_3$

The results for the group 10 acetylide complexes listed in Table 1.11. have been given as nonlinear refractive indices n_2; once again, these data are available for internal comparison only, because other experimental parameters are needed to derive γ values that are required for comparision to the results given earlier. The results are consistent with increased nonlinearity on chromophore chain lengthening (as observed with acetylide complexes cited earlier) and with a metal efficiency series nickel > platinum > palladium.[83]

Table 1.11. Nonlinear Refractive Index Measurements for Group 10 Acetylide Complexes[a]

Complex	n_2 (10^{-18} m^2 W^{-1})	Ref.
trans-[Ni(C≡CPh)$_2$(PBu$^n_3$)$_2$]	-16 ± 5	83
trans-[Pd(C≡CPh)$_2$(PBu$^n_3$)$_2$]	-0.5 ± 0.1	83
trans-[Pd(C≡CC$_6$H$_4$-4-C≡CPh)$_2$(PBu$^n_3$)$_2$]	-25 ± 3	83
trans-[Pt(C≡CPh)$_2$(PBu$^n_3$)$_2$]	-3.0 ± 0.1	83
trans-[Pt(C≡CC$_6$H$_4$-4-C≡CPh)$_2$(PBu$^n_3$)$_2$]	-209 ± 27	83

[a] Z-scan, thf, 0.53 μm

Many applications in nonlinear optics require materials that are processable, e.g. as thin films, so acetylide polymers are clearly of interest. Group 10 acetylide polymers have proven a fertile area of study. In many of the acetylide polymers of square planar nickel, palladium, and platinum listed in Tables 1.12. (SI units) and 1.13. (cgs units), the imaginary part of the nonlinearity is the major contributor, implying significant two-photon absorption. Some of the polymers have nonlinearities that are significantly larger than related monometallic acetylide complexes. There does not seem to be a consistent trend in nonlinearity resultant upon increasing polymer size. Although it is hard to compare data across metal (because the polymers vary in length as well as composition), the platinum polymers are in many cases more efficient than the analogous palladium polymers. The nonlinearities of these polymers do not depend dramatically on aromatic ring substitution, but increasing the number of diethynylarenes in the repeat unit increases the nonlinearity.[79,84,85]

Table 1.12. Molecular Cubic NLO Results for Group 10 Acetylide Polymers[a]

Complex	λ_{max} (nm)	γ_{real} (10^{-42} m^5 V^{-2})	γ_{imag} (10^{-42} m^5 V^{-2})	γ (10^{-42} m^5 V^{-2})	Solvent	Ref.
$[Ni(C{\equiv}CC{\equiv}C)(PBu^n_3)_2]_n$	412	-2.63	-2.41	3.57	$CHCl_3$	80,81.86
	410	-2.63	-2.41	3.57		82
$[Ni(C{\equiv}CC_6H_4\text{-}4\text{-}C{\equiv}C)(PBu^n_3)_2]_n$		-10	20	20	$CHCl_3$	86
$[Ni(C{\equiv}CC_6H_4\text{-}4\text{-}C{\equiv}C)(POc^n_3)_2]_n$		-40	100	100	$CHCl_3$	86
$[Ni(C{\equiv}CC{\equiv}C)\{P(C_8H_{17})_3)\}]_n$		-40	30	50	$CHCl_3$	86
$[Pd_2(C{\equiv}CC_6H_4\text{-}4\text{-}C{\equiv}C)(\mu\text{-dppm})_2]_n$		-20	20	20	$CHCl_3$	86
$[Pt(C{\equiv}CC{\equiv}C)(PBu^n_3)_2]_n$	364	-1.48	1.74	2.28	$CHCl_3$	80,81.86
	360	-1.48	1.74	2.28		82

[a] 1.06 μm, DFWM

Table 1.13. Molecular Cubic NLO Results for Group 10 Acetylide Polymers

Complex	γ_{real} (10^{-36} esu)	γ_{imag} (10^{-36} esu)	γ (10^{-36} esu)	Technique	Solvent	Fund. (μm)	Ref.
$[Pd(C{\equiv}CC_6H_4\text{-}4\text{-}C{\equiv}C)(PBu^n{}_3)_2]_n$	390	380	490	FWM		0.63	78
$[Pd(C{\equiv}CC_6H_4\text{-}4\text{-}C{\equiv}C)(PBu^n{}_3)_2]_n$ n = 112	102	3401		OKG/IDA[a]	thf	1.06/0.53	84
$[Pd(C{\equiv}CC_6H_2\text{-}2,5\text{-}Me_2\text{-}4\text{-}C{\equiv}C)(PBu^n{}_3)_2]_n$ n = 4	19	1169		OKG/IDA[a]	thf	1.06/0.53	79
$[Pd(C{\equiv}CC_6H_3\text{-}3\text{-}NH_2\text{-}4\text{-}C{\equiv}C)(PBu^n{}_3)_2]_n$ n = 12	15	1753		OKG/IDA[a]	thf	1.06/0.53	79
$[Pd(C{\equiv}CC_6H_2\text{-}2,5\text{-}(OMe)_2\text{-}4\text{-}C{\equiv}C)(PBu^n{}_3)_2]_n$ n = 67	22	2432		OKG/IDA[a]	thf	1.06/0.53	79
$[Pd(C{\equiv}CC_6H_4\text{-}4\text{-}C{\equiv}CC{\equiv}CC_6H_4\text{-}4\text{-}C{\equiv}C)(PBu^n{}_3)_2]_n$ oligomer	66	2094		OKG/IDA[a]	thf	1.06/0.53	79
$[Pd(C{\equiv}CC_6H_2\text{-}2,5\text{-}Et_2\text{-}4\text{-}C{\equiv}CC{\equiv}CC_6H_2\text{-}2,5\text{-}Et_2\text{-}4\text{-}C{\equiv}C)(PBu^n{}_3)_2]_n$ n = 16	106	3490		OKG/IDA[a]	thf	1.06/0.53	79
$[Pt(C{\equiv}CC_6H_4\text{-}4\text{-}C{\equiv}C)(PBu^n{}_3)_2]_n$ ~32 000 amu			1470	THG	benzene	1.06	87
$[Pt(C{\equiv}CC_6H_4\text{-}4\text{-}C{\equiv}C)(PBu^n{}_3)_2]_n$ n = 112	37	1906		OKG/IDA[a]	thf	1.06/0.53	79
$[Pt(C{\equiv}CC_6H_2\text{-}2,5\text{-}Me_2\text{-}4\text{-}C{\equiv}C)(PBu^n{}_3)_2]_n$ n = 26	29	1200		OKG/IDA[a]	thf	1.06/0.53	79
	56	1199		OKG/IDA[a]	thf	1.06/0.53	88
$[Pt(C{\equiv}CC_6H_2\text{-}2,5\text{-}Et_2\text{-}4\text{-}C{\equiv}C)(PBu^n{}_3)_2]_n$ n = 15	43	956		OKG/IDA[a]	thf	1.06/0.53	79
$[Pt(C{\equiv}CC_6H_3\text{-}3\text{-}F\text{-}4\text{-}C{\equiv}C)(PBu^n{}_3)_2]_n$ n = 18	56	1260		OKG/IDA[a]	thf	1.06/0.53	79
$[Pt(C{\equiv}CC_6H_2\text{-}2,5\text{-}(OMe)_2\text{-}4\text{-}C{\equiv}C)(PBu^n{}_3)_2]_n$ n = 111, 105, 62	48,65,43	1724,1330,1586		OKG/IDA[a]	thf	1.06/0.53	79
$[Pt(C{\equiv}CC_6Me_4\text{-}4\text{-}C{\equiv}C)(PBu^n{}_3)_2]_n$ oligomer	28	1324		OKG/IDA[a]	thf	1.06/0.53	79
$[Pt(C{\equiv}CC_6H_3\text{-}3\text{-}NH_2\text{-}4\text{-}C{\equiv}C)(PBu^n{}_3)_2]_n$ n = 76	18	1342		OKG/IDA[a]	thf	1.06/0.53	79

Table 1.13. (continued) Molecular Cubic NLO Results for Group 10 Acetylide Polymers

Complex	γ_{real} (10^{-36} esu)	γ_{imag} (10^{-36} esu)	γ (10^{-36} esu)	Technique	Solvent	Fund. (μm)	Ref.
$[Pt(C{\equiv}CC_6H_3\text{-}3\text{-}CF_3\text{-}4\text{-}C{\equiv}C)(PBu^n_3)_2]_n$ n = 44	34	2148		OKG/IDA[a]	thf	1.06/0.53	79
$[Pt\{C{\equiv}C(1\text{-naphthyl})\text{-}4\text{-}C{\equiv}C\}(PBu^n_3)_2]_n$ n = 62	19	2474		OKG/IDA[a]	thf	1.06/0.53	79
$[Pt\{3\text{-}C{\equiv}C(C_5H_3N)\text{-}2\text{-}C{\equiv}C\}(PBu^n_3)_2]_n$ n = 47, 35	33	2263		OKG/IDA[a]	thf	1.06/0.53	79
$[Pt(C{\equiv}CC_6H_4\text{-}4\text{-}C{\equiv}C)(PBu^n_3)_2]_n$	890	130	1450	FWM		0.63	78
$[Pt(C{\equiv}CC_6H_4\text{-}4\text{-}C{\equiv}CC{\equiv}CC_6H_4\text{-}4\text{-}C{\equiv}C)(PBu^n_3)_2]_n$ n = 223, 97	90,121	4558,4025		OKG/IDA[a]	thf	1.06/0.53	79
$[Pt(C{\equiv}CC_6H_4\text{-}4\text{-}C{\equiv}CC{\equiv}CC_6H_4\text{-}4\text{-}C{\equiv}C)(PBu^n_3)_2]_n$ n > 144	856	3570		OKG/IDA[a]	thf	1.06/0.53	84
$[Pt(C{\equiv}CC_6H_2\text{-}2,5\text{-}Me_2\text{-}4\text{-}C{\equiv}CC{\equiv}CC_6H_2\text{-}2,5\text{-}Me_2\text{-}4\text{-}C{\equiv}C)\text{-}(PBu^n_3)_2]_n$ n = 52,38	116	2432		OKG/IDA[a]	thf	1.06/0.53	79
$[Pt(C{\equiv}CC_6H_2\text{-}2,5\text{-}Me_2\text{-}4\text{-}C{\equiv}CC{\equiv}CC_6H_2\text{-}2,5\text{-}Me_2\text{-}4\text{-}C{\equiv}C)\text{-}(PBu^n_3)_2]_n$ n = 52	181	4366		OKG/IDA[a]	thf	1.06/0.53	79,84
	120 ± 30	5400 ± 500		OKG	thf	0.53	
$[Pt(C{\equiv}CC_6H_2\text{-}2,5\text{-}Et_2\text{-}4\text{-}C{\equiv}CC{\equiv}CC_6H_2\text{-}2,5\text{-}Et_2\text{-}4\text{-}C{\equiv}C)\text{-}(PBu^n_3)_2]_n$ n = 146	79	4933		OKG/IDA[a]	thf	1.06/0.53	79
$[Pt(C{\equiv}CC_6H_4\text{-}4\text{-}C{\equiv}C)(PBu^n_3)_2Pt(C{\equiv}CC_6H_4C_6H_4\text{-}4\text{-}C{\equiv}C)(PBu^n_3)_2]_n$ n = 66		4466		OKG/IDA[a]	thf	1.06/0.53	79

[a] IDA = Intensity Dependent Absorption

1.5.4. *Group 11 Acetylide Complexes*

Most of the group 11 acetylide complexes to have been examined thus far are gold complexes, probed by Z-scan at 0.80 μm; the results of these studies are collected in Table 1.14., with structural formulas of some of the more efficient examples being displayed in Figure 1.14. Cubic nonlinearities for many of these 14 electron gold complexes are larger than those of their 18 electron ruthenium analogues, the opposite trend to that observed with β.[89] Replacing PMe_3 by PPh_3 and extending the acetylide ligand both increase π-delocalization possibilities and both result in an increase in $|\gamma|$ values. Introduction of polarizing nitro substituent has a similar effect, but progression from the most efficient monometallic complexes to the iron-digold complexes $[Fe\{\eta^5\text{-}C_5H_4\text{-}(E)\text{-}CH{=}CHC_6H_4\text{-}4\text{-}C{\equiv}CAu(L)\}_2]$ (L = PMe_3, PPh_3, PCy_3) does not result in significant further increase in $|\gamma|$.[77]

Three silver phenylacetylide complexes were examined by heterodyned optical Kerr gate measurements; the data for polymeric compounds are presented in Table 1.15. ($[Ag(C{\equiv}CPh)(PPh_3)]_4$ exhibited negligible third-order nonlinearity). The nonlinear responses are in the femtosecond domain and follow the trend silver phenylacetylide polymer > silver phenylacetylide-silver *tert*-butylthiolate double salt > (triphenylphosphine)silver phenylacetylide tetramer.[91]

Table 1.14. Molecular Cubic NLO Measurements of Gold Acetylide Complexes[a]

Complex	λ_{max} (nm)	γ_{real} (10^{-36} esu)	γ_{imag} (10^{-36} esu)	γ (10^{-36} esu)	Solvent	Ref.
$[Au(C{\equiv}CPh)(PPh_3)]$	296	39 ± 20	--	39 ± 20	thf	75
$[Au(C{\equiv}CC_6H_4\text{-}4\text{-}NO_2)(PPh_3)]$	338	120 ± 40	20 ± 15	120 ± 40	thf	75
$[Au(C{\equiv}CC_6H_4\text{-}4\text{-}C_6H_4\text{-}4\text{-}NO_2)(PPh_3)]$	350	540 ± 150	120 ± 50	550 ± 160	thf	75
$[Au(C{\equiv}CC_6H_4\text{-}4\text{-}(E)\text{-}CH{=}CHC_6H_4\text{-}4\text{-}NO_2)(PPh_3)]$	386	1200 ± 200	470 ± 150	1300 ± 250	thf	75
$[Au(C{\equiv}CC_6H_4\text{-}4\text{-}(Z)\text{-}CH{=}CHC_6H_4\text{-}4\text{-}NO_2)(PPh_3)]$	362	420 ± 150	92 ± 30	430 ± 150	thf	75
$[Au(C{\equiv}CC_6H_4\text{-}4\text{-}C{\equiv}CC_6H_4\text{-}4\text{-}NO_2)(PPh_3)]$	362	1300 ± 400	560 ± 150	1400 ± 430	thf	75
$[Au(C{\equiv}CC_6H_4\text{-}4\text{-}N{=}CHC_6H_4\text{-}4\text{-}NO_2)(PPh_3)]$	392	130 ± 30	330 ± 60	350 ± 70	thf	75
$PPN[Au(C{\equiv}CC_6H_4\text{-}4\text{-}NO_2)_2]$	376	-800 ± 30	115 ± 50	810 ± 60	CH_2Cl_2	90
$NPr_4[Au(C{\equiv}CC_6H_4\text{-}4\text{-}NO_2)_2]$	374	90 ± 150	190 ± 50	210 ± 160	CH_2Cl_2	90
$[Au(C{\equiv}CC_6H_4\text{-}4\text{-}NO_2)(CNBu^t)]$	332	≤ 130	≤ 50	≤ 130	CH_2Cl_2	90
$[Au(C{\equiv}CC_6H_4\text{-}4\text{-}C_6H_4\text{-}4\text{-}NO_2)(CNBu^t)]$	343	20 ± 100	70 ± 50	70 ± 110	CH_2Cl_2	90
$[Au(C{\equiv}CC_6H_4\text{-}4\text{-}(E)\text{-}CH{=}CHC_6H_4\text{-}4\text{-}NO_2)(CNBu^t)]$	381	390 ± 200	1050 ± 300	1120 ± 360	CH_2Cl_2	90
$[Au(C{\equiv}CC_6H_4\text{-}4\text{-}C_6H_4\text{-}4\text{-}NO_2)\{C(NHBu^t)(NEt_2)\}]$	354	10 ± 100	160 ± 40	160 ± 110	CH_2Cl_2	90
$[Au(C{\equiv}CC_6H_4\text{-}4\text{-}(E)\text{-}CH{=}CHC_6H_4\text{-}4\text{-}NO_2)\{C(NHBu^t)(NEt_2)\}]$	389	-200 ± 360	610 ± 200	640 ± 410	CH_2Cl_2	90
$Au\{C{\equiv}CC_6H_4\text{-}(E)\text{-}4\text{-}CH{=}CHPh\}(PPh_3)$	338	0 ± 300	0 ± 50	0	thf	76
$Au(C{\equiv}CC_6H_4\text{-}4\text{-}C{\equiv}CPh)(PPh_3)$	336	-900 ± 400	0 ± 100	900 ± 400	thf	76
$Au(C{\equiv}CC_6H_4\text{-}4\text{-}C{\equiv}CPh)(PMe_3)$	335	-200 ± 150	0 ± 50	200 ± 150	thf	76
$[Fe\{\eta^5\text{-}C_5H_4\text{-}(E)\text{-}CH{=}CHC_6H_4\text{-}4\text{-}C{\equiv}CAu(PCy_3)\}_2]$	468	-500 ± 500	500 ± 100	640 ± 390	thf	77
$[Fe\{\eta^5\text{-}C_5H_4\text{-}(E)\text{-}CH{=}CHC_6H_4\text{-}4\text{-}C{\equiv}CAu(PPh_3)\}_2]$	465	-1100 ± 300	300 ± 60	1140 ± 310	thf	77

Table 1.14. Molecular Cubic NLO Measurements of Gold Acetylide Complexes[a]

Complex	λ_{max} (nm)	γ_{real} (10^{-36} esu)	γ_{imag} (10^{-36} esu)	γ (10^{-36} esu)	Solvent	Ref.
$[Fe\{\eta^5\text{-}C_5H_4\text{-}(E)\text{-}CH{=}CHC_6H_4\text{-}4\text{-}C{\equiv}CAu(PMe_3)\}_2]$	463	200 ± 150	0 ± 30	200 ± 150	thf	77
$[Au(C{\equiv}CC_6H_4\text{-}4\text{-}NO_2)(PCy_3)]$	342	100 ± 50	--	100 ± 50	thf	62
$[Au(C{\equiv}CC_6H_4\text{-}4\text{-}NO_2)(PPh_3)]$	338	120 ± 40	20 ± 15	120 ± 40	thf	62
$[Au(C{\equiv}CC_6H_4\text{-}4\text{-}NO_2)(PMe_3)]$	339	150 ± 50	--	150 ± 50	thf	62
$[(PCy_3)AuC{\equiv}CC_6H_4\text{-}4\text{-}C{\equiv}CAu(PCy_3)]$	325	≤250	--	≤250	thf	62
$[(PCy_3)AuC{\equiv}CC_6H_4\text{-}4\text{-}C_6H_4\text{-}4\text{-}C{\equiv}CAu(PCy_3)]$	324	-300 ± 200	0 ± 30	300 ± 200	thf	62
$[Au(C{\equiv}CC_6H_4\text{-}4\text{-}CHO)(PPh_3)]$	322	300 ± 50	0	300 ± 50	thf	49
$[Au(C{\equiv}CC_6H_4\text{-}4\text{-}CHO)(PMe_3)]$	322	35 ± 20	45 ± 30	60 ± 35	thf	49
$[Au(C{\equiv}CC_6H_4\text{-}4\text{-}\overline{CHO(CH_2)_3O})(PPh_3)]$	296	-300 ± 200	0 ± 30	300 ± 200	thf	49
$[Au(C{\equiv}CC_6H_4\text{-}4\text{-}\overline{CHO(CH_2)_3O})(PMe_3)]$	292	too low	too low		thf	49
$[Au(C{\equiv}CC_6H_4\text{-}3\text{-}CHO)(PPh_3)]$	318	scattered	scattered		thf	49
$[Au(C{\equiv}CC_6H_4\text{-}3\text{-}CHO)(PMe_3)]$	322	scattered	scattered		thf	49

[a] Z-scan, 0.80 μm

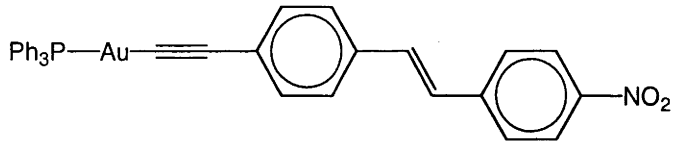

γ_{real} = 1200 ± 200 x 10^{-36} esu
γ_{imag} = 470 ± 150 x 10^{-36} esu
$|\gamma|$ = 1300 ± 250 x 10^{-36} esu

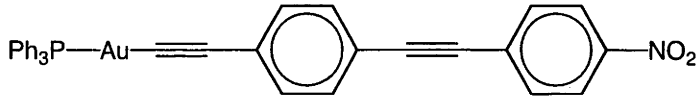

γ_{real} = 1300 ± 400 x 10^{-36} esu
γ_{imag} = 560 ± 150 x 10^{-36} esu
$|\gamma|$ = 1400 ± 430 x 10^{-36} esu

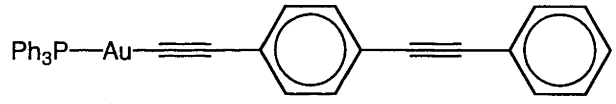

γ_{real} = -900 ± 400 x 10^{-36} esu
γ_{imag} = 0 ± 100 x 10^{-36} esu
$|\gamma|$ = 900 ± 400 x 10^{-36} esu

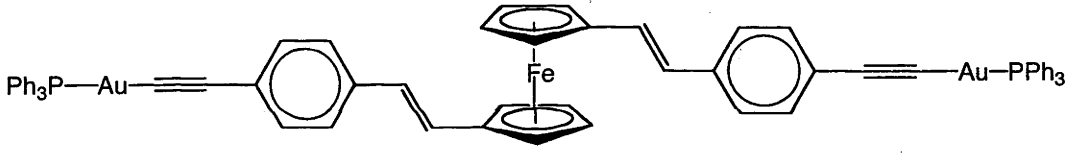

γ_{real} = -1100 ± 300 x 10^{-36} esu
γ_{imag} = 300 ± 60 x 10^{-36} esu
$|\gamma|$ = 1140 ± 310 x 10^{-36} esu

Figure 1.14. Selected gold acetylide complexes with large γ values.

Table 1.15. Molecular and Bulk Cubic NLO Measurements of Silver Acetylide Polymers[a]

Complex	λ_{max} (nm)	$\chi^{(3)}$ (10^{-14} esu)	γ^b (10^{-36} esu)	Solvent	Ref.
$[AgC{\equiv}CPh]_n$	260	2.40	90 700	1:1 DMSO/$CHCl_3$	91
	271	-1.11	-105 900	1:1:1 DMSO/$CHCl_3$/CH_2Cl_2	91
$[AgC{\equiv}CPh{\bullet}AgS(t\text{-}Bu)]_n$	264	1.10	74 400	1:1 DMSO/$CHCl_3$	91
	271	-0.68	-64 900	1:1:1 DMSO/$CHCl_3$/CH_2Cl_2	91

[a] Optical heterodyned optical Kerr effect, 0.647 μm

[b] Calculated with the assumption that n = 7

1.5.5. *Vinylidene Complexes*

All reports of cubic nonlinearities for vinylidene complexes thus far are of ruthenium complexes assessed by Z-scan at 0.80 μm, the results from which are collected in Table 1.16. As with many ruthenium acetylide complexes, the real components of the cubic nonlinearities for the aryldiazovinylidene complexes are negative and the imaginary components are significant, suggestive of two-photon absorption contributing to the observed response. The data are consistent with incorporation of nitro substituent resulting in a significant increase in $|\gamma|$, but nonlinearities for the other monometallic vinylidene complexes are uniformly low. In contrast, the two trimetallic vinylidene complexes to be examined thus far display large cubic NLO efficiencies.[54,77]

Table 1.16. Molecular Cubic NLO Measurements of Vinylidene Complexes[a]

Complex	λ_{max} (nm)	γ_{real} (10^{-36} esu)	γ_{imag} (10^{-36} esu)	γ (10^{-36} esu)	Solvent	Ref.
$[Fe\{\eta^5\text{-}C_5H_4\text{-}(E)\text{-}CH{=}CHC_6H_4\text{-}4\text{-}CH{=}CRuCl(dppm)_2\}_2](PF_6)_2$	383	-3000 ± 1200	2300 ± 800	3800 ± 1400	thf	77
$[Ru(C{=}CPhN{=}NPh)(PPh_3)_2(\eta^5\text{-}C_5H_5)]BF_4$	363	-160 ± 60	75 ± 25	180 ± 65	CH_2Cl_2	63
$[Ru(C{=}CPhN{=}NC_6H_4\text{-}2\text{-}OMe)(PPh_3)_2(\eta^5\text{-}C_5H_5)]Cl$	377	-220 ± 150	70 ± 30	230 ± 150	CH_2Cl_2	63
$[Ru(C{=}CPhN{=}NC_6H_4\text{-}3\text{-}OMe)(PPh_3)_2(\eta^5\text{-}C_5H_5)]BF_4$	389	-310 ± 60	90 ± 30	320 ± 65	CH_2Cl_2	63
$[Ru(C{=}CPhN{=}NC_6H_4\text{-}4\text{-}OMe)(PPh_3)_2(\eta^5\text{-}C_5H_5)]Cl$	374	-20 ± 40	80 ± 40	80 ± 50	CH_2Cl_2	63
$[Ru(C{=}CPhN{=}NC_6H_4\text{-}4\text{-}NO_2)(PPh_3)_2(\eta^5\text{-}C_5H_5)]BF_4$	413	-320 ± 100	160 ± 40	360 ± 110	CH_2Cl_2	63
$[Ru(C{=}CPhN{=}NC_6H_4\text{-}4\text{-}NO_2)(PPh_3)_2(\eta^5\text{-}C_5H_5)]Cl$	413	-630 ± 200	160 ± 50	650 ± 210	CH_2Cl_2	63
$[Ru(C{=}CPhN{=}NC_6H_4\text{-}4\text{-}NO_2)(PPh_3)_2(\eta^5\text{-}C_5H_5)]Br$	413	-570 ± 150	150 ± 40	590 ± 160	CH_2Cl_2	63
$[Ru(C{=}CPhN{=}NC_6H_4\text{-}4\text{-}NO_2)(PPh_3)_2(\eta^5\text{-}C_5H_5)]I$	413	-460 ± 50	140 ± 50	480 ± 60	CH_2Cl_2	63
$[Ru(C{=}CPhN{=}NC_6H_4\text{-}4\text{-}NO_2)(PPh_3)_2(\eta^5\text{-}C_5H_5)](4\text{-}MeC_6H_4SO_3)$	413	-580 ± 200	210 ± 50	620 ± 210	CH_2Cl_2	63
$[Ru(C{=}CPhN{=}NC_6H_4\text{-}4\text{-}NO_2)(PPh_3)_2(\eta^5\text{-}C_5H_5)]NO_3$	413	-460 ± 150	200 ± 50	500 ± 160	CH_2Cl_2	63
trans-$[Ru(C{=}CHPh)Cl(dppm)_2]PF_6$	320	<440	<50	<440	thf	48
trans-$[Ru(C{=}CHC_6H_4\text{-}4\text{-}C{\equiv}CPh)Cl(dppm)_2]PF_6$	380	<500	0	<500	thf	48
trans-$[Ru(C{=}CHC_6H_4\text{-}4\text{-}CHO)Cl(dppm)_2]PF_6$	403	0	<20	<20	thf	48
trans-$[Ru(C{=}CHC_6H_4\text{-}4\text{-}NO_2)Cl(dppm)_2]PF_6$	470	<50	<30	<50	thf	48
trans-$[Ru(C{=}CHC_6H_4\text{-}4\text{-}C{\equiv}CC_6H_4\text{-}4\text{-}NO_2)Cl(dppm)_2]PF_6$	326	<500	420 ± 60	420 ± 60	thf	48
trans-$[Ru(C{=}CHPh)Cl(dppe)_2]PF_6$	317	380 ± 400	<50	380 ± 400	thf	48
trans-$[Ru(C{=}CHC_6H_4\text{-}4\text{-}CHO)Cl(dppe)_2]PF_6$	412	<260	0	<260	thf	48
trans-$[Ru(C{=}CHC_6H_4\text{-}4\text{-}NO_2)Cl(dppm)_2]PF_6$	476	250 ± 300	<50	250 ± 300	thf	48
trans-$[Ru\{C{=}CHC_6H_4\text{-}4\text{-}(E)\text{-}CH{=}CHC_6H_4\text{-}4\text{-}NO_2\}Cl(dppe)_2]PF_6$	473	650 ± 500	<50	650 ± 500	thf	48

Table 1.16. (continued) Molecular Cubic NLO Measurements of Vinylidene Complexes[a]

Complex	λ_{max} (nm)	γ_{real} (10^{-36} esu)	γ_{imag} (10^{-36} esu)	γ (10^{-36} esu)	Solvent	Ref.
trans-[Ru{C=CHC$_6$H$_4$-4-CHO(CH$_2$)$_3$O}Cl(dppm)$_2$]PF$_6$	317	75 ± 75	0	75 ± 75	thf	49
trans-[Ru(C=CHC$_6$H$_4$-3-CHO)Cl(dppm)$_2$]PF$_6$	320	200 ± 200	0	200 ± 200	thf	49
trans-[Ru(C=CHC$_6$H$_4$-4-CHO)Cl(dppm)$_2$]PF$_6$	403	0	<20	<20	thf	49
[1,3,5-*trans*-[RuCl(dppm)$_2${C=CHC$_6$H$_4$-(*E*)-4-CH=CH}$_3$C$_6$H$_3$](PF$_6$)$_3$	396	-900 ± 500	700 ± 400	1100 ± 700	thf	54

[a] Z-scan, 0.800 μm

1.6. *Conclusions*

The studies of the NLO properties of acetylide and vinylidene complexes summarized above have resulted in development of structure – NLO response relationships for quadratic optical nonlinearities, while low nonlinearities and large error margins for many of the studies with small acetylide complexes have resulted in less success at developing relationships for cubic nonlinearities. Some of the acetylide complexes are amongst the most efficient organic or inorganic quadratic NLO molecules thus far, while the ruthenium acetylide dendrimers possess two-photon absorption cross-sections of the same order of magnitude as the best organic performers.

1.7. *References*

(1) Chemla, D. S.; Zyss, J., Eds. *Nonlinear Optical Properties of Organic Molecules and Crystals II*; Academic Press: Orlando, 1987.

(2) Chemla, D. S.; Zyss, J., Eds. *Nonlinear Optical Properties of Organic Molecules and Crystals I*; Academic Press: Orlando, 1987.

(3) Williams, D. J., Ed. *Nonlinear Optical Properties of Organic and Polymeric Materials*; American Chemical Society, 1983; Vol. 233.

(4) Kirtman, B.; Champagne, B. *Int. Rev. Phys. Chem.* **1997**, *16*, 389.

(5) Hann, R. A.; Bloor, D., Eds. *Organic Materials for Non-Linear Optics*; Royal Society of Chemistry: London, 1989.

(6) Hann, R. A.; Bloor, D., Eds. *Organic Materials for Non-linear Optics II*; Royal Society of Chemistry: London, 1991.

(7) Verbiest, T.; Houbrechts, S.; Kauranen, M.; Clays, K.; Persoons, A. *J. Mater. Chem.* **1997**, *7*, 2175.

(8) Long, N. J. *Angew. Chem. Int. Ed. Engl.* **1995**, *34*, 21.

(9) Di Bella, S. *Chem. Soc. Rev.* **2001**, *30*, 355.

(10) Whittall, I. R.; McDonagh, A. M.; Humphrey, M. G.; Samoc, M. *Adv. Organomet. Chem.* **1998**, *43*, 291.

(11) Whittall, I. R.; McDonagh, A. M.; Humphrey, M. G.; Samoc, M. *Adv. Organomet. Chem.* **1999**, *43*, 349.

(12) Marder, S. R. In *Inorganic Materials*; Bruce, D. W., O'Hare, D., Eds.; Wiley: Chichester, 1992; p 116.

(13) Nie, W. *Adv. Mater.* **1993**, *5*, 520.

(14) Allen, S. *New Scientist* **1989**, *1 July*, 31.

(15) Heeger, A. J.; Orenstein, J.; Ulrich, D., Eds. *Nonlinear Optical Properties of Polymers*; Materials Research Society: Pittsburgh, 1988.

(16) Ashwell, G. J.; Bloor, D., Eds. *Organic Materials for Non-linear Optics III*; Royal Society of Chemistry: Cambridge, 1993.

(17) Messier, J.; Kajzar, F.; Prasad, P.; Ulrich, D., Eds. *Nonlinear Optical Effects in Organic Polymers*; Kluwer Academic Publishers: Dordrecht, 1989; Vol. E162.

(18) Messier, J.; Kajzar, F.; Prasad, P., Eds. *Organic Molecules for Nonlinear Optics and Photonics*; Kluwer Academic Publishers: Dordrecht, 1991.

(19) Kobayashi, T., Ed. *Nonlinear Optics of Organics and Semiconductors*; Springer-Verlag: Berlin, 1989.

(20) Lyons, M. H., Ed. *Materials for Non-linear and Electro-optics 1989*; Institute of Physics: Bristol, 1989.

(21) Marder, S. R.; Sohn, J. E.; Stucky, G. D., Eds. *Materials for Nonlinear Optics, Chemical Perspectives*; American Chemical Society: Washington D.C., 1991.

(22) Williams, D. J. *Angew. Chem. Int. Ed.* **1984**, *23*, 690.

(23) Nalwa, H. S. *Adv. Mater.* **1993**, *5*, 341.

(24) Nalwa, H. S. *Appl. Organomet. Chem.* **1991**, *5*, 1.

(25) Nalwa, H. S.; Watanabe, T.; Miyata, S. *Adv. Mater.* **1995**, *7*, 754.

(26) Kanis, D. R.; Ratner, M. A.; Marks, T. J. *Chem. Rev.* **1994**, *94*, 195.

(27) Nast, R. *Angew. Chem. Int. Ed.* **1960**, *72*, 26.

(28) Humphrey, M. G. *J. Organomet. Chem.* **2003**, *670*, 1.

(29) Long, N. J.; Williams, C. K. *Angew. Chem. Int. Ed.* **2003**, *42*, 2586.

(30) Boyd, R. W. *Nonlinear Optics*; Academic Press: New York, 1992.

(31) Zyss, J.; Chemla, D. S. In *Nonlinear Optical Properties of Organic Molecules and Crystals I*; Chemla, D. S., Zyss, J., Eds.; Academic Press: New York, 1987; p23.

(32) Sutherland, R. L. *Handbook of Nonlinear Optics*; Marcel Dekker: New York, 1996; Vol. 52.

(33) Chemla, D. S.; Oudar, J. L.; Jerphagon, J. *J. Phys. Rev. B* **1975**, *12*, 4534.

(34) Clays, K.; Persoons, A. *Rev. Sci. Intrum.* **1992**, *63*, 3285.

(35) Sheik-Bahae, M.; Said, A. A.; Wei, T.; Hagan, D. J.; van Stryland, E. W. *IEEE J. Quantum Electr.* **1990**, *26*, 760.

(36) Di Bella, S.; Ratner, M. A.; Marks, T. J. *J. Am. Chem. Soc.* **1992**, *114*, 5842.

(37) Di Bella, S.; Marks, T. J.; Ratner, M. A. *J. Am. Chem. Soc.* **1994**, *116*, 4440.

(38) Oudar, J. L. *J. Chem. Phys.* **1977**, *67*, 446.

(39) Oudar, J. L.; Hierle, R. J. *J. Appl. Phys.* **1977**, *48*, 2699.

(40) Naulty, R. H.; Cifuentes, M. P.; Humphrey, M. G.; Houbrechts, S.; Boutton, C.; Persoons, A.; Heath, G. A.; Hockless, D. C. R.; Luther-Davies, B.; Samoc, M. *J. Chem. Soc., Dalton Trans.* **1997**, 4167.

(41) Naulty, R. H.; McDonagh, A. M.; Whittall, I. R.; Cifuentes, M. P.; Humphrey, M. G.; Houbrechts, S.; Maes, J.; Persoons, A.; Heath, G. A.; Hockless, D. C. R. *J. Organmet. Chem* **1998**, *563*, 137.

(42) Cadierno, V.; Conejero, S.; Gamasa, M. P.; Gimeno, J.; Asselberghs, I.; Houbrechts, S.; Clays, K.; Persoons, A.; Borge, J.; Garcia-Granda, S. *Organometallics* **1999**, *18*, 582.

(43) Wu, I.-Y.; Lin, J. T.; Luo, J.; Li, C.-S.; Tsai, C.; Wen, Y. S.; Hsu, C.-C.; Yeh, F.-F.; Sean, L. *Organometallics* **1998**, *17*, 2188.

(44) McDonagh, A. M.; Cifuentes, M. P.; Lucas, N. T.; Humphrey, M. G.; Houbrechts, S.; Persoons, A. *J. Organomet. Chem.* **2000**, *605*, 184.

(45) McDonagh, A. M.; Lucas, N. T.; Cifuentes, M. P.; Humphrey, M. G.; Houbrechts, S.; Persoons, A. *J. Organomet. Chem.* **2000**, *605*, 193.

(46) Houbrechts, S.; Clays, K.; Persoons, A.; Cadierno, V.; Gamasa, M. P.; Gimeno, J.; Whittall, I. R.; Humphrey, M. G. *Proc. SPIE-Int. Soc. Opt. Eng.* **1996**, *2852*, 97.

(47) Houbrechts, S.; Clays, K.; Persoons, A.; Cadierno, V.; Gamasa, M. P.; Gimeno, J. *Organometallics* **1996**, *15*, 5266.

(48) Hurst, S.; Cifuentes, M. P.; Morrall, J. P.; Lucas, N. T.; Whittall, I. R.; Humphrey, M. G.; Asselberghs, I.; Persoons, A.; Samoc, M.; Luther-Davies, B.; Willis, A. C. *Organometallics* **2001**, *20*, 4664.

(49) Hurst, S.; Lucas, N. T.; Cifuentes, M. P.; Humphrey, M. G.; Samoc, M.; Luther-Davies, B.; Asselberghs, I.; Boxel, R. V.; Persoons, A. *J. Organomet. Chem.* **2001**, *633*, 114.

(50) Powell, C.; Cifuentes, M. P.; McDonagh, A. M.; Hurst, S.; Lucas, N. T.; Delfs, C. D.; Stranger, R.; Humphrey, M. G.; Houbrechts, S.; Asselberghs, I.; Persoons, A.; Hockless, D. C. R. *Inorg. Chim. Acta.* **2003**, *352*, 9.

(51) Whittall, I. R.; Humphrey, M. G.; Persoons, A.; Houbrechts, S. *Organometallics* **1996**, *15*, 1935.

(52) Weyland, T.; Ledoux, I.; Brasselet, S.; Zyss, J.; Lapinte, C. *Organometallics* **2000**, *19*, 5235.

(53) McDonagh, A. M.; Humphrey, M. G.; Samoc, M.; Luther-Davies, B.; Houbrechts, S.; Wada, T.; Sasabe, H.; Persoons, A. *J. Am. Chem. Soc.* **1999**, *121*, 1405.

(54) Hurst, S.; Humphrey, M. G.; Isoshima, T.; Wostyn, K.; Asselberghs, I.; Clays, K.; Persoons, A.; Samoc, M.; Luther-Davies, B. *Organometallics* **2002**, *21*, 2024.

(55) McDonagh, A. M.; Cifuentes, M. P.; Humphrey, M. G.; Houbrechts, S.; Maes, J.; Persoons, A.; Samoc, M.; Luther-Davies, B. *J. Organomet. Chem.* **2000**, *610*, 71.

(56) Whittall, I. R.; Cifuentes, M. P.; Humphrey, M. G.; Luther-Davies, B.; Samoc, M.; Houbrechts, S.; Persoons, A.; Heath, G. A.; Hockless, D. C. R. *J. Organomet. Chem.* **1997**, *549*, 127.

(57) Wu, I.-Y.; Lin, J. T.; Luo, J.; Sun, S.-S.; Li, C.-S.; Lin, K. J.; Tsai, C.; Hsu, C.-C.; Lin, J.-L. *Organometallics* **1997**, *16*, 2038.

(58) Whittall, I. R.; Humphrey, M. G.; Houbrechts, S.; Maes, J.; Persoons, A.; Schmid, S.; Hockless, D. C. R. *J. Organomet. Chem.* **1997**, *544*, 277.

(59) Hurst, S.; Lucas, N. T.; Humphrey, M. G.; Asselberghs, I.; Boxel, R. V.; Persoons, A. *Aust. J. Chem.* **2001**, *54*, 447.

(60) Whittall, I. R.; Cifuentes, M. P.; Humphrey, M. G.; Luther-Davies, B.; Samoc, M.; Houbrechts, S.; Persoons, A.; Heath, G. A.; Bogsányi, D. *Organometallics* **1997**, *16*, 2631.

(61) Whittall, I. R.; Humphrey, M. G.; Houbrechts, S.; Persoons, A.; Hockless, D. C. R. *Organometallics* **1996**, *15*, 5738.

(62) Hurst, S. K.; Cifuentes, M. P.; McDonagh, A. M.; Humphrey, M. G.; Samoc, M.; Luther-Davies, B.; Asselberghs, I.; Persoons, A. *J. Organomet. Chem.* **2002**, *642*, 259.

(63) Cifuentes, M. P.; Driver, J.; Humphrey, M. G.; Asselberghs, I.; Persoons, A.; Samoc, M.; Luther-Davies, B. *J. Organomet. Chem.* **2000**, *607*, 72.

(64) Marder, S. R.; Perry, J. W.; Schaefer, W. P.; Tiemann, B. G. *Proc. SPIE-Int. Soc. Opt. Eng.* **1989**, *1147*, 108.

(65) Whittall, I. R.; Cifuentes, M. P.; Costigan, M. J.; Humphrey, M. G.; Goh, S. C.; Skelton, B. W.; White, A. H. *J. Organomet. Chem.* **1994**, *471*, 193.

(66) Whittall, I. R.; Humphrey, M. G.; Samoc, M.; Luther-Davies, B.; Hockless, D. C. R. *J. Organomet. Chem.* **1997**, *544*, 189.

(67) Whittall, I. R.; Humphrey, M. G.; Hockless, D. C. R.; Skelton, B. W.; White, A. H. *Organometallics* **1995**, *14*, 3970.

(68) McDonagh, A. M.; Whittall, I. R.; Humphrey, M. G.; Skelton, B. W.; White, A. H. *J. Organomet. Chem.* **1996**, *519*, 229.

(69) McDonagh, A. M.; Whittall, I. R.; Humphrey, M. G.; Hockless, D. C. R.; Skelton, B. W.; White, A. H. *J. Organomet. Chem.* **1996**, *523*, 33.

(70) Myers, L. K.; Langhoff, C.; Thompson, M. E. *J. Am. Chem. Soc.* **1992**, *114*, 7560.

(71) Thompson, M. E.; Chiang, W.; Myers, L. K.; Langhoff, C. *Proc. SPIE-Int. Soc. Opt. Eng.* **1991**, *1497*, 423.

(72) Myers, L. K.; Ho, D. M.; Thompson, M. E.; Langhoff, C. *Polyhedron* **1995**, *14*, 57.

(73) Whittall, I. R.; Humphrey, M. G.; Samoc, M.; Swiatkiewicz, J.; Luther-Davies, B. *Organometallics* **1995**, *14*, 5493.

(74) McDonagh, A. M.; Humphrey, M. G.; Samoc, M.; Luther-Davies, B. *Organometallics* **1999**, *18*, 5195.

(75) McDonagh, A. M.; Cifuentes, M. P.; Whittall, I. R.; Humphrey, M. G.; Samoc, M.; Luther-Davies, B.; Hockless, D. C. R. *J. Organomet. Chem.* **1996**, *526*, 99.

(76) Hurst, S.; Lucas, N. T.; Humphrey, M. G.; Isoshima, T.; Wostyn, K.; Asselberghs, I.; Clays, K.; Persoons, A.; Samoc, M.; Luther-Davies, B. *Inorg. Chim. Acta.* **2003**, *350*, 62.

(77) Hurst, S.; Humphrey, M. G.; Morrall, J. P.; Cifuentes, M. P.; Samoc, M.; Luther-Davies, B.; Heath, G. A.; Willis, A. C. *J. Organomet. Chem.* **2003**, *670*, 56.

(78) Frazier, C. C.; Chauchard, E. A.; Cockerham, M. P.; Porter, P. L. *Mater. Res. Soc. Symp. Proc.* **1988**, *109*, 323.

(79) Porter, P. L.; Guha, S.; Kang, K.; Frazier, C. C. *Polymer* **1991**, *32*, 1756.

(80) Blau, W. J.; Byrne, H. J.; Cardin, D. J.; Davey, A. P. *J.Mater. Chem.* **1991**, *1*, 245.

(81) Davey, A. P.; Cardin, D. J.; Byrne, H. J.; Blau, W. J. In *Organic Molecules for Nonlinear Optics and Photonics*; Messier, J., Kajzar, F., Prasad, P., Eds.; Kluwer: Dordrecht, 1991; Vol. 194, p 391.

(82) Davey, A. P.; Page, H.; Blau, W. J. *Synthetic Metals* **1993**, *55-57*, 3980.

(83) Haub, J.; Johnson, M.; Orr, B.; Woodruff, M.; Crisp, G. In *CLEO/QEIS*: Baltimore, 1991.

(84) Guha, S.; Kang, K.; Porter, P. L.; Roach, J. F.; Remy, D. E.; Aranda, F. J.; Rao, D. V. G. *Opt. Lett.* **1992**, *17*, 264.

(85) Guha, S.; Frazier, C. C.; Chen, W. P.; Porter, P. L.; Kang, K. *Proc. SPIE-Int. Soc. Opt. Eng.* **1989**, *1105*, 14.

(86) Page, H.; Blau, W. J.; Davey, A. P.; Lou, X.; Cardin, D. J. *Synth. Met.* **1994**, *63*, 179.

(87) Frazier, C. C.; Guha, S.; Chen, W. P.; Cockerham, M. P.; Porter, P. L.; Lee, C. H. *Polymer* **1987**, *28*, 553.

(88) Guha, S.; Frazier, C. C.; Porter, P. L.; Kang, K.; Finberg, S. E. *Opt. Lett.* **1989**, *14*, 952.

(89) Whittall, I. R.; Humphrey, M. G.; Samoc, M.; Luther-Davies, B. *Angew. Chem. Int. Ed. Engl.* **1997**, *36*, 370.

(90) Vicente, J.; Chicote, M. T.; Abrisqueta, M. D.; Ramirez de Arellano, M. C.; Humphrey, M. G.; Cifuentes, M. P.; Samoc, M.; Luther-Davies, B. *Organometallics* **2000**, *19*, 2968.

(91) Teo, B. K.; Xu, Y. H.; Zhong, B. Y.; He, Y. K.; Chen, H. Y.; Qian, W.; Deng, Y. J.; Zou, Y. H. *Inorg. Chem.* **2001**, *40*, 6794.

Chapter 2

Computational Investigation into the Optical and Nonlinear Optical Properties of Group 8 Metal Acetylide Complexes

Chapter 2

Computational Investigation into the Optical and Nonlinear Optical Properties of Group 8 Metal Acetylide Complexes

---

Contents

2.1. *Introduction*

2.2. *Cyclopentadienyl Group 8 Metal Acetylide Complexes*

2.3. *Octahedral Bis(bidentate phosphino)Ruthenium Acetylide Complexes*

2.4. *Octahedral Osmium Acetylide Complexes*

2.5. *Conclusions*

2.6. *Experimental*

2.7. *References*

Chapter 2

Computational Investigation into the Optical and Nonlinear Optical Properties of Group 8 Metal Acetylide Complexes

2.1. *Introduction*

This Chapter presents the results of a series of ADF calculations on Group 8 metal acetylide complexes. Model complexes consisting of metal acetylides with a combination of chloro-, cyclopentadienyl and phosphine ligands have been examined, and the calculated optical and nonlinear optical properties compared with existing experimental data for analogous molecules.

This work has been divided into three sections. The first section involves calculations on a series of cyclopentadienyl group 8 metal acetylide complexes in order to evaluate the capacity of ADF to accurately calculate optical and nonlinear optical spectra. The second section contains the results of a study of a series of ruthenium mono- and bis- acetylide complexes, and includes attempts to characterize the optical spectra for both the neutral and oxidized states. The third section involves examination of a series of osmium acetylide complexes in order to test assumptions made in the previous section. The complexes investigated are displayed in Figure 2.1.

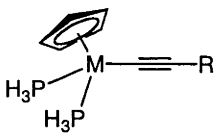

M = Fe, Ru, Os
R = H, Ph, 4-$C_6H_4NO_2$

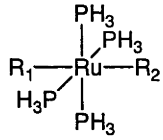

R_1 = Cl, R_2 = Cl, C≡CPh, C≡CC_6H_4-4-C≡CPh
R_1 = C≡CPh, R_2 = C≡CPh, C≡CC_6H_4-4-C≡CPh

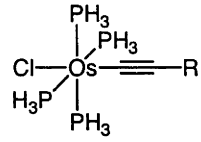

R = Ph, 4-C_6H_4C≡CPh

Figure 2.1. Model complexes studied in this work

These were chosen because of the existence of a considerable amount of experimental data for related complexes against which their various optical properties can be compared.[1-6]

As shown in the preceding Chapter, the molecular NLO properties of group 8 metal acetylides have been studied extensively in recent years. When compared with their precursor acetylenes, these complexes tend to show significantly higher thermal stability, molecular NLO properties, and structural diversity. In addition, the presence of a metal centre allows for relatively accessible multiple oxidation states.

Theoretical investigations of group 8 metal acetylide complexes are less common. DFT has been used by Stranger and co-workers to calculate ionization potentials and the degree of back-bonding in a series of cyclopentadienyl ruthenium acetylide complexes.[7] Similar work concentrating on back-bonding has been performed on (chloro)tetra(phosphine) group 8 metal acetylide complexes (Figure 2.2).[8]

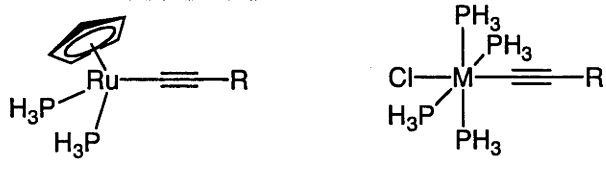

M = Fe, Ru, Os
R = H, Ph, C_6H_4-4-NO_2

Figure 2.2. Model complexes investigated by Stranger and co-workers[7,8]

2.1.1. *Density Functional Theory*

Whereas most computational chemistry techniques attempt to find numerical solutions to the Schrödinger wave equation, $H\psi = E\psi$, DFT focuses on the electron density of the system rather than the wavefunction. At the heart of DFT is the Kohn-Sham equation:

$$(-1/2\nabla^2 + V_{ext}(\mathbf{r}) + V_C(\mathbf{r}) + V_{XC}(\mathbf{r}))\varphi_i(\mathbf{r}) = \varepsilon_i\phi_i(\mathbf{r})$$

where $V_{XC}(\mathbf{r})$ is a suitable local exchange-correlation potential, $V_{ext}(\mathbf{r})$ is the external potential, $V_C(\mathbf{r})$ is the Coulombic potential of the electron cloud, ε_i is the one-electron MO, and ϕ_i is the corresponding orbital energy. Solving these equations is considerably less computationally expensive than are the corresponding *ab initio* techniques. As a consequence DFT has become a popular technique, particularly when large molecules are studied.

2.1.2. *ADF in the calculation of optical and nonlinear optical properties*

In the calculation of optical spectra and frequency-dependent hyperpolarizabilities, it is necessary to incorporate a time dependence to the Kohn-Sham equations:

$$i\delta/\delta t\ \varphi_i(\mathbf{r},t) = H\varphi_i(\mathbf{r},t) = (-\nabla^2/2 + V[\rho](\mathbf{r},t))\varphi_i(\mathbf{r},t)$$

ADF has been used to successfully calculate optical spectra in the past. Nonlinear optical spectra (specifically β values) have also been calculated, but with only partial success. The systems investigated have ranged from atoms[9] to simple molecules[9-12] to quite complex systems such as porphyrins[13-15] and transition metal complexes.[16-18] Where ADF has been used to calculate optical spectra the results generated are comparable to those from other advanced theoretical techniques, such as CCSD(T), with differences of up to 8000 cm^{-1} between experimental and calculated data being observed.[19] Results are generally comparable to sophisticated *ab initio* methods.

There are far fewer examples of the calculation of second-order hyperpolarizabilities employing ADF in the chemical literature. Some small molecules have been studied,[9,20] but a zirconium tetrapyrrole sandwich is the only moderately-sized molecule to have been examined thus far.[21] There is therefore, a need to apply ADF to a greater range of experimental data.

Baerends and co-workers calculated the first and second hyperpolarizabilities of a variety of small molecules (N_2, CO_2, CS_2, C_2H_4, NH_3, CO, HF, H_2O, and CH_4), and compared results with both experimental data and high level *ab initio* calculations.[9] TD-DFT gives a reasonable correlation to the experimental data, the differences being comparable to those seen with the *ab initio* results. The authors suggested that improvements in the exchange-correlation potentials should lead to a considerable improvement in the results. Similar calculations have been performed by the authors on helium and *p*-nitroaniline.[20]

A zirconium tetrapyrrole sandwich complex (Figure 2.3.) has been studied using the TD-DFT module of ADF by Rosa and co-workers;[21] unfortunately, because the experimental second-order hyperpolarizabilities were measured close to the resonance frequency, a clear correlation between the calculated and experimental results could not be obtained.

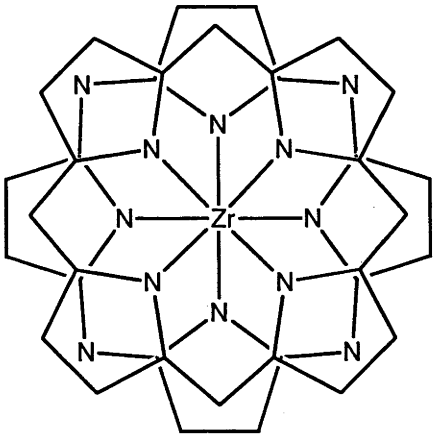

Figure 2.3. Tetrapyrrole zirconium sandwich complex investigated by Rosa and co-workers[21]

2.2. *Cyclopentadienyl Group 8 Metal Acetylide Complexes*

Recently, the effect of metal replacement on second-order hyperpolarizabilities for some cyclopentadienyl group 8 metal *p*-nitrophenylacetylide complexes has been examined.[3,5] Additionally, other cyclopentadienyl complexes have been previously synthesized by Dr Ian Whittall, and their second-order hyperpolarizabilities measured.[2,22,23] The existence of this experimental data provides a well defined basis on which to assess ADF's ability to calculate optical spectra and β hyperpolarizabilities.

Initial geometries of the model complexes (Figure 2.4.) were defined using the results from crystal structure studies. These geometries were then refined by a geometry optimization, and the resultant Cartesian coordinates were used in input files for the subsquent calculations. In examples where the acetylide ligand includes a phenyl group, the centroid of the cyclopentadienyl ring was in the plane of the phenyl ring.

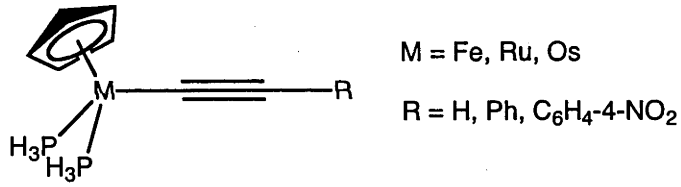

Figure 2.4. Model complexes examined in this study

2.2.1. *Geometry Optimization*

Initial geometries of the cyclopentadienyl metal acetylide complexes were refined by use of an ADF geometry optimization calculation. In order to reduce computational expense, C_s symmetry was imposed upon the molecules. This prevents the optimization calculation from breaking a mirror plane defined by the metal acetylide-cyclopentadienyl centroid.

Selected calculated bond lengths are shown in Table 2.1. The M–C, C≡C, M–P, and C–R bond lengths are tabulated (R refers to the atom adjacent to the C≡C, either C or H depending on the acetylide ligand). The M–C bonds are in the range 1.88 – 2.04 Å, and the C≡C bonds are 1.23 – 1.24 Å. The results indicate that the M–C bond strengthens and the C≡C bonds weaken as the acetylide ligand becomes more electron withdrawing.

The trends upon metal replacement are more complex. For example, the trend in C≡C bond length is Ru > Fe > Os for complexes containing a 4-nitrophenylacetylide ligand. When the phenylacetylide-containing complexes are examined, the trend changes to Fe > Ru > Os. It should be noted that the differences in bond lengths are small.

Table 2.1. Calculated bond lengths (Å)

Complex	M–C	C≡C	C–R	M–P
$Fe(C{\equiv}CH)(PH_3)_2(\eta^5\text{-}C_5H_5)$	1.90660	1.22911	1.06921	2.17577
$Fe(C{\equiv}CPh)(PH_3)_2(\eta^5\text{-}C_5H_5)$	1.89626	1.23481	1.41641	2.17872
$Fe(C{\equiv}CC_6H_4\text{-}4\text{-}NO_2)(PH_3)_2(\eta^5\text{-}C_5H_5)$	1.87750	1.23751	1.40610	2.18511
$Ru(C{\equiv}CH)(PH_3)_2(\eta^5\text{-}C_5H_5)$	2.04206	1.22968	1.06895	2.28696
$Ru(C{\equiv}CPh)(PH_3)_2(\eta^5\text{-}C_5H_5)$	2.00306	1.23442	1.41410	2.28224
$Ru(C{\equiv}CC_6H_4\text{-}4\text{-}NO_2)(PH_3)_2(\eta^5\text{-}C_5H_5)$	1.98825	1.23762	1.40336	2.28889
$Os(C{\equiv}CH)(PH_3)_2(\eta^5\text{-}C_5H_5)$	2.02130	1.22807	1.06941	2.28355
$Os(C{\equiv}CPh)(PH_3)_2(\eta^5\text{-}C_5H_5)$	2.0028	1.23152	1.41326	2.27949
$Os(C{\equiv}CC_6H_4\text{-}4\text{-}NO_2)(PH_3)_2(\eta^5\text{-}C_5H_5)$	1.90417	1.23515	1.40297	2.28664

These calculated bond lengths can be compared against experimental data derived from crystallography. Humphrey and co-workers have synthesized a number of ruthenium acetylide complexes, similar to the model complexes used in this study.[1,5,24] Some important experimental bond lengths are tabulated in Table 2.2, with M–C bonds in the range 1.99 – 2.02 Å and C≡C bonds varying as 1.20 – 1.23 Å. These results show good agreement with the calculated values (the calculated bond lengths are 1.99 – 2.04 Å and 1.23 – 1.24 Å for the Ru–C and C≡C bonds, respectively); however, it is impossible to determine if the trends in the calculated values are replicated in the crystallographic results, due to limited data and the inherent uncertainties.

Table 2.2. Crystallographic bond lengths (Å)				
Complex	M–C	C≡C	C–C	Reference
$Ru(C{\equiv}CPh)(PPh_3)_2(\eta^5\text{-}C_5H_5)$	2.017(5)	1.214(7)	1.462(8)	24
$Ru(C{\equiv}CPh)(PMe_3)_2(\eta^5\text{-}C_5H_5)$	1.989(7)	1.224(10)	1.430(9)	1
$Ru(C{\equiv}CC_6H_4\text{-}4\text{-}NO_2)(PPh_3)_2(\eta^5\text{-}C_5H_5)$	1.994(5)	1.202(8)	1.432(7)	1
$Ru(C{\equiv}CC_6H_4\text{-}4\text{-}NO_2)(PMe_3)_2(\eta^5\text{-}C_5H_5)$	1.99(2)	1.23(2)	1.43(3)	1
$Ru(C{\equiv}CC_6H_4\text{-}4\text{-}NO_2)(dppe)(\eta^5\text{-}C_5H_5)$	1.993(3)	1.214(4)	1.424(4)	3

Calculated dipole moments are tabulated in Table 2.3. Two trends are immediately obvious: the dipole moment increases upon metal variation as Fe < Ru < Os, and upon acetylide ligand variation as $C{\equiv}CH < C{\equiv}CPh < C{\equiv}CC_6H_4NO_2$. Both trends are expected: the dipole should increase on increasing the strength of the electron withdrawing group, and on increasing ease of polarization of the transition metal atom.

Table 2.3. Calculated dipole moments	
Complex	Dipole (D)
$Fe(C{\equiv}CH)(PH_3)_2(\eta^5\text{-}C_5H_5)$	3.011
$Fe(C{\equiv}CPh)(PH_3)_2(\eta^5\text{-}C_5H_5)$	4.263
$Fe(C{\equiv}CC_6H_4\text{-}4\text{-}NO_2)(PH_3)_2(\eta^5\text{-}C_5H_5)$	12.455
$Ru(C{\equiv}CH)(PH_3)_2(\eta^5\text{-}C_5H_5)$	3.293
$Ru(C{\equiv}CPh)(PH_3)_2(\eta^5\text{-}C_5H_5)$	5.018
$Ru(C{\equiv}CC_6H_4\text{-}4\text{-}NO_2)(PH_3)_2(\eta^5\text{-}C_5H_5)$	12.709
$Os(C{\equiv}CH)(PH_3)_2(\eta^5\text{-}C_5H_5)$	3.452
$Os(C{\equiv}CPh)(PH_3)_2(\eta^5\text{-}C_5H_5)$	5.881
$Os(C{\equiv}CC_6H_4\text{-}4\text{-}NO_2)(PH_3)_2(\eta^5\text{-}C_5H_5)$	13.698

2.2.2. *Back-Bonding*

The role of back-bonding in metal acetylide complexes has been of recent interest. There is very little information on back-bonding available from structural data, as the C≡C bond is relatively insensitive to changes in the π and π* orbitals resulting in most C≡C bond lengths falling within a narrow range. While the M–C bond length is considerably more variable, it is dominated by the σ bonding contribution and thus does not readily provide information on the presence and strength of back-bonding in a metal acetylide complex. IR spectroscopy can potentially provide valuable information on the strength of back-bonding (the presence of back-bonding should lead to a decrease in the C≡C stretching frequency), but the presence of coupling reduces the utility of this technique as an effective means of measuring the strength of back-bonding. This has resulted in most useful studies into back-bonding of metal acetylides being performed either computationally or with photoelectron spectroscopy.

Lichtenberger and co-workers have used photoelectron spectroscopy to study the MOs of iron acetylide complexes.[25-28] They found that the acetylide ligand is a stronger π donor and a weaker π acceptor than is a CO ligand. This is consistent with metal-acetylide complexes involving considerably less back-bonding than metal carbonyl complexes. A further computational investigation into back-bonding, involving titanium acetylide complexes, and using *ab initio* techniques, found that the titanium d orbitals are too far removed from both the acetylide π bonding and anti-bonding orbitals for effective interaction with either; Ti acetylide complexes can therefore be said to be π neutral.[29]

Interestingly, there are some physical measurements that suggest the presence of back-bonding in transition metal acetylide complexes. The electronic spectra of $W(C{\equiv}CR)(\equiv CH)(dmpe_2)$[30] and the ^{57}Fe Mössbauer spectra of $[Fe(C{\equiv}CR)_6]^{4-}$ [31] have been interpreted as indicating significant back-bonding. Both of these systems involved molecules that are more electron rich than the molecules studied by Lichtenberger and co-workers,[25-28] suggesting that in electron-rich systems, back-bonding becomes more prevalent. Back-bonding in metal acetylide complexes has been examined computationally

with ADF recently,[7,8] both studies finding significant back-bonding which increases in importance upon proceeding to a more strongly electron-withdrawing acetylide ligand.

The current series of compounds affords an opportunity to investigate the effects on MOs and hence back-bonding of descending a group and proceding to a more electron withdrawing acetylide ligand. The presence of back-bonding in metal acetylide complexes is particularly interesting, as there has been a suggestion that the increasing M–C multiple bond character increases quadratic hyperpolarizabilities.[32]

Stranger *et al* have constructed simple MO diagrams showing the bonding between an acetylide ligand and a group 8 metal centre, but these diagrams are simplified by only considering the acetylide C≡CH.[7,8] An additional complication is introduced with the π bonding and anti-bonding orbitals of the phenyl group. Because strongly electron withdrawing ligand such as $C{\equiv}CC_6H_4\text{-}4\text{-}NO_2$ will cause significant back-bonding, the MO diagram of $Fe(C{\equiv}CC_6H_4\text{-}4\text{-}NO_2)(PH_3)_2(\eta^5\text{-}C_5H_5)$ is considerably more complex than that obtained for the C≡CH analogue.

Figure 2.5. presents a MO diagram for $Fe(C{\equiv}CC_6H_4\text{-}4\text{-}NO_2)(PH_3)_2(\eta^5\text{-}C_5H_5)$. The square pyramidal $Fe(PH_3)_2(\eta^5\text{-}C_5H_5)$ fragment (in which the $\eta^5\text{-}C_5H_5$ ligand occupies three facially-disposed coordination sites) and the planar $C{\equiv}C\,C_6H_4\text{-}4\text{-}NO_2$ ligand interact strongly via overlap of the singly-occupied 15a' orbital of the former (essentially d_{z2} in character) with the singly occupied 18a' orbital of the latter (an sp-hybridized σ orbital). For the $Fe(PH_3)_2(\eta^5\text{-}C_5H_5)$ unit, 13a' and 11a'' (essentially d_{xy} and d_{x2-y2} in character, respectively) are non-bonding, transforming to 34a' and 18a'' in the alkynyl complex. Orbitals 14a' and 10a'' of the ligated metal unit (comprised, principally, of d_{xz} and d_{yz} contributions) have π symmetry with respect to the alkynyl-metal axis, and interact with filled arylalkynyl π orbitals (3a'', 19a', 6a'') in a destabilizing manner and with vacant π orbitals (7a'', 9a'', 22a', 10a'') in a stabilizing manner.

As Figure 2.5. demonstrates, a number of acetylide virtual orbitals (9a'', 22a' and 10a'') interact with iron d orbitals in a back-bonding fashion. Because of the number of virtual orbitals involved in back-bonding, it is difficult to quantify the amount of back-bonding, but the MO diagram clearly shows that it is significant.

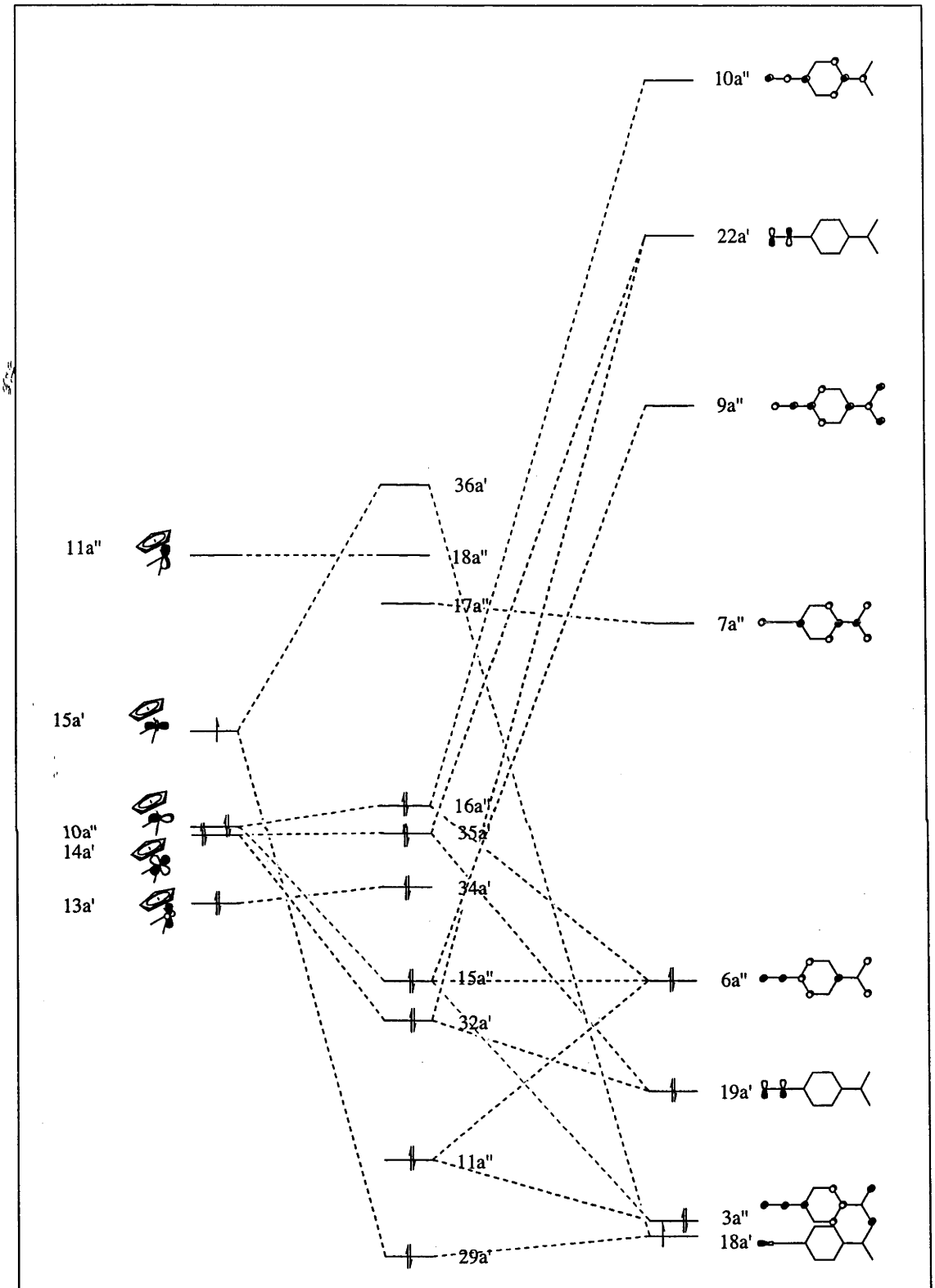

Figure 2.5. MO diagram for $Fe(C{\equiv}CC_6H_4\text{-}4\text{-}NO_2)(PH_3)_2(\eta^5\text{-}C_5H_5)$.

2.2.3. *Optical Spectra*

Calculated optical transitions of the *p*-nitrophenylacetylide-containing complexes and experimental data for comparison are tabulated in Table 2.4. The correlation between the calculated and observed ν_{max} metal-to-ligand charge-transfer bands is extremely good, given the replacement of dppe by PH_3 and the absence of solvent effects for the former. The largest difference is approximately 3000 cm^{-1}, significantly less than the 8000 cm^{-1} differences which are sometimes observed in the literature. The differences in the phenyl → phenyl* transitions are greater, an unsurprising result, given the replacement of dppe with PH_3 in the model complexes.

2.2.4. *Nonlinear Optical Properties*

Molecular second-order hyperpolarizabilities can be directly calculated by ADF's RESPONSE module. This module is particularly useful as it determines all of the components of the β tensor. The static and frequency dependent (1064 nm) tensorial components of the molecular second-order hyperpolarizabilities have been calculated and the results tabulated (Tables 2.5. and 2.6. respectively).

The quadratic hyperpolarizabilities of the model complexes consist of 14 non-zero components. The static hyperpolarizability tensor components contain a significant number of identical components. For example, β_{xxy} always has the same value as β_{xyx} and β_{yxx}. The number of non-identical components increases when the hyperpolarizabilities at 1064 nm are examined; whereas the static hyperpolarizabilities consist of six non-identical components, the 1064 nm tensors have ten non-identical components.

Table 2.4. Calculated and experimental optical spectra of $M(C{\equiv}CC_6H_4\text{-}4\text{-}NO_2)(PH_3)_2(\eta^5\text{-}C_5H_5)$

Complex	ν_{max}, cm^{-1} (expt) *a*	ε, M^{-1} cm^{-1} (expt) *a*	ν_{max}, cm^{-1} (calc) *b*	f (calc) *b*	Transition
$Fe(C{\equiv}CC_6H_4\text{-}4\text{-}NO_2)(PH_3)_2(\eta^5\text{-}C_5H_5)$	20 000	13 000	18 000	0.36	MLCT
	31 490	9800	28 700	0.25	Phenyl → Phenyl*
$Ru(C{\equiv}CC_6H_4\text{-}4\text{-}NO_2)(PH_3)_2(\eta^5\text{-}C_5H_5)$	22 200	18 000	19 000	0.45	MLCT
	33 700	8800	32 400	0.18	Phenyl → Phenyl*
$Os(C{\equiv}CC_6H_4\text{-}4\text{-}NO_2)(PH_3)_2(\eta^5\text{-}C_5H_5)$	21 600	17 000	20 100	0.49	MLCT
	36 800	10 400	30 800	0.18	Phenyl → Phenyl*

a Experimental results are taken from $M(C{\equiv}CC_6H_4\text{-}4\text{-}NO_2)(dppe)(\eta^5\text{-}C_5H_5)$[5]

b All other calculated transitions are at least two orders of magnitude lower in oscillator strength

Table 2.5. Calculated tensorial static hyperpolarizabilities

M =	Fe			Ru			Os		
R =	H	Ph	C_6H_4-4-NO_2	H	Ph	C_6H_4-4-NO_2	H	Ph	C_6H_4-4-NO_2
β_{xxx}	-0.60	12.61	70.31	-0.36	12.89	67.75	-0.26	13.73	67.73
β_{xxy}	0.64	11.81	58.27	0.83	11.63	54.95	0.75	12.56	56.85
β_{xxz}	0.00	0.00	0.00	0.00	0.00	0.00	0.00	0.00	0.00
β_{xyx}	0.64	11.81	58.27	0.83	11.63	54.95	0.75	12.56	56.85
β_{xyy}	-0.35	8.49	43.56	-0.65	7.22	39.20	-0.96	6.84	39.25
β_{xyz}	0.00	0.00	0.00	0.00	0.00	0.00	0.00	0.00	0.00
β_{xzx}	0.00	0.00	0.00	0.00	0.00	0.00	0.00	0.00	0.00
β_{xzy}	0.00	0.00	0.00	0.00	0.00	0.00	0.00	0.00	0.00
β_{xzz}	-1.48	-2.39	-2.97	-1.49	-2.41	-2.97	-1.66	-3.17	-3.79
β_{yxx}	0.64	11.81	58.27	0.83	11.63	54.95	0.75	12.56	56.85
β_{yxy}	-0.35	8.49	43.56	-0.65	7.22	39.20	-0.96	6.84	39.25
β_{yxz}	0.00	0.00	0.00	0.00	0.00	0.00	0.00	0.00	0.00
β_{yyx}	-0.35	8.49	43.56	-0.65	7.22	39.20	-0.96	6.84	39.25
β_{yyy}	1.87	7.97	32.64	2.88	8.01	29.81	0.62	4.45	26.07
β_{yyz}	0.00	0.00	0.00	0.00	0.00	0.00	0.00	0.00	0.00
β_{yzx}	0.00	0.00	0.00	0.00	0.00	0.00	0.00	0.00	0.00
β_{yzy}	0.00	0.00	0.00	0.00	0.00	0.00	0.00	0.00	0.00
β_{yzz}	1.49	0.46	-0.14	1.99	0.96	0.38	2.13	0.94	0.28
β_{zxx}	0.00	0.00	0.00	0.00	0.00	0.00	0.00	0.00	0.00
β_{zxy}	0.00	0.00	0.00	0.00	0.00	0.00	0.00	0.00	0.00
β_{zxz}	-1.48	-2.39	-2.97	-1.49	-2.41	-2.97	-1.66	-3.17	-3.79
β_{zyx}	0.00	0.00	0.00	0.00	0.00	0.00	0.00	0.00	0.00
β_{zyy}	0.00	0.00	0.00	0.00	0.00	0.00	0.00	0.00	0.00
β_{zyz}	1.49	0.46	-0.14	1.99	0.96	0.38	2.13	0.94	0.28
β_{zzx}	-1.48	-2.39	-2.97	-1.49	-2.41	-2.97	-1.66	-3.17	-3.79
β_{zzy}	1.49	0.46	-0.14	1.99	0.96	0.38	2.13	0.94	0.28
β_{zzz}	0.00	0.00	0.00	0.00	0.00	0.00	0.00	0.00	0.00

All values are in units of 10^{-30} esu

Table 2.6. Calculated tensorial SHG hyperpolarizabilities at 1064 nm

M =	Fe			Ru			Os		
R =	H	Ph	C_6H_4-4-NO_2	H	Ph	C_6H_4-4-NO_2	H	Ph	C_6H_4-4-NO_2
β_{xxx}	-1.50	31.67	1134.97	-0.75	24.93	1579.45	-0.68	26.73	1211.51
β_{xxy}	1.65	26.37	-912.85	1.14	24.06	1206.78	0.86	24.16	925.18
β_{xxz}	0.00	0.00	0.00	0.00	0.00	0.00	0.00	0.00	0.00
β_{xyx}	1.65	26.37	-912.85	1.14	24.06	1206.78	0.86	24.16	925.18
β_{xyy}	-0.14	18.53	-697.66	-0.82	16.17	879.30	-1.32	14.06	659.00
β_{xyz}	0.00	0.00	0.00	0.00	0.00	0.00	0.00	0.00	0.00
β_{xzx}	0.00	0.00	0.00	0.00	0.00	0.00	0.00	0.00	0.00
β_{xzy}	0.00	0.00	0.00	0.00	0.00	0.00	0.00	0.00	0.00
β_{xzz}	-2.71	-3.18	15.73	-1.97	-4.11	-19.05	-2.14	-4.94	-17.78
β_{yxx}	4.71	22.35	-675.05	1.70	26.44	1173.59	1.09	24.31	903.52
β_{yxy}	-5.46	28.09	-674.46	-1.43	14.02	891.86	-1.38	14.74	679.80
β_{yxz}	0.00	0.00	0.00	0.00	0.00	0.00	0.00	0.00	0.00
β_{yyx}	-5.46	28.09	-674.46	-1.43	14.02	891.86	-1.38	24.16	679.80
β_{yyy}	0.66	26.97	-561.64	3.41	12.09	650.62	0.51	9.07	481.92
β_{yyz}	0.00	0.00	0.00	0.00	0.00	0.00	0.00	0.00	0.00
β_{yzx}	0.00	0.00	0.00	0.00	0.00	0.00	0.00	0.00	0.00
β_{yzy}	0.00	0.00	0.00	0.00	0.00	0.00	0.00	0.00	0.00
β_{yzz}	7.39	-2.97	44.40	3.18	2.01	-10.05	2.83	0.81	-9.12
β_{zxx}	0.00	0.00	0.00	0.00	0.00	0.00	0.00	0.00	0.00
β_{zxy}	0.00	0.00	0.00	0.00	0.00	0.00	0.00	0.00	0.00
β_{zxz}	-2.20	-4.04	-4.60	-1.97	-3.38	-4.22	-2.13	-4.25	-5.68
β_{zyx}	0.00	0.00	0.00	0.00	0.00	0.00	0.00	0.00	0.00
β_{zyy}	0.00	0.00	0.00	0.00	0.00	0.00	0.00	0.00	0.00
β_{zyz}	2.05	0.32	-0.53	2.61	1.16	0.23	2.68	1.07	-0.36
β_{zzx}	-2.20	-4.04	-4.60	-1.97	-3.38	-4.22	-2.13	-4.25	-5.68
β_{zzy}	2.05	0.32	-0.53	2.61	1.16	0.23	2.68	1.07	-0.36
β_{zzz}	0.00	0.00	0.00	0.00	0.00	0.00	0.00	0.00	0.00

All values are in units of 10^{-30} esu

Very few experimental techniques afford the tensorial components of the quadratic hyperpolarizability, so the results from Tables 2.5. and 2.6.. have been converted to the overall β values. These values are tabulated in Table 2.7., and displayed graphically in Figures 2.6. and 2.7.

Table 2.7. Calculated static and 1064 nm molecular second-order hyperpolarizabilities

Compound	β_0	β_{SHG}
$[Fe(C{\equiv}CH)(PH_3)_2(\eta^5\text{-}C_5H_5)]$	3.81	13.04
$[Fe(C{\equiv}CPh)(PH_3)_2(\eta^5\text{-}C_5H_5)]$	29.58	74.79
$[Fe(C{\equiv}CC_6H_4\text{-}4\text{-}NO_2)(PH_3)_2(\eta^5\text{-}C_5H_5)]$	148.03	2263.77
$[Ru(C{\equiv}CH)(PH_3)_2(\eta^5\text{-}C_5H_5)]$	5.50	7.60
$[Ru(C{\equiv}CPh)(PH_3)_2(\eta^5\text{-}C_5H_5)]$	28.51	57.67
$[Ru(C{\equiv}CC_6H_4\text{-}4\text{-}NO_2)(PH_3)_2(\eta^5\text{-}C_5H_5)]$	138.47	3093.93
$[Os(C{\equiv}CH)(PH_3)_2(\eta^5\text{-}C_5H_5)]$	5.18	6.71
$[Os(C{\equiv}CPh)(PH_3)_2(\eta^5\text{-}C_5H_5)]$	29.24	61.06
$[Os(C{\equiv}CC_6H_4\text{-}4\text{-}NO_2)(PH_3)_2(\eta^5\text{-}C_5H_5)]$	140.10	2263.88

All values are in units of 10^{-30} esu.

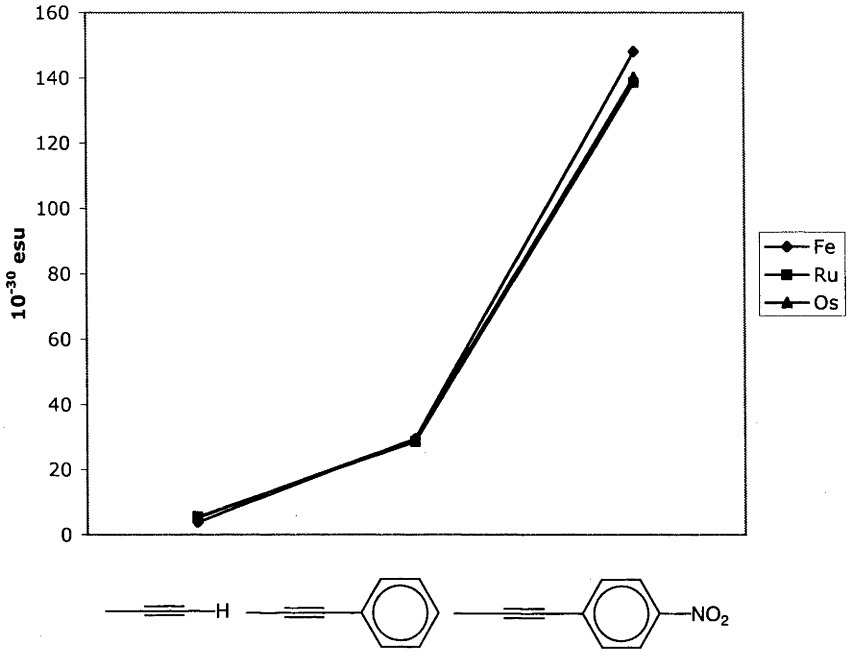

Figure 2.6. Calculated static hyperpolarizabilities. Legend refers to the metal in the formula $[M(C{\equiv}CR)(PH_3)_2(\eta^5\text{-}C_5H_5)]$

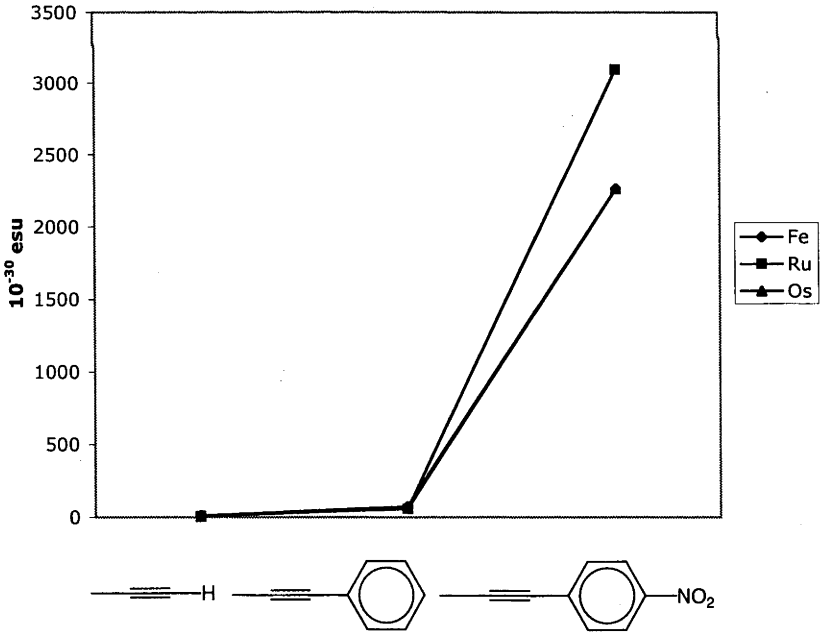

Figure 2.7. Calculated hyperpolarizabilities at 1064 nm. Legend refers to the metal in the formula $[M(C{\equiv}CR)(PH_3)_2(\eta^5\text{-}C_5H_5)]$

These results present a clear trend across all metal centers: there is a significant increase in quadratic nonlinearity as the acetylide ligand proceeds from C≡CH to C≡CPh and then to $C{\equiv}CC_6H_4$-4-NO_2. The effect of metal variation, in moving from iron to ruthenium and then to osmium, is less clear, showing considerable dependence on the acetylide and the frequency-dependence of the nonlinearity.

The experimentally derived molecular second-order nonlinearities (both frequency independent and at 1064 nm) for a number of complexes are presented in Table 2.8. This data can be contrasted with the calculated second-order hyperpolarizabilities in two ways: the absolute numbers can be compared, and the trends in the data. In addition to the aforementioned (cyclopentadienyl)bis(phosphine) transition metal acetylide complexes, the data for a series of chiral bis(chiral-at-phosphorus bidentate phosphine) containing transition metal acetylides complexes have been included. While these results can not be compared with the calculated hyperpolarizabilities directly, they demonstrate the trend in hyperpolarizabilities upon metal replacement.

A comparision of the data presented indicates discrepency between the absolute calculated and experimental hyperpolarizabilities. The experimental observed trend of Fe < Ru ≤ Os is not reproduced with the calculated data. Because there was no apparent correlation between calculated and experimental results, it appears that ADF is not an useful tool for the investigation of hyperpolarizabilities in transition metal acetylide systems.

Table 2.8. Experimental results

Compound	λ_{max} (nm)	ε (10^4 M^{-1} cm^{-1})	β_{HRS} (10^{-30} esu)	β_0 (10^{-30} esu)	Reference
$Fe(C{\equiv}CC_6H_4\text{-}4\text{-}NO_2)(dppe)(\eta^5\text{-}C_5H_5)$	498	1.3	665	64	5
$Ru(C{\equiv}CC_6H_4\text{-}4\text{-}NO_2)(dppe)(\eta^5\text{-}C_5H_5)$	447	1.8	664	161	5
$Os(C{\equiv}CC_6H_4\text{-}4\text{-}NO_2)(dppe)(\eta^5\text{-}C_5H_5)$	461	1.7	929	188	5
$(-)_{436}$-*trans*-$Fe(C{\equiv}CC_6H_4\text{-}4\text{-}NO_2)Cl\{(R,R)\text{-diph}\}_2$	543	1.7	440	-14	3
$(-)_{589}$-*trans*-$Ru(C{\equiv}CC_6H_4\text{-}4\text{-}NO_2)Cl\{(R,R)\text{-diph}\}_2$	467	2.1	528	97	3
$(-)_{365}$-*trans*-$Os(C{\equiv}CC_6H_4\text{-}4\text{-}NO_2)Cl\{(R,R)\text{-diph}\}_2$	490	1.8	620	74	3
$Ru(C{\equiv}CC_6H_4\text{-}4\text{-}NO_2)(PPh_3)_2(\eta^5\text{-}C_5H_5)$	460	1.1	468	96	5
$Os(C{\equiv}CC_6H_4\text{-}4\text{-}NO_2)(PPh_3)_2(\eta^5\text{-}C_5H_5)$	474	2.2	1051	174	5

diph ≡ 1,2-bis(methylphenylphosphino)benzene

2.3. *Octahedral Bis(bidentate phosphino)Ruthenium Acetylide Complexes*

Recently a series of octahedral ruthenium mono- and bis- acetylide complexes have been synthesized and their UV-vis-NIR spectroelectrochemistry examined.[33] The spectra are particularly interesting because of the appearance of an intense low-energy NIR band upon oxidation (Figure 2.8.). This band occurs at technologically-important wavelengths (this will be expanded upon in Chapter 3). Additionally, these compounds can be visualised as model complexes of the larger dendritic complexes. In order to fully characterize the optical spectra of both the neutral and oxidized complexes (focussing, in particular, on the strong NIR band), a TD-DFT computational investigation has been performed.

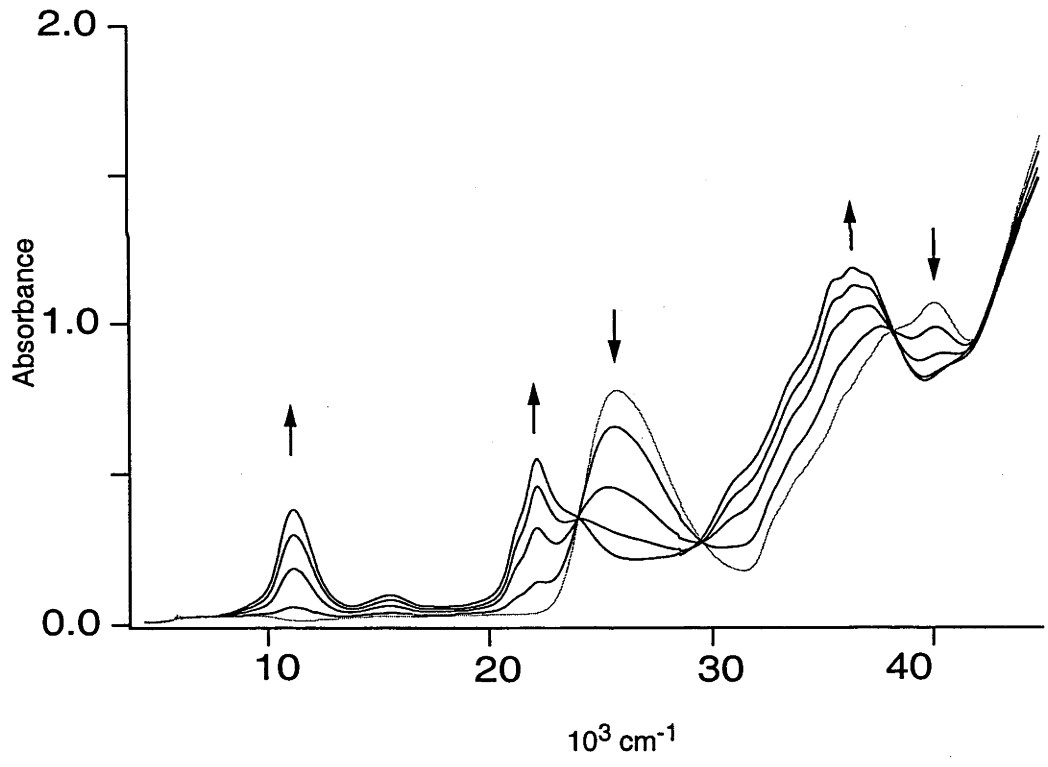

Figure 2.8. UV-vis-NIR spectral changes during electrochemical oxidation of *trans*-[Ru(C≡CC_6H_4-4-C≡CPh)Cl(dppe)$_2$]

(M.P. Cifuentes)

2.3.1. *Geometry Optimatization*

ADF geometry optimatization calculations were performed on the model complexes (Figure 2.9.) and the bond lengths of the neutral species are shown in Figure 2.10. As can be seen, the bond lengths are reasonably similar. The Ru–C bonds range from 2.03 to 2.10 Å with the mono-acetylide complexes, *trans*-[RuCl(C≡CPh)(PH_3)$_4$] and *trans*-[RuCl(C≡CC_6H_4-4-C≡CPh)(PH_3)$_4$], being at the lower end of the range and the bis-acetylide complexes, *trans*-[Ru(C≡CPh)$_2$(PH_3)$_4$] and *trans*-[Ru(C≡CPh)(C≡CC_6H_4-4-C≡CPh)(PH_3)$_4$], being slightly longer. The bis-chloride complex, *trans*-[$RuCl_2$(PH_3)$_4$], has a Ru–Cl bond length of 2.50 Å. The C≡C bonds adjacent to the ruthenium are all approximately 1.24 Å in length. The C≡C bonds furthest from the ruthenium atom on *trans*-[RuCl(C≡CC_6H_4-4-C≡CPh)(PH_3)$_4$] and *trans*-[Ru(C≡CPh)(C≡CC_6H_4-4-C≡CPh)(PH_3)$_4$] are shorter, approximately 1.22 Å.

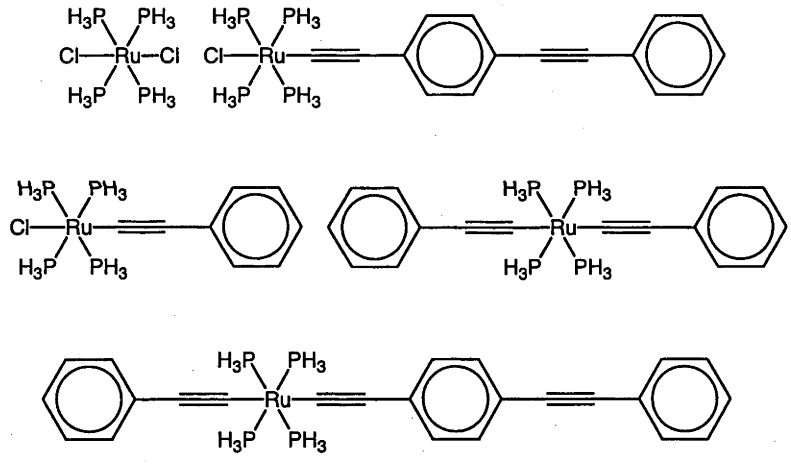

Figure 2.9. Model complexes investigated in this study

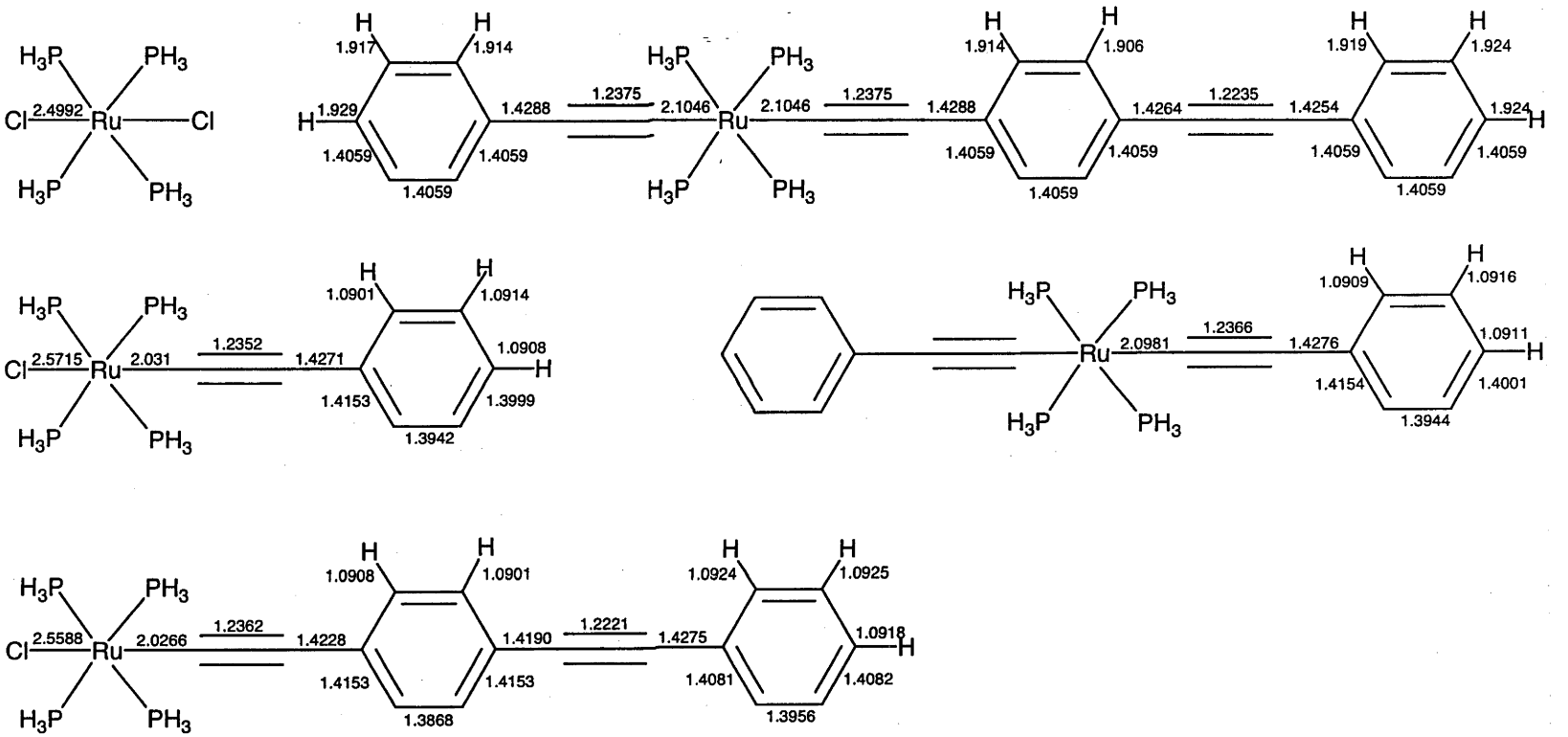

Figure 2.10. Calculated bond lengths (Å) for ruthenium acetylide complexes

Lewis and co-workers have collected crystallographic data on *trans*-[RuCl(C≡CPh)(dppe)$_2$] and *trans*-[Ru(C≡CPh)$_2$(dppe)$_2$].[34,35] The mono-acetylide complex has a Ru–C bond length of 2.007(5) Å, and a C≡C bond length of 1.198(7) Å. Conversely, the bis-acetylide complex shows Ru–C bond lengths of 2.061(5) and 2.064(5), and C≡C bond lengths of 1.207(7) and 1.194(7) Å.

Because of the symmetry imposed upon the metal complexes and their rigid rod conformation, the bond angles only show minor deviations from idealized geometries. These small deviations are due to electronic and steric effects.

Upon oxidation, the changes in geometry are rather minor: the C≡C bond is lengthened and the Ru–C and C–C bonds are shortened. These changes in bond lengths are shown in Table 2.9 and can be readily explained by considering the orbital which loses the electron (the HOMO). Figure 2.11. displays the HOMO of *trans*-[Ru(C≡CPh)Cl(PH$_3$)$_4$]. This orbital is delocalized across the ruthenium d_{xy} orbital and a phenylacetylide π-orbital. The orbital contains nodes at the Ru–C and C–C bonds. In the case of mono-acetylide complexes, there is also a node at the Ru–Cl bond. It is therefore expected that loss of electron density from this orbital should lead to a strengthening of the Ru–C and C–C bonds and, conversely, the C≡C bond is expected to weaken.

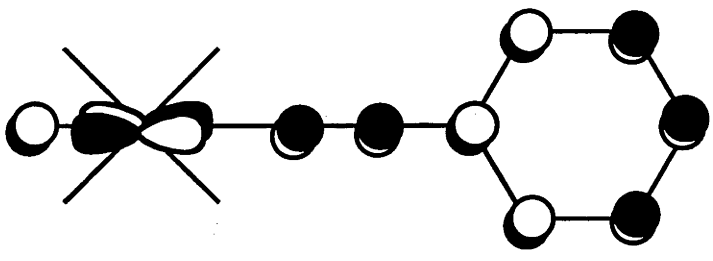

Figure 2.11. HOMO of *trans*-[Ru(C≡CPh)Cl(PH$_3$)$_4$]

Table 2.9. Changes in bond lengths upon oxidation[a]

Complex	C≡CPh			C≡CC$_6$H$_4$-4-C≡CPh			
	Ru–C	C≡C	C–C	Ru–C	C≡C	C–C	Ru–Cl
trans-[RuCl$_2$(dppe)$_2$]							-0.1148
trans-[RuCl(C≡CPh)(dppe)$_2$]	-0.0667	0.0179	-0.0221				-0.0799
trans-[RuCl(C≡CC$_6$H$_4$C≡CPh)(PH$_3$)$_4$]				-0.0544	0.0154	-0.0233	-0.0558
trans-[Ru(C≡CPh)$_2$(dppe)$_2$]	-0.0444	0.0108	-0.0138				
trans-[Ru(C≡CPh)(C≡CC$_6$H$_4$C≡CPh)(PH$_3$)$_4$]	-0.0364	0.0082	-0.0105	-0.0364	0.0082	-0.0104	

[a] All bond lengths are in Å. Change in bond length = bond length of oxidized complex – bond length of neutral complex

2.3.2. *Optical Spectra*

The coordinate system used in the geometry optimizations was maintained for subsequent calculations of optical excitation energies. The frequencies and oscillator strengths from TD-DFT calculations are summarized below (Tables 2.10. to 2.12.), together with assignment of the most important contributions to the optical transitions (note: the considerable mixing of Ru d orbitals with alkynyl and/or chloro orbitals has been ignored to retain descriptive utility). Also shown below are diagrams comparing the measured optical spectra and the calculated optical transitions (Figures 2.12. to 2.16.). As the calculated oscillator strength (f) is not directly comparable to the extinction coefficient,* the height of the oscillator strength bars relative to the absorbance is arbitrary.

2.3.2.1. *trans*-$[RuCl_2(PH_3)_4]$

Figure 2.12. presents the UV-vis-NIR absorption spectrum of *trans*-$[RuCl_2(dppe)_2]$ along with the calculated absorption transitions of *trans*-$[RuCl_2(PH_3)_4]$. Table 2.10. details the exact optical transitions. It is important to note that phenyl → phenyl* transitions have not been calculated because the phenyl groups have been removed to simplify the calculations.

These calculations indicate that the main absorption band consists of transfer of electron density from a Cl p orbital to a molecular orbital consisting of Ru d_{yz} and phosphine

---

* The oscillator strength for a transition between two energy levels i and j, f_{ij}, is defined as:

$f_{ij} = 8\pi^2 mc\nu GR_{ij}^2/3h$

where m is the mass of an electron, c is the speed of light, ν is the frequency, G is the degeneracy of the final state, R_{ij} is the transition length, and h is Planck's constant.

Experimentally, f_{ij} is determined by integration of the absorption band, given by the equation:

$f_{ij} = (k/n)\int\varepsilon(\sigma)d\sigma$

where $\varepsilon(\sigma)$ is the molar absorption coefficient at wavelength σ, n is the average refractive index of the medium, and $k = 4.32 \times 10^{-9}$ L^{-1} mol cm^{-1}.

character (LMCT). The difference between the experimentally observed ν_{max} and the calculated ν_{max} is very small (<2000 cm^{-1}).

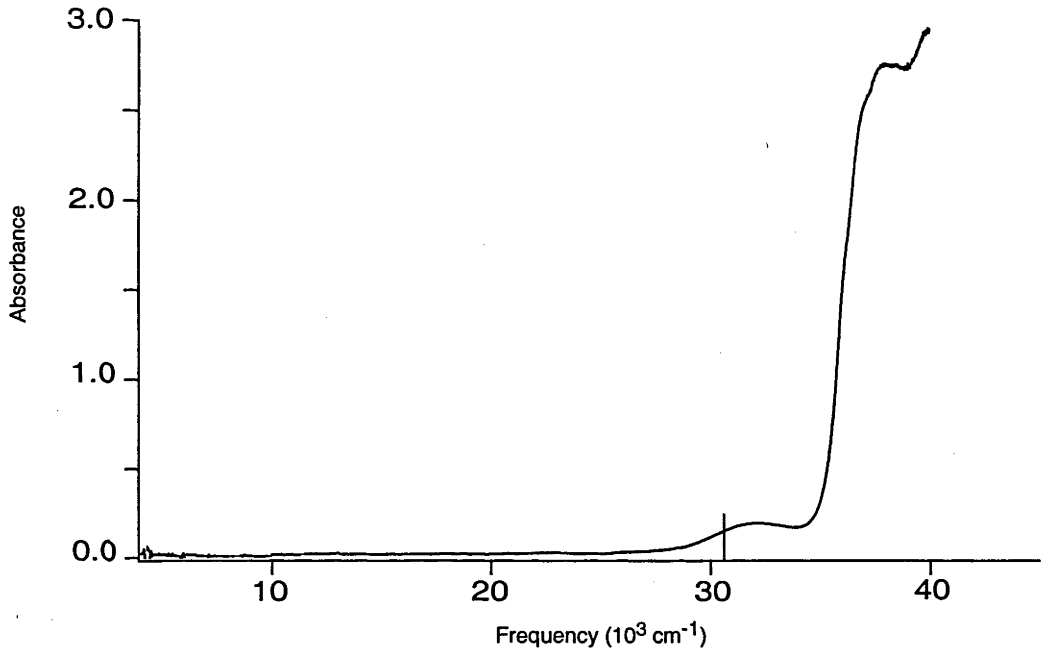

Figure 2.12. UV-vis-NIR absorption spectra of *trans*-$[RuCl_2(dppe)_2]$ and the calculated absorption transitions of *trans*-$[RuCl_2(PH_3)_4]$ (vertical line)

Table 2.10. Calculated optical transitions for *trans*-$[RuCl_2(PH_3)_4]$ and relevant experimental data for *trans*-$[RuCl_2(dppe)_2]$

ν_{max} [ε] (expt) [a]	ε (expt) [a]	ν_{max} (calc) [a]	f (calc)	Composition	Major Assignment
22 660	0.04	28 630	7.3×10^{-4}	$10a_1 \rightarrow 11a_1$	Cl $p_z \rightarrow$ Ru d_{x2-y2} + Ru d_{z2}
		29 520	2.2×10^{-5}	$6b_1 \rightarrow 7b_1$	Ru d_{xz} + Cl $\rightarrow PH_3$
32 170	0.6	30 250	0.018	$7b_2 \rightarrow 8b_2$	Cl $p_y \rightarrow$ Ru d_{yz} + PH_3
38 006	sh, 5.7	*b*			Phenyl $\rightarrow$ Phenyl*
39 939	6.1	*b*			Phenyl $\rightarrow$ Phenyl*

[a] ν_{max} in cm^{-1}, ε in 10^4 M^{-1} cm^{-1}

[b] Not applicable

2.3.2.2. *Trans*-[Ru(C≡CPh)Cl(PH$_3$)$_4$]

Figure 2.13. presents the UV-vis-NIR absorption spectrum of *trans*-[Ru(C≡CPh)Cl(dppe)$_2$] and the calculated optical transitions of *trans*-[Ru(C≡CPh)Cl(PH$_3$)$_4$]. Table 2.11. gives further details on the composition of these optical transitions.

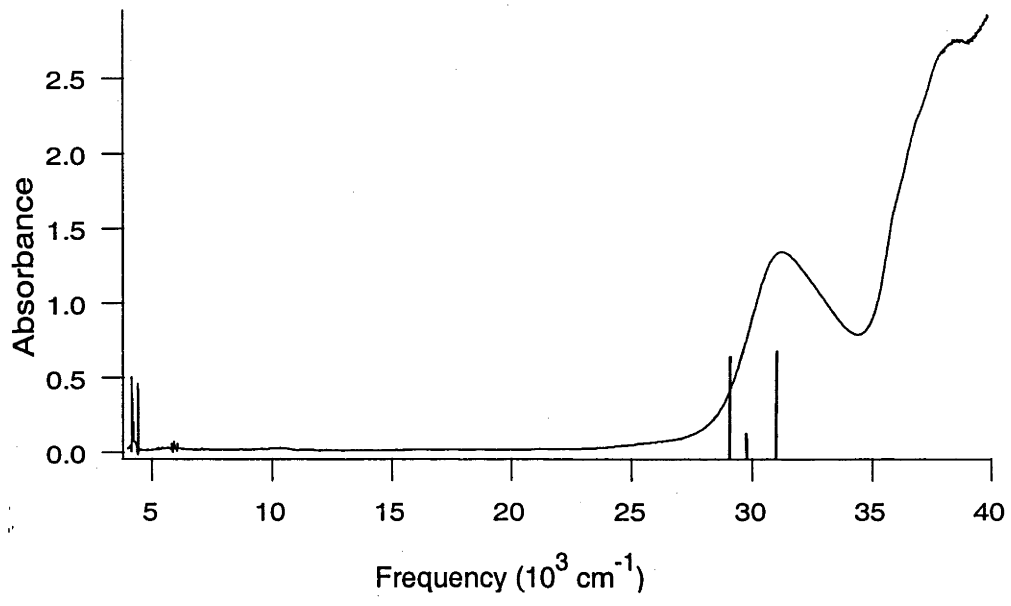

Figure 2.13. UV-vis-NIR absorption spectrum of *trans*-[Ru(C≡CPh)Cl(dppe)$_2$] and the calculated absorption transitions of *trans*-[Ru(C≡CPh)Cl(PH$_3$)$_4$] (vertical lines)

These calculations show that the MLCT band is made up of two significant transitions. One primarily involves a 9b$_2$ (the HOMO, which is an anti-bonding orbital consisting of Ru d_{yz}, Cl p_y and phenylacetylide π character) to 10b$_2$ (which consists of phenylacetylide π character with a small admixture of Ru d_{yz}) transition. The other transition consists primarily of a HOMO to the 11b$_2$ orbital (a phosphine orbital) transition. It is important to note that these optical transitions cannot be purely described as involving only two orbitals. The first major transition has a significant amount of 9b$_2$ to 11b$_2$ character, and likewise, the second major transition has a significant amount of 9b$_2$ to 10b$_2$ character. Therefore, the

energy difference between these two optical transitions is less than that which may have been expected from a simple inspection of the relevant orbitals. Located between these two optical transitions is a significantly weaker transition, which consists primarily of transfer of electron density from a $12b_1$ orbital (a MO made up of Ru d_{xz}, Cl p_x and acetylide π character) to a $13b_1$ orbital (a phosphine MO).

2.3.2.3. *Trans*-[Ru(C≡CC$_6$H$_4$-4-C≡CPh)Cl(PH$_3$)$_4$]

Figure 2.14. compares the UV-vis-NIR absorption spectrum of *trans*-[Ru(C≡CC$_6$H$_4$-4-C≡CPh)Cl(dppe)$_2$] and the calculated optical transitions of *trans*-[Ru(C≡CC$_6$H$_4$-4-C≡CPh)Cl(PH$_3$)$_4$], further detail on the composition of these optical transitions is given in Table 2.11.

The calculations indicate that the optical spectrum is made up of four optical transitions, the strongest of which occurs at approximately 22 000 cm^{-1}. There is a significant difference between this transition and the observed optical absorption maximum (which is centred at approximately 26 000 cm^{-1}). The difference between the calculated and observed values is consistent with other attempts at calculating optical spectra of large molecules using ADF. This major transition consists mostly of a $12b_2$ to $13b_2$ component, which involves transfer of electron density from a Ru d_{yz} MO to a phenylacetylide π MO.

The other three transitions all involve transfer of electron density from a Ru d_{yz} orbital to either a phosphine MO, a phenylacetylide π MO, or a delocalized phenylacetylide π and phosphine MO. All of these are weak relative to the major transition, however, as ν_{max} increases, so does the strength of the transition. These transitions may account for the shoulder on the optical absorption maximum in the UV-vis-NIR spectrum.

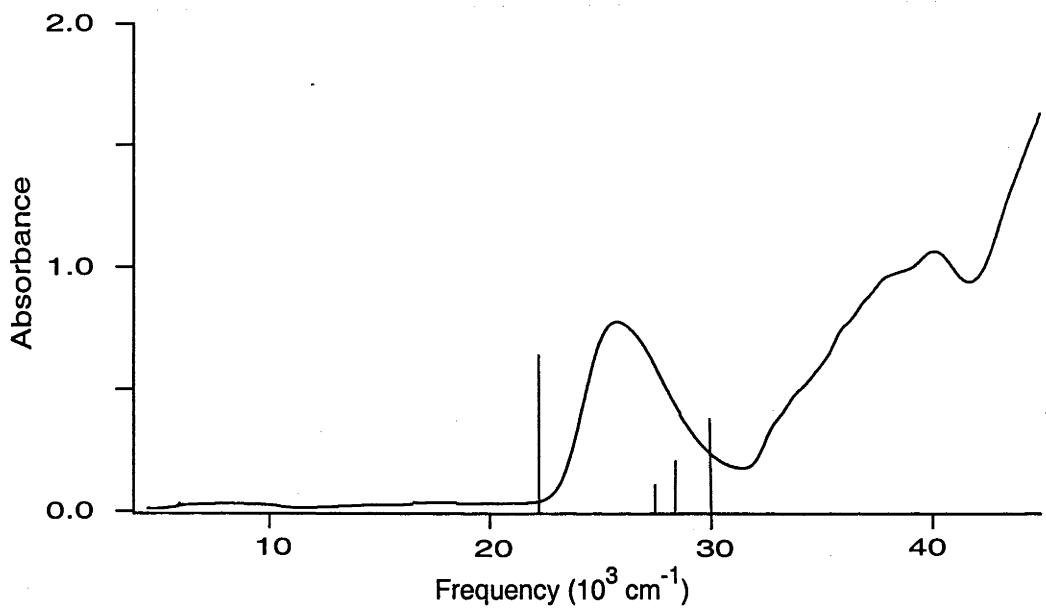

Figure 2.14. UV-vis-NIR absorption spectrum of *trans*-[Ru(C≡CC_6H_4-4-C≡CPh)Cl(dppe)$_2$] and the calculated absorption transitions of *trans*-[Ru(C≡CC_6H_4-4-C≡CPh)Cl(PH_3)$_4$] (vertical lines)

Table 2.11. Calculated optical transitions and relevant experimental data for mono-acetylide complexes

trans-[Ru(C≡CPh)Cl(PH$_3$)$_4$]					
ν_{max} (expt) [a]	ε (expt)[a]	ν_{max} (calc)	f (calc)	Composition	Major Assignment
31 350	2.3	29 250	0.16	$9b_2 \rightarrow 10b_2$	Ru $d_{yz} \rightarrow C_2Ph$
		29 780	0.039	$12b_1 \rightarrow 13b_1$	Ru $d_{xz} \rightarrow PH_3$
		31 260	0.18	$9b_2 \rightarrow 11b_2$	Ru $d_{yz} \rightarrow PH_3$
38 480	5.0	*b*			Phenyl → Phenyl*
trans-[Ru(C≡CC$_6$H$_4$-4-C≡CPh)Cl(PH$_3$)$_4$]					
ν_{max} (expt) [a]	ε (expt)[a]	ν_{max} (calc)	f (calc)	Composition	Major Assignment [c]
25 760	3.6	21 950	0.82	$12b_2 \rightarrow 13b_2$	Ru $d_{yz} \rightarrow C_2R$
		27 690	0.15	$12b_2 \rightarrow 14b_2$	Ru $d_{yz} \rightarrow PH_3$
		28 390	0.27	$11b_2 \rightarrow 13b_2$	Ru $d_{yz} \rightarrow C_2R$
37 880	sh, 4.5	30 030	0.49	$12b_2 \rightarrow 15b_2$	Ru $d_{yz} \rightarrow C_2R + PH_3$
40 150	5.0	*b*			Phenyl → Phenyl*

[a] ν_{max} in cm^{-1}, ε in 10^4 M^{-1} cm^{-1}. [b] Not applicable. [c] R = C$_6$H$_4$-4-C≡CPh.

2.3.2.4. *Trans*-[Ru(C≡CPh)$_2$(PH$_3$)$_4$]

Figure 2.15. presents the UV-vis-NIR absorption spectrum of *trans*-[Ru(C≡CPh)$_2$(dppe)$_2$] and the calculated optical transitions of *trans*-[Ru(C≡CPh)$_2$(PH$_3$)$_4$]. Table 2.12. gives more detail on the composition of these optical transitions.

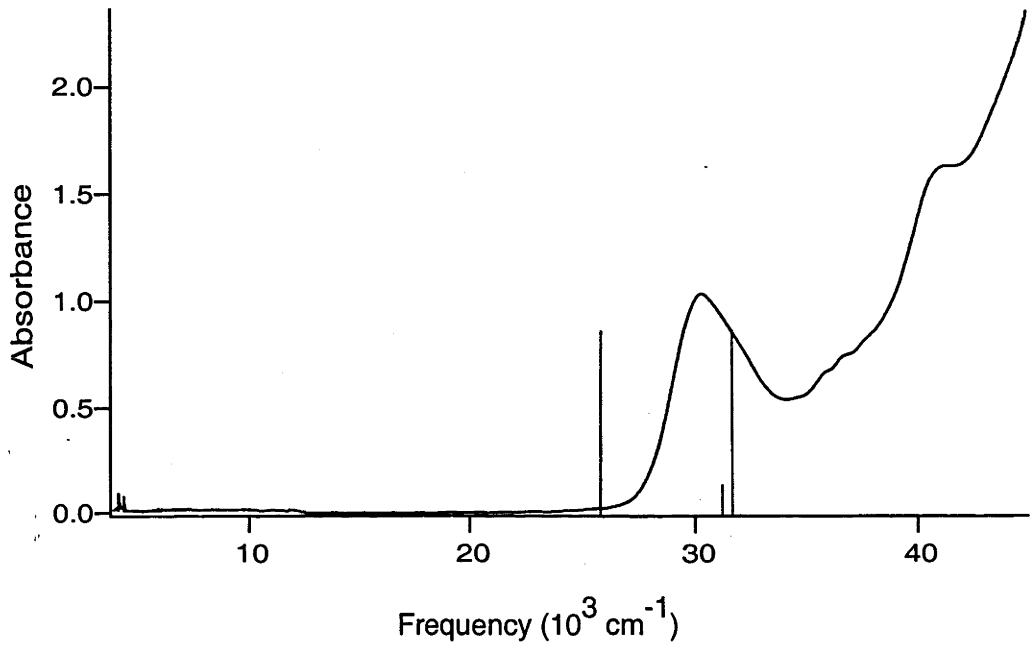

Figure 2.15. UV-vis-NIR absorption spectrum of *trans*-[Ru(C≡CPh)$_2$(dppe)$_2$] and the calculated absorption transitions of *trans*-[Ru(C≡CPh)$_2$(PH$_3$)$_4$]

The calculated optical absorption spectrum of *trans*-[Ru(C≡CPh)$_2$(PH$_3$)$_4$] is more complicated than those of the compounds above. It consists of three strong transitions and four weaker transitions. The first strong transition appears at ca 26 000 cm^{-1}, and involves a transition from the HOMO (11b$_2$) to a phenylacetylide MO (12b$_2$). There is a significant difference between the calculated ν_{max} of this transition, and the ν_{max} of the observed MLCT band. This large apparent discrepancy is, however, not surprising given that calculated ν_{max} can differ by up to 8000 cm^{-1}.

The second and third strong transitions are interesting because they don't have a significant contribution from the $11b_2$ HOMO orbital. Rather, they involve the $10b_2$ orbital, a large delocalized orbital made up of phenylacetylide π anti-bonding contributions from both acetylide ligands. The second transition is a π MO internal transition, whereas the third transition predominantly involves transfer of electron density to a phosphine MO.

The first weak transition is mainly $11b_2$ to $13b_2$ (a phosphine MO in character), but has significant mixing with an $11b_2$ to $14b_2$ (another phosphine MO) transition. The second weak transition is predominantly $11b_2$ to $14b_2$ in character, with small amounts of $10b_2$ to $12b_2$ (one of the major transitions detailed above).

The third weak transition is significant in that it can be described as LMCT. The ground state is the $10b_2$ orbital described above, whereas the excited state is a $13b_2$ MO. The $13b_2$ MO is delocalized about the Ru d_{yz} orbital and a π phenylacetylide MO.

The fourth weak transition is also unusual, as it is the only significant transition which has a x-axis component (in the plane of the phenyl rings). It involves the Ru d_{xz} orbital and the π orbitals on the acetylide bonds ($17b_1$). The excited state is the $18b_1$ orbital (a phosphine orbital).

2.3.2.5. *Trans*-[Ru(C≡CPh)(C≡CC$_6$H$_4$-4-C≡CPh)(PH$_3$)$_4$]

Figure 2.16. displays the UV-vis-NIR absorption spectrum of *trans*-[Ru(C≡CPh)(C≡CC$_6$H$_4$-4-C≡CPh)(dppe)$_2$] and the calculated optical transitions of *trans*-[Ru(C≡CPh)(C≡CC$_6$H$_4$-4-C≡CPh)(PH$_3$)$_4$]. Table 2.12. gives more detail on the composition of these optical transitions.

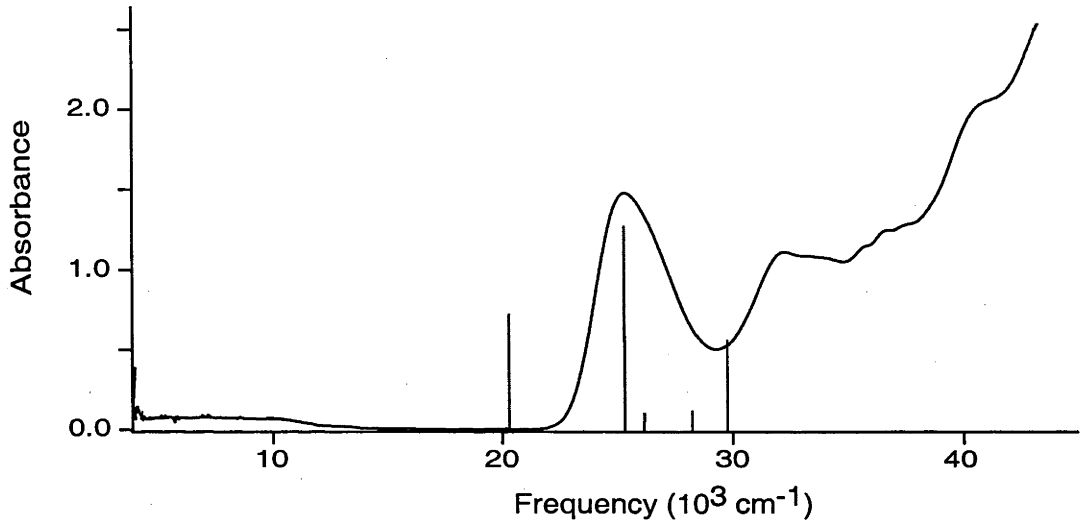

Figure 2.16. UV-vis-NIR absorption spectrum of *trans*-[Ru(C≡CPh)(C≡CC$_6$H$_4$-4-C≡CPh)(dppe)$_2$] and the calculated absorption transitions of *trans*-[Ru(C≡CPh)(C≡CC$_6$H$_4$-4-C≡CPh)(PH$_3$)$_4$] (vertical lines)

As with *trans*-[Ru(C≡CPh)$_2$(PH$_3$)$_4$], the calculated absorption spectrum of *trans*-[Ru(C≡CPh)(C≡CC$_6$H$_4$-4-C≡CPh)(PH$_3$)$_4$] is fairly complicated. It consists of three major transitions and two much weaker transitions.

The first strong optical transition appears at *ca* 20 000 cm^{-1}, and corresponds to a 14b$_2$ → 15b$_2$ transition. There is a very significant difference between the location of this transition and the location of the experimentally observed transition (*ca* 25 500 cm^{-1}). This may be due to the extra stabilization of certain conjugated virtual orbitals as discussed above.

The second and third major transitions each involve transfer of electron density from an orbital delocalized over the acetylide ligands and the Ru d_{yz} orbital to an acetylide virtual

orbital. The second significant transition is $13b_2 \rightarrow 15b_2$, whereas the third transition is $14b_2 \rightarrow 18b_2$.

The first minor transition ($14b_2 \rightarrow 16b_2$) is similar in nature to the first major transition. However, while the stronger transition involves promotion of electron density to a C≡CC_6H_4-4-C≡CPh acetylide virtual orbital, the weaker transition involves promotion to a C≡CPh virtual orbital.

The second minor transition ($14b_2 \rightarrow 17b_2$) involves promotion of an electron from the orbital delocalized over the acetylide ligands and a Ru d_{yz} orbital to a phosphine-based orbital.

Table 2.12. Calculated optical transitions for and relevant experimental data for ruthenium bis-acetylide complexes

trans-[Ru(C≡CPh)$_2$(PH$_3$)$_4$]

ν_{max} (expt)[a]	ε (expt)[a]	ν_{max} (calc)	f (calc)	Composition	Major Assignment
30 310	8.1	26 050	0.37	$11b_1 \rightarrow 12b_1$	Ru $d_{yz} \rightarrow C_2Ph$
		26 680	0.023	$11b_1 \rightarrow 13b_1$	Ru $d_{yz} \rightarrow PH_3$
				$11b_1 \rightarrow 14b_1$	Ru $d_{yz} \rightarrow PH_3$
		28 110	0.091	$11b_1 \rightarrow 14b_1$	Ru $d_{yz} \rightarrow PH_3$
				$10b_1 \rightarrow 12b_1$	$C_2Ph \rightarrow C_2Ph$
		31 350	0.061	$10b_1 \rightarrow 13b_1$	$C_2Ph \rightarrow PH_3$
				$10b_1 \rightarrow 14b_1$	$C_2Ph \rightarrow PH_3$
		31 750	0.037	$17b_2 \rightarrow 18b_2$	Ru $d_{xz} \rightarrow PH_3$
		33 360	0.23	$10b_1 \rightarrow 12b_1$	$C_2Ph \rightarrow C_2Ph$
		34 200	0.24	$10b_1 \rightarrow 14b_1$	$C_2Ph \rightarrow PH_3$
41 160	12.8	*b*			Phenyl → Phenyl*

trans-[Ru(C≡CPh)(C≡CC$_6$H$_4$-4-C≡CPh)(PH$_3$)$_4$]

ν_{max} (expt) [a]	ε (expt)[a]	ν_{max} (calc)	f (calc)	Composition	Major Assignment *c*
25 540	6.8	20 130	0.47	$14b_2 \rightarrow 15b_2$	Ru d_{yz} + $PhC_2C_6H_4C_2RuC_2Ph \rightarrow C_2C_6H_4C{\equiv}CPh$
		24 910	0.81	$13b_2 \rightarrow 15b_2$	Ru d_{yz} + $PhC_2C_6H_4C_2RuC_2Ph \rightarrow C_2C_6H_4C{\equiv}CPh$

Table 2.12. (continued) Calculated optical transitions for and relevant experimental data for ruthenium bis-acetylide complexes

ν_{max} (expt) a	ε (expt)[a]	ν_{max} (calc)	f (calc)	Composition	Major Assignment *c*
32 440	5.0	26 490	0.046	$14b_2 \rightarrow 16b_2$	Ru d_{yz} + $PhC_2C_6H_4C_2RuC_2Ph \rightarrow C_2Ph$
33 880	4.9	27 804	0.053	$14b_2 \rightarrow 17b_2$	Ru d_{yz} + $PhC_2C_6H_4C_2RuC_2Ph \rightarrow PH_3$
36 750	5.5	29 690	0.35	$14b_2 \rightarrow 18b_2$	Ru d_{yz} + $PhC_2C_6H_4C_2RuC_2Ph \rightarrow C_2C_6H_4C{\equiv}CPh$
41 010	8.7	*b*			Phenyl → Phenyl*

a ν_{max} in cm^{-1}, ε in 10^4 M^{-1} cm^{-1}. *b* Not applicable. *c* R = C_6H_4-4-C≡CPh.

2.3.3. *Oxidized Complexes*

Direct calculation of the optical spectra of the oxidized species was not performed because ADF is currently unable to calculate optical spectra of open-shell molecules. The optical spectra have therefore been determined by the ΔSCF method. In order to determine the energy of the transition, the following assumptions were made about the nature of the transition:

- The transition is A_1 symmetry
- The donor orbital of the transition is below the HOMO
- The electron is excited into the 'hole' in the HOMO formed by oxidation

The first assumption is justified as A_1 symmetry transitions are electric-dipole allowed, and therefore significantly stronger than other transitions. The calculated transitions of the neutral complexes confirm this, with all significant transitions having A_1 symmetry. The second assumption arises from the observation that the new transition is significantly lower in energy than the FMO gap. Therefore, the transition must not involve the virtual orbitals. The third assumption is an outgrowth of the second: as the electron must be promoted into a unfilled or partially filled orbital which is not a virtual orbital, the only candidate is the HOMO.

MO diagrams of three relevant examples, namely *trans*-$[RuCl_2(PH_3)_4]$, *trans*-$[Ru(C{\equiv}CPh)Cl(PH_3)_4]$ and *trans*-$[Ru(C{\equiv}CPh)_2(PH_3)_4]$, have been constructed to demonstrate the effects of oxidation on the MOs. Results can be applied to the related complexes, *trans*-$[Ru(C{\equiv}CC_6H_4\text{-}4\text{-}C{\equiv}CPh)Cl(dppe)_2]$ and *trans*-$[Ru(C{\equiv}CPh)(C{\equiv}CC_6H_4\text{-}4\text{-}C{\equiv}CPh)(dppe)_2]$.

2.3.3.1. *trans-[$RuCl_2(PH_3)_4$]*

A MO diagram of the model complex *trans*-$[RuCl_2(PH_3)_4]$ is shown in Figure 2.17. The molecular orbitals are represented schematically, and hence orbital mixing is not depicted.

As can be seen from the MO diagram, the HOMO is made up of a Ru d_{yz} orbital and two Cl p_y orbitals interacting in an anti-bonding fashion. The LUMO also consists of Ru and Cl anti-bonding orbitals but, in contrast, the orbitals are d_{x2-y2} and p_z for the respective atoms. Upon oxidation, the HOMO-LUMO energy gap appears to be unchanged.

2.3.3.2. *trans-[Ru(C≡CPh)Cl(PH$_3$)$_4$]*

A MO diagram of *trans*-[Ru(C≡CPh)Cl(PH_3)$_4$] is shown in Figure 2.18. As can be seen from MO diagram, the HOMO ($9b_2$) is made up of a Ru d_{yz} orbital, a Cl p_y orbital and delocalized π–bonding from the phenylacetylide unit interacting in an anti-bonding fashion. The LUMO ($6a_2$) is a Ru d_{xy} orbital with a small amount of mixing from phosphine MOs. Upon oxidation, the HOMO-LUMO band gap appears to increase by approximately 20%. As a general rule of thumb, upon oxidation the virtual orbitals increase in energy whereas the filled orbitals decrease in energy, relative to each other.

The significant transitions in the optical spectra can be visualised by examining Figure 2.18. The calculated optical spectra (Table 2.11.) show that the two transitions are $9b_2 \rightarrow 10b_2$ and $9b_2 \rightarrow 11b_2$. The $9b_2$ level is described in the paragraph above, whereas $10b_2$ has a much smaller Ru d_{xy} contribution, and a proportionally larger phenylacetylide π–bonding contribution. The $11b_2$ orbital on the other hand, has virtually no ruthenium d character, and is best described as a phosphine molecular orbital. Therefore, the MLCT band is made up of both metal-to-acetylide and metal-to-phosphine charge transfer.

The MO diagram allows the low energy absorption band which appears upon oxidation to be characterized. The transition is $8b_2 \rightarrow 9b_2$. The $8b_2$ orbital is a p_y orbital localized on the Cl atom. The transition can hence be defined as ligand-to-metal charge transfer in nature.

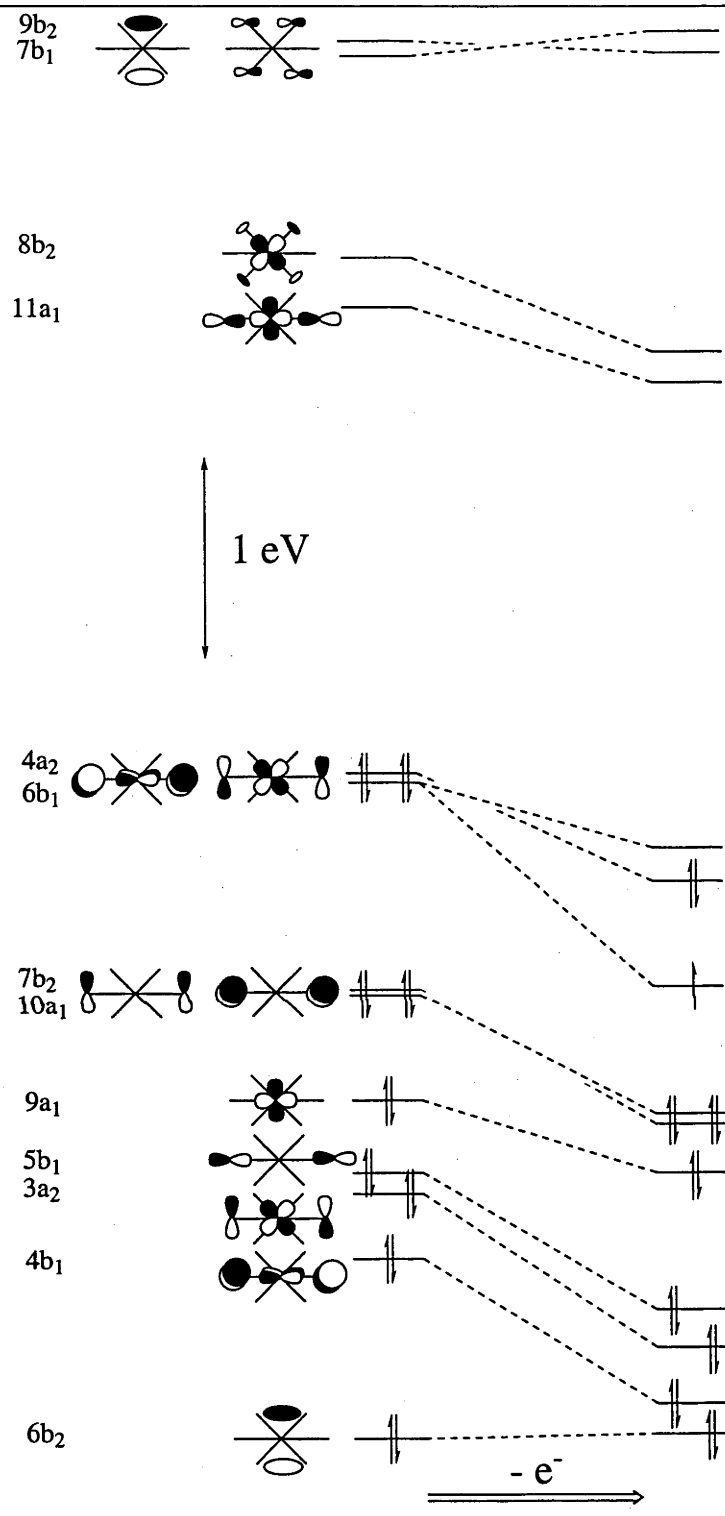

Figure 2.17. MO diagram for *trans*-$[RuCl_2(PH_3)_4]$ showing the effect of oxidation on the energy levels

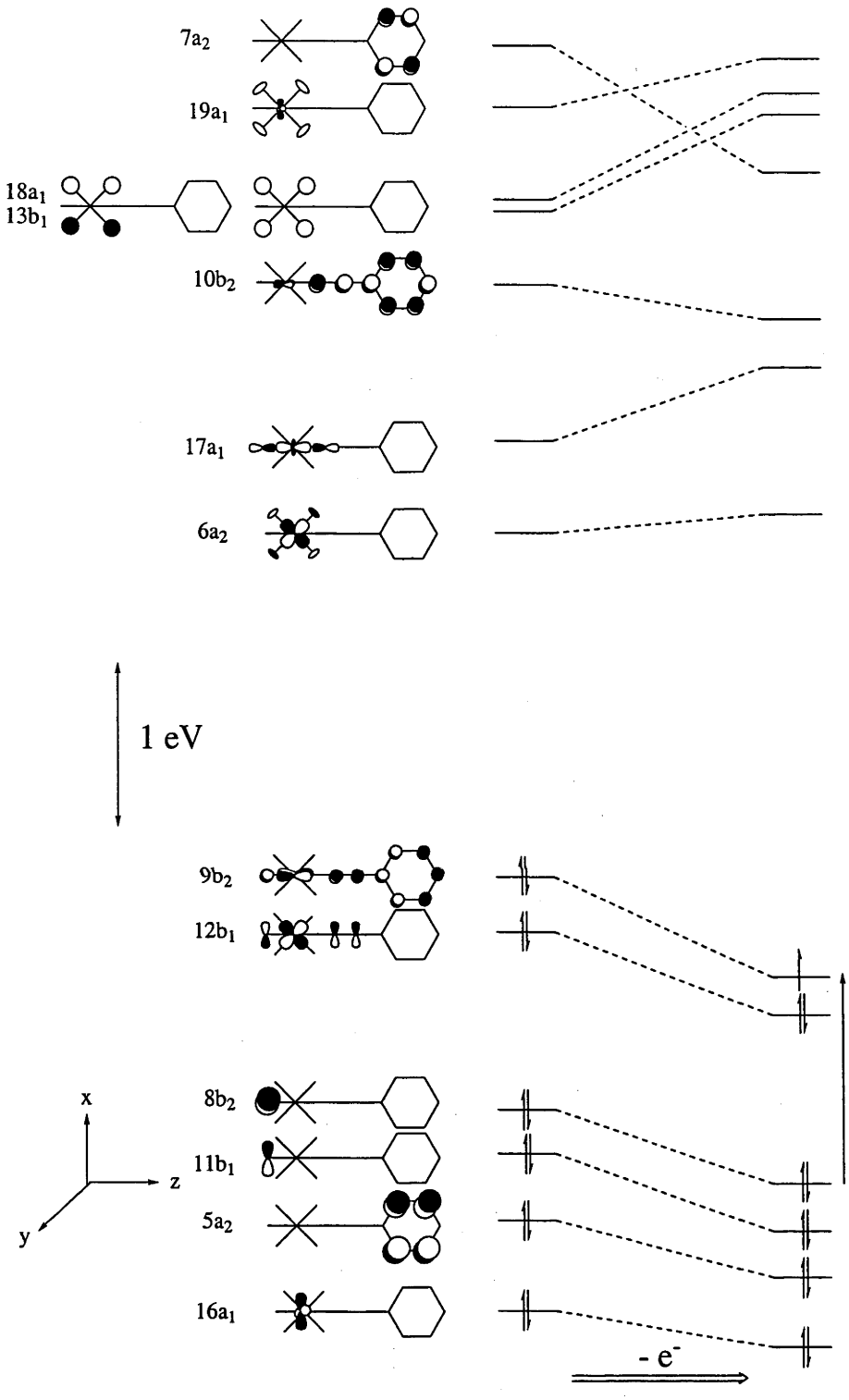

Figure 2.18. MO diagram for *trans*-[Ru(C≡CPh)Cl(PH_3)$_4$] showing the effect of oxidation on the energy levels

2.3.3.3. *trans-[Ru(C≡CPh)$_2$(PH$_3$)$_4$]*

A MO diagram showing the effects of oxidation on the MO of *trans*-Ru(C≡CPh)$_2$(PH$_3$)$_4$] is displayed in Figure 2.19. The HOMO ($11b_1$) consists of a Ru d_{yz} orbital mixed with considerable acetylide $\pi - \pi^*$ antibonding character. The LUMO ($7a_2$) is similar to that in *trans*-[Ru(C≡CPh)Cl(dppe)$_2$] in that it consists of a Ru d_{xy} orbital with a small amount of mixing from phosphine MOs. The increase in the HOMO–LUMO gap is smaller than that observed for *trans*-[RuCl(C≡CPh)(dppe)$_2$], in the region of 10%. This is due to a smaller decrease in the stabilization of the HOMO relative to the LUMO upon oxidation for the bis-acetylide complex.

The optical spectrum of neutral *trans*-[Ru(C≡CPh)$_2$(dppe)$_2$] is dominated by three transitions: $11b_1 \rightarrow 12b_1$, $10b_1 \rightarrow 12b_1$ and $10b_1 \rightarrow 13b_1$. The MO diagram allows these orbitals to be rapidly identified. The $10b_1$ orbital is a π anti-bonding orbital delocalized over both of the phenylacetylide ligands. The $11b_1$ orbital is an anti-bonding orbital delocalized over the phenylacetylide ligands and the Ru d_{xy} orbital. The $12b_1$ and $13b_1$ orbitals are similar in nature to the $10b_1$ and $11b_1$ orbitals, respectively.

The low energy band arises from the $10b_1 \rightarrow 11b_1$ transition. It can therefore be characterized as a ligand-to-metal charge transfer band.

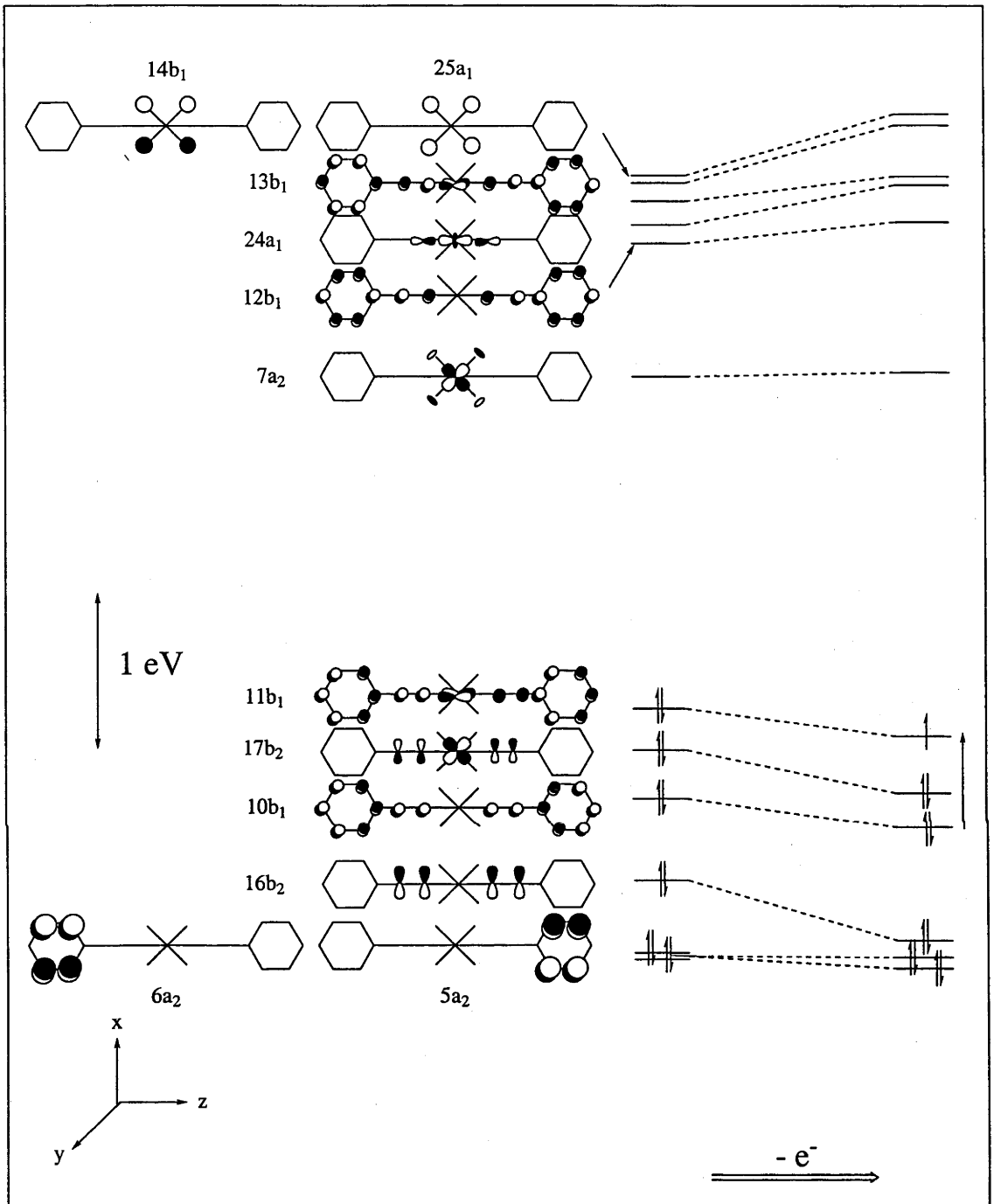

Figure 2.19. MO diagram for *trans*-[Ru(C≡CPh)$_2$(PH$_3$)$_4$] showing the effect of oxidation on the energy levels

2.3.4. *Comparisons with Experimental Data*

Table 2.13. lists experimental results and calculated transition energies for the low energy band which emerges on oxidation. As with the neutral complexes, the calculated values correlate well with the experimental energies. Some predicted transitions were not observed, presumably due to poor overlap between the relevant orbitals.

Generally, the correlation between the experimental ν_{max} and the calculated ΔE values are close. The largest difference is just over 3000 cm^{-1}, which is small when compared with the intrinsic errors common to this style of calculation (solution measurements vs molecules in isolation, diphenylphosphine vs PH_3, and neglect of spin-coupling).

Interestingly, more than one low energy band appears upon oxidation, and these other, much weaker bands are also apparent in the calculations. For example, the weak low energy band at approximately 17 000 cm^{-1} in *trans*-[Ru(C≡CPh)Cl(dppe)$_2$] is due to a $7b_2 \rightarrow 9b_2$ transition, or the promotion from a bonding orbital delocalized on the Ru d_{yz} and phenylacetylide ligand to its corresponding anti-bonding orbital.

Table 2.13. Calculated energies of the low energy transitions of oxidized acetylide complexes

Complex	ν_{max} (expt)	ε (expt)	Transition	ΔE (calc)	Major Assignment
trans-[Ru(C≡CPh)Cl(dppe)$_2$]$^+$	12 040	1.0	8 b_2 → 9 b_2	9 300	Cl p_y → Ru d_{yz} + C_2Ph
	16 980	0.1	7 b_2 → 9 b_2	17 400	Ru d_{yz} + C_2Ph → Ru d_{yz} + C_2Ph
			6 b_2 → 9 b_2	24 100	Ru d_{yz} + C_2Ph → Ru d_{yz} + C_2Ph
trans-[Ru(C≡CC_6H_4-4-C≡CPh)Cl(dppe)$_2$]$^+$			11 b_1 → 12 b_1	7 200	Cl p_y → Ru d_{yz} + C_2
	11 160	2.0	10 b_1 → 12 b_1	11 600	Cl p_y → Ru d_{yz} + C_2
	15 560	0.5	9 b_1 → 12 b_1	18 100	Cl p_y → C_2Ph
trans-[Ru(C≡CPh)$_2$(dppe)$_2$]$^+$	8 920	3.6	10 b_1 → 11b_1	5 700	C_2Ph → Ru d_{yz} + C_2
	16 200	0.6	9 b_1 → 11b_1	15 800	Ph → Ru d_{yz} + C_2
			8 b_1 → 11b_1	20 000	C_2Ph → Ru d_{yz} + C_2
trans-[Ru(C≡CPh)(C≡CC_6H_4-4-C≡CPh)(dppe)$_2$]$^+$			13 b_2 → 14 b_2	4 200	C_2 → Ru d_{yz}
	8 440	2.9	12 b_2 → 14 b_2	9 600	Ph$C_2C_6H_4C_2$ → Ru d_{yz} + C_2
	15 960	0.2	11 b_2 → 14 b_2	16 700	Ru d_{yz} + C_2Ph → Ru d_{yz} + C_2

ν_{max} in cm^{-1}, ε in x 10^4 M^{-1} cm^{-1}, ΔE in cm^{-1}

2.4. *Octahedral Osmium Acetylide Complexes*

Recently, a series of osmium acetylide complexes (analogous to several studied in the above section) have been synthesized, and their UV-vis-NIR spectroelectrochemical spectra measured.[6] Figure 2.20. shows some of the molecules that were studied. This data permits the assumptions made in the characterization of the oxidized species in Section 2.3. to be tested with a related system.

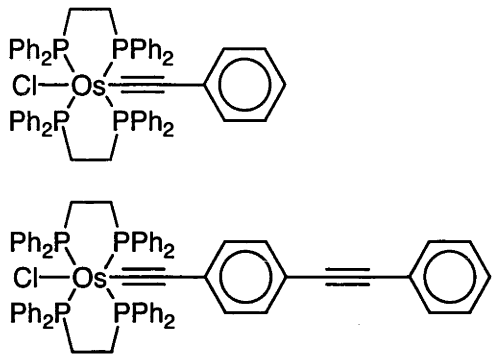

Figure 2.20. Osmium Acetylide Complexes

2.4.1. Geometry Optimizations

Geometry optimizations were initially performed on model complexes. To reduce computational expense, each dppe ligand has been replaced with two PH_3 ligands. These PH_3 groups are staggered with respect to the plane of the phenyl rings (Figure 2.21.). These calculated geometries were then used to generate optical spectra, and single point calculations were performed on the oxidized species. C_{2v} symmetry was imposed upon the system.

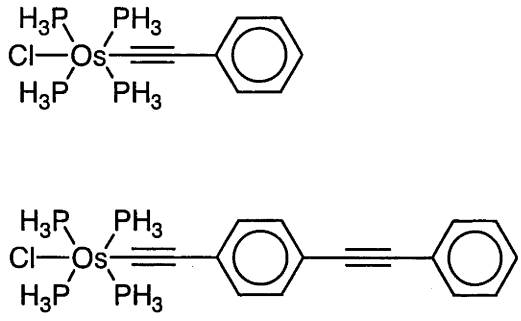

Figure 2.21. Model osmium acetylide complexes

The bond lengths generated from the geometry optimizations are presented in Figure 2.22. As can been seen, the Os–C bond distances are approximately 2.06 Å, whereas the C≡C bonds are approximately 1.23 Å. When the two C≡C bonds in *trans*-[Os(C≡CC_6H_4-4-C≡CPh)Cl(PH_3)$_4$] are compared, the one closest to the metal centre is slightly longer (1.2361 Å vs. 1.2223 Å). This is probably due to donation of osmium d electron density into the π anti-bonding orbital of the acetylide unit.

The Os–C distance for *trans*-[Os(C≡CPh)Cl(PH_3)$_4$] is slightly longer than the corresponding bond length in *trans*-[Os(C≡CC_6H_4-4-C≡CPh)Cl(PH_3)$_4$] (2.0653 Å vs 2.0623 Å), while the C≡C bond length of *trans*-[Os(C≡CPh)Cl(PH_3)$_4$] is slightly shorter than, that of the extended chain analogue (1.2344 Å vs. 1.2361 Å). This is indicative of increased back-bonding with the C≡CC_6H_4-4-C≡CPh ligand. However, it should be emphasized that these differences in bond length are small.

There are very few examples of osmium acetylide X-ray structure studies in the chemical literature to which these bond lengths can be compared (there are many examples of osmium acetylide clusters,[36-41] but these cannot be used as a comparison because of the different mode of bonding). Table 2.14. compares the calculated bond lengths with some literature values: all the calculated bond lengths in the present work are similar to crystallographically determined bond lengths.

Bond angles can also be determined from the geometry optimization calculations, but because of the symmetry constraints placed on the calculation (C_{2v}), very little significant information can be obtained. Hence, this data has not been presented.

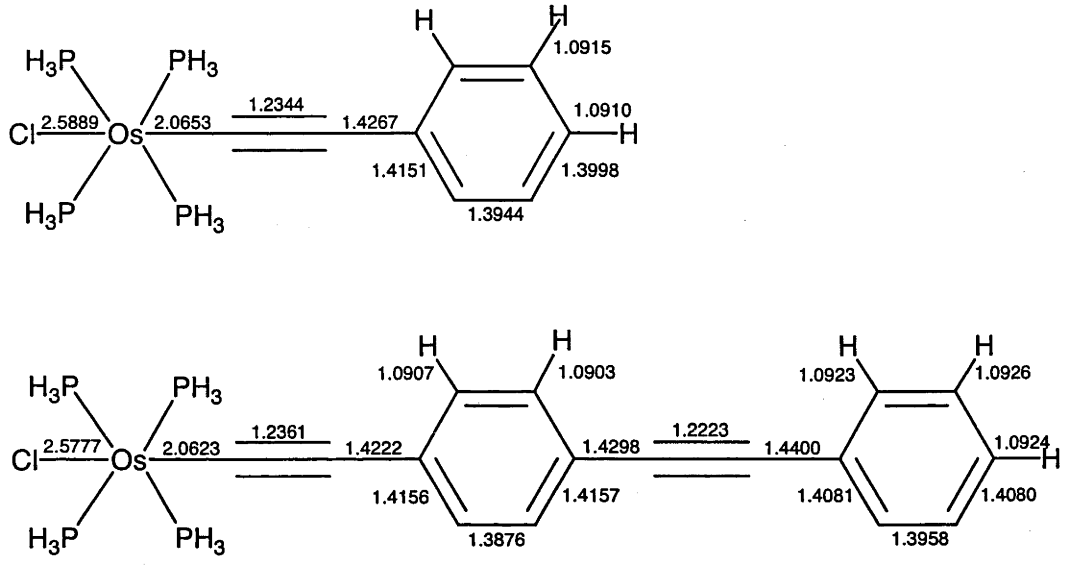

Figure 2.22. Calculated osmium acetylide bond lengths. All bond lengths are in Å.

Table 2.14. Comparison between calculated osmium acetylide bond lengths and related crystallographically-derived bond lengths

Complex	Os–C	C≡C	C–C	Reference
trans-[Os(C≡CPh)Cl(PH_3)$_4$]	2.0653	1.2344	1.4267	This Work
trans-[Os(C≡CC_6H_4-4-C≡CPh)Cl(PH_3)$_4$]	2.0623	1.2361	1.4222	This Work
[Os(C≡CC_6H_4-4-Me)(C≡CC_6H_4-4-NO_2)(dppm)$_2$]	2.066(2)	1.158(5)	1.470(5)	42
[OsH(C≡CPh)($GePh_3$)(P^iPr_3)]	2.008(4)	1.214(4)	1.424(5)	43

All bond lengths in Å

2.4.2. *Calculation of Optical Spectra of Neutral Species*

The results of the calculation of optical spectra are shown in Table 2.15. The spectrum for the complex *trans*-[Os(C≡CPh)Cl(PH_3)$_4$] consists of one major transition at 28 300 cm^{-1} which is largely osmium to acetylide charge transfer. Additionally, there are several minor transitions (all of which have an oscillator strength lower by an order of magnitude relative to the major transition). Three minor transitions all involve transfer of electron density from osmium d orbitals to phosphine-based orbitals. These transitions appear at 29 600, 30 700, 31 100 and 36 300 cm^{-1}, and, with the exception of the transition at 31 100 cm^{-1}, they possess A_1 symmetry.

The longer acetylide complex, *trans*-[Os(C≡CC_6H_4-4-C≡CPh)Cl(PH_3)$_4$], has a more complex absorption spectrum, as determined by ADF. It consists of three strong transitions, all of which involve charge transfer from osmium d orbitals to acetylide orbitals. The location of these transitions ranges from 19 900 to 28 500 cm^{-1}. All of these transitions have a larger oscillator strength than the major transition in *trans*-[Os(C≡CPh)Cl(PH_3)$_4$]. Additionally, there are two smaller transitions (oscillator strengths of 0.10 and 0.014, respectively) which occur at 29 800 and 31 100 cm^{-1}. Both of these transitions involve osmium-to-phosphine charge transfer.

The experimental absorption spectrum derived from *trans*-[Os(C≡CPh)Cl(dppe)$_2$] and *trans*-[Os(C≡CC_6H_4-4-C≡CPh)Cl(dppe)$_2$] shows metal-to-ligand charge transfer bands at 30 825 and 25 575 cm^{-1}, respectively.[6] The correlation between the calculated absorption spectrum of *trans*-[Os(C≡CPh)Cl(PH_3)$_4$] and the experimentally determined absorption spectrum of *trans*-[Os(C≡CPh)Cl(dppe)$_2$] is quite close. Comparison of the two calculated absorption spectra suggests that *trans*-[Os(C≡CC_6H_4-4-C≡CPh)Cl(PH_3)$_4$] possesses a metal-to-ligand charge-transfer band at lower energies than does *trans*-[Os(C≡CPh)Cl(PH_3)$_4$] (the smaller complex has one transition at 28 300 cm^{-1}, whereas the larger complex has transitions at 19 900, 27 400 and 28 500 cm^{-1}). This trend is also observed in the experimental data. One of the major transitions in *trans*-[Os(C≡CC_6H_4-4-C≡CPh)Cl(PH_3)$_4$] is at considerably lower energy than is the MLCT band in *trans*-[Os(C≡CC_6H_4-4-C≡CPh)Cl(dppe)$_2$]. This is probably due to the additional stabilization of

some conjugated virtual orbitals, as discussed in the section of ruthenium mono- and bis-acetylide complexes.

Table 2.15. Calculated optical spectra of model osmium acetylide complexes

trans-[Os(C≡CPh)Cl(PH$_3$)$_4$]				
ν_{max}	f	Symmetry	Composition	Assignment
28 300	0.32	A_1	85% $10b_2 \rightarrow 11b_2$	Metal to Phenylacetylide CT
29 600	0.024	A_1	96% $13b_1 \rightarrow 14b_1$	Metal to Phosphine CT
30 700	0.011	A_1	96% $10b_2 \rightarrow 12b_2$	Metal to Phosphine CT
31 100	0.010	B_1	88% $9b_2 \rightarrow 6a_2$	Metal to Phosphine CT
36 300	0.19	A_1	77% $9b_2 \rightarrow 11b_2$	Metal to Phenylacetylide CT
trans-[Os(C≡CC$_6$H$_4$-4-C≡CPh)Cl(PH$_3$)$_4$]				
ν_{max}	f	Symmetry	Composition	Assignment
19 900	0.66	A_1	91% $13b_2 \rightarrow 14b_2$	Metal to Acetylide CT
27 400	0.39	A_1	74% $12b_2 \rightarrow 14b_2$	Metal to Acetylide CT
28 500	0.43	A_1	77% $13b_2 \rightarrow 15b_2$	Metal to Acetylide CT
29 800	0.10	A_1	93% $13b_2 \rightarrow 16b_2$	Metal to Phosphine CT
31 100	0.014	A_1	97% $19b_1 \rightarrow 20b_1$	Metal to Phosphine CT

2.4.3. *Oxidized Species*

Single point calculations were performed on *trans*-$[Os(C{\equiv}CPh)Cl(PH_3)_4]^+$ and *trans*-$[Os(C{\equiv}CC_6H_4\text{-}4\text{-}C{\equiv}CPh)Cl(PH_3)_4]^+$, providing information on the molecular orbitals of these oxidised model complexes. Figures 2.23. and 2.24. show the effect of oxidation on the MOs.

Unsurprisingly, both *trans*-$[Os(C{\equiv}CPh)Cl(PH_3)_4]^+$ and *trans*-$[Os(C{\equiv}CC_6H_4\text{-}4\text{-}C{\equiv}CPh)Cl(PH_3)_4]^+$ have similar MOs. The HOMO consists of a large delocalized orbital made up of Os d_{yz}, Cl p_y and acetylide π character. Although it is not apparent from Figure 2.24., it is important to note that there is considerably more electron density on the phenylacetylide unit closest to the osmium centre than on the second phenylacetylide unit in *trans*-$[Os(C{\equiv}CC_6H_4\text{-}4\text{-}C{\equiv}CPh)Cl(PH_3)_4]$.

The LUMO of *trans*-$[Os(C{\equiv}CPh)Cl(PH_3)_4]$ consists of a Os d_{xy} orbital with small amounts of mixing with phosphine MOs. In contrast, the LUMO of *trans*-$[Os(C{\equiv}CC_6H_4\text{-}4\text{-}C{\equiv}CPh)Cl(PH_3)_4]$ is a phenylacetylide π MO. This results from the increased stabilization of the phenylacetylide MOs due to extra conjugation. The MO analogous to the LUMO for *trans*-$[Os(C{\equiv}CPh)Cl(PH_3)_4]$ is the LUMO + 1 in the longer chain complex. This extra stabilization leads to the FMO gap of *trans*-$[Os(C{\equiv}CPh)Cl(PH_3)_4]$ being approximately 4760 cm^{-1} larger than the FMO gap of $[Os(C{\equiv}CC_6H_4\text{-}4\text{-}C{\equiv}CPh)Cl(PH_3)_4]$.

Upon oxidation, the FMO gap of *trans*-$[Os(C{\equiv}CPh)Cl(PH_3)_4]$ increases by approximately 2900 cm^{-1} (an increase of around 13%), whereas the FMO of *trans*-$[Os(C{\equiv}CC_6H_4\text{-}4\text{-}C{\equiv}CPh)Cl(PH_3)_4]$ increases by approximately 1770 cm^{-1} (an increase of around 10%).

The assignment of the low energy transitions is tabulated in Table 2.16: experimental results for *trans*-$[Os(C{\equiv}CPh)Cl(dppe)_2]^+$ and *trans*-$[Os(C{\equiv}CC_6H_4\text{-}4\text{-}C{\equiv}CPh)Cl(dppe)_2]^+$ are compared to calculated values of the model oxidized osmium complexes. Calculated values are shown to correlate well with the experimental results for the oxidized species; some predicted transitions were not observed, presumably due to poor overlap between relevant orbitals.

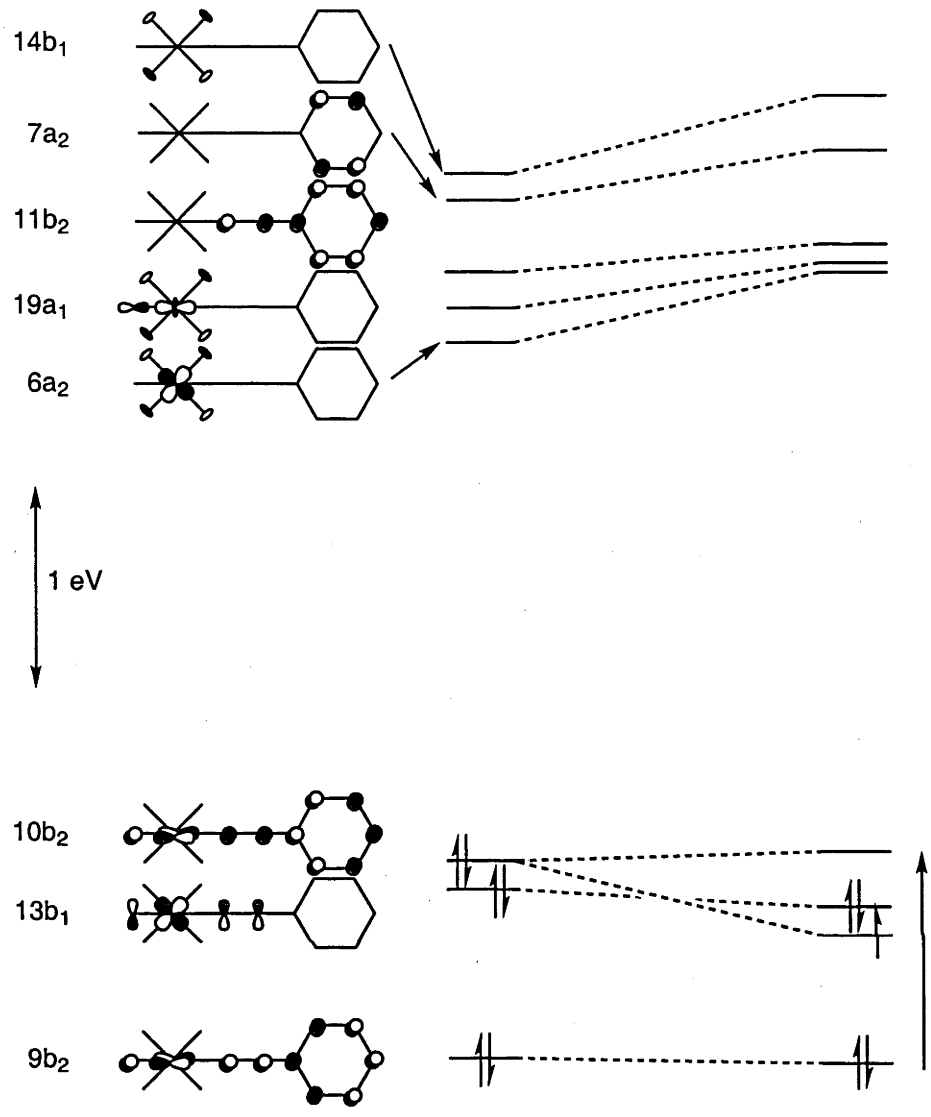

Figure 2.23. Effect of oxidation on MOs of *trans*-[Os(C≡CPh)Cl(PH_3)$_4$]

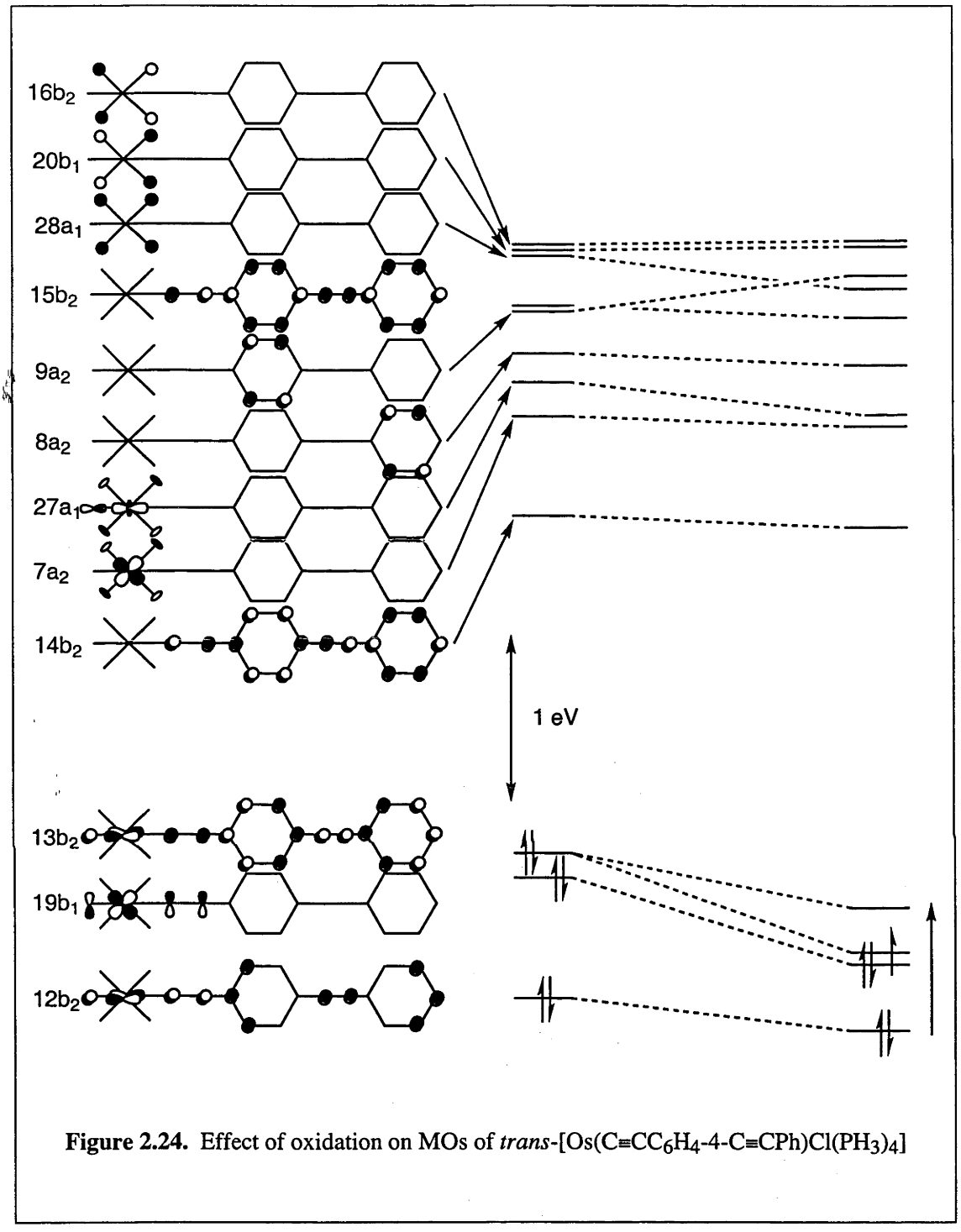

Figure 2.24. Effect of oxidation on MOs of *trans*-[Os(C≡CC$_6$H$_4$-4-C≡CPh)Cl(PH$_3$)$_4$]

Table 2.16. Observed and calculated low energy optical transitions of oxidized osmium acetylide complexes[a]

Complex	ν_{max} (expt)	ε (expt)	Transition	ΔE (calc)	Assignment
trans-$[Os(C{\equiv}CPh)Cl(PH_3)_4]^+$			$9b_2 \rightarrow 10b_2$	9030	Os d_{yz} + C_2Ph + Cl $p_y \rightarrow$ Os d_{yz} + C_2Ph + Cl p_y
	14 000	0.9	$8b_2 \rightarrow 10b_2$	16 620	Os d_{yz} + C_2Ph + Cl $p_y \rightarrow$ Os d_{yz} + C_2Ph + Cl p_y
			$7b_2 \rightarrow 10b_2$	22 670	$C_2Ph \rightarrow$ Os d_{yz} + C_2Ph + Cl p_y
trans-$[Os(C{\equiv}CC_6H_4\text{-}4\text{-}C{\equiv}CPh)Cl(PH_3)_4]^+$			$12b_2 \rightarrow 13b_2$	6210	Os d_{yz} + $C_2R \rightarrow$ Os d_{yz} + C_2R + Cl p_y
	13 130	1.9	$11b_2 \rightarrow 13b_2$	11 410	C_2R + Cl $p_y \rightarrow$ Os d_{yz} + C_2R + Cl p_y
	23 220	1.2	$10b_2 \rightarrow 13b_2$	17 260	Os d_{yz} + Cl $p_y \rightarrow$ Os d_{yz} + C_2R + Cl p_y

[a] Experimental data taken from Ref 6. ν_{max} in cm^{-1}, ε in 10^4 M^{-1} cm^{-1}

2.5. *Conclusions*

The optical properties of a number of related group 8 metal acetylide complexes have been investigated via the ADF density functional program and the results compared against pre-existing experimental data. This work necessitated the construction of model complexes, geometry optimizations, and then calculation of the desired optical properties. Where possible, the results were calculated directly using TD-DFT and examples containing an unpaired electron were calculated using indirect methods.

Data from a series of cyclopentadienyl group 8 acetylide complexes have been used to evaluate the suitability of ADF in calculating molecular second-order hyperpolarizabilities in these types of compounds, hyperpolarizabilities were calculated directly using TD-DFT and were shown to be incompatible with the experimental data. While the observed trend in hyperpolarizabilities upon addition of a more electron-withdrawing acetylide ligand was apparent in the calculations, the experimentally observed trends upon metal replacement were not.

The optical spectra of a series of ruthenium acetylide complexes have been calculated; the resultant deviations from the experimental optical spectra were found to be similar to those from other advanced computational techniques. Likewise, geometry optimization calculations yielded bond lengths which are comparable to the experimentally observed values. These results indicate that the metal-to-ligand charge-transfer band is primarily metal-to-acetylide in character, mixed with significant amounts of metal-to-phosphine component.

The experimentally observed low-energy absorption band which appears upon oxidation has been characterized indirectly. By assuming that the transition is symmetry allowed, and that it involves promotion of an electron from an occupied orbital to the partially filled HOMO, the exact transitions can been determined. The calculated results are comparable to the experimentally observed values.

The above assumptions were tested by application to a new series of metal-acetylide complexes. In this case, a series of osmium acetylide complexes were examined, and similar results to the ruthenium series were observed. Geometry optimizations gave similar results to crystallographically derived bond lengths.

2.6. *Experimental*

2.6.1. *ADF Calculations*

All calculations described in this chapter were performed on a Linux-based Pentium III computer (600 MHz) using the Amsterdam Density Functional Theory (ADF) Release 1999.[44-46] The local exchange correlation approximation of Vosko, Wilk, and Nusair[47] was used with the corrections of Becke[48] and Perdew.[49,50] Triple-ξ basis sets (Type IV) were used for all atoms. Core orbitals were frozen through 1s (C), 2p (P), 3p (Fe), 3p (Ru) and 4f (Os). Relativistic corrections were incorporated using the ZORA functionality.[51] Geometries were optimized using the algorithm of Versluis and Ziegler.[52] Optical spectra and hyperpolarizabilities of closed shell complexes were calculated using the time-dependent DFT functionality available in ADF.[53]

The cyclopentadienyl metal acetylide complexes used C_s symmetry with a coordinate system having the acetylide bond in the xy plane, and the PH_3 ligands in the xz plane. In order to reduce computational expense, the bidentate phosphine ligands were replaced with PH_3 ligands. In the case of the 4-nitrophenylacetylide-containing complexes, the nitro groups were constrained to be in the plane of the phenyl rings.

The ruthenium acetylide complexes used C_{2v} symmetry with a coordinate system having the z-axis running in the same direction as the acetylides, and the x axis in the plane of the phenyl rings. In order to reduce computational expense, each dppe ligand was replaced with two PH_3 ligands. Phenyl rings were constrained to be coplanar and the PH_3 ligands are staggered with respect to the phenyl rings.

2.7. *References*

(1) Whittall, I. R.; Humphrey, M. G.; Hockless, D. C. R.; Skelton, B. W.; White, A. H. *Organometallics* **1995**, *14*, 3970.

(2) Whittall, I. R.; Cifuentes, M. P.; Humphrey, M. G.; Luther-Davies, B.; Samoc, M.; Houbrechts, S.; Persoons, A.; Heath, G. A.; Hockless, D. C. R. *J. Organomet. Chem.* **1997**, *549*, 127.

(3) McDonagh, A. M.; Cifuentes, M. P.; Humphrey, M. G.; Houbrechts, S.; Maes, J.; Persoons, A.; Samoc, M.; Luther-Davies, B. *J. Organomet. Chem.* **2000**, *610*, 71.

(4) Cifuentes, M. P.; Powell, C. E.; Humphrey, M. G.; Heath, G. A.; Samoc, M.; Luther-Davies, B. *J. Phys. Chem. A* **2001**, *105*, 9625.

(5) Powell, C.; Cifuentes, M. P.; McDonagh, A. M.; Hurst, S.; Lucas, N. T.; Delfs, C. D.; Stranger, R.; Humphrey, M. G.; Houbrechts, S.; Asselberghs, I.; Persoons, A.; Hockless, D. C. R. *Inorg. Chim. Acta.* **2003**, *352*, 9.

(6) Morrall, J. P.; Powell, C. E.; Stranger, R.; Cifuentes, M. P.; Humphrey, M. G.; Heath, G. A. *J. Organomet. Chem.* **2003**, *670*, 248.

(7) McGrady, J. E.; Lovell, T.; Stranger, R.; Humphrey, M. G. *Organometallics* **1997**, *16*, 4004.

(8) Delfs, C. D.; Stranger, R.; Humphrey, M. G.; McDonagh, A. M. *Journal of Organometallic Chemistry* **2000**, *607*, 208.

(9) Van Gisbergen, S. J. A.; Snijders, J. G.; Baerends, E. J. *J. Chem. Phys.* **1998**, *109*, 10657.

(10) Gritsenko, O. V.; Van Gisbergen, S. J. A.; Gorling, A.; Baerends, E. J. *J. Chem. Phys.* **2000**, *113*, 8478.

(11) Gruning, M.; Gritsenko, O. V.; Van Gisbergen, S. J. A.; Baerends, E. J. *J. Chem. Phys.* **2001**, *114*, 652.

(12) Schipper, P. R. T.; Gritsenko, O. V.; Van Gisbergen, S. J. A.; Baerends, E. J. *J. Chem. Phys.* **2000**, *112*, 1344.

(13) Van Gisbergen, S. J. A.; Rosa, A.; Ricciardi, G.; Baerends, E. J. *J. Chem. Phys.* **1999**, *111*, 2499.

(14) Baerends, E. J.; Ricciardi, G.; Rosa, A.; Van Gisbergen, S. J. A. *Coordination Chemistry Reviews* **2002**, *230*, 5.

(15) Ricciardi, G.; Rosa, A.; Baerends, E. J.; Van Gisbergen, S. J. A. *J. Am. Chem. Soc.* **2002**, *124*, 12319.

(16) Gisbergen, S. J. A. v.; Groeneveld, J. A.; Rosa, A.; Snijders, J. G.; Baerends, E. J. *J. Phys. Chem. A* **1999**, *103*, 6835.

(17) Bencini, A.; Ciofini, I.; Daul, C. A.; Ferretti, A. *J. Am. Chem. Soc.* **1999**, *121*, 11418.

(18) Rosa, A.; Baerends, E. J.; Van Gisbergen, S. J. A.; van Lenthe, E.; Groeneveld, J. A.; Snijders, J. G. *J. Am. Chem. Soc* **1999**, *121*, 10356.

(19) Te Velde, G.; Bickelhaupt, F. M.; Baerends, E. J.; Fonseca Guerra, C.; Van Gisbergen, S. J. A.; Snijders, J. G.; Ziegler, T. *J. Comput. Chem.* **2001**, *22*, 931.

(20) Van Gisbergen, S. J. A.; Snijders, J. G.; Baerends, E. J. *J. Chem. Phys.* **1998**, *109*, 10644.

(21) Ricciardi, G.; Rosa, A.; Van Gisbergen, S. J. A.; Baerends, E. J. *J. Phys. Chem. A* **2000**, *104*, 635.

(22) Houbrechts, S.; Clays, K.; Persoons, A.; Cadierno, V.; Gamasa, M. P.; Gimeno, J.; Whittall, I. R.; Humphrey, M. G. *Proc. SPIE-Int. Soc. Opt. Eng.* **1996**, *2852*, 97.

(23) Whittall, I. R.; Humphrey, M. G.; Persoons, A.; Houbrechts, S. *Organometallics* **1996**, *15*, 1935.

(24) Bruce, M. I.; Humphrey, M. G.; Snow, M. R.; Tiekink, E. R. T. *J. Organomet. Chem.* **1986**, *314*, 213.

(25) Schilling, B. E. R.; Hoffmann, R.; Lichtenberger, D. L. *J. Am. Chem. Soc.* **1979**, *101*, 585.

(26) Lichtenberger, D. L.; Renshaw, S. K.; Wong, A.; Tagge, C. D. *Organometallics* **1993**, *12*, 3522.

(27) Lichtenberger, D. L.; Renshaw, S. K.; Bullock, R. M. *J. Am. Chem. Soc.* **1993**, *115*, 3276.

(28) Lichtenberger, D. L.; Kellogg, G. E. *Acc. Chem. Res.* **1987**, *20*, 379.

(29) Knight, E. T.; Myers, L. K.; Thompson, M. E. *Organometallics* **1992**, *11*, 3691.

(30) Birchall, T.; Myers, R. D. *Spectrosc. Int. J.* **1983**, *2*, 22.

(31) Manna, J.; Geib, S. J.; Hopkins, M. D. *J. Am. Chem. Soc.* **1992**, *114*, 9199.

(32) Calabrese, J. C.; Cheng, L. T.; Green, J. C.; Marder, S. R.; Tam, W. *J. Am. Chem. Soc.* **1991**, *113*, 7227.

(33) Powell, C. E.; Cifuentes, M. P.; Morrall, J. P.; Stranger, R.; Humphrey, M. G.; Samoc, M.; Luther-Davies, B.; Heath, G. A. *J. Am. Chem. Soc.* **2003**, *125*, 602.

(34) Faulkner, C. W.; Ingham, S. L.; Khan, M. S.; Lewis, J.; Long, N. J.; Raithby, P. R. *J. Organomet. Chem.* **1994**, *482*, 139.

(35) Atherton, Z.; Faulkner, C. W.; Ingham, S. L.; Kakkar, A. K.; Khan, M. S.; Lewis, J.; Long, N. J.; Raithby, P. R. *J. Organomet. Chem.* **1993**, *462*, 265.

(36) Kizas, O. A.; Krivykh, V. V.; Vorontsov, E. V.; Tok, O. L.; Dolgushin, F. M.; Koridze, A. A. *Organometallics* **2001**, *20*, 4170.

(37) Koridze, A. A.; Sheloumov, A. M.; Dolgushin, F. M.; Yanovsky, A. I.; Struchkov, Y. T.; Petrovskii, P. V. *J. Organomet. Chem.* **1997**, *536-537*, 381.

(38) Koridze, A. A.; Kizas, O. A.; Petrovskii, P. V.; Kolobova, N. E.; Struchkov, Y. T.; Yanovsky, A. I. *J. Organomet. Chem.* **1988**, *338*, 81.

(39) Chi, Y.; Huttner, G.; Imhof, W. *J. Organomet. Chem.* **1990**, *384*, 93.

(40) Chi, Y.; Lin, R.-C.; Chen, C.-C.; Peng, S.-M.; Lee, G.-H. *Journal of Organometallic Chemistry* **1992**, *439*, 347.

(41) Ewing, P.; Farrugia, L. J. *J. Organomet. Chem.* **1987**, *320*, C47.

(42) Younus, M.; Long, N. J.; Raithby, P. R.; Lewis, J.; Page, N. A.; White, A. J. P.; Williams, D. J.; Colbert, M. C. B.; Hodge, A. J.; Khan, M. S.; Parker, D. G. *J. Organomet. Chem.* **1999**, *578*, 198.

(43) Baya, M.; Esteruelas, M. A.; Onate, E. *Organometallics* **2001**, *20*, 4875.

(44) Baerends, E. J.; Ellis, D. E.; Ros, P. *Chem. Phys.* **1973**, *2*, 42.

(45) Baerends, E. J.; Ros, P. *Chem. Phys.* **1973**, 2, 52.

(46) Baerends, E. J.; Ros, P. *Int. J. Quantum Chem.* **1978**, *S12*, 169.

(47) Vosko, S. H.; Wilk, L.; Nusair, M. *Can. J. Phys.* **1980**, *58*, 1200.

(48) Becke, A. D. J. *Chem. Phys.* **1986**, *84*, 4524.

(49) Perdew, J. P. *Phys. Rev. B.* **1986**, *33*, 8822.

(50) Perdew, J. P.; Cherary, J. A.; Vosko, S. H.; Jackson, K. A.; Pederson, M. R.; Singh, D. J.; Fiolhais, C. *Phys. Rev. A.* **1992**, *46*, 6671.

(51) van Lenthe, E.; Baerends, E. J.; Snijders, J. G. *Chem. Phys.* **1993**, *99*, 4597.

(52) Versluis, L.; Ziegler, T. *J. Chem. Phys.* **1988**, *88*, 322.

(53) Van Gisbergen, S. J. A.; Snijders, J. G.; Baerends, E. J. *Comput. Phys. Commun.* **1999**, *118*, 119.

Chapter 3

Electrochemical Switching of Third–Order Nonlinear Optical Properties

Chapter 3

Electrochemical Switching of Third–Order Nonlinear Optical Properties

Contents

3.1. *Introduction*

3.2. *Synthesis*

3.3. *Experimental Procedures to Switch Nonlinearities*

3.4. *Results and Discussion*

3.5. *Conclusions*

3.6. *Experimental*

3.7. *References*

Chapter 3

Electrochemical Switching of Third–Order Nonlinear Optical Properties

3.1. *Introduction*

An important cornerstone of modern electronics is the ability to modulate (switch) a physical property. Generally switching devices are built around switching electric currents, but the switching of other properties is also of considerable interest. As fabrication technology improves, the dimensions of electronic devices has shrunk. However, there appears to be a fundamental limit to the size reduction possible with current manufacturing technology. For this reason, research into optical molecular switches (a molecular switch is a molecule which alters its structural or electronic properties upon the addition of an external stimuli) has become popular,[1-6] and several patents have been granted.[7,8] Herein is reported the first practical switching of molecular third–order hyperpolarizabilities using electrochemical stimuli.

3.1.1. *Switching of Nonlinearities*

It is only relatively recently that reports of switching NLO properties have appeared in the chemical literature. This area was reviewed in 1999,[9] but, considerable work has since appeared. The current Section contains a brief review of developments in the field prior to the work presented here. Previous examples of NLO-switchable materials include proteins,[10] both organic and inorganic molecules,[11-16] azafulleroids,[17] and polymers.[18] These switches have been activated by a variety of methods: photochemical, chemical oxidation/reduction, protonation/deprotonation and through other chemical reactions.

3.1.1.1. *Switching via Protonation/Deprotonation Sequences*

A large number of acetylide/vinylidene complex pairs have been synthesized and their quadratic and molecular NLO properties reported in the literature. These results are tabulated in Table 3.1. for quadratic nonlinearities, and Table 3.2. for cubic nonlinearities. While switching via protonation/deprotonation sequences can be effective, the chemical manipulations remote from the optical bench may render this of academic interest only. Many of the vinylidene and acetylide complex pairs in Table 3.1. have similar nonlinearities, which significantly limits their applicability as effective NLO active switches, but a five-fold increase in β and β_0 values is observed on deprotonating the vinylidene complex *trans*-[Ru(C=CHC$_6$H$_4$-4-(*E*)-CH=CHC$_6$H$_4$-4-NO$_2$)Cl(dppe)$_2$]PF$_6$ to afford *trans*-[Ru(C≡CC$_6$H$_4$-4-(*E*)-CH=CHC$_6$H$_4$-4-NO$_2$)Cl(dppe)$_2$].[11] Proton/deprotonation switching of cubic NLO properties suffers from low nonlinearities and significant error margins, which have frustrated most attempts to demonstrate switching with vinylidene/acetylide complex pairs – perhaps the most clear-cut example afforded a five-fold increase in γ value on proceeding from *trans*-[Ru(C=CHC$_6$H$_4$-4-NO$_2$)Cl(dppm)$_2$]PF$_6$ to *trans*-[Ru(C≡CC$_6$H$_4$-4-NO$_2$)Cl(dppm)$_2$].[11,12]

Another interesting example of the protonation/deprotonation switching of second-order nonlinearities was performed by Clays and co-workers on an azafullaroid system.[17] Protonation of a dimethylamino group by trifluoroacetic acid lead to a substantial decrease in the molecular second-order hyperpolarizability. This decrease was not quantified, but could be reversed by the addition of Hünig's base.

Table 3.1. Switching of Molecular Quadratic NLO Properties via Protonation/Deprotonation Sequences[a]

Complex	λ (nm)	β (10^{-30} esu)	β_0 (10^{-30} esu)	Ref.
trans-[Ru(C≡CPh)Cl(dppm)$_2$]	308	20	12	11
trans-[Ru(C=CHPh)Cl(dppm)$_2$]PF_6	320	24	16	11
trans-[Ru(C≡CPh)Cl(dppe)$_2$]	319	6	3	11
trans-[Ru(C=CHPh)Cl(dppe)$_2$]PF_6	317	b	b	11
trans-[Ru(C≡CC_6H_4-4-C≡CPh)Cl(dppm)$_2$]	381	101	43	11
trans-[Ru(C=CHC_6H_4-4-C≡CPh)Cl(dppm)$_2$]PF_6	380	64	31	11
trans-[Ru(C≡CC_6H_4-4-CHO)Cl(dppm)$_2$]	405	106	38	11
trans-[Ru(C=CHC_6H_4-4-CHO)Cl(dppm)$_2$]PF_6	403	108	39	11
trans-[Ru(C≡CC_6H_4-4-CHO)Cl(dppe)$_2$]	413	120	40	11
trans-[Ru(C=CHC_6H_4-4-CHO)Cl(dppe)$_2$]PF_6	412	181	61	11
trans-[Ru(C≡CC_6H_4-4-NO_2)Cl(dppm)$_2$]	473	767	129	20
trans-[Ru(C=CHC_6H_4-4-NO_2)Cl(dppm)$_2$]PF_6	470	721	127	11
trans-[Ru(C≡CC_6H_4-4-NO_2)Cl(dppe)$_2$]	477	351	55	11
trans-[Ru(C=CHC_6H_4-4-NO_2)Cl(dppe)$_2$]PF_6	476	1130	180	11
trans-[Ru(C≡CC_6H_4-4-C≡CC_6H_4-4-NO_2)Cl(dppm)$_2$]	464	833	161	11
trans-[Ru(C=CHC_6H_4-4-C≡CC_6H_4-4-NO_2)Cl(dppm)$_2$]PF_6	326	424	122	11
trans-[Ru(C≡CC_6H_4-4-(*E*)-CH=CHC_6H_4-4-NO_2)Cl(dppm)$_2$]	490	1964	235	20
trans-[Ru(C≡CC_6H_4-4-(*E*)-CH=CHC_6H_4-4-NO_2)Cl(dppm)$_2$]PF_6	369	1899	314	11

Table 3.1. (continued) Switching of Molecular Quadratic NLO Properties via Protonation/Deprotonation Sequences[a]				
Complex	λ (nm)	β (10^{-30} esu)	β_0 (10^{-30} esu)	Ref.
trans-[Ru(C≡CC_6H_4-4-(*E*)-CH=CHC_6H_4-4-NO_2)Cl(dppe)$_2$]	489	2676	342	11
trans-[Ru(C≡CC_6H_4-4-(*E*)-CH=CHC_6H_4-4-NO_2)Cl(dppe)$_2$]PF_6	473	441	74	11

[a] HRS, 1.064 μm, thf

[b] scatters

Table 3.2. Switching of Molecular Cubic NLO Properties via Protonation/Deprotonation Sequences[a]

Complex	λ (nm)	Re γ (10^{-36} esu)	Im γ (10^{-36} esu)	γ (10^{-36} esu)	Solvent	Ref.
trans-[Ru(C≡CPh)Cl(dppm)$_2$]	308	<120	0	<120	thf	11
trans-[Ru(C=CHPh)Cl(dppm)$_2$]PF_6	320	<440	<50	<440	thf	11
trans-[Ru(C≡CPh)Cl(dppe)$_2$]	319	-170 ± 40	71 ± 20	180 ± 45	CH_2Cl_2	21
trans-[Ru(C=CHPh)Cl(dppe)$_2$]PF_6	317	380 ± 400	<50	380 ± 400	thf	11
trans-[Ru(C≡CC_6H_4-4-C≡CPh)Cl(dppm)$_2$]	381	65 ± 40	520 ± 200	520 ± 200	thf	11
trans-[Ru(C=CHC_6H_4-4-C≡CPh)Cl(dppm)$_2$]PF_6	380	<500	0	<500	thf	11
trans-[Ru(C≡CC_6H_4-4-CHO)Cl(dppm)$_2$]	405	<120	210 ± 60	210 ± 60	thf	11
trans-[Ru(C=CHC_6H_4-4-CHO)Cl(dppm)$_2$]PF_6	403	0	<20	<20	thf	11
trans-[Ru(C≡CC_6H_4-4-CHO)Cl(dppe)$_2$]	413	-300 ± 500	<200	300 ± 500	thf	11
trans-[Ru(C=CHC_6H_4-4-CHO)Cl(dppe)$_2$]PF_6	412	<260	0	<260	thf	11
trans-[Ru(C≡CC_6H_4-4-NO_2)Cl(dppm)$_2$]	473	170 ± 34	230 ± 46	290 ± 60	CH_2Cl_2	12
trans-[Ru(C=CHC_6H_4-4-NO_2)Cl(dppm)$_2$]PF_6	470	<50	<30	<50	thf	11
trans-[Ru(C≡CC_6H_4-4-NO_2)Cl(dppe)$_2$]	477	320 ± 55	<50	320 ± 55	thf	11
trans-[Ru(C=CHC_6H_4-4-NO_2)Cl(dppe)$_2$]PF_6	476	250 ± 300	<50	250 ± 300	thf	11
trans-[Ru(C≡CC_6H_4-4-C≡CC_6H_4-4-NO_2)Cl(dppm)$_2$]	464	-160 ± 80	160 ± 60	230 ± 100	thf	11
trans-[Ru(C=CHC_6H_4-4-C≡CC_6H_4-4-NO_2)Cl(dppm)$_2$]PF_6	326	<500	420 ± 60	420 ± 60	thf	11
trans-[Ru(C≡CC_6H_4-4-(*E*)-CH=CHC_6H_4-4-NO_2)Cl(dppm)$_2$]	490	200 ± 40	1100 ± 220	1100 ± 220	CH_2Cl_2	12
trans-[Ru(C≡CC_6H_4-4-(*E*)-Ch=CHC_6H_4-4-NO_2)Cl(dppm)$_2$]PF_6	369	b	b	b	thf	11

Table 3.2. (continued) Switching of Molecular Cubic NLO Properties via Protonation/Deprotonation Sequences[a]						
Complex	λ (nm)	Re γ (10^{-36} esu)	Im γ (10^{-36} esu)	γ (10^{-36} esu)	Solvent	Ref.
trans-[Ru(C≡CC_6H_4-4-(*E*)-CH=CHC_6H_4-4-NO_2)Cl(dppe)$_2$]	489	40 ± 200	<100	40 ± 200	thf	11
trans-[Ru(C≡CC_6H_4-4-(*E*)-CH=CHC_6H_4-4-NO_2)Cl(dppe)$_2$]PF_6	473	650 ± 500	<50	650 ± 500	thf	11

[a] Z-scan, 0.80 μm

[b] scatters

3.1.1.2. *Switching via Chemical Oxidation/Reduction Sequences*

A series of second-order NLO molecular switches have been synthesized by Coe and co-workers.[13] Ruthenium pentammine bipyridinium chlorides (Figure 3.1.) can be oxidized by H_2O_2 and HCl. These oxidized complexes show a very significant reduction in β (estimated to be in the order of 10 – 20 fold, relative to the neutral species). This reduction can be reversed by the addition of a hydrazine hydrate solution. By the successive addition of oxidizing and reducing agents, the switch can be shuttled back and forth. This approach is, however, unsuitable for devices as each successive switching process is carried out at the laboratory bench, and with every switching process, the solution gets progressively more dilute.

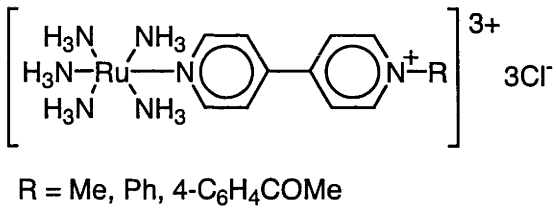

R = Me, Ph, 4-C_6H_4COMe

Figure 3.1. Ru^{II}-4,4'-bipyridinium chromophores of Coe and co-workers[13]

Sortino and co-workers have likewise demonstrated the applicability of a pentammine ruthenium bipyridinium complex for NLO switching.[22] They attached the complex to an ultrathin platinum film, and oxidized the complex with a cerium sulfate solution. Reduction was achieved with addition of hydrazine. While the change in nonlinearities was not measured, the large change in the optical absorption spectra provides evidence for a similar change in the nonlinearities.

Similar results have also been obtained by Ward and co-workers.[14] Oxidation [by the addition of $(NBu_4)Br_3$] of an octamethylferrocene donor linked to a nitrothiophene acceptor via an ethenyl bridge (Figure 3.2.) leads to a significant reduction of the quadratic hyperpolarizability. This can be reversed by addition of hydrazine. The neutral species has a static β value of 95 x 10^{-30} esu, whereas the oxidized species has a β value of 10 x 10^{-30} esu (the β value at 1064 nm likewise change from 316 x 10^{-30} esu to 25 x 10^{-30} esu upon

oxidation). The hexafluorophosphine salt of the cation was also reduced then oxidized, affording similar results.

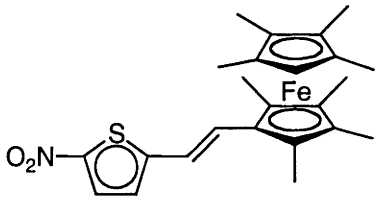

Figure 3.2. Switchable chromophore of Ward and co-workers[14]

A series of iron acetylide complexes have been synthesized by Lapinte and co-workers (Figure 3.3.).[19] Because of the close proximity of the iron centres, it is possible to synthesize and isolate the hexafluorophosphate salt of all of the various combinations of Fe^{II} and Fe^{III} oxidation states. For example, the trimetallic octopolar complex shown at the bottom of Figure 3.3. is available in the following states: $Fe^{II}/Fe^{II}/Fe^{II}$, $Fe^{II}/Fe^{II}/Fe^{III}$, $Fe^{II}/Fe^{III}/Fe^{III}$, and $Fe^{III}/Fe^{III}/Fe^{III}$. As each of these states has a different hyperpolarizability, there exists considerable scope for molecular switches.

Of particular interest is the mixed valence complex $[Fe^{II}(dppe)(\eta^5\text{-}C_5Me_5)(C{\equiv}CC_6H_4\text{-}4\text{-}C{\equiv}C)Fe^{III}(dppe)(\eta^5\text{-}C_5Me_5)](PF_6)$. This complex undergoes a substantial decrease in second-order nonlinearities upon either reduction or oxidation to the Fe^{II}/Fe^{II} or Fe^{III}/Fe^{III} states, respectively.

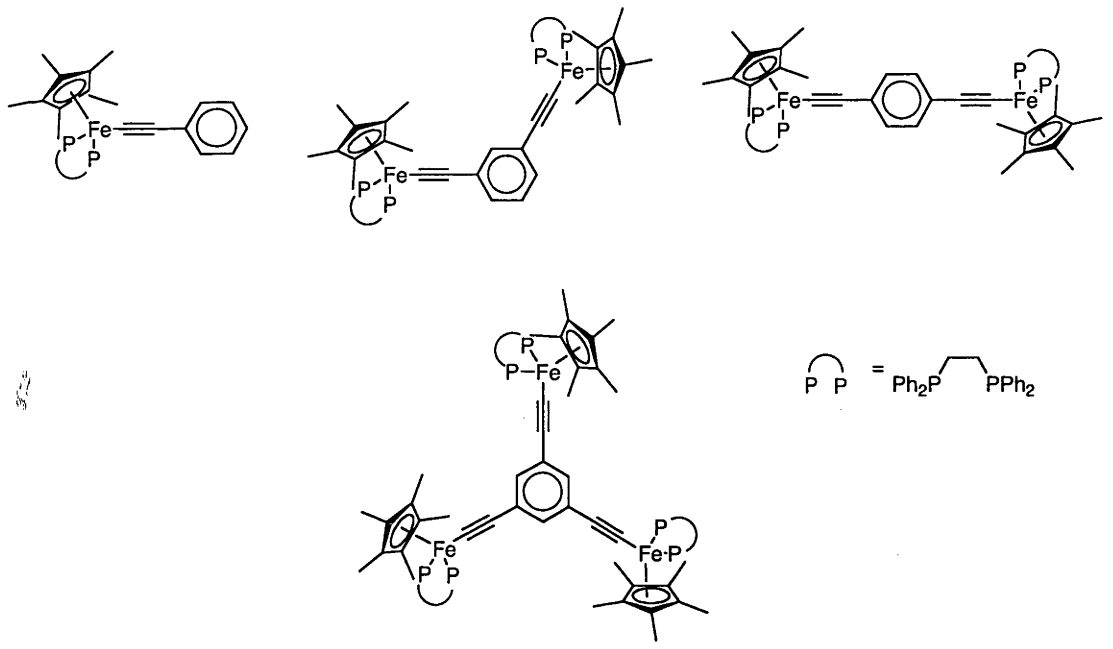

Figure 3.3. Iron acetylides of Lapinte and co-workers[19]

3.1.1.3. *Switching via Other Chemical Reactions*

Other examples of switching NLO properties by chemical reactions include recent work by Di Bella and co-workers.[15] A series of Schiff bases have been synthesized, upon incorporation of a metal, a significant increase in β_μ is observed (Figure 3.4.). This approach is limited, as it has not been shown to be reversible, so the switch is essentially "one-way", and, as the switch involves a chemical reaction, significant time and effort must be expended in "turning on" the NLO response.

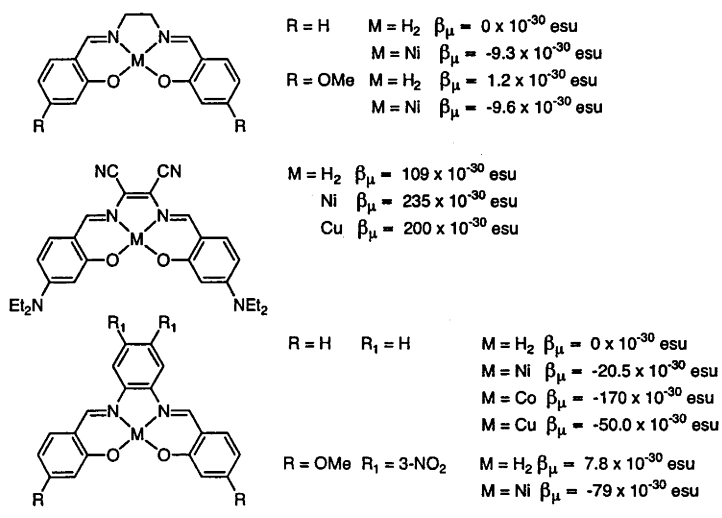

Figure 3.4. Metalloorganic chromophores used by Di Bella and co-workers[15]

3.1.1.4. *Switching via Photochemistry*

The switching of molecular second-order hyperpolarizabilities has been observed in the protein *bacteriorhodopsin* (bR). In nature bR plays an important role in energy generation systems of bacteria as a photon-driven H+ pump. Analogues of bR are found in most animal species, where they play a role in vision. Structurally, bR can be described as consisting of seven α-helixes surrounding a retinal chromophore.[23] The photocycle of bR is summarized in Figure 3.5. The molecular second-order hyperpolarizability at 1064 nm has been measured by HRS, and found to be very large (2100 x 10^{-30} esu).[24] Song and co-workers have observed 532 nm SHG from suspensions of the purple membrane of *Halobacterium halogium* (which contains significant amounts of orientated bR) in water.[10] When 570 nm light is used to photoexcite the protein, the observed SHG drops by 60 – 90% depending on the degree of dilution. Some model complexes of the chromophores have been synthesised and their molecular second-order hyperpolarizabilities studied (Figure 3.6.).[25] The differing optical properties of the different states of bR allows the demonstration of many interesting optical effects.[26]

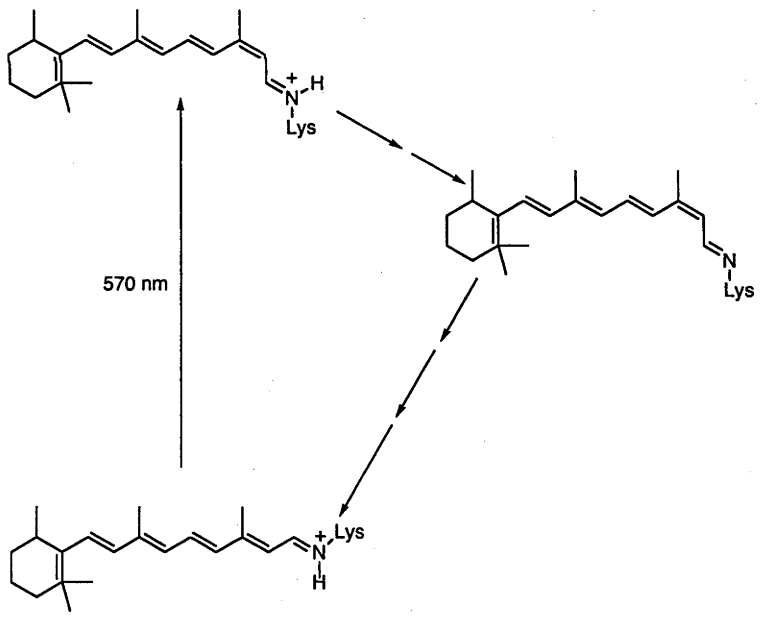

Figure 3.5. Chromophore of bR during the photocycle

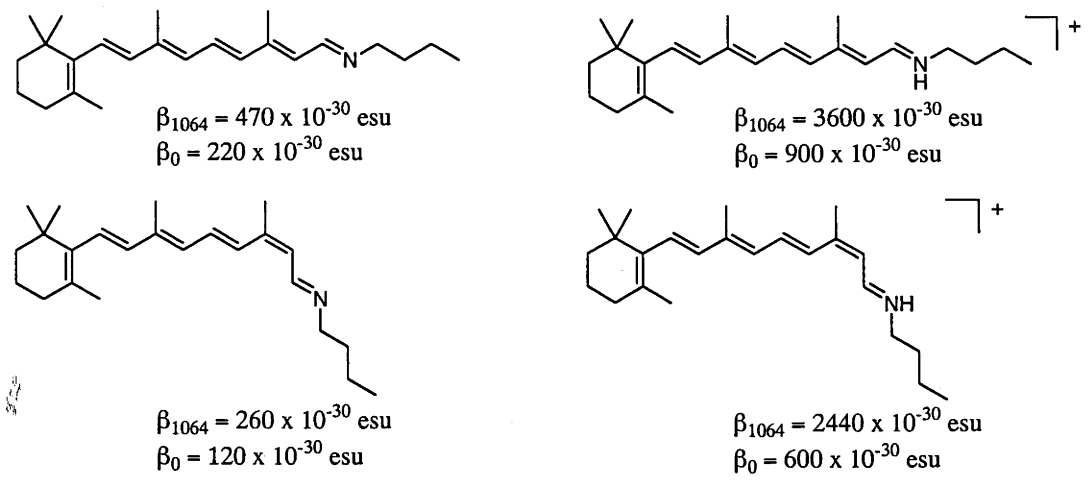

Figure 3.6. Model complexes of the bR chromophore and their molecular second-order hyperpolarizabilities[25]

Another method of switching hyperpolarizabilities involves photoisomerization of polymers. Sekkat and co-workers have synthesized azo polyimide polymers (Figure 3.7.) and examined switching third-order hyperpolarizabilities.[18] In the resting state, the polymers (spin cast onto glass slides) have the azo linkage in a *trans* conformation. Upon irradiation with green light (543.5 nm) from a He-Ne laser, the observed second-harmonic light drops considerably. As the polymers have a β value of approximately zero, the authors constructed a theoretical argument for the change in second-harmonic light arising from a decrease in γ. Once irradiation with green light is stopped, the polymers thermally revert back to a *trans* conformation, leading to an increase in third-order hyperpolarizabilities.

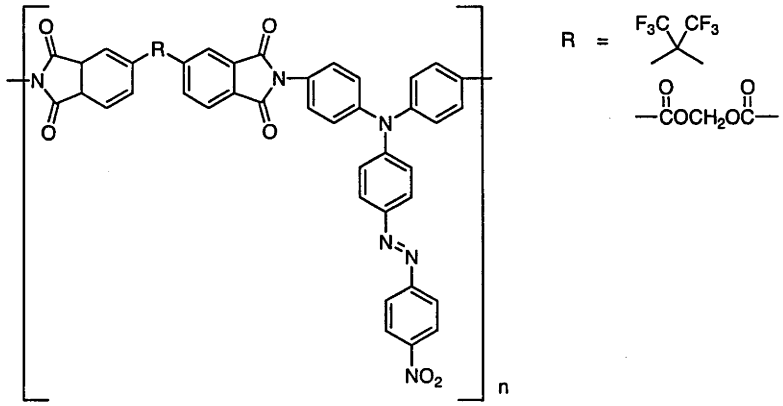

Figure 3.7. Azo polyimide polymers of Sekkat and co-workers[18]

Sortino and co-workers have used the pair of complexes $[Ru^{III/II}(NH_3)_5(N\text{-methyl-4,4'-bipyridinium})](PF_6)_n$ as a dipolar multifunctional molecular switch.[27] The Ru^{II} species undergoes photooxidation upon irradiation of light at 254 nm, whereas the Ru^{III} species undergoes photoreduction when irradiated with light at 528 nm. While the switching of nonlinearities on this system has yet to be demonstrated, the large change in the optical absorption spectrum suggests that switching of the nonlinearities is possible.

3.1.1.5. *Switching via Magnetic Spin Crossover*

An interesting possibility to afford a NLO-active molecular switch is the exploitation of spin-cross. Létard and co-workers have examined the second-order nonlinearities and magnetism data for a large number of coordination compounds ($[M(PM\text{-}L)_2(NCS)_2]$, where M = Mn, Fe, Co, Ni and Zn, and PM-L represents a variety of large aromatic ligands), although a working switch has yet to be demonstrated.[16]

3.1.1.6. *Overview*

While the switching of nonlinearities summarized above has been demonstrated by several means, all examples exhibit practical difficulties which limit their usefulness. These difficulties include long periods of time required to perform the switch (this is particularly acute when a chemical reaction is required to switch), relaxation of one state to an other, and an inability to quantify the change in nonlinearities induced by the switch.

It is proposed that the use of an electrochemical switch may reduce some of these difficulties. As electrochemical reactions tend to be diffusion limited, the time required to perform a switch can be significantly reduced from that of a chemical reaction.

Prior to the completion of this Thesis, but subsequent to the initial publication of our results,[28,29] Clays and co-workers demonstrated the electrochemical switching of the first hyperpolarizability of the chromophore depicted in Figure 3.2.[30] A similar change in the hyperpolarizabilities to that achieved with the previous chemical redox switching was observed.

3.1.2. *Theoretical Background*

As discussed in Chapter 2, oxidation of bis(bidentate phosphine)ruthenium acetylide complexes results in the appearance of a strong absorption band in the range 8400 – 12 000 cm^{-1}. Upon reduction to the neutral species, this band disappears (an example is shown in Figure 3.8.). The presence of this reversible absorption band affords the possibility of an electrochemical molecular NLO switch.

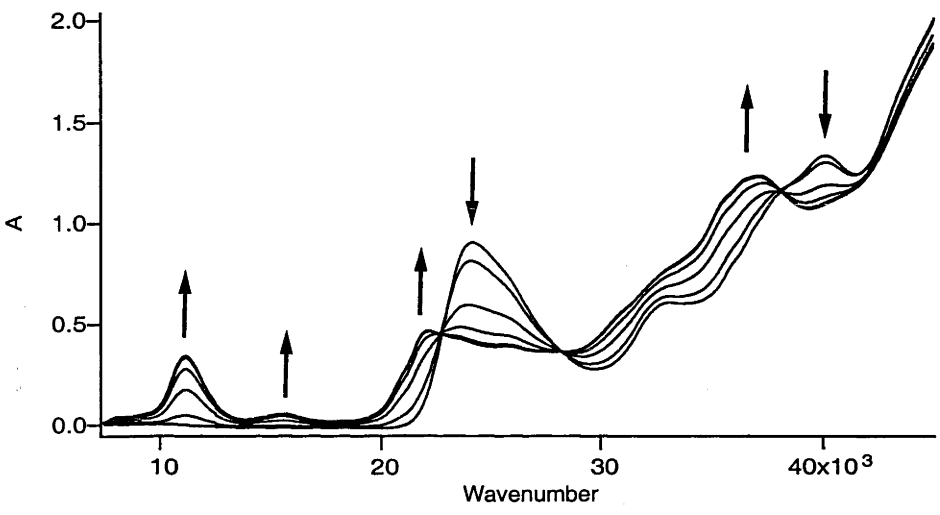

Figure 3.8. UV-Vis-NIR spectra of a CH_2Cl_2 solution of 1,3,5-C_6H_3{4-C≡CC_6H_4C≡C-*trans*-[RuCl(dppe)$_2$]}$_3$ (**4**) during oxidation at $E_{appl} \approx 0.80$ V at 248 K.

(M. P. Cifuentes)

The relationship between hyperpolarizabilities and optical absorption bands can be described by perturbation theory:

$$\beta \approx 3(\mu_{ee} - \mu_{gg})(\mu_{ge}^2/E_{ge}^2)$$

$$\gamma \propto -\mu_{ge}^4/E_{ge}^3 + \mu_{ge}^2\mu_{ee'}^2/E_{ge}^2E_{ge'} + \mu_{ge}^2(\mu_{ee} - \mu_{gg})^2/E_{ge}^3$$

where μ_{gg} is the ground state dipole moment, μ_{ee} is the excited state dipole moment, $\mu_{ee'}$ and μ_{ge} are transition dipole moments, and E_{ge} and $E_{ge'}$ are the optical absorption energies.[31] As E_{ge} and μ_{ge} are related to λ_{max} and ε, respectively, the existence of a strong reversible absorption band should ensure a significant change in the hyperpolarizabilities at the relevant wavelength (8400 – 12 000 cm^{-1}).

This range of wavelengths encompasses several technologically interesting frequencies. Many biological materials have high optical transparency at 12 500 cm^{-1}, whereas silica has a high optical transparency at wavelengths corresponding to 8300 and 7700 cm^{-1} (the so-called telecommunications wavelengths). For these reasons, a series of ruthenium mono- and bis-acetylide complexes (*trans*-[Ru(C≡CPh)Cl(dppm)$_2$] (**1**), *trans*-[Ru(C≡CC$_6$H$_4$-4-C≡CPh)Cl(dppe)$_2$] (**2**), *trans*-[Ru(C≡CPh)(C≡CC$_6$H$_4$-4-C≡CPh)(dppe)$_2$] (**3**), 1,3,5-C$_6$H$_3${C≡CC$_6$H$_4$-4-C≡C-*trans*-[RuCl(dppe)$_2$]}$_3$ (**4**) and 1,3,5-C$_6$H$_3${C≡CC$_6$H$_4$-4-C≡C-*trans*-[Ru(C≡CPh)(dppe)$_2$]}$_3$ (**5**) have been synthesized (Figure 3.9. and 3.10.) and their utility as reversible molecular third-order hyperpolarizability switches investigated.

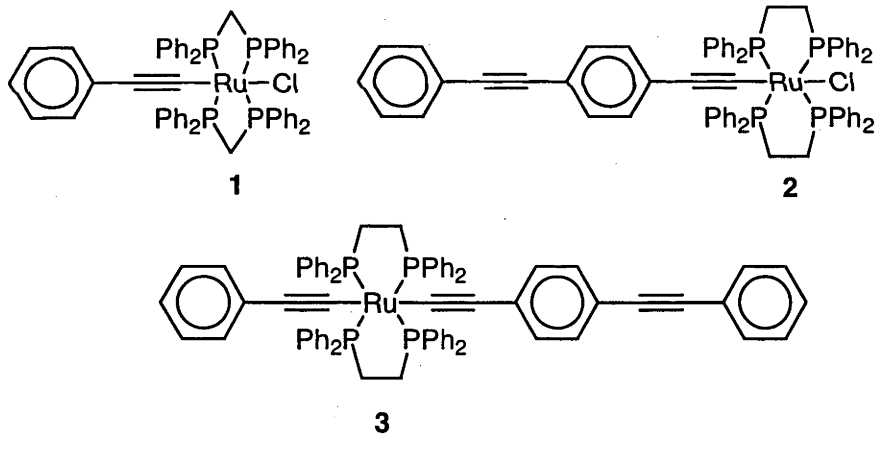

Figure 3.9. Linear ruthenium mono- and bis-acetylide complexes investigated as NLO switches

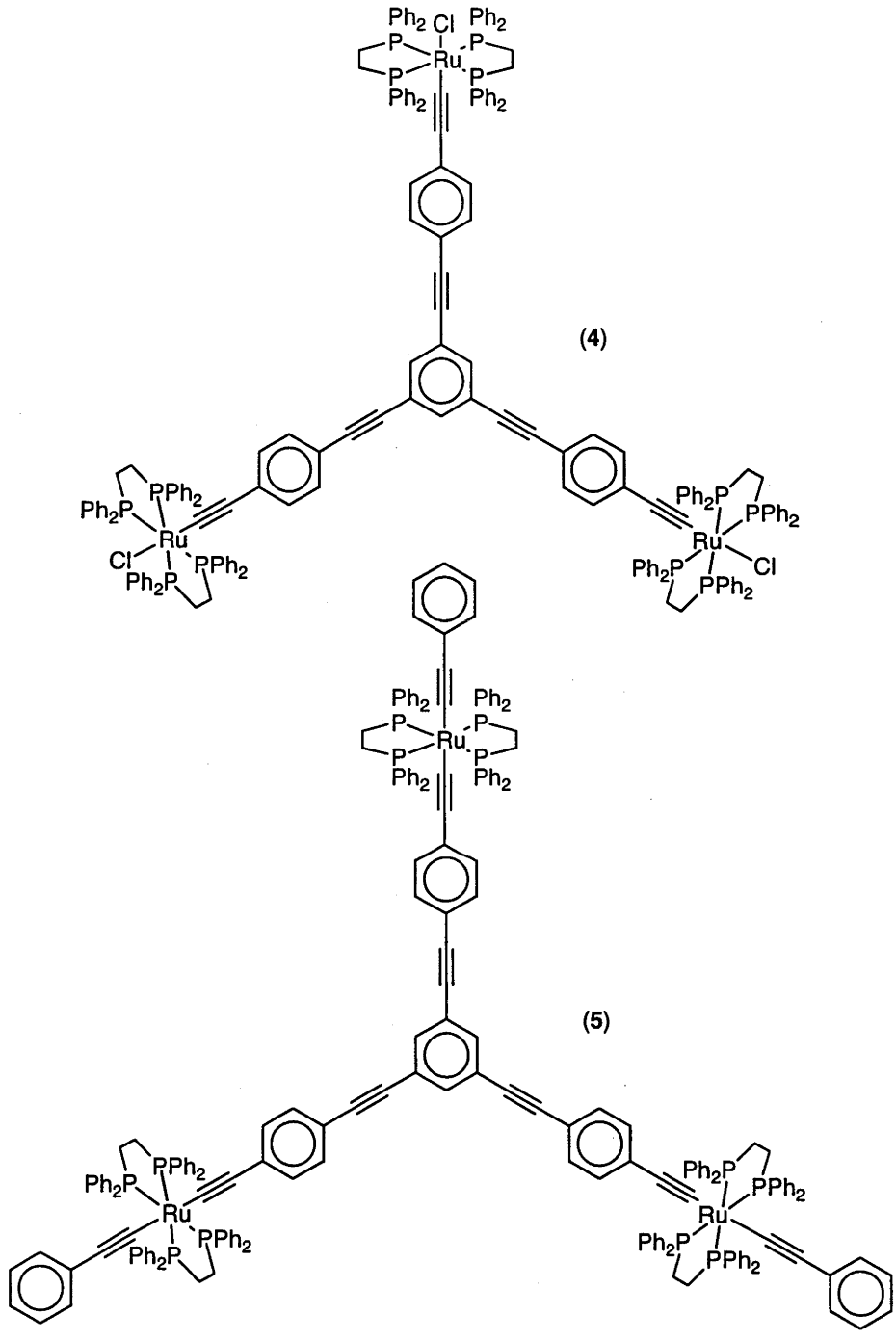

Figure 3.10. Octopolar ruthenium mono- and bis- acetylide complexes investigated as NLO switches

3.2. *Synthesis*

Most of the compounds studied in this section have been previously reported in the literature,[32-36] the exception being *trans*-[Ru(C≡CC$_6$H$_4$-4-C≡CPh)Cl(dppe)$_2$] (**2**). All of the acetylide complexes were synthesized by coupling an acetylene onto a bis(bidendatephosphine)ruthenium chloride complex (Schemes 3.1. and 3.2.).

Trans-[Ru(C≡CC$_6$H$_4$-4-C≡CPh)Cl(dppe)$_2$] (**2**) was characterized by MALDI mass spectrometry, satisfactory microanalysis, UV-vis spectroscopy, ^{1}H, and ^{31}P NMR spectroscopy. The MALDI mass spectrum contains the parent ion as well as peaks corresponding to the loss of the chlorine and acetylide ligands. The ^{1}H NMR spectrum shows the complex phenyl region ranging from 6.5 – 7.5 ppm, and the dppe bridging protons displaying a broad peak at 5.3 ppm. The ^{31}P NMR shows a singlet at 49.7 ppm, confirming the *trans* geometry of the phosphine ligands.

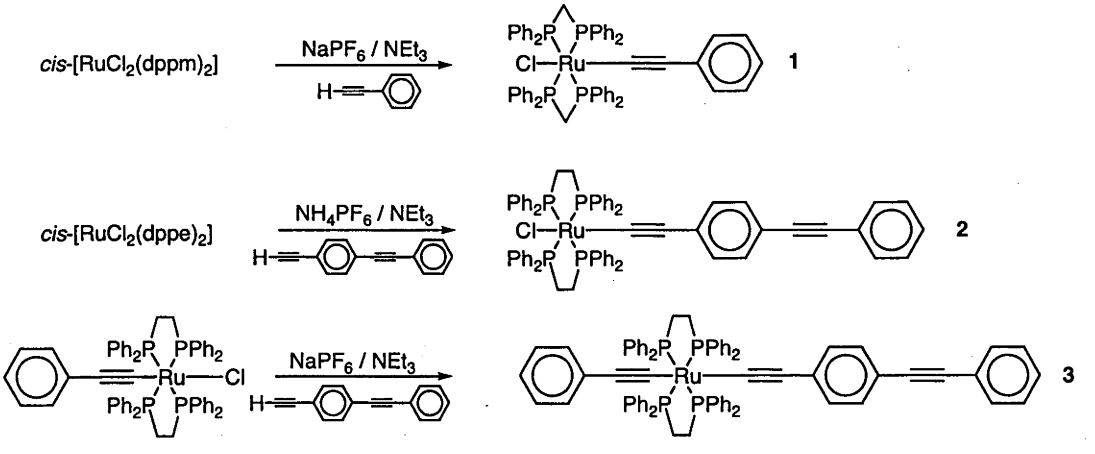

Scheme 3.1. Syntheses of linear ruthenium acetylide complexes.
1 and **3** were synthesized by the literature method.[32,34]

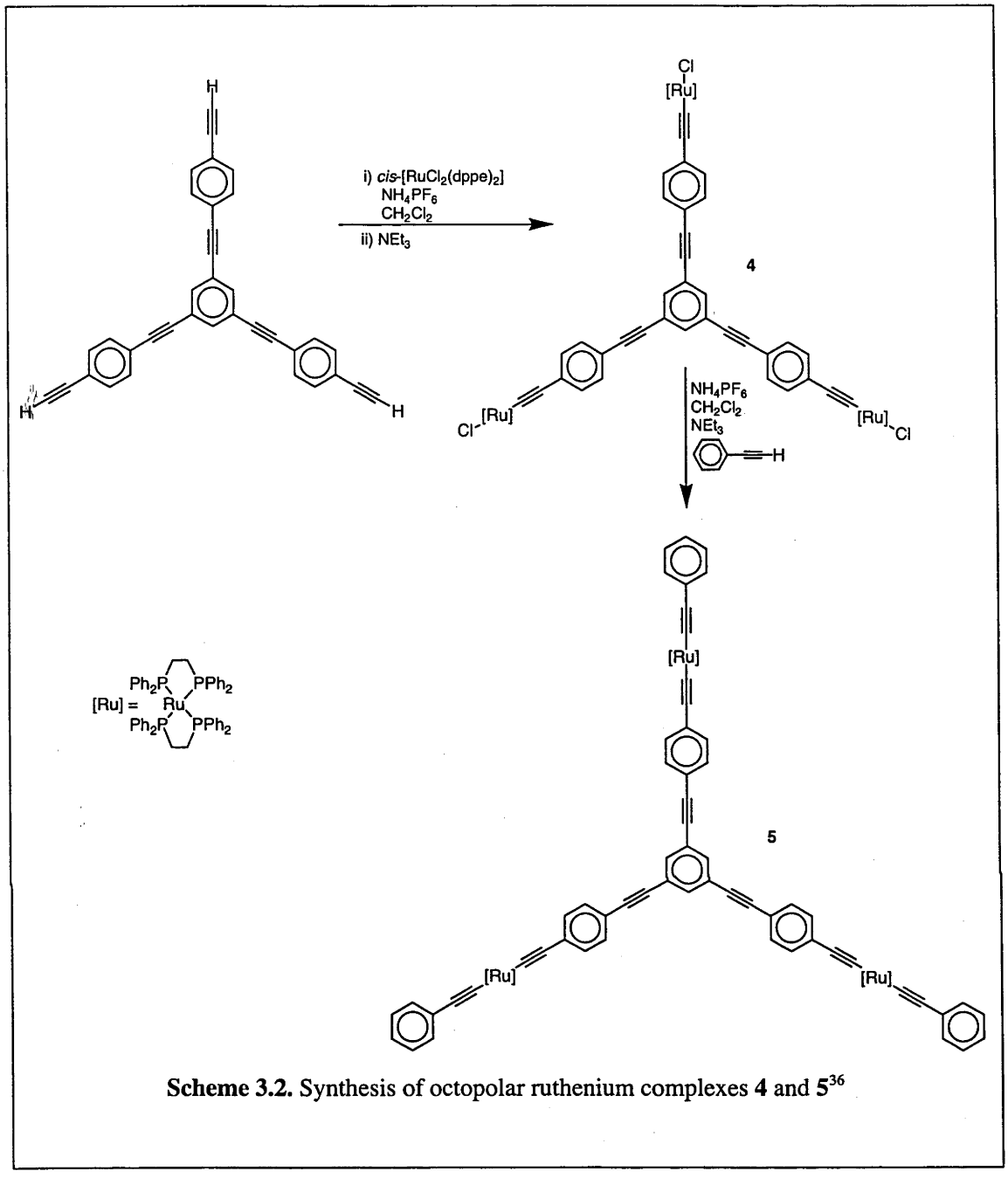

Scheme 3.2. Synthesis of octopolar ruthenium complexes **4** and **5**[36]

3.3. *Experimental Procedures to Switch Nonlinearities*

The switching of the third-order nonlinearities was examined with two different experimental set-ups. Initially, a modified Z-scan set-up was used to determine the molecular third-order nonlinearities of both the neutral and oxidized species. Both open and closed aperture Z-scans were undertaken. In order to extract further information, in particular the temporal nature of the response, a modified DFWM set-up was used to investigate one complex (**4**) in greater detail. To perform the electrochemical oxidation and reduction on the complexes, it was necessary to incorporate a potentiostat and OTTLE cell into both the Z-scan and DFWM set-up. Details of the modified apparatus are given below.

3.3.1. *OTTLE Cell*

The OTTLE cell consisted of a 0.5 mm quartz cell containing a thin platinum working electrode immersed in a dichloromethane solution of the sample and electrolyte $(NBu^n_4)PF_6$. The electrode had a 1.5 mm hole to allow the passage of the laser pulses. Above the 0.5 mm section of the cell was a larger solvent reservoir containing the reference (Ag/AgCl wire) and counter electrode (platinum wire). The cell was isolated from the atmosphere and was purged with argon before being filled with an argon-saturated solution of the sample and electrolyte in dichloromethane.

3.3.2. *Z-Scan Apparatus*

The Z-scan set-up is based on the description in Chapter 1, and is shown in Figure 3.11. Two different laser sources were used, depending on the wavelength of the switchable absorption band. A Ti-sapphire laser was used to supply 800 nm femtosecond pulses for studying the mono-acetylide complexes, and a tuneable Topas optical parametric amplifier was used to supply femtosecond pulses of 1180 and 1200 nm for studying the bis-acetylide complexes.

In addition to the closed aperture measurements, open aperture measurements were also carried out. This measures the total transmission of the beam, as the sample moves through the focal point. From this, the nonlinear absorption can be determined. If the transmission

dips downwards as the sample transverses the focal point of the laser, the sample is acting as a two-photon absorber. Likewise, if the transmission increases as the sample transverses the focal point, the sample is acting as a saturable absorber.

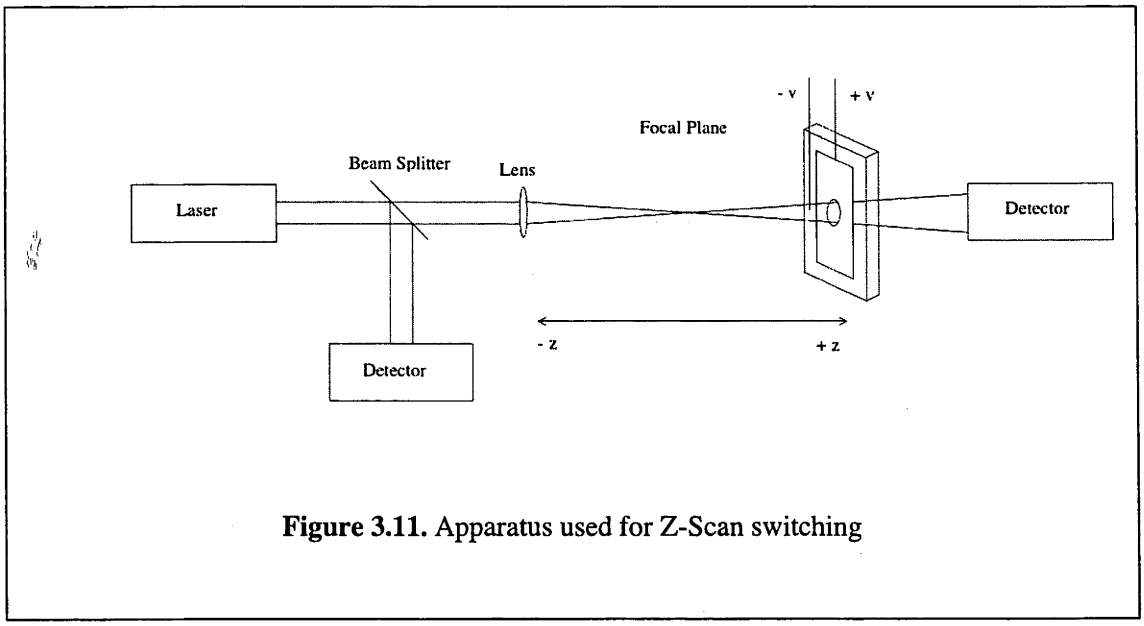

Figure 3.11. Apparatus used for Z-Scan switching

3.3.3. *Degenerate Four-Wave Mixing Apparatus*

Figure 3.12. displays the experimental set-up of the simultaneous DFWM and pump-probe experiments for in-situ measurements of electrochemical switching of third-order nonlinearity. A Ti-sapphire laser was used to supply 800 nm femtosecond pulses. Beams 1 and 2 were timed to arrive at the sample (a hole in the Pt electrode) simultaneously while the delay of beam 3 was scanned with a computer-controlled delay line. The phase-matched DFWM signal appearing in the fourth corner of the rectangle defined by the three incident beams was monitored as a function of the beam 3 delay. The intensity of beam 3 transmitted through the sample was also monitored: this provided a pump-probe (transient absorption, TA) signal where beams 1 and 2 were pumps and beam 3 was the probe monitoring transmission changes induced by the pumps.

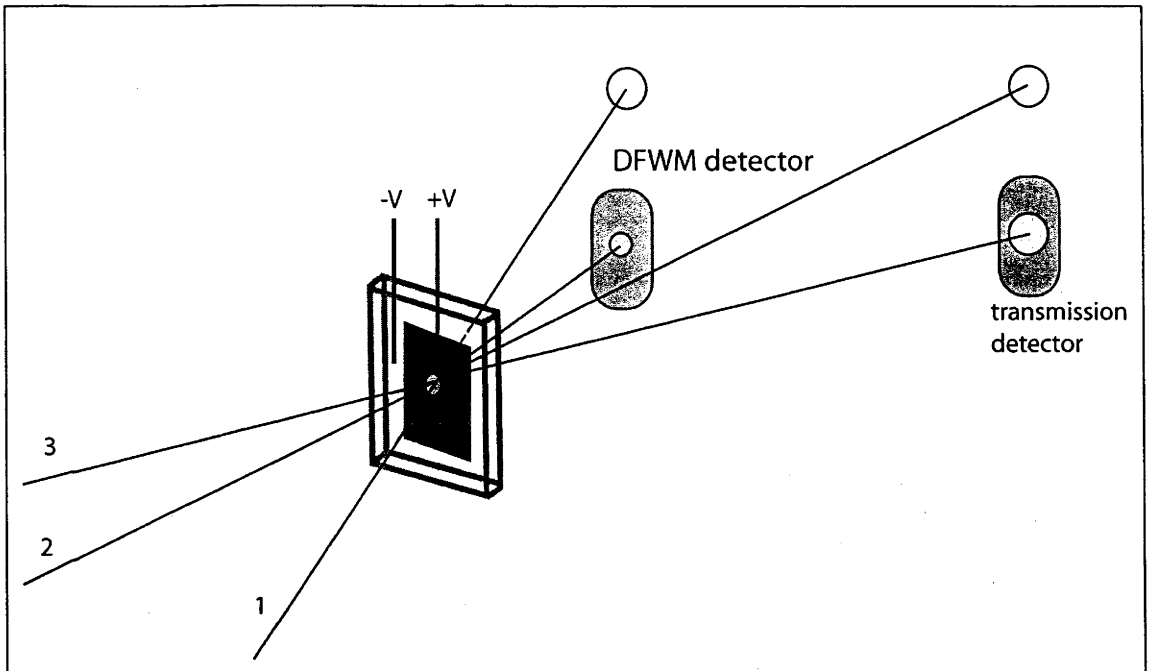

Figure 3.12. DFWM and OTTLE cell set-up used to probe third-order nonlinearities of **4**

3.4. *Results and Discussion*

3.4.1. *Z-Scan Switching*

3.4.1.1. *Switching of Mono-Acetylide Complexes*

Complexes **1**, **2**, and **4** all show similar changes in optical behaviour during oxidation and reduction. Therefore only one example will be examined in detail. Figure 3.13. shows the effect of oxidation and reduction on the open and closed aperture Z-scan traces (800 nm, 100 fs pulses) of octopolar complex **4** (0.18% w/w solution in dichloromethane). The upper two curves (empty squares and circles) show the Z-scan data for the neutral complex (the open aperture results are plotted with squares, and the closed aperture results are plotted with circles). These two traces are indicative of a strong nonlinear absorption. The lower two traces (filled squares and circles) are from the oxidized complex. The different shapes of these traces are consistent with the solution changing from showing strong nonlinear absorption to acting as a saturable absorber.

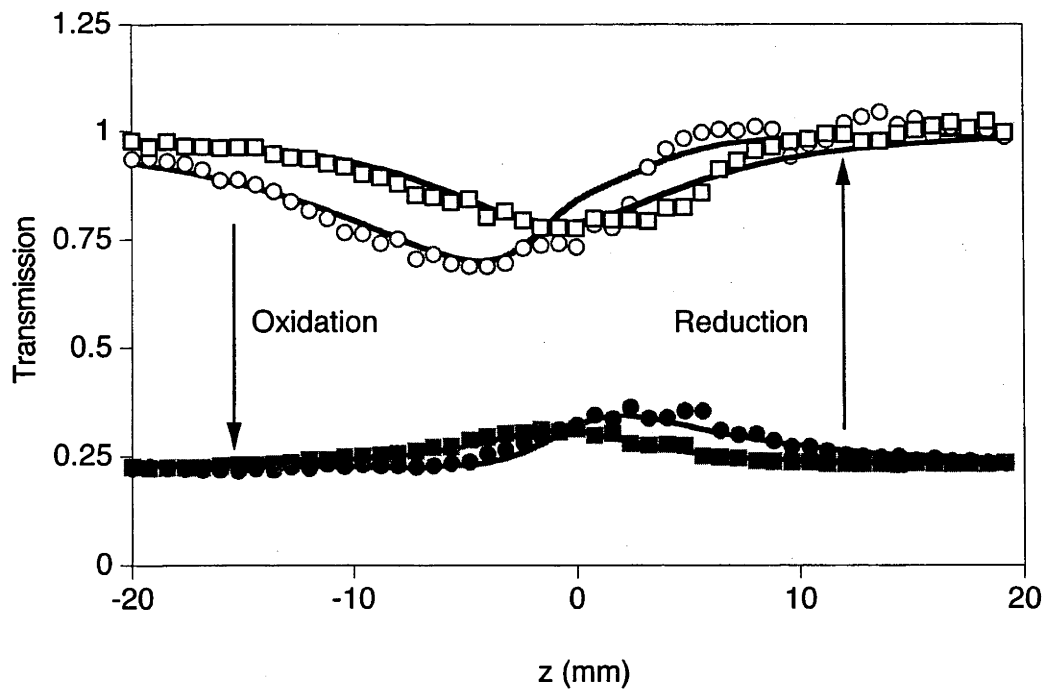

Figure 3.13. Closed and open aperture Z-scan traces for the neutral and oxidized forms of **4**

The change in transmission of the open aperture Z-scan experiment during oxidation and reduction of complex **4** is illustrated in Figure 3.14. Panel (a) depicts the open aperture trace of the neutral complex. The strong nonlinear absorption is easily observable. Upon introduction of the oxidation potential (0.8 V), there is a transition period (Panel (b)) where the transmission plunges (due to the growth of the strong absorption band). This starts to level out as all of the complex is fully converted into the oxidized form (Panel (c)). After sufficient time has elapsed, a new equilibrium between the oxidized and neutral complexes around the electrode is reached and the signal stabilizes (Panel (d)). At this point the third-order properties of the oxidized complex were determined (it is assumed that the amount of neutral molecules in the beam is very low relative to the amount of oxidized molecules). The open aperture results indicate that the solution is now acting as a saturable absorber. Finally, the potential is changed to 0 volts (Panel (e)). This leads to a gradual increase in the transmission (due to the loss of the strong absorption band) (Panels (f) and (g)). Panel (h) shows the endpoint, where the neutral complex has been fully regenerated, once again showing strong nonlinear absorption.

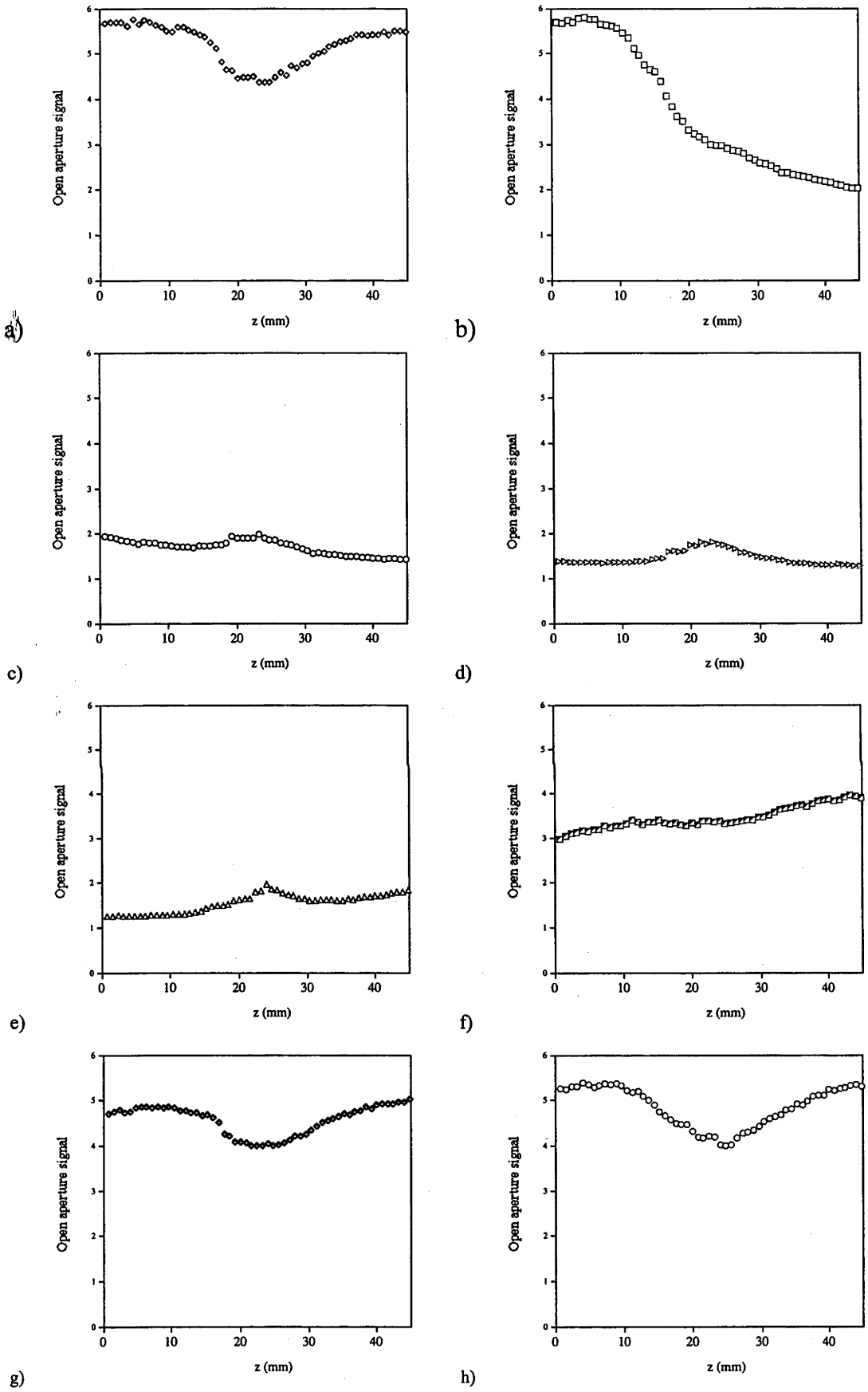

Figure 3.14. Change in open aperture Z-Scan traces over an oxidation/reduction cycle

The electrochemical potentials, linear optical data, and third-order hyperpolarizabilities for mono-acetylide complexes and the corresponding complex cations, **1/1**$^{+}$, **2/2**$^{+}$ and **4/4**$^{+}$ are tabulated in Table 3.3.

Complex **1** has either a very low, or non-existent third-order response. Upon oxidation, it has moderate third-order nonlinearities. Complex **2** has a small negative component of the real third-order hyperpolarizability, and a moderate imaginary component of the third-order nonlinear response, and therefore two-photon absorption. Upon oxidation the real component of the hyperpolarizability changes in sign and increases in magnitude considerably. Similar behaviour is observed with the imaginary component of the hyperpolarizability, leading to the complex changing from a weak two-photon absorber to a saturable absorber. The octopolar complex **4** shows similar behaviour to **2**, except that the absolute values of the hyperpolarizability of both the neutral and oxidized complexes are larger.

An important consideration to take into account is the stability of the oxidized complexes. If oxygen is not rigorously excluded from the cell, the strong absorption band which is crucial for the switching phenomenon is observed to decay, disappearing after approximately half an hour. If the cell is maintained under anaerobic conditions, the oxidized complex does not appear to decay. A sample was maintained under an inert atmosphere overnight with no observable decay (as measured by UV/vis spectroscopy).

Table 3.3. Third-order hyperpolarizabilities of neutral and oxidized mono-acetylide complexes

Complex / complex cation	$E_{1/2}$ (V) ($Ru^{II/III}$)	ν_{max} (cm^{-1})	ε (10^4 M^{-1} cm^{-1})	γ_{real} (10^{-36} esu)	γ_{imag} (10^{-36} esu)	$\lvert\gamma\rvert$ (10^{-36} esu)	$\sigma 2$ (10^{-50} cm^4 s)
1	0.55	31400	2.3	<300	<200	≅0	≅0
1+		12000	1.0	1300 ± 500	-2200 ± 1000	2600 ± 1000	–540 ± 200
2	0.55	25800	3.6	-100 ± 100	450 ± 200	460 ± 200	110 ± 50
2+		11200	2.0	2900 ± 1000	-1200 ± 600	3100 ± 1000	–300 ± 70
4	0.51	24200	9.9	-330 ± 100	2200 ± 500	2200 ± 600	530 ± 120
4+		11200	7.8	13500 ± 3000	-4700 ± 500	14000 ± 3000	–1200 ± 100

3.4.1.2. *Switching of Bis-Acetylide Complexes*

Results obtained at longer wavelengths can only be considered preliminary at this stage. Analysis of these results indicates that they are influenced to some degree by additional effects which may be due to nonlinearities of non-electronic origin, possibly thermal nonlinearities. Unlike the 800 nm measurements which were performed with the rather low repetition rate of 30 Hz, the laser system for the 1180 and 1300 nm measurements was operating with a repetition rate of 1 kHz. This, together with possibility of overtone absorption, may be a factor producing effectively negative nonlinearity of the electrochemical cell with the electrolyte solution that is observed. In essence, the nonlinearity due to the solutes could be observed (positive in the case of all compounds investigated at 1.18 and 1.3 micron), but the background solvent/cell nonlinearity could not be subtracted from the total effect in a precise way.

Figure 3.15. shows an example of the results obtained during electrochemical switching of a 0.2% w/w solution of **3** at 1180 nm in dichloromethane. Similar to the results above for the mono-acetylide complex **4** (Section 3.4.1.1.), the electrochemically induced change of transmission (or electrochromic effect) also results in a change of nonlinear optical properties of the complex. The filled circles plot the open aperture Z-scan results of the neutral complexes, and the filled squares plot the closed aperture results of the same complex. The open symbols plot the same results for the oxidized complex. The characteristic shapes of open and closed aperture scans allow a simple interpretation of the changes of the optical properties of the molecule. While the neutral molecule is a strong two-photon absorber (as evidenced by a dip in the open aperture scan at zero potential), the oxidized molecule has the sign of the absorptive nonlinearity reversed: the maximum in the middle of the scan (distorted by drift of the background transmission due to the electrochemical reaction not yet in equilibrium) is a result of the absorptivity being a decreasing function of the light intensity, which is a characteristic of a saturable absorber.

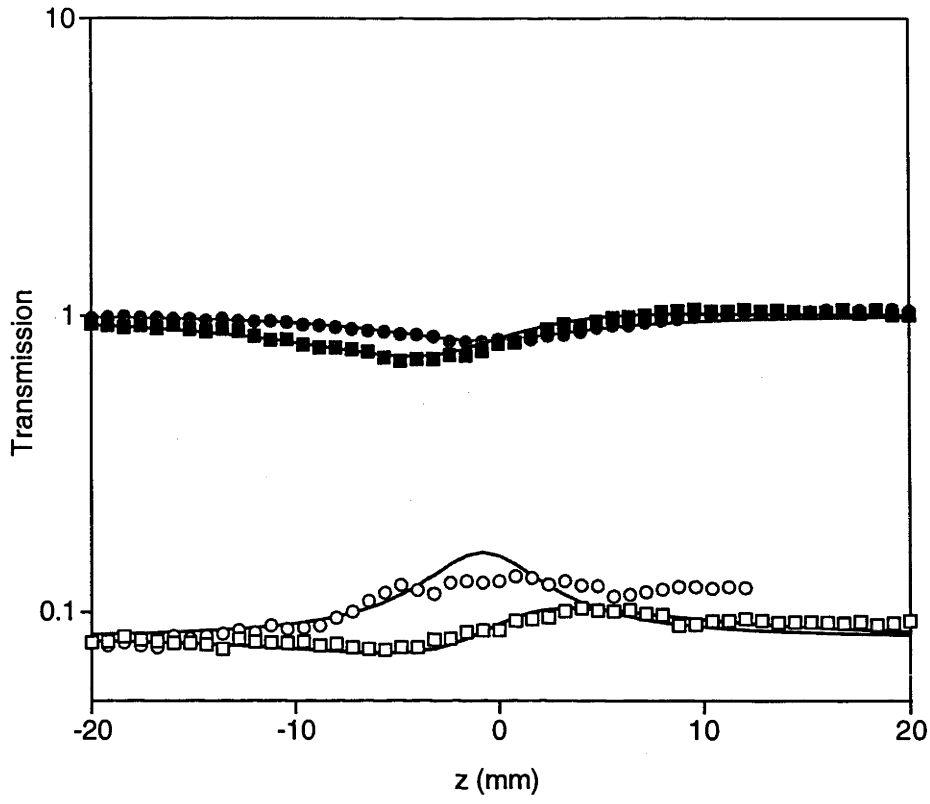

Figure 3.15. Closed and open aperture Z-scan traces for neutral (filled symbols) and oxidized (unfilled symbols) forms of **3**

Figure 3.16. shows this nonlinear electrochromic switching effect in a solution of **5** at 1180 nm. Circles denote the closed aperture results of the neutral species, the squares show the closed aperture results after oxidation at 0.8 V. The triangles represent the closed aperture Z-scan results after the potential is returned to 0.0 V. The deviations from the theoretical curves are thought to be partially due to thermal effects. The closed aperture Z-scans indicates that the refractive nonlinearity of the solution is positive for the neutral form of **5**, but becomes close to zero for the oxidized form at the 0.8 V potential. As the curve after the oxidation-reduction cycle is essentially identical to the starting curve, this indicates that the effect is reversible. However, nonlinear absorptive effects appear to be of lesser significance than in the case of 800 nm measurements.

Thus, the main effect observed at 1180 nm is the "switching off" of the large refractive nonlinearity of **5**. This observation should, however, be confirmed by other experimental techniques, since the difficulties with the presence of a suspected thermal component of the nonlinearity (which may also be modified by the electrochemical reactions) preclude an

unequivocal attribution of the Z-scan changes to the electronic hyperpolarizability modification only.

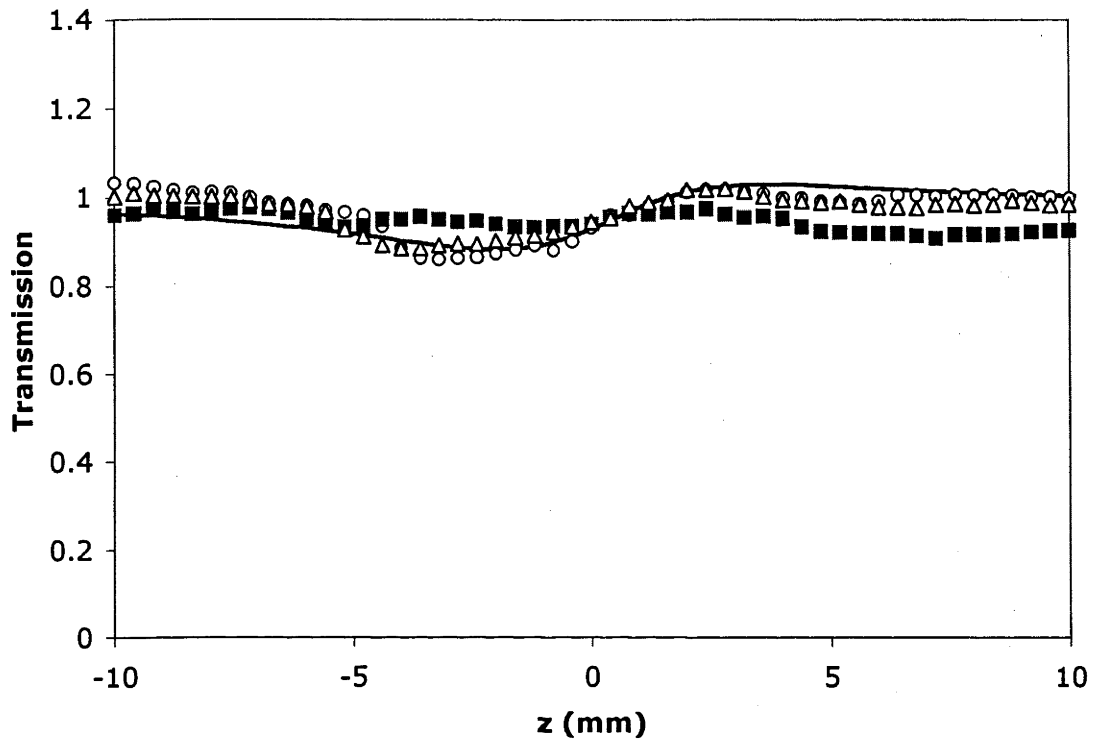

Figure 3.16. Closed aperture results from the electrochromic switching of **5**

3.4.2. *DFWM Switching*

Typical DFWM and TA scans at 12 500 cm^{-1} recorded on pristine samples of **4** in the same electrochemical cell are presented in Figure 3.17. The DFWM curve is somewhat unsymmetrical, with a slight "tail" for positive delays. The magnitude of the response of **4** (*ca* 22 times that of 1 mm silica) was used to estimate an approximate value of n_2 of the solution and hence $|\gamma|$ for the solute. The resulting value $|\gamma| \approx 2000 \times 10^{-36}$ esu is in good agreement with that from literature Z-scan results ($2200 \pm 600 \times 10^{-36}$ esu).[32] The changes of transmission (a dip at the delay time close to zero) seen in the pump-probe signal in Figure 3.17. are consistent with these previous results, indicating efficient two-photon absorption in **4**. The depth of the dip affords the two-photon absorption coefficient $\beta = 0.05$ cm GW^{-1} for

the 0.3% w/w solution, leading to $\sigma_2 \approx 10^{-47}$ cm^4 W^{-1} (10^3 GM units), again in reasonable agreement with $\sigma_2 = 0.53 \times 10^{-47}$ cm^4 W^{-1} determined by the previous Z-scan studies of γ_{imag}.

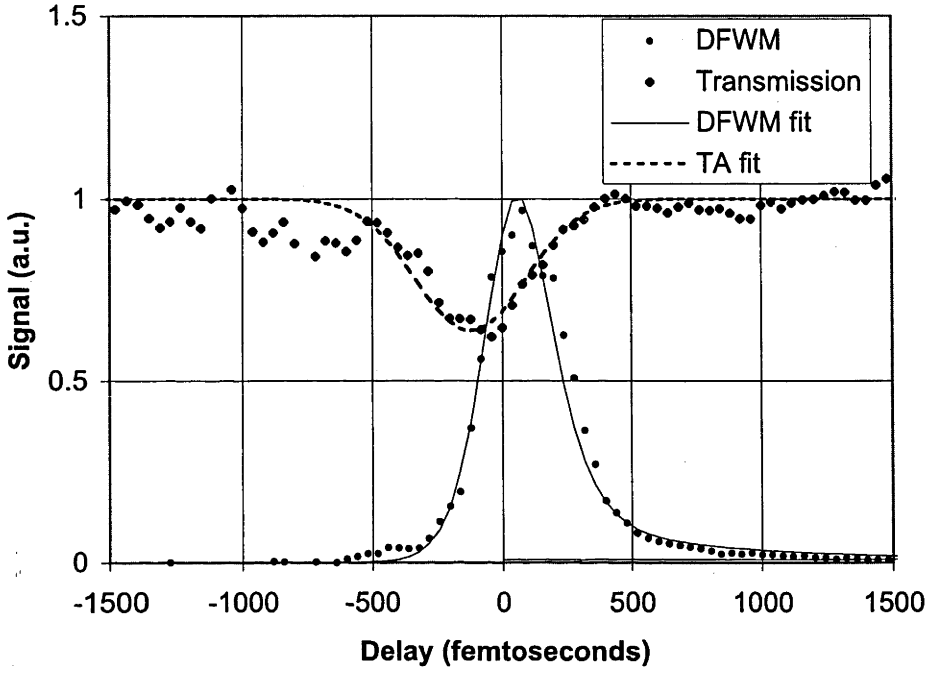

Figure 3.17. Simultaneous DFWM and pump-probe measurements on a solution of **4** (0.3% w/w in CH_2Cl_2) in an electrochemical cell before oxidation.

Oxidation and reduction cycles in the electrochemical cell were then carried out, while monitoring both the transmission signal and the DFWM signal. Oxidation of the 0.3% w/w solution of **4** to **4**$^{3+}$ caused the transmission at 800 nm to decrease to about 10% of that before oxidation, while the DFWM signal increased to about 1.4 times its intensity before oxidation. Figure 3.17. shows the time-resolved signals obtained on a solution of **4**$^{3+}$. Two major differences are seen compared to the signals in Figure 3.16.: the DFWM signal is now dominated by a delayed response with a characteristic time of about 1 ps, and the TA signal is now positive (indicating absorption saturation effects) with a decay time that is also in the order of 1 ps. From the magnitude of the DFWM signal after oxidation (and taking into account a suitable absorption correction), one can calculate the value of $|\gamma|$ of **4**$^{3+}$ to be *ca* 20 x 10^{-33} esu, about ten times larger than that for the neutral molecule, and once again in good

agreement with the Z-scan result reported previously (14 000 ± 3000 x 10^{-36} esu). The change of the character of the TA signal also confirms the change of sign of γ_{imag}.

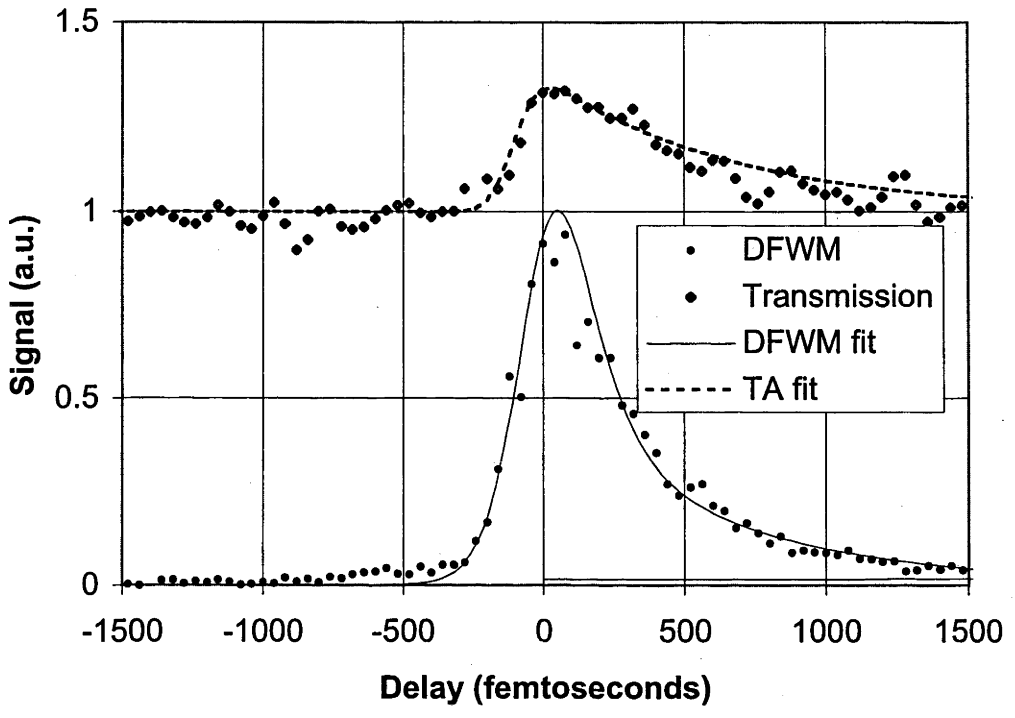

Figure 3.18. Simultaneous DFWM and pump-probe measurements on a solution of **4** (0.3% w/w in CH_2Cl_2) in an electrochemical cell after oxidation.

When the DFWM results are combined with the Z-scan results they conclusively prove that the switching of the third-order nonlinearity represents the first demonstrable example of nonlinear electrochromism originating in femtosecond scale processes. It is of interest to investigate the temporal characteristics of the relaxation of the transient absorption and DFWM signals in more detail: the fast relaxation may be due to efficient energy transfer from the excited complex molecules, and to solution interactions (including fast reorientation of molecules). However, this was not possible within the scope of the present study.

3.5. *Conclusions*

A recent theme in the literature has been investigations into the reversible modulation ("switching") of NLO properties. Currently, most papers in this field have looked at switching of quadratic NLO properties, via photoisomerization, protonation/deprotonation, or chemical oxidation/reduction. The work presented here is the first example of electrochemical switching of third-order molecular NLO properties.

An OTTLE cell has been incorporated into a Z-Scan set-up, which, drawing upon the spectroelectrochemical spectra described in Chapter 2, allows reversible switching of cubic NLO properties of a number of mono-acetylide complexes. As long as the cell is kept in a strictly anaerobic environment, the switch is stable. An attempt to extend this to bis-acetylide complexes has been less successful, possibly due to the high repetition rate of the laser used; however, these preliminary results indicate that a lower powered laser may allow the demonstration of electrochemically induced modulation of cubic NLO properties at wavelengths useful for telecommunications.

Incorporation of the OTTLE cell into a DFWM set-up has extended this work by confirmation of the original results and determination of the time response of the phenomena. The experimentally determined time decay indicates that this is an electronic process.

3.6. *Experimental*

3.6.1. *Synthetic Procedures*

All reactions were performed under a nitrogen atmosphere with the use of standard Schlenk techniques unless otherwise stated. Dichloromethane was dried by distilling over calcium hydride, diethyl ether was dried by distilling over sodium/benzophenone and triethylamine was deoxygenated under reduced pressure. "Petrol" refers to a fraction of petroleum ether of boiling range 60 – 80 °C. Chromatography was on basic ungraded alumina.

MALDI mass spectra were recorded using a Micromass TofSpec-2e MALDI-TOF MS instrument at the Research School of Chemistry, Australian National University (ANU); peaks are reported as m/z (assignment, relative intensity). The microanalysis was carried out at the Research School of Chemistry, ANU. ^{1}H and ^{31}P NMR spectra were recorded using a Varian Gemini-300 FT NMR spectrometer and are referenced to residual chloroform (7.24 ppm) or external 85% H_3PO_4 (0.0 ppm), respectively. UV-vis spectra of solutions were recorded in tetrahydrofuran in 1 cm quartz cells using a Cary 5 spectrophotometer.

The complexes *trans*-[RuXY(dppe)$_2$], [X = Cl, Y = Cl[33] C≡CPh,[34] X = C≡CPh, Y = C≡CPh,[34] C≡CC_6H_4-4-C≡CPh[32]], 1,3,5-C_6H_3-{C≡CC_6H_4-4-C≡C-*trans*-[RuCl(dppe)$_2$]}$_3$,[36] 1,3,5-C_6H_3-{C≡CC_6H_4-4-C≡C-*trans*-[Ru(C≡CPh)(dppe)$_2$]}$_3$[36] and the alkyne HC≡CC_6H_4-4-C≡CPh[37] were prepared using literature procedures.

3.6.1.1. *Synthesis of trans-[Ru(C≡CC_6H_4-4-C≡CPh)Cl(dppe)$_2$]* (3)

A mixture of *cis*-[$RuCl_2$(dppe)$_2$] (161 mg, 0.149 mmol), 4-HC≡CC_6H_4C≡CPh (41 mg, 0.203 mmol) and ammonium hexafluorophosphate (43 mg, 0.264 mmol) was stirred in dichloromethane (40 mL) for 16 h. The mixture was taken to dryness *in vacuo* and triturated with ether (3 x 15 mL). Dichloromethane (30 mL) and triethylamine (2 mL) were added, and the resultant solution stirred for 30 s. The solution was taken to dryness *in vacuo*, and the residue purified by column chromatography on alumina, eluting with 20% dichloromethane / 80% petrol to remove the bis-alkynyl product (trace quantities), and then with acetone to remove the product. The product was recrystallized by liquid diffusion of methanol into a dichloromethane solution to afford orange crystals of *trans*-[Ru(4-C≡CC_6H_4C≡CPh)Cl(dppe)$_2$] as the hemi-dichloromethane solvate, yield 94 mg (54 %).

MALDI MS: 1134 ([M]$^+$, 90), 1100 (MH – Cl)+, 90), 934 (MH – $C_2C_6H_4C_2Ph$)+, 95), 899 (MH – $C_2C_6H_4C_2Ph$ - Cl)+, 100). Anal. Calcd for $C_{68}H_{57}ClP_4Ru.0.5CH_2Cl_2$: C: 69.90, H 4.97%. Found: C 69.74, H 5.02 %. ^1H NMR: (δ, 300 MHz, $CDCl_3$); 2.67 (m, 8H, CH_2), 5.28 (s, 1H, CH_2Cl_2), 6.53 to 7.52 (m, 49H, phenyl). ^{31}P NMR: (δ, 121 MHz, $CDCl_3$); 49.7 (s, PPh_2).

3.6.2. *Electrochemical and spectroelectrochemical studies*

Electrochemical and spectroelectrochemical measurements were performed at the Department of Chemistry, Australian National University and the Research School of Chemistry, Australian National University by Dr M. P. Cifuentes. Cyclic voltammetric measurements were recorded using a MacLab 400 interface and MacLab potentiostat from AD Instruments (using Pt disc working-, Pt auxiliary- and Ag-AgCl reference mini-electrodes from Cypress Systems). Scan rates were typically 100 mV s^{-1}. Electrochemical solutions contained 0.1 M $(NBu^n_4)PF_6$ and *ca* 10^{-3} M complex in dichloromethane. Solutions were purged and maintained under an atmosphere of nitrogen. All values are referenced to an internal ferrocene/ferrocenium couple (E^0 at 0.56 V). Electronic spectra (45 000 - 4 000 cm^{-1}) were recorded on a Perkin-Elmer Lambda 9 spectrophotometer. Solution spectra of the oxidized species at 253 K were obtained by electrogeneration (Thompson 401E potentiostat) at a Pt gauze working electrode within a cryostatted optically-transparent thin-layer electrochemical (OTTLE) cell, path-length 0.5 mm, mounted within the spectrophotometer.[38] The electrogeneration potential was *ca* 300 mV beyond $E_{1/2}$ for each couple, to ensure complete electrolysis. The efficiency and reversibility of each step was tested by applying a sufficiently negative potential to reduce the product; stable isosbestic points were observed in the spectral progressions for all the transformations reported herein.

3.6.3. *Z-Scan*

Z-scan measurements were performed at the Laser Physics Centre, Research School of Physical Sciences and Engineering, Australian National University, by the author, Dr Marek Samoc and Mr Joseph Morrall. Measurements were performed at 800 nm (12 500 cm^{-1}) using 100 fs pulses from a system consisting of a Coherent Mira Ti-sapphire laser pumped with a

Coherent Verdi cw pump and a Ti-sapphire regenerative amplifier pumped with a frequency-doubled Q-switched pulsed Nd:YAG laser (Spectra Physics GCR) at 30 Hz and employing chirped pulse amplification. Z-scan measurements were also attempted at 1180 nm (8470 cm^{-1}) and 1300 nm (7690 cm^{-1}) using another high-power femtosecond laser system with a 775 nm Ti-sapphire regenerative amplifier (Clark-MXR CPA-2001A) pumping a Light Conversion Topas optical parametric amplifier. This system provides tunable, approximately 150 fs pulses with a repetition rate of 1 kHz. For both femtosecond systems, the energy per pulse used in the experiments was limited (using a halfwave plate/polarizer combination and/or neutral density filters) to approximately 1 μJ. Argon-saturated dichloromethane solutions of the complexes containing *ca* 0.3 M $(NBu^n_4)PF_6$ supporting electrolyte were examined in an OTTLE cell (with Pt auxiliary-, Pt working- and Ag-AgCl reference electrodes), path length 0.5 mm, with the laser beam passing through a focussing lens and directed along the axis passing through a 1.5 mm diameter hole in the Pt sheet working electrode. The electrochemical cell was mounted on a computer driven translation stage, as usual in Z-scan measurements.[39] The w_0 parameter of the beam (the radius at the $1/e^2$ intensity point) was chosen to be in the range 35 - 45 μm. The Rayleigh length $z_R = \frac{\pi w_0^2}{\lambda}$, where w_0 is the Gaussian beam waist and λ is the wavelength, was thus taken to be $z_R > 3$ mm (which corresponds to $w_0 > 30$ μm for $\lambda = 0.8$ μm). A "thin sample" assumption was therefore considered to be justified. In effect, one can then treat the total effect of the third-order nonlinearity of all the components of the system, the solution (solvent and dissolved materials) and the glass walls of the cell, as being an additive quantity. The beam "cropping" by the aperture was also negligible over the range of travel of the cell (z = -3 cm to +3 cm from the focal plane), the beam radius growing by roughly a factor of ten (i.e. to about 350-450 μm) over the distance of ten Rayleigh lengths, but still providing for almost complete transmission. The beam transmitted through the electrochemical cell was split in two, one part being focussed on an "open aperture" detector, the other part being transmitted through a 1 mm aperture to provide the "closed aperture" signal. Z-scans were collected with the electrochemical cell. The electrogeneration potential was 0.8 V to ensure complete electrolysis; this required approximately 5 min. The Z-scan measurements were carried out during the electrolysis and were continued while the electrode potential was cycled from zero to 0.8 V and back to zero again. The real and imaginary parts of the nonlinear phase change were determined by numerical fitting using equations given in the literature,[39] assuming that the absorption saturation process can be modelled by a linear dependence of the absorption coefficient on the light intensity.[31] The nonlinearities and light intensities were calibrated

using measurements of a 1 mm thick silica plate for which the nonlinear refractive index n_2 = 3 x 10^{-16} cm^2 W^{-1} was assumed.

3.6.4. *DFWM*

DFWM measurements were performed at the Laser Physics Centre, Research School of Physical Sciences and Engineering, Australian National University, by the author, Dr Marek Samoc and Mr Joseph Morrall. Measurements were performed at 800 nm (12 500 cm^{-1}) using 100 fs pulses from a system consisting of a Coherent Mira Ti-sapphire laser pumped with a Coherent Verdi cw pump and a Ti-sapphire regenerative amplifier pumped with a frequency-doubled Q-switched pulsed Nd:YAG laser (Spectra Physics GCR) at 30 Hz and employing chirped pulse amplification. Argon-saturated dichloromethane solutions of **4** containing *ca* 0.3 M $(NBu^n_4)PF_6$ supporting electrolyte were examined in an OTTLE cell (with Pt auxiliary-, Pt working- and Ag-AgCl reference electrodes), path length 0.5 mm, with the laser beams directed through a 1.5 mm diameter hole in the Pt sheet working electrode. The DFWM measurements were carried out during the electrolysis and were continued while the electrode potential was cycled from zero to 0.8 V. The NLO measurements were performed at 12 500 cm^{-1} in a forward (i.e. BOXCARS) DFWM geometry[31] with the output beam from the laser system split into three beams which were aligned so as to overlap on the sample (spot size ca 150 μm). The beams were timed with optical delay lines in such a way that two of the beams arrived at the sample at the same time, while the delay of beam 3 was scanned between negative values (corresponding to beam 3 arriving at the sample before the pump beams 1 and 2) and positive values (corresponding to beam 3 arriving at the sample after the pump beams). Two detectors were employed, one monitoring the phase-matched DFWM signal appearing in the fourth corner of the rectangle formed by the three interacting beams, and the other monitoring the intensity of the probe beam (beam 3) after the sample. With this arrangement, the DFWM signal originating from the formation of a transient grating and the transient absorption (TA) signal originating from modification of the sample absorptivity by the presence of high intensity pump beams could be measured simultaneously. The results were referenced to those of a 1 mm thick silica glass plate, for which the nonlinear index n_2 = 3 x 10^{-16} cm^2 W^{-1} was assumed.

3.7. *References*

(1) Raymo, F. M. *Adv. Mater.* **2002**, *14*, 401.

(2) Porres, L.; Alain, V.; Thouin, L.; Hapiot, P.; Blanchard-Desce, M. *Phys. Chem. Chem. Phys.* **2003**, *5*, 4576.

(3) Giordani, S.; Raymo, F. M. *Org. Lett.* **2003**, *5*, 3559.

(4) Szacilowski, K.; Stasicka, Z. *Coord. Chem. Rev.* **2002**, *229*, 17.

(5) Fabbrizzi, L.; Licchelli, M.; Mascheroni, S.; Poggi, A.; Sacchi, D.; Zema, M. *Inorganic Chemistry* **2002**, *41*, 6129.

(6) Feringa, B. L. *Molecular Switches*; Wiley-VCH, 2001.

(7) Honda, M.; Naito, T.; Sugita, T.; Ando, M. In *Eur. Pat. Appl.*; (Hitachi, Ltd., Japan). Ep, 2003.

(8) McCoy, C. H.; Chen, J. In *PCT Int. Appl.*; (Surface Logix, Inc., USA). Wo, 2003..

(9) Coe, B. J. *Chem. Eur. J.* **1999**, *5*, 2464.

(10) Song, Q.; Wan, C.; Johnson, C. K. *J. Phys. Chem* **1994**, *98*, 1999.

(11) Hurst, S.; Cifuentes, M. P.; Morrall, J. P.; Lucas, N. T.; Whittall, I. R.; Humphrey, M. G.; Asselberghs, I.; Persoons, A.; Samoc, M.; Luther-Davies, B.; Willis, A. C. *Organometallics* **2001**, *20*, 4664.

(12) McDonagh, A. M.; Whittall, I. R.; Humphrey, M. G.; Skelton, B. W.; White, A. H. *J. Organomet. Chem.* **1996**, *519*, 229.

(13) Coe, B. J.; Houbrechts, S.; Asselberghs, I.; Persoons, A. *Angew. Chem. Int. Ed.* **1999**, *38*.

(14) Malaun, M.; Paul, R. L.; Jeffery, J. C.; McCleverty, J. A.; Ward, M. D.; Asselberghs, I.; Clays, K.; Persoons, A. *Chem. Commun.* **2001**, 49.

(15) Di Bella, S.; Fragalâ, I. *Synthetic Metals* **2000**, *115*, 191.

(16) Gaudry, J.-B.; Capes, L.; Langot, P.; Marcén, S.; Kollmannsberger, M.; Lavastre, O.; Freysz, E.; Létard, J.-F.; Kahn, O. *Chem. Phys. Lett.* **2000**, *324*, 321.

(17) Asselberghs, I.; Zhao, Y.; Clays, K.; Persoons, A.; Comito, A.; Rubin, Y. *Chem. Phys. Lett.* **2002**, *364*, 279.

(18) Sekkat, Z.; Knoesen, A.; Lee, V. L.; Miller, R. D. *J. Phys. Chem. B* **1997**, *104*, 4733.

(19) Weyland, T.; Ledoux, I.; Brasselet, S.; Zyss, J.; Lapinte, C. *Organometallics* **2000**, *19*, 5235.

(20) Naulty, R. H.; McDonagh, A. M.; Whittall, I. R.; Cifuentes, M. P.; Humphrey, M. G.; Houbrechts, S.; Maes, J.; Persoons, A.; Heath, G. A.; Hockless, D. C. R. *J. Organmet. Chem* **1998**, *563*, 137.

(21) Whittall, I. R.; McDonagh, A. M.; Humphrey, M. G.; Samoc, M. *Adv. Organomet. Chem.* **1999**, *43*, 349.

(22) Sortino, S.; Petralia, S.; Conoci, S.; Di Bella, S. *J. Am. Chem. Soc.* **2003**, *125*, 1122.

(23) Grigorieff, N.; Ceska, T. A.; Downing, K. H.; Baldwin, J. M.; Henderson, R. *J. Mol. Bio.* **1996**, *259*, 393.

(24) Clays, K.; Hendrickx, E.; Triest, M.; Verbiest, T.; Persoons, A.; Dehu, C.; Brédas, J.-L. *Science* **1993**, *262*.

(25) Hendrickx, E.; Clays, K.; Persoons, A.; Dehu, C.; Brédas, J.-L. *J. Am. Chem. Soc.* **1995**, *117*, 3547.

(26) Wang, C. H.; Bacon, M.; Kar, A. K.; Wherrett, B. S.; Baxter, R. L. *J. Opt. Soc. Am. B* **1997**, *14*, 2304.

(27) Sortino, S.; Petralia, S.; Di Bella, S. *J. Am. Chem. Soc.* **2003**, *125*, 5610.

(28) Cifuentes, M. P.; Powell, C. E.; Humphrey, M. G.; Heath, G. A.; Samoc, M.; Luther-Davies, B. *J. Phys. Chem. A* **2001**, *105*, 9625.

(29) Powell, C. E.; Cifuentes, M. P.; Morrall, J. P.; Stranger, R.; Humphrey, M. G.; Samoc, M.; Luther-Davies, B.; Heath, G. A. *J. Am. Chem. Soc.* **2003**, *125*, 602.

(30) Asselberghs, I.; Clays, K.; Persoons, A.; McDonagh, A. M.; Ward, M. D.; McCleverty, J. A. *Chem. Phys. Lett.* **2003**, *368*, 408.

(31) Sutherland, R. L. *Handbook of Nonlinear Optics*; Marcel Dekker: New York, 1996; Vol. 52.

(32) McDonagh, A. M.; Humphrey, M. G.; Samoc, M.; Luther-Davies, B.; Houbrechts, S.; Wada, T.; Sasabe, H.; Persoons, A. *J. Am. Chem. Soc.* **1999**, *121*, 1405.

(33) Chatt, J.; Hayter, R. G. *J. Chem. Soc., Dalton Trans.* **1961**, 896.

(34) Touchard, D.; Haquette, P.; Guesmi, S.; Pichon, L. L.; Daridor, A.; Toupet, L.; Dixneuf, P. H. *Organometallics* **1997**, *16*, 3640.

(35) Touchard, D.; Haquette, P.; Pirio, N.; Toupet, L.; Dixneuf, P. H. *Organometallics* **1993**, *12*, 3132.

(36) McDonagh, A. M.; Powell, C. E.; Morrall, J. P.; Cifuentes, M. P.; Humphrey, M. G. *Organometallics* **2003**, *22*, 1402.

(37) Lavastre, O.; Cabioch, S.; Dixneuf, P. H.; Vohlidal, J. *Tetrahedron* **1997**, *53*, 7595.

(38) Duff, C. M.; Heath, G. A. *Inorg. Chem.* **1991**, *30*, 2528.

(39) Sheik-Bahae, M.; Said, A. A.; Wei, T.; Hagan, D. J.; van Stryland, E. W. *IEEE J. Quantum Electr.* **1990**, *26*, 760.

Chapter 4

Ruthenium Acetylide Dendrimers and Related Complexes

Chapter 4

Ruthenium Acetylide Dendrimers and Related Complexes

Contents

4.1. *Introduction*

4.2. *Synthesis of Dendrimers with Electron-Donating Peripheral Substituents*

4.3. *Synthesis of Peripherally-Metalated Dendrimers*

4.4. *Improved Methods of Dendrimer Synthesis*

4.5. *Physical Properties*

4.6. *Nonlinear Optical Properties*

4.7. *Conclusion*

4.8. *Experimental*

4.9. *References*

Chapter 4

Ruthenium Acetylide Dendrimers and Related Complexes

4.1. *Introduction*

The traditional design of molecules with high molecular nonlinearities has focused on dipolar complexes. These molecules tend to have high second-order nonlinearities because of the increased stability of the first excited state. This concept has been used in organic, inorganic and organometallic complexes. A different design motif, however, is to examine octupolar compounds. Many examples of octupolar compounds exhibit high second-order hyperpolarizabilities.[1-12] Octupolar molecules are less likely to pack in a centrosymmetric space group, or to have dipoles aligned in an antiparallel fashion, both of which would eliminate a bulk response. Additionally, octupolar molecules can possess substantial off-diagonal tensor components, which can lead to high nonlinearities.

Dendrimera are regular hyperbranched polymers which, because of their regular repeating units, possess well defined molecular weights. The dendrimers synthesized in this Chapter have three arms at each branching point. A dendrimer generation is defined by the number of branching points (Figure 4.1.) such that a zero-generation dendrimer possesses one branching point and a first-generation dendrimer possesses a second branching point at the terminus of each zero-generation arm.

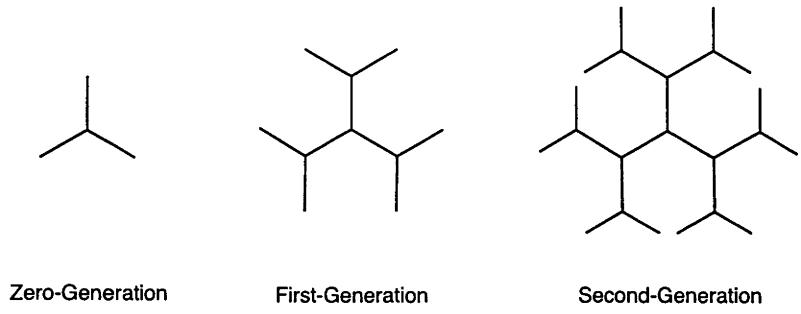

Figure 4.1. Idealized dendrimer geometry

Two different synthetic methodologies are used to construct dendrimers: divergent and convergent (Figure 4.2.). The divergent strategy involves reaction of a zero-generation core with a branching point, to give the first generation dendrimer. This, in turn, is reacted with another branching point to give the second-generation dendrimer. The convergent strategy involves construction of a dendritic wedge, which is then coupled to a core to give the desired dendrimer. Both methodologies involve trade-offs. Because the divergent route uses smaller branching points, there is less steric strain; however, separation of defective dendrimers tends to be more difficult, as the two dendrimers tend to be quite similar. The convergent route increases the problem of steric strain, but makes the purification of the final product simpler.

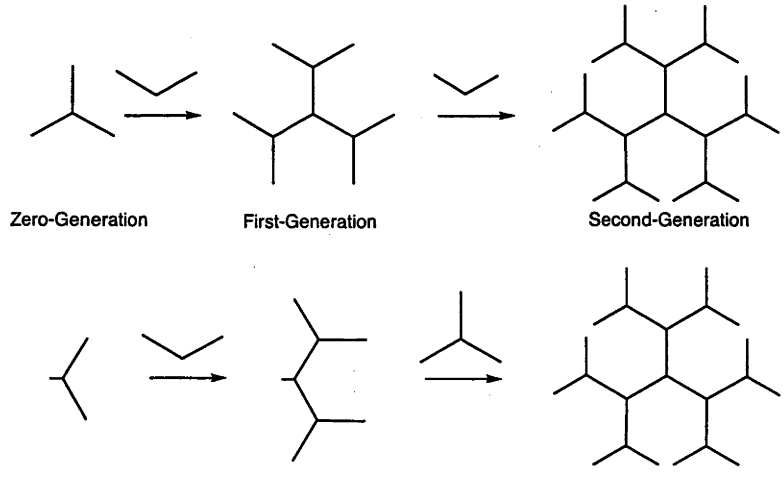

Figure 4.2. Divergent (above) and convergent (below) dendrimer construction methodologies

Dendrimers have been used for a variety of different purposes including drug delivery,[13-16] biochips,[17] nanoscopic containers,[15] and catalysts.[16] Dendrimers have a well-established role in photonics; there have been a number of recent studies into their effectiveness as light harvesting molecules,[18-24] as nonlinear optical materials,[25-27] as materials for high performance waveguides[28] and as electro-optical materials.[29]

While most dendrimers are organic,[30-33] organometallic dendrimers have been reported in the literature.[34-67] A review on organometallic dendrimers and other related complexes was published in 1998.[68] There are a small number of transition-metal acetylide dendrimers that have been reported.[26,27,62-67,69]

The existing transition-metal acetylide dendrimers have utilized two different transition metals: platinum and ruthenium. Sections 4.2. and 4.3. include details of literature-extant ruthenium-acetylide dendrimers. Figure 4.3. displays an example of a platinum-acetylide dendrimer developed by Takahashi and co-workers.[64] Dendrimers with the same design motif, and up to six generations in size, have been synthesized.[67] Novel variants have also been synthesized, such as a dendrimer incorporating a porphyrin core. Figure 4.4. displays an example of a platinum-acetylide dendrimer with a porphyrin core, but it should be noted that examples of up to two generations larger have been reported.[66]

The synthetic work in this Chapter is divided into three broad themes. The first theme involves the incorporation of an electron donating group (diethylamino) onto the outside of a ruthenium acetylide dendrimer. The second theme is an investigation into dendrimers with an organic core and metals on the periphery. Because of the large numbers of chemical reactions required to synthesize these dendrimers, the last synthetic motif involves an investigation into new synthetic routes to reduce the number of steps required for the synthesis of new dendrimers.

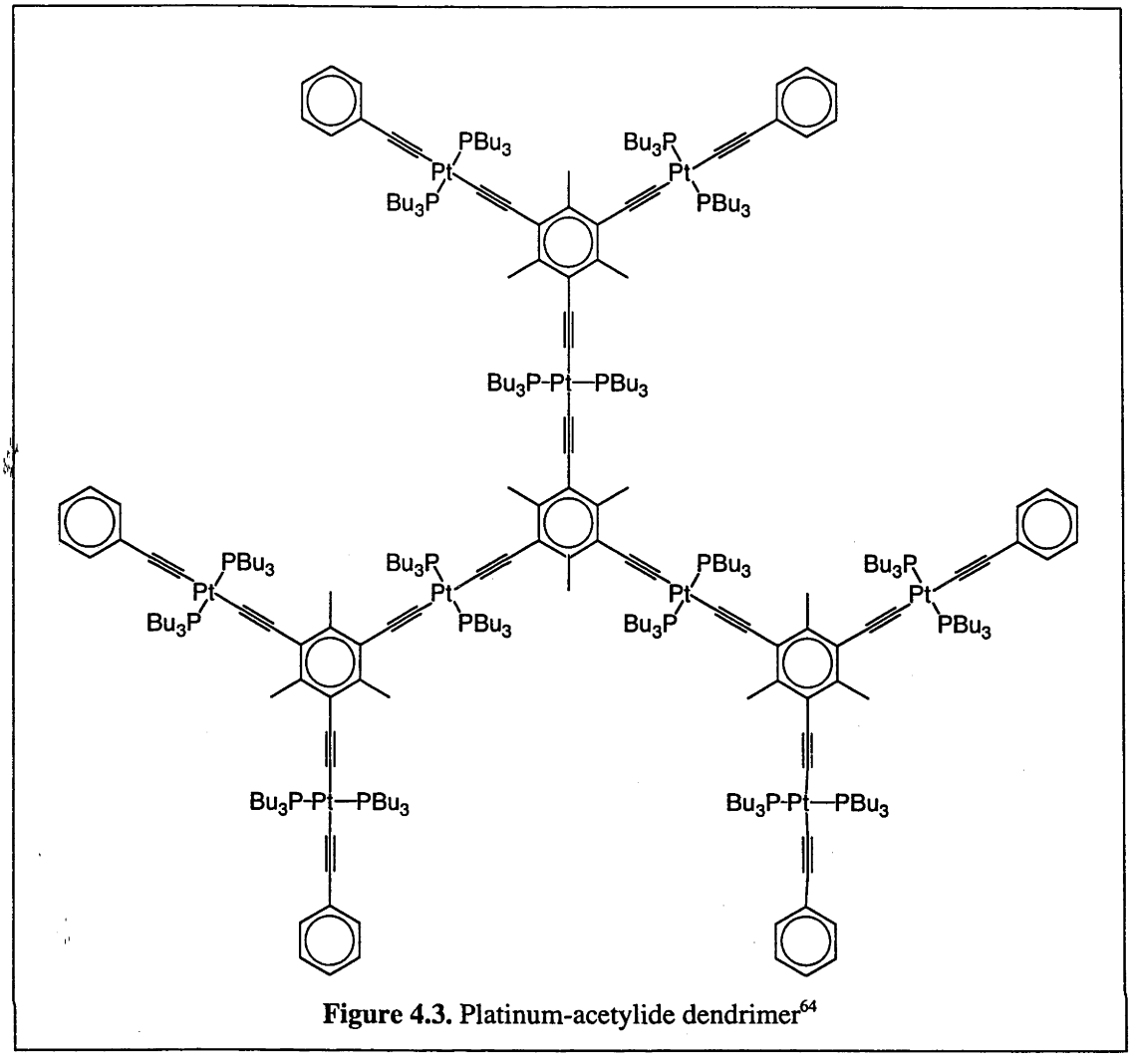

Figure 4.3. Platinum-acetylide dendrimer[64]

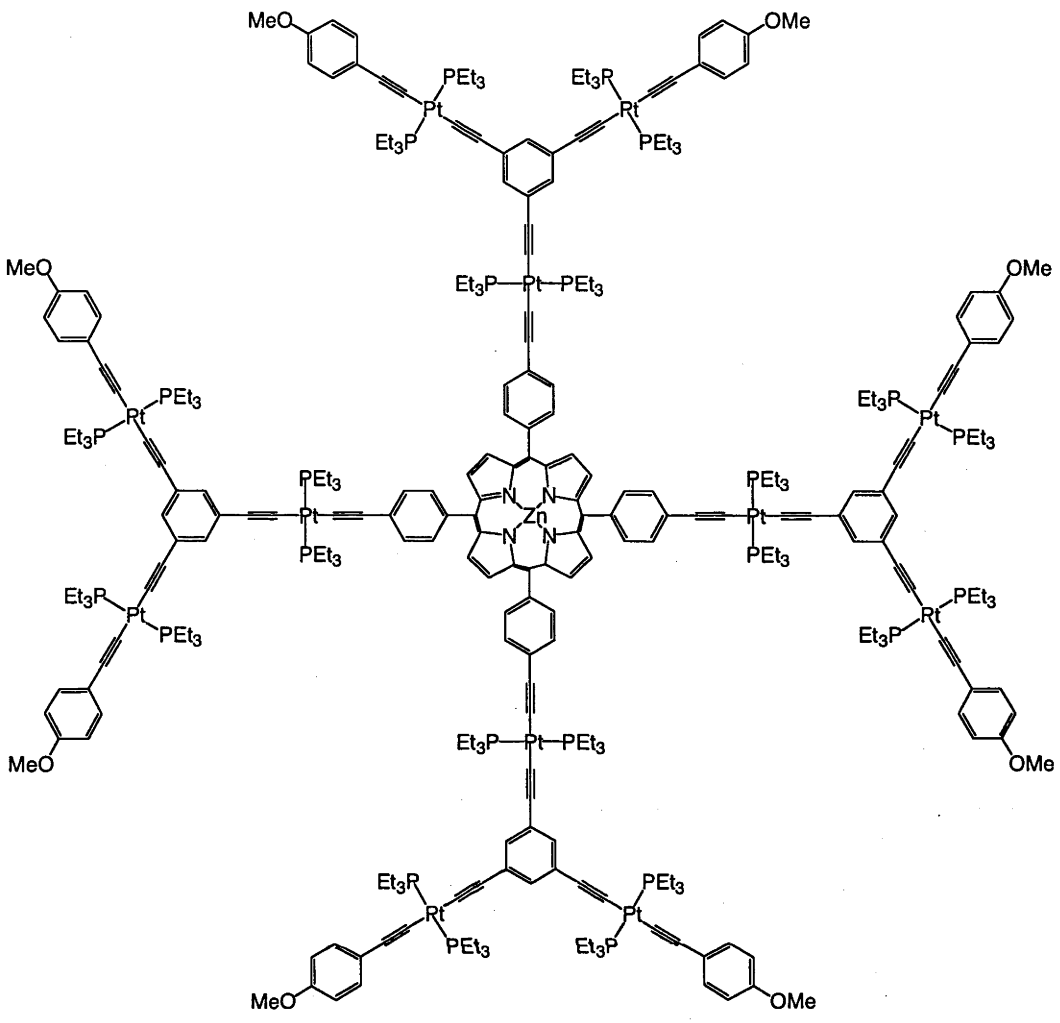

Figure 4.4. Porphyrin-containing platinum-acetylide dendrimer[66]

4.2. *Synthesis of Dendrimers with Electron-Donating Peripheral Substituents*

4.2.1. *Introduction*

Two motifs are common in the design of materials with high nonlinearities: dipolar and octupolar geometry. Dipolar molecules rely on large charge asymmetry and extensive π delocalization to generate high nonlinearities. Dipolar complexes tend to use a donor–π-conjugated bridge–acceptor system (Figure 4.5.), but while producing high nonlinearities, it also leads to a loss of optical transparency. Octupolar complexes provide a means of obtaining high nonlinearities without a corresponding loss of optical transparency. For example, the zero generation dendrimer 1,3,5-{*trans*-[Ru(C≡CPh)(dppe)$_2$](C≡CC$_6$H$_4$-4-C≡C)}$_3$C$_6$H$_3$ has a $|\gamma|$ of 3000 ± 600 x 10^{-36} esu, whereas the first generation analogue 1,3,5-C$_6$H$_3$-(C≡CC$_6$H$_4$-4-C≡C-*trans*-[Ru(dppe)$_2$]C≡C-3,5-C$_6$H$_3$-{C≡CC$_6$H$_4$-4-C≡C-*trans*-[Ru(C≡CPh)(dppe)$_2$]}$_2$)$_3$ has a $|\gamma|$ of 20 700 ± 2000 x 10^{-36} esu. The two complexes display a MLCT band in almost identical locations (λ_{max} = 411 nm and 402 nm, respectively).[27] The incorporation of an electron-withdrawing nitro- group on the periphery of the first generation dendrimer mentioned above leads to a substantial increase in the nonlinearities.[70] The purpose of this section is to investigate the effect of incorporation of an electron-donating substituent on the periphery of a dendrimer.

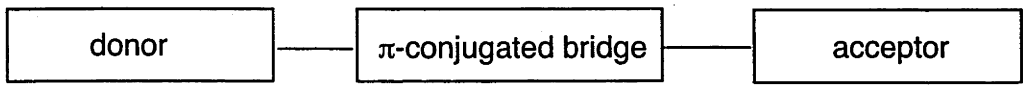

Figure 4.5. Donor–π-conjugated bridge–acceptor system

4.2.2. *Synthesis of Et$_2$NC$_6$H$_4$-4-C≡CH*

The standard literature preparation of a functionalized *p*-benzaldehyde involves reaction of the aldehyde (Et$_2$NC$_6$H$_4$-4-CHO, in this case) with triphenylphosphine, Zn dust and carbon

tetrabromide to give the compound $Et_2NC_6H_4$-4-CH=CBr_2. This compound is then converted to $Et_2NC_6H_4$-4-C≡CLi by reaction with *n*-butyllithium, and then protonated *in situ* by reaction with water (Scheme 4.1.) to give the NEt_2 functionalized phenylacetylene.

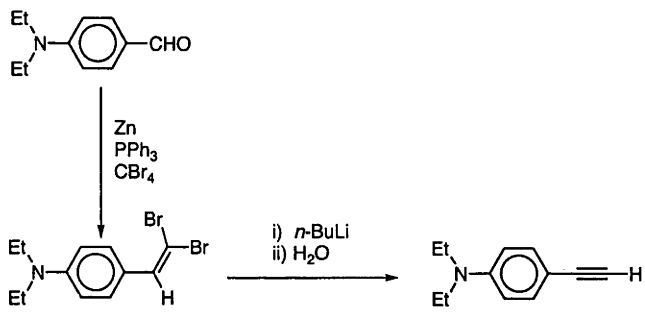

Scheme 4.1. Preparation of $Et_2NC_6H_4$-4-C≡CH[71]

An alternative synthetic route was devised. The compound $Et_2NC_6H_4$-4-I was formed by reaction of NEt_2Ph and iodine. The product, $Et_2NC_6H_4$-4-I (**1**), was in turn reacted with trimethylsilylacetylene via a Sonogashira coupling to give $Et_2NC_6H_4$-4-C≡$CSiMe_3$ (**2**) which was desilylated with tetrabutylammonium fluoride to give the desired acetylene (Scheme 4.2.). The identity of the acetylene **3** was confirmed by comparison of the ^1H NMR and low resolution EI mass spectrometry data to the literature.[72] The trimethylsilyl-protected precursor **2** was characterized by ^1H NMR and high resolution EI mass spectrometry.

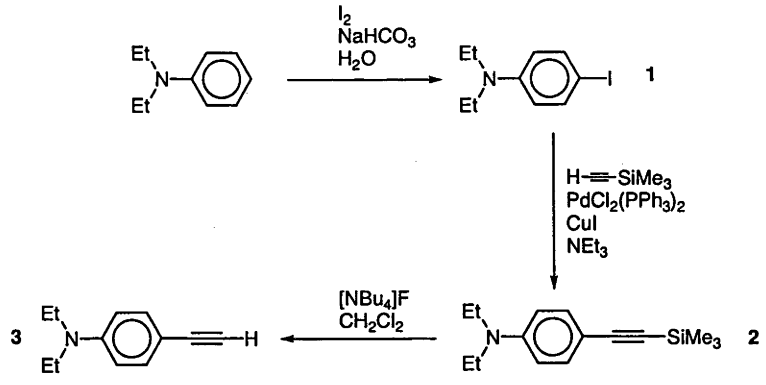

Scheme 4.2. Synthesis of $Et_2NC_6H_4$-4-C≡CH

4.2.3. *Synthesis of Ruthenium-Acetylide Complexes*

In order to enact a full comparison with the neutral and electron withdrawing dendrimers, an attempt was made to synthesize a linear analogue, *trans*-[Ru(C≡C C_6H_4-4-C≡CPh)(C≡CC_6H_4-4-NEt_2)(dppe)$_2$] (**5**). Initially, it was planned to react the ligand, $Et_2NC_6H_4$-4-C≡CH (**3**), with *cis*-[$RuCl_2$(dppe)$_2$] to give the mono-acetylide *trans*-[Ru(C≡CC_6H_4-4-NEt_2)Cl(dppe)$_2$]. This would in turn be reacted with PhC≡CC_6H_4-4-C≡CH to give the desired linear analogue **5** (Scheme 4.3.). However, reaction of *cis*-[$RuCl_2$(dppe)$_2$] with **3** was found to give a dark green solid before the addition of the triethylamine base. Unknown **6** was isolated. Only poor ^{1}H NMR data could be collected, presumably due to the paramagnetic nature of the complex. It was suspected that the basic ligand had caused the vinylidene complex to deprotonate *in situ* to give the desired acetylide, which then in turn reacted with another diethylamino-substituted acetylene to give the bis-acetylide complex **6**. Because of the presence of two strong electron donating groups, the Ru^{III} oxidation state may be favoured over the Ru^{II} state (Figure 4.6.), but this identification should be treated as tentative.

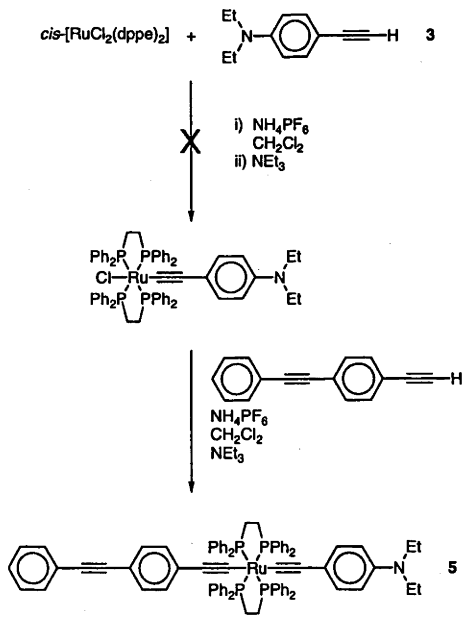

Scheme 4.3. Planned reaction pathway for the synthesis of *trans*-[Ru(C≡CC_6H_4-4-C≡CPh)(C≡CC_6H_4-4-NEt_2)(dppe)$_2$] (**5**)

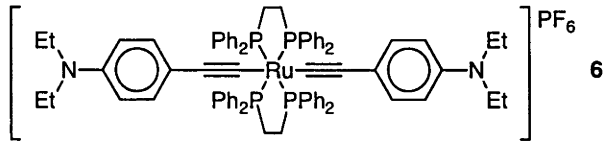

Figure 4.6. Proposed green complex **6** from attempted synthesis of *trans*-[Ru(C≡CC$_6$H$_4$-4-NEt$_2$)Cl(dppe)$_2$]

A new approach designed to preclude the possibility of bis-substitution on the Ru center by **3**, was trialed. *cis*-[RuCl$_2$(dppe)$_2$] was reacted with PhC≡CC$_6$H$_4$-4-C≡CH to give *trans*-[Ru(C≡CC$_6$H$_4$-4-C≡CPh)Cl(dppe)$_2$] (**4**) (the characterization of this complex is described in Chapter 3). This was in turn reacted with **3** to give **5** (Scheme 4.4.), characterized by ^{1}H and ^{31}P NMR, UV-vis, IR, FAB mass spectrometry and a satisfactory microanalysis. The yield (31%) was low due to the instability of the complex on the alumina column used in purification.

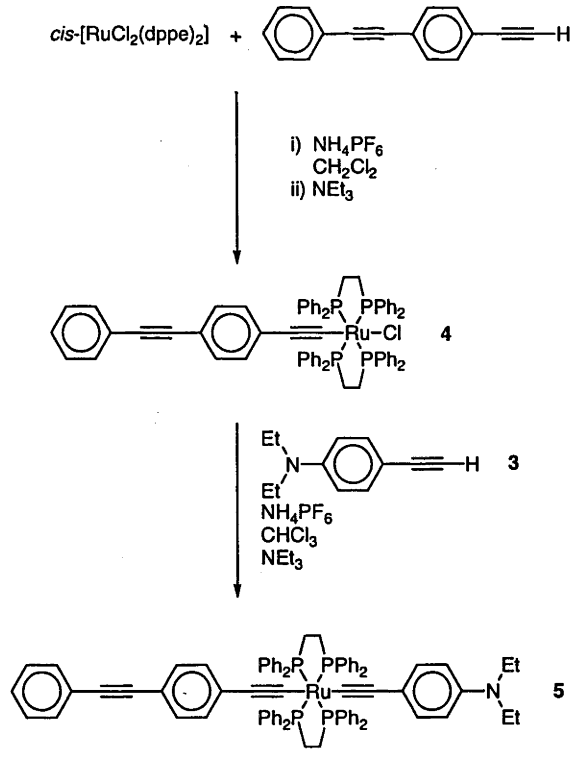

Scheme 4.4. Synthesis of *trans*-[Ru(C≡CC$_6$H$_4$-4-C≡CPh)(C≡CC$_6$H$_4$-4-NEt$_2$)(dppe)$_2$] (**5**)

The synthesis of the triruthenium organometallic octupolar core 1,3,5-C_6H_3{C≡CC_6H_4-4-C≡C-*trans*-[RuCl(dppe)$_2$]}$_3$ (**9**) was carried out following the published procedure.[73] 1,3,5-triethynylbenzene reacted with IC_6H_4-4-C≡C$SiMe_3$ to give octupolar organic compound **7**, desilylation with TBAF gave the extended organic core compound **8**, which was then reacted with *cis*-[$RuCl_2$(dppe)$_2$] to give the desired dendritic core **9** (Scheme 4.5.).

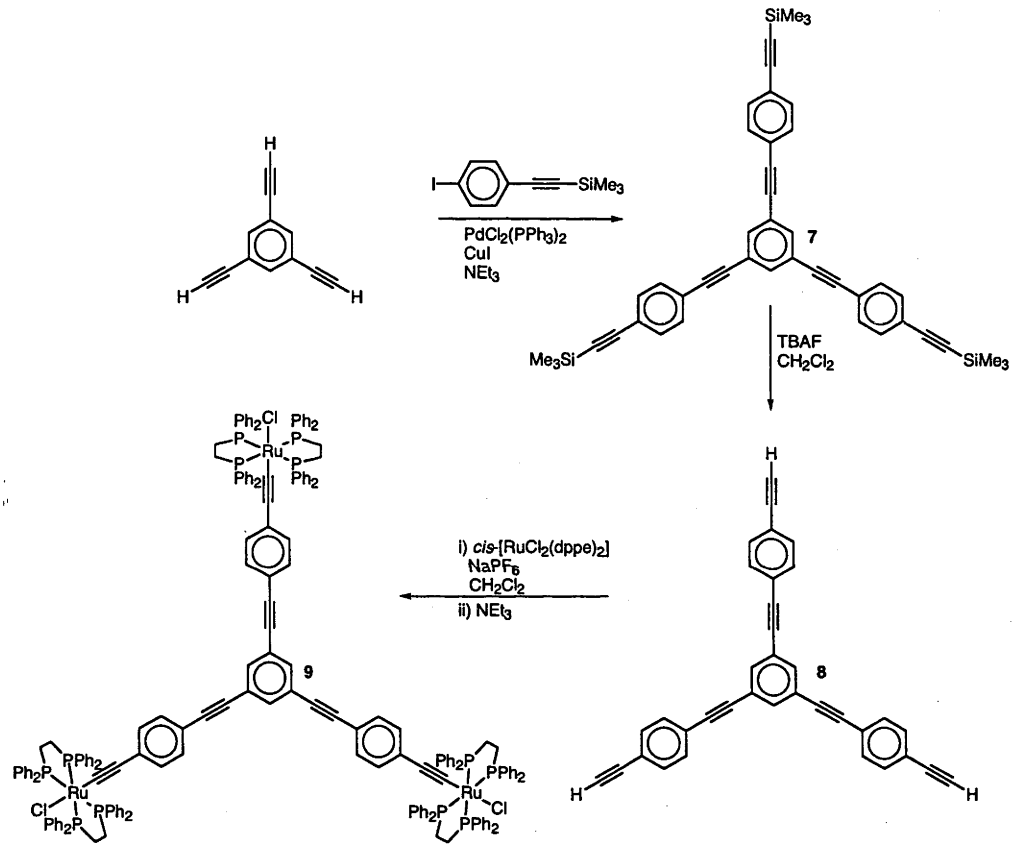

Scheme 4.5. Synthesis of 1,3,5-C_6H_3{C≡CC_6H_4-4-C≡C-*trans*-[RuCl(dppe)$_2$]}$_3$ (**9**)[73]

The synthesis of the zero generation triruthenium dendrimer (**10**) was undertaken by reaction of the diethylamino-substituted acetylene (**3**) with the core **9** via a Dixneuf coupling (Scheme 4.6.). **10** was characterized by ^{1}H and ^{31}P NMR, UV-vis, IR, FAB mass spectrometry and a satisfactory microanalysis. As with the linear analogue **5**, the yield

(26%) was low due to the instability of the complex on the alumina column used in purification.

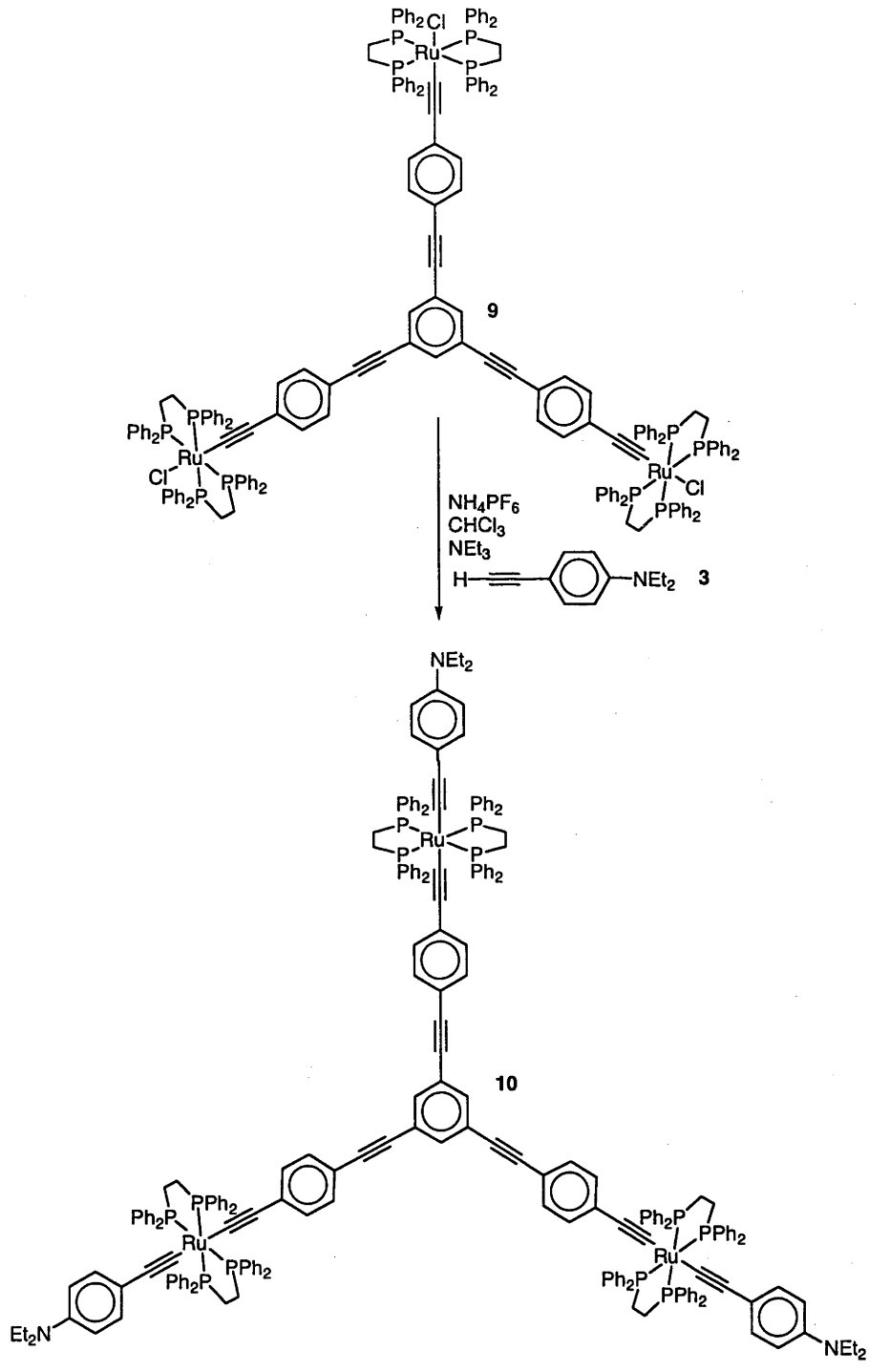

Scheme 4.6. Synthesis of **10**

The synthesis of the dendritic wedge intermediate required for the synthesis of the electron-donating wedge was performed by the published procedure (Scheme 4.7).[27] 1,3,5-Tribromobenzene was selectively transhalogenated to form 1,3-dibromo-5-iodobenzene **11**, which was then reacted with trimethylsilylacetylene via a Sonogashira coupling to form **12**. The bromine atoms were then replaced with iodine to give **13**. This was reacted with 4-bromophenylacetylene to afford **14**. A second transhalogenation reaction formed **15**, which was in turn reacted with an organozinc reagent to give the organic wedge **16**. Reaction with *cis*-$[RuCl_2(dppe)_2]$ gave the dendritic wedge **17** required for further synthesis.

The reaction of the diethylamino-substituted acetylene with 1-$(Me_3SiC{\equiv}C)C_6H_3$-3,5-$\{C{\equiv}CC_6H_4$-4-$C{\equiv}C$-*trans*-$[RuCl(dppe)_2]\}_2$ (**17**) and $NaPF_6$ in refluxing CH_2Cl_2/NEt_3 gave the electron withdrawing dendritic wedge complex 1-$(Me_3SiC{\equiv}C)C_6H_3$-3,5-$\{C{\equiv}CC_6H_4$-4-$C{\equiv}C$-*trans*-$[Ru(C{\equiv}CC_6H_4$-4-$NEt_2)(dppe)_2]\}_2$ (**18**) (Scheme 4.8.). This complex was characterized by ^1H and ^{31}P NMR, UV-vis and IR spectroscopy. The poor stability of this complex on basic alumina prevented the purification required for a satisfactory microanalysis. **18** was desilylated by reaction with potassium carbonate in dichloromethane. This gave a yellow-green solid which decomposed during attempts to purify it by alumina column chromatography.

Because of the instability of the species incorporating the diethylamino-substituted acetylene, this work was discontinued. There is, however, considerable value in exploring the effects of electron-withdrawing and electron-donating substituents on nonlinearities in octupolar complexes. Hence Section 4.3. continues with this theme, with a different electron-donating ligand, and a more facile dendrimer synthesis.

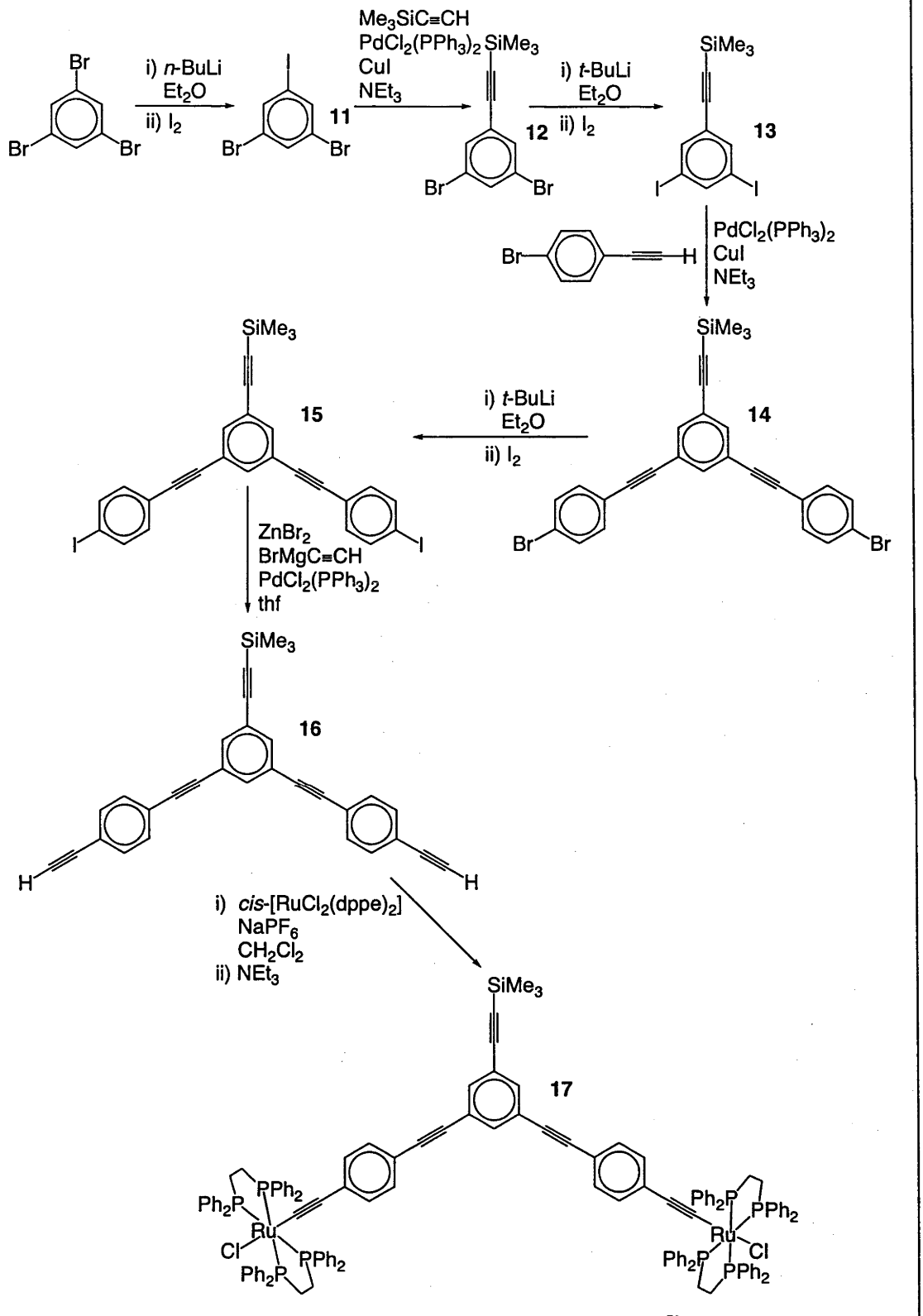

Scheme 4.7. Synthesis of dendritic wedge **17**.[73]

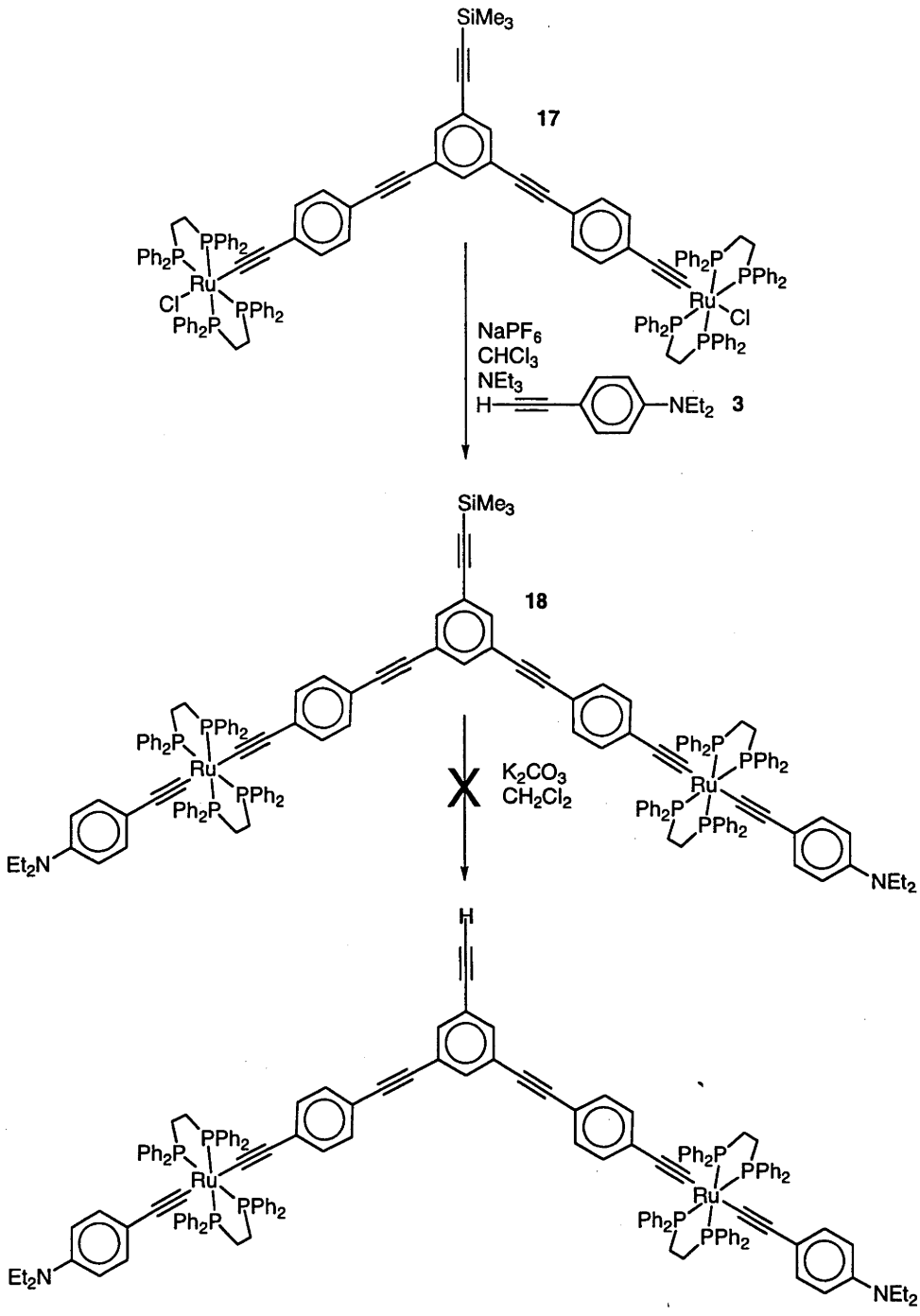

Scheme 4.8. Attempted synthesis of an electron-donating wedge

4.3. *Synthesis of Peripherally-Metallated Dendrimers*

Despite the relative lack of success in the generation of a significant number of electron-donating dendrimers (Section 4.2.), there is still utility in the incorporation of ligands with both strong electron-donors and –acceptors on the periphery of dendrimers. For this reason, two dendrimers and their associated wedges were synthesized.

The synthesis of the wedges is displayed in Scheme 4.9. 1,3,5-Tribromobenzene was reacted with 2-methyl-3-butyn-2-ol in the presence of CuI and a Pd^{II} catalyst, and deprotected with potassium hydroxide to give 1,3,5-triethynylbenzene, following the method of Trumbo and co-workers.[74] The literature preparation[69] for **22a** was modified at this stage to include an alternative work up of **19** (which limits decomposition of the product during work-up) and a longer reaction time during the synthesis of **20a** (which eliminates the need to remove excess starting materials). 1,3,5-Triethynylbenzene was then reacted with *cis*-$[RuCl_2(dppe)_2]$ and ammonium hexafluorophosphate to afford the bis-metallated complex 1,3-{*trans*-$[(dppe)_2ClRuC{\equiv}C]\}_2$-5-$HC{\equiv}CC_6H_3$ (**19**). Chloro- replacement by reaction with phenylacetylene, ammonium hexafluorophosphate and triethylamine then afforded the complex 1,3-{*trans*-$[(dppe)_2(PhC{\equiv}C)RuC{\equiv}C]\}_2$-5-$HC{\equiv}CC_6H_3$ (**20a**). In order to decrease the steric strain about the ethynyl group, the complex was coupled with 4-iodo(trimethylsilylethynyl)benzene to give 1,3-{*trans*-$[(dppe)_2(PhC{\equiv}C)RuC{\equiv}C]\}_2$-5-$(Me_3SiC{\equiv}C\text{-}4\text{-}C_6H_4C{\equiv}C)C_6H_3$ (**21a**) via a Pd^0-catalyzed Sonogashira reaction. This was then desilylated with tetrabutylammonium fluoride to give the desired wedge, 1,3-{*trans*-$[(dppe)_2(PhC{\equiv}C)RuC{\equiv}C]\}_2$-5-$(HC{\equiv}C\text{-}4\text{-}C_6H_4C{\equiv}C)C_6H_3$ (**22a**).

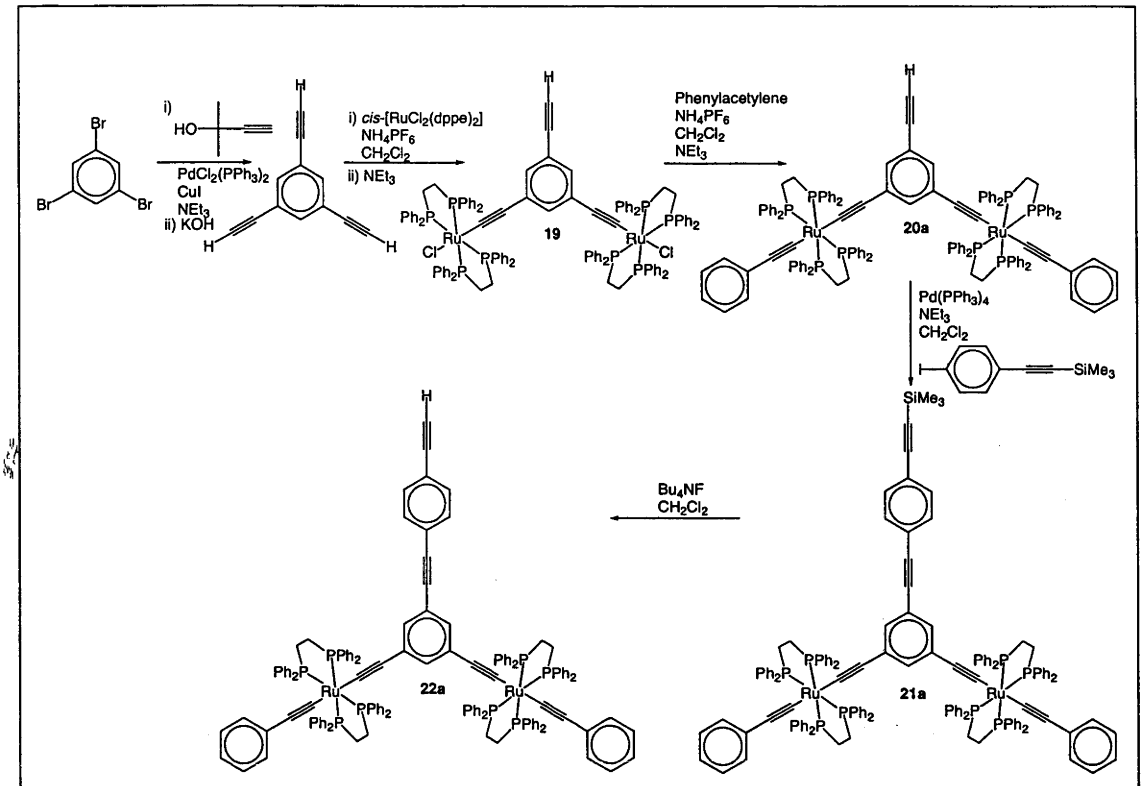

Scheme 4.9. Synthesis of dendritic wedge **22a**

Replacement of phenylacetylene in the above synthetic route with the electron-withdrawing 4-nitrophenylacetylene and the electron-donating 4-ethynylaniline has afforded both electron-withdrawing (**20b** - **22b**) and electron-donating (**20c** - **22c**) dendritic wedges (Figure 4.7.).

The various wedges, **22b** - **22c**, were reacted with 1,3,5-triiodobenzene via a Pd^0 catalyzed Sonogashira reaction to form the dendritic complexes **23b** - **23c** (Scheme 4.10.). Because of the instability of the diethylamino- complexes reported earlier, **20c** - **23c** were purified by recrystallization rather than column chromatography.

These complexes (**20b,c** - **23b,c**) have been characterized by ^1H and ^{31}P NMR, satisfactory microanalysis, UV-vis and IR spectroscopy. FAB mass spectrometry was found to be unreliable; larger molecules failed to give a parent ion, in common with other ruthenium-acetylide dendrimers.[69,73] In order to further characterize one example (**23b**), molecular modeling was performed to determine the dendrimer dimensions (Figure 4.8.), and these were compared with a TEM image (Figure 4.9.). The molecular modeling indicates that the dendrimer is approximately 50 Å in diameter, this value comparing well with the TEM

results (~50 Å).

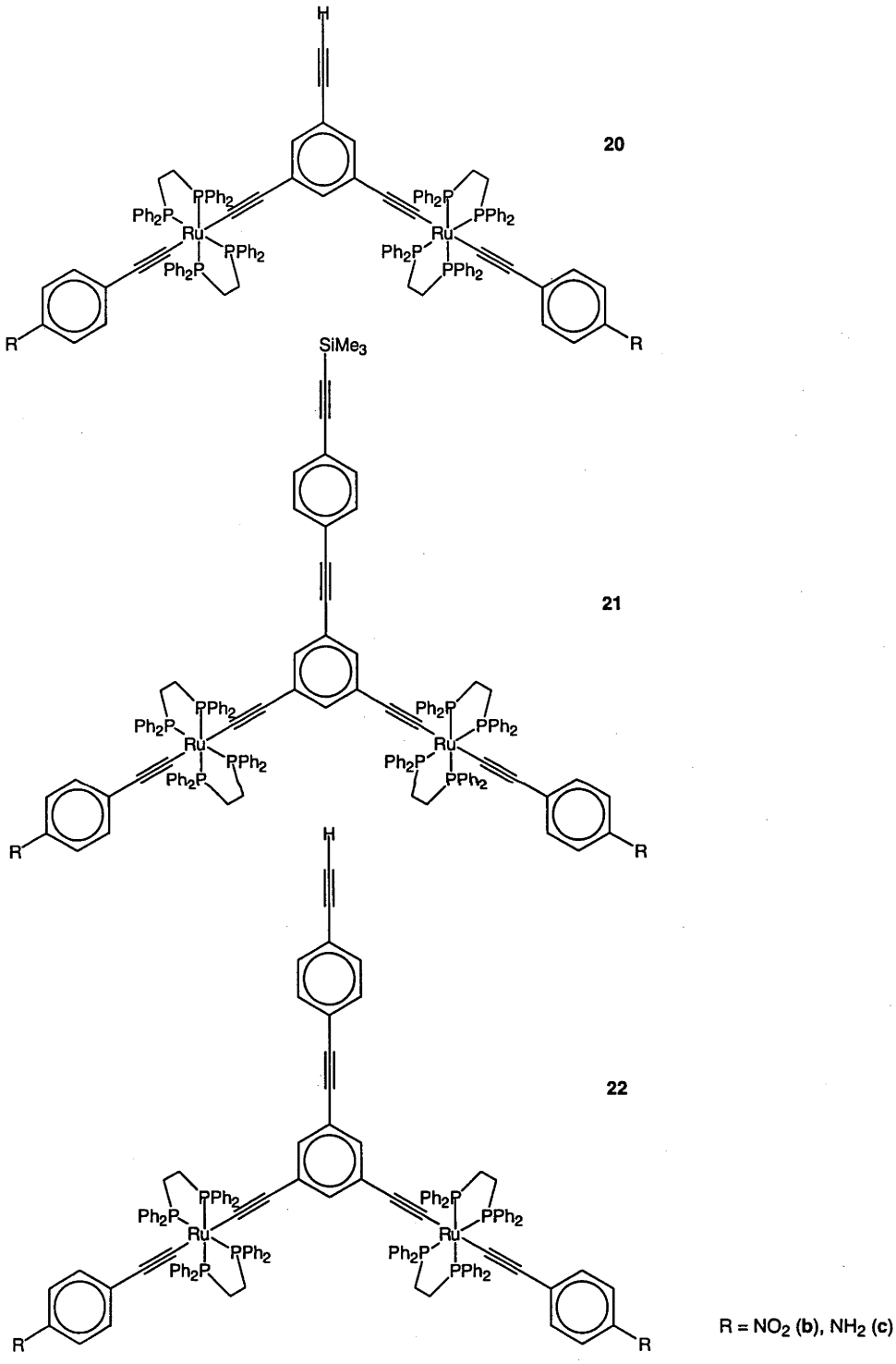

Figure 4.7. Electron-withdrawing and electron-donating dendritic wedges

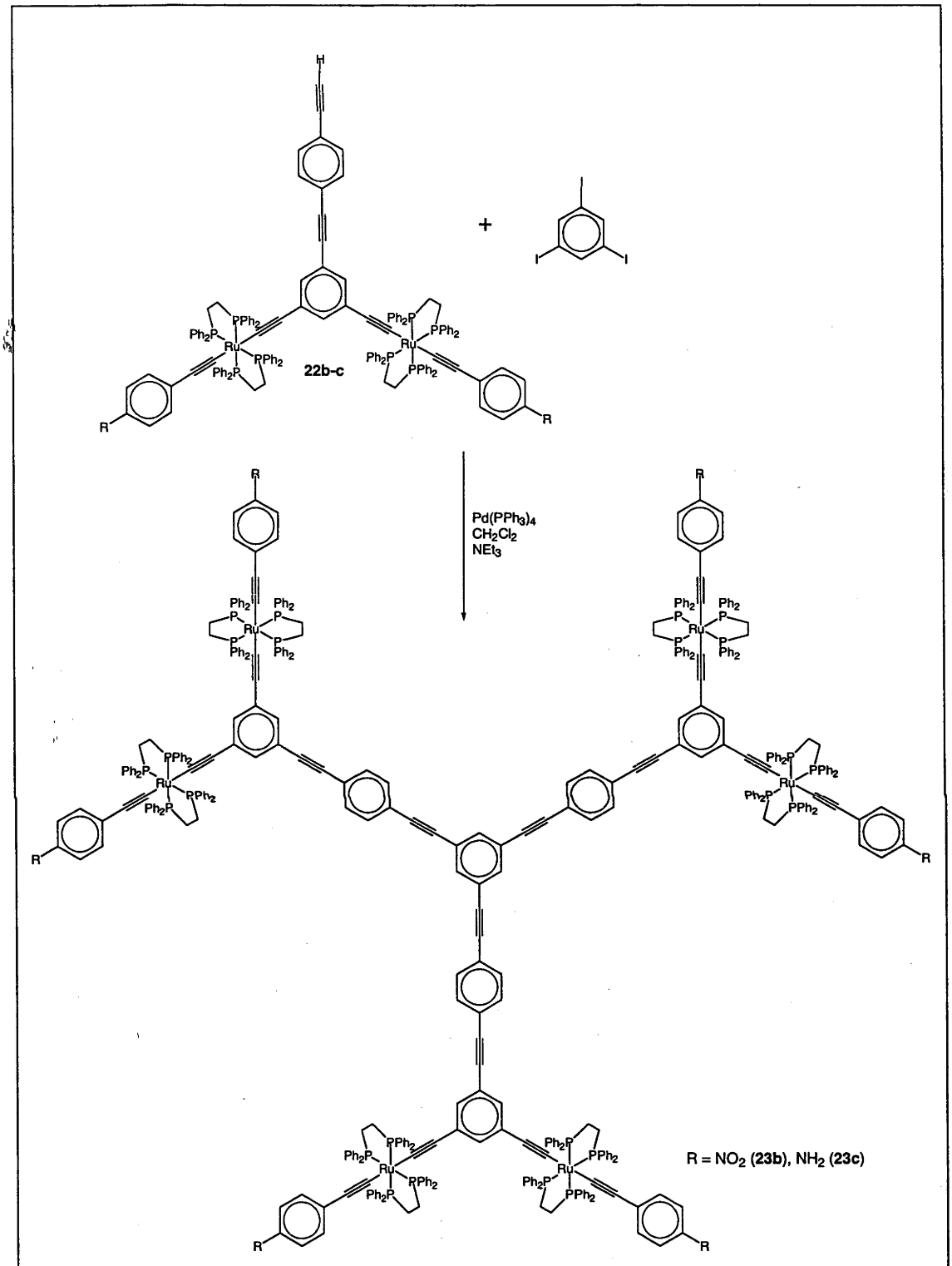

Scheme 4.10. Synthesis of dendrimers **23b** and **23c**

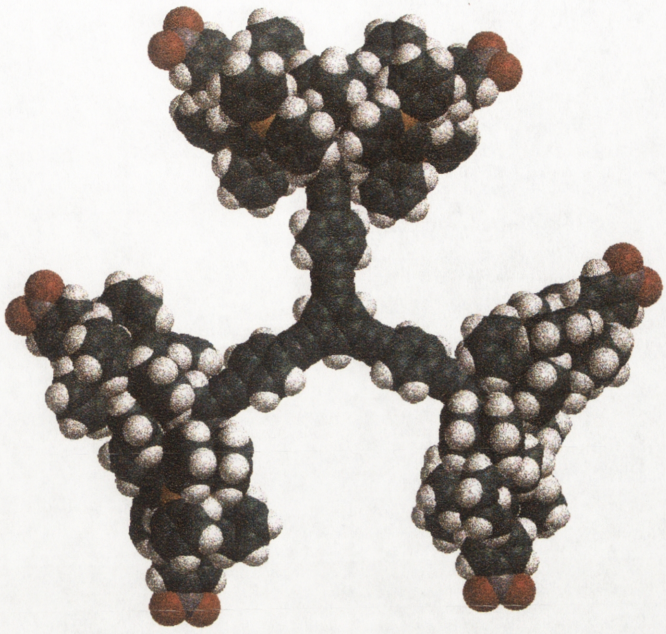

Figure 4.8. Geometry of **23b** as derived by molecular modelling. Calculations indicate that **23b** is approximately 50 Å in diameter.

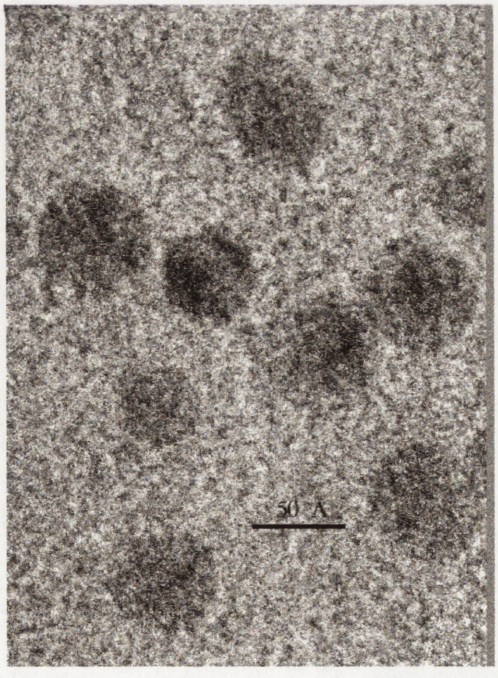

(M. P. Cifuentes and E. G. A. Notaras)

Figure 4.9. TEM image of **23b**

4.4. *Improved Methods of Dendrimer Synthesis*

4.4.1. *Introduction*

An important constraint in the synthesis of transition metal acetylide dendrimers is the large number of reactions required for their synthesis. Recently, a new method of dendrimer wedge synthesis has been published[69] which requires considerably fewer steps than the earlier synthetic route.[26] A comparison of the structures of both wedges is displayed in Figure 4.10.

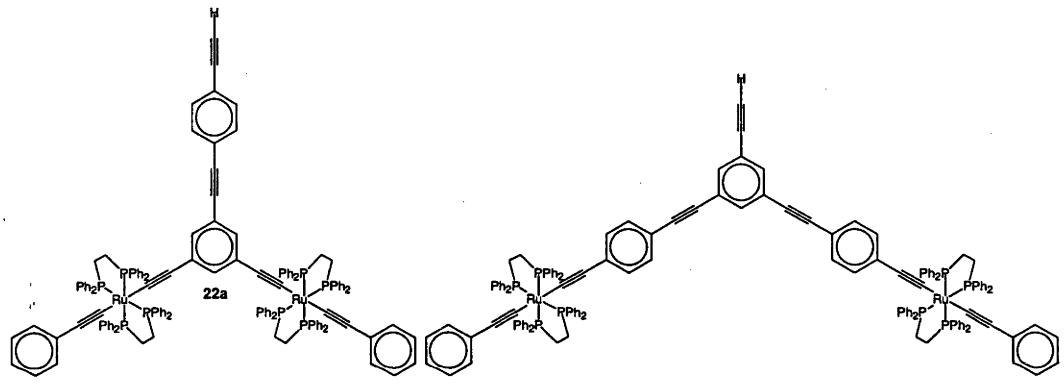

Figure 4.10. Dendritic wedges **22a**[69] (left) and **22d**[26] (right)

The two wedges differ significantly in the complexity of the synthetic route used to construct them. The synthesis of both wedges start with 1,3,5-tribromobenzene, but wedge **22d** requires an earlier selective *trans*-halogenation reaction to introduce the required asymmetry around the central ring, whereas the preparation of **22a** relies on the steric bulk of ruthenium-bis(diphosphine) centres to introduce asymmetry. The synthesis of **22d** requires 11 reactions from commercially available starting materials, whereas preparation of **22a** requires 10 reactions from commercially available starting materials, the majority of which are significantly simpler than the analogous reactions for **22d**.

Wedge **22d** has been successfully reacted with 1,3,5-C_6H_3{C≡CC_6H_4-4-C≡C-*trans*-[RuCl(dppe)$_2$]}$_3$ (**9**) to form a Ru_9 dendrimer with ruthenium-acetylide units in both the inner and outer generations. By comparison, wedge **22a** has only been reacted with 1,3,5-triiodobenzene, to give a Ru_6 dendrimer with ruthenium-acetylide units in the outer generation. The third-order hyperpolarizabilities of the two dendrimers are 20 700 ± 2000 and 1600 ± 2000 x 10^{-36} esu, respectively,[27,75] indicating that the presence of additional metals in the core of the dendrimer leads to a major increase in the third-order nonlinearities. There is, therefore, considerable utility in coupling the synthetically less demanding wedge with a transition metal-acetylide containing core.

4.4.2. *Reaction between Wedge and Core*

The method used to synthesize the wedge is described in Section 4.3. In order to simplify the synthesis, only one style of wedge was examined, **22a**, which was reacted with the organometallic core **9**. Initial attempts at coupling **22a** to **9** via a Dixneuf reaction (Scheme 4.11.) returned only starting materials. Replacement of ammonium hexafluorophosphate with the more reactive sodium hexafluorophosphate had no discernible effect. Attempting the reaction in refluxing dichloromethane and $CHCl_3$ afforded starting materials or decomposition of the wedge.

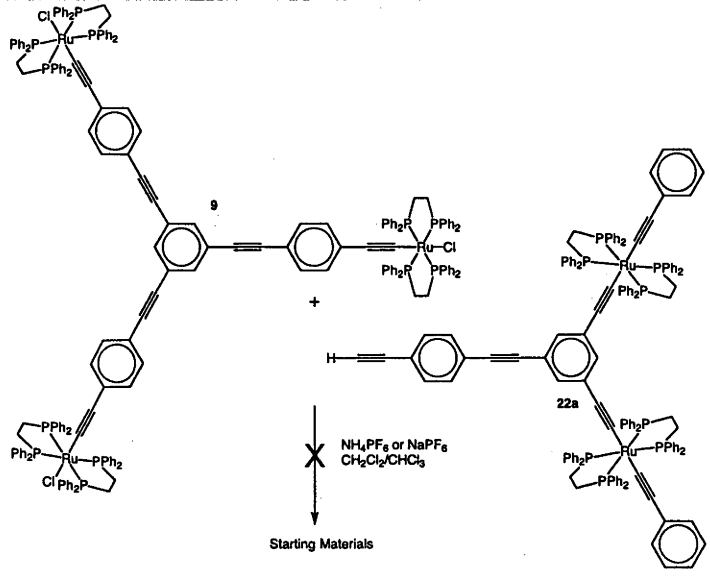

Scheme 4.11. Reaction between wedge and core

It was therefore proposed to attempt to increase the reactivity of either the core or the wedge by structural modification allowing coupling by a Sonogashira or a Negishi coupling, rather than a Dixneuf coupling. Other possible routes to the desired dendrimer include replacement of the chloride on the core **9** with a better leaving group, such as acetonitrile or dihydrogen, or activation of the wedge, by either acetylenic proton abstraction by BuLi or conversion of the wedge **22a** to a trimethylstannyl analogue. Finally, the steric load can be reduced by incorporation of a less bulky wedge (ie. increasing the distance of the phenylalkynyl chain to remove the ruthenium metal centers from the reaction center), or use of a less bulky core.

4.4.3. *Sonogashira Coupling*

The Sonogashira reaction is a well established means of coupling an acetylene with an aryl-halide with palladium and copper catalysts.[76] The biggest problem with the reaction is the formation of an unwanted homo-coupled byproduct. This homo-coupling requires the presence of oxygen and has been observed to be significantly more important when electron rich substituents are present with the acetylene. The unwanted coupling can be avoided by the removal of the copper catalyst, and the replacement of the Pd^{II} catalyst with a Pd^{0} phosphine catalyst. The mechanism is displayed in Scheme 4.12.

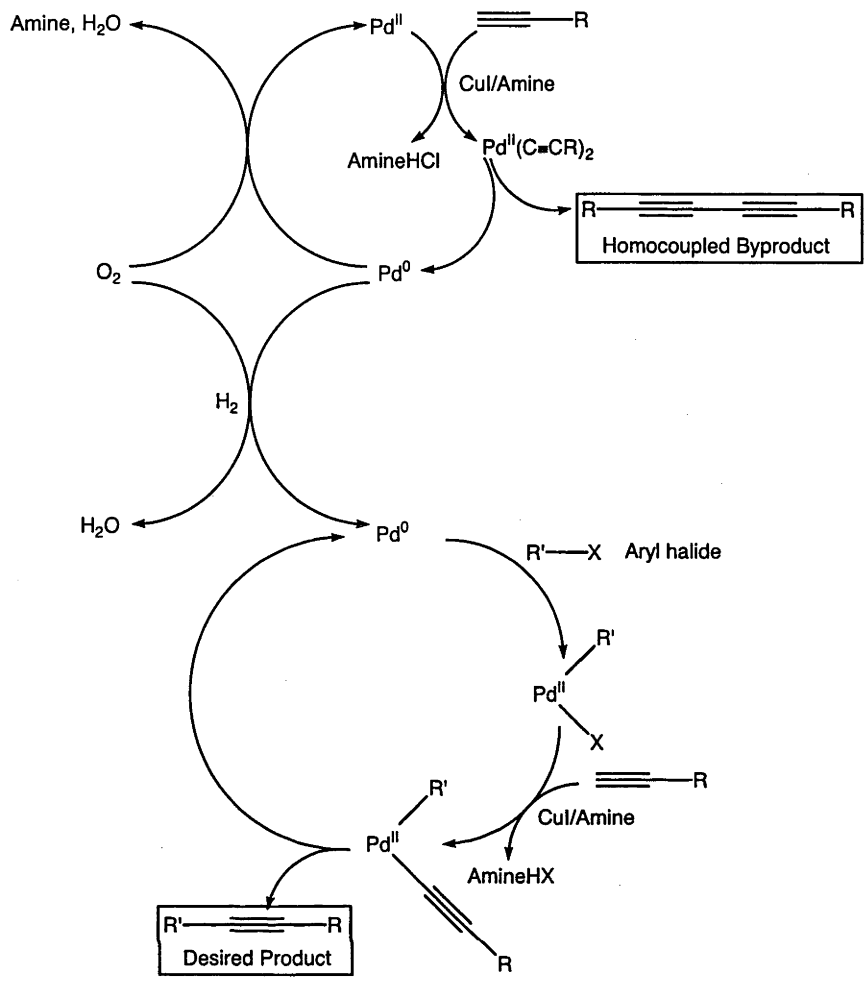

Scheme 4.12. Mechanism of Sonogashira coupling and associated homocoupling reactions as proposed by Ho and co-workers[77]

The syntheses of the required aryl halide precursors, *trans*-[Ru(C≡CC_6H_4-4-I)$_2$(dppe)$_2$] (**24**) and 1,3,5-C_6H_3{C≡CC_6H_4-4-C≡C-*trans*-[Ru(C≡CC_6H_4-4-I)(dppe)$_2$]}$_3$ (**25**), are displayed in Schemes 4.13. and 4.14., respectively. The ruthenium chloride starting material, *cis*-[$RuCl_2$(dppe)$_2$], was stirred with 4-iodophenylacetylene in the presence of ammonium hexafluorophosphate to form the vinylidene *trans*-[Ru(C=CHC_6H_4-4-I)Cl(dppe)$_2$]PF_6. This was then deprotonated *in situ* to the mono-acetylide *trans*-[Ru(C≡CC_6H_4-4-I)Cl(dppe)$_2$] *via* the addition of triethylamine. This complex was then free to react with surplus 4-iodophenylacetylene to form the desired bis-acetylide product. The octopolar triruthenium complex **25** was synthesized in a similar manner by the reaction of 4-iodophenylacetylene

with the octupolar complex **9** in the presence of ammonium hexafluorophosphate and triethylamine.

The successful synthesis of the two iodoaryl complexes **24** and **25** allows a Sonogashira coupling to be attempted by reaction with 1,3-{*trans*-[(dppe)$_2$(PhC≡C)RuC≡C]}$_2$-5-HC≡CC$_6$H$_3$ (**20a**) in an attempt to synthesize the dendrimer **26** (e.g. Scheme 4.15.). The linear bis-acetylide complex **24** can be used as a model for the more synthetically complex octupolar complex. However the reaction between **25** and **20a** resulted in the formation of the homo-coupled product (3-5-{*trans*-[(dppe)$_2$(PhC≡C)RuC≡C]}$_2$C$_6$H$_3$-1-C≡C)$_2$, rather than the desired first generation dendrimer (Figure 4.11.). This complex was identified by comparison with the literature ^{1}H and ^{31}P NMR spectral data (similar results were observed in the analogous reaction between **24** and **22a**).[69]

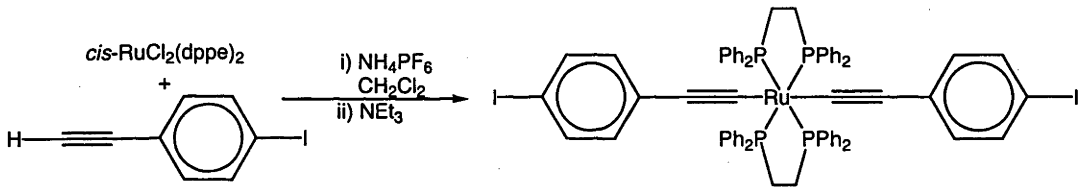

Scheme 4.13. Synthesis of *trans*-[Ru(C≡CC$_6$H$_4$-4-I)$_2$Cl$_2$] (**24**)

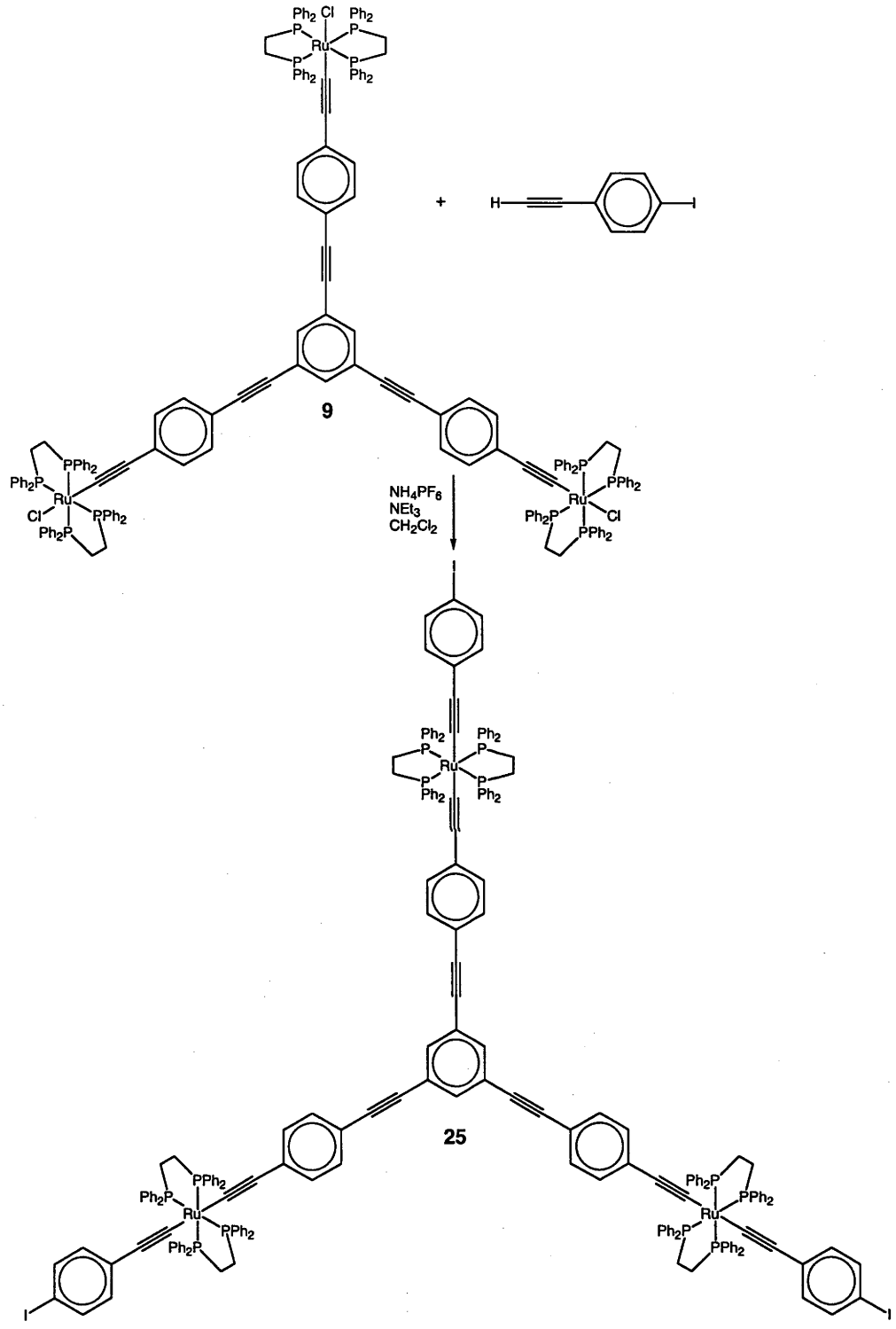

Scheme 4.14. Synthesis of 1,3,5-C_6H_3{$C{\equiv}CC_6H_4$-4-$C{\equiv}C$-*trans*-[$Ru(C{\equiv}CC_6H_4$-4-I)$(dppe)_2$]}$_3$ (**25**)

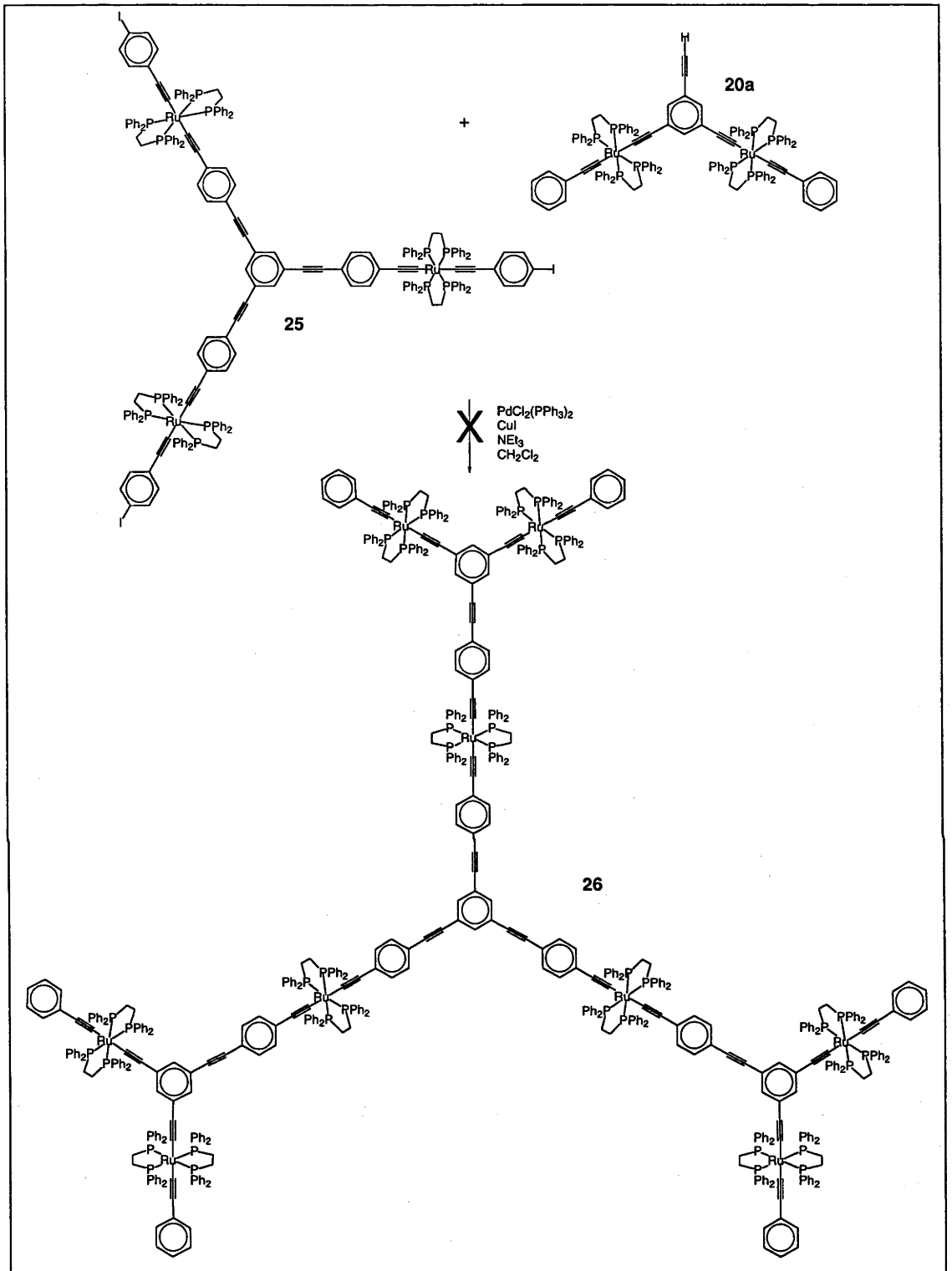

Scheme 4.15. Attempted Reaction between **25** and **20a**

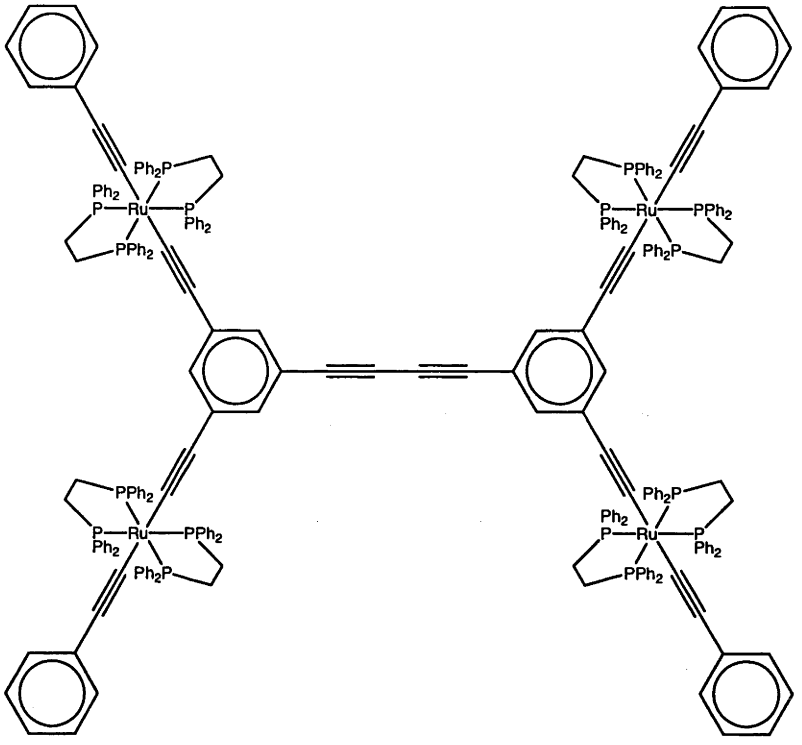

Figure 4.11. {3,5-(*trans*-[(dppe)$_2$(PhC≡C)RuC≡C)$_2$C$_6$H$_3$-1-C≡C}$_2$

Another possible synthetic route to the formation of a metal-actylide containing dendrimer is reaction between **19** and **24** in the presence of $PdCl_2(PPh_3)_2$ and CuI, leading to the formation of *trans*-[Ru(dppe)$_2$]{C≡CC$_6$H$_4$-4-C≡C-1-C$_6$H$_3$-3,5-(C≡C-*trans*-[RuCl(dppe)$_2$])$_2$}$_2$ (**27**) (Scheme 4.16.). Instead of the desired quadrapolar complex **27**, the complex {3,5-(*trans*-[(dppe)$_2$ClRuC≡C)$_2$C$_6$H$_3$-1-C≡C}$_2$ (**28**) was synthesized (this complex is a product of the homo-coupling of wedge **19**). Because of difficulties in separating **28** from the unreacted **24**, **28** was synthesized by a more rational method (Scheme 4.17.) which allowed the complex to be characterized. Upon conversion of **19** to **28**, the acetylene proton resonance in the ^{1}H nmr disappears, and there is a substantial increase in the extinction coefficient of the MLCT band in the UV-vis spectrum.

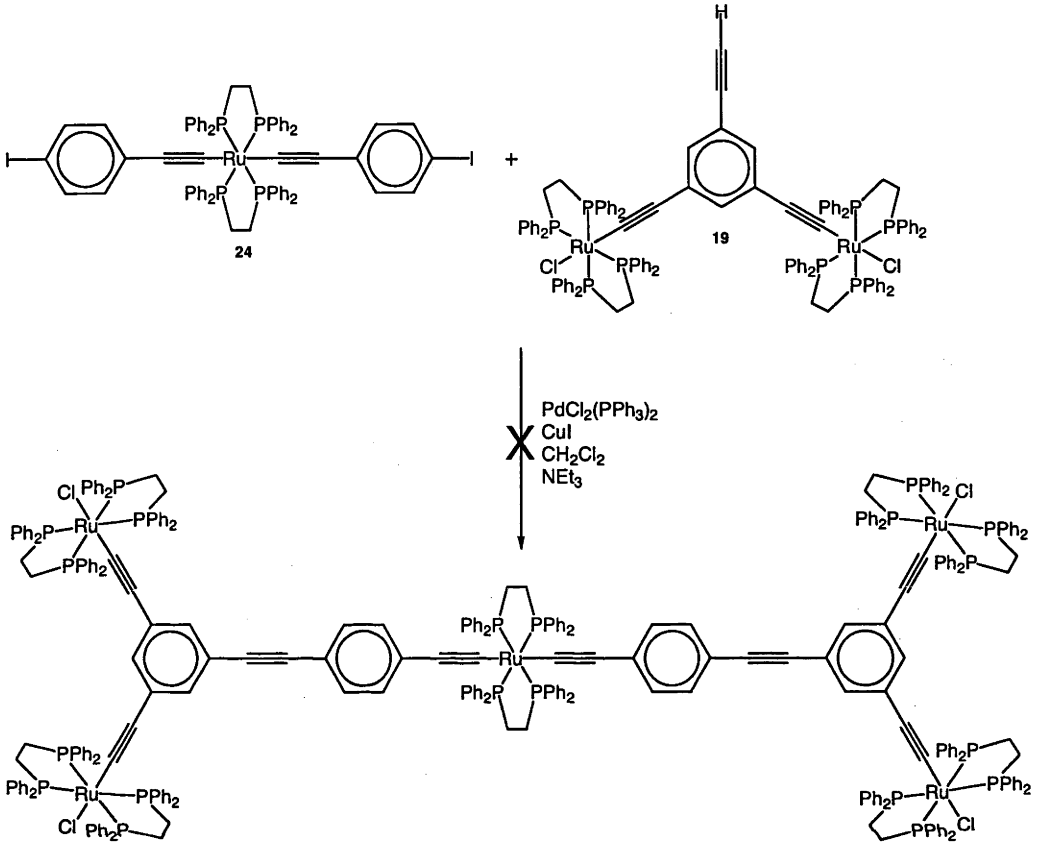

Scheme 4.16. Attempted synthesis of *trans*-[Ru(dppe)$_2$]{C≡CC$_6$H$_4$-4-C≡C-1-C$_6$H$_3$-3,5-(C≡C-*trans*-[RuCl(dppe)$_2$])$_2$}$_2$ (**27**)

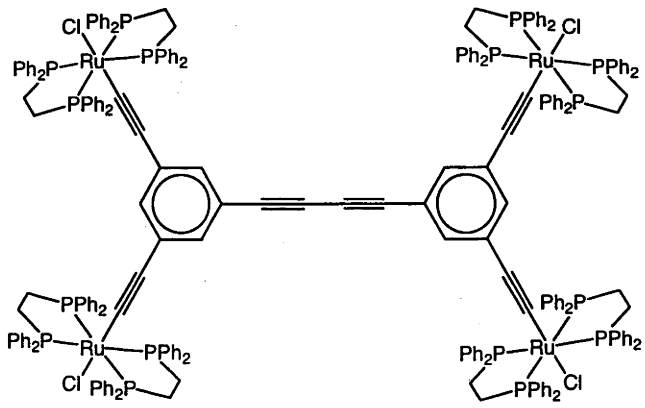

Figure 4.12. {3,5-(*trans*-[(dppe)$_2$ClRu]C≡C)$_2$C$_6$H$_3$-1-C≡C}$_2$ (**28**)

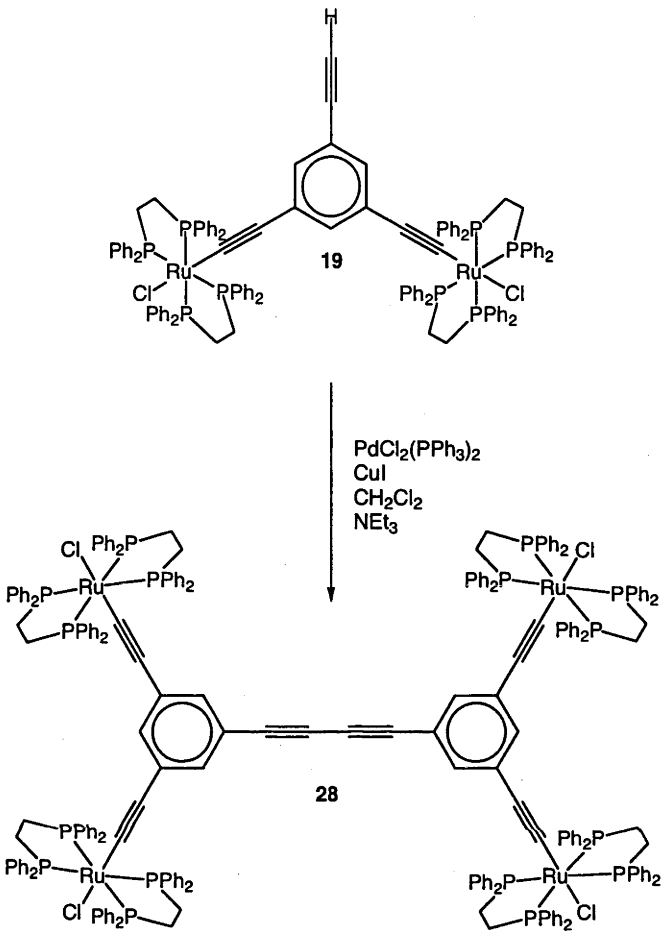

Scheme 4.17. Synthesis of {3,5-(*trans*-[(dppe)$_2$ClRuC≡C)$_2$C$_6$H$_3$-1-C≡C}$_2$ (**28**)

In an attempt to eliminate the homo-coupling reaction of the wedge complexes, the Pd^{II}/CuI catalyst system was replaced with Pd^0 in the form of $Pd(PPh_3)_4$. Reaction of **20a** with either **24** or **25** in the presence of $Pd(PPh_3)_4$ led to the same result: **20a** would remain unreacted, while the core would decompose. Closer investigation revealed an ether soluble ruthenium acetylide species. This was suspected to be a result of reaction with the Pd^0 catalyst, because of the large increase in the integral of phenyl region in the ^{1}H NMR, but further investigation was beyond the scope of this project. The suspected side-product is displayed in Figure 4.13.

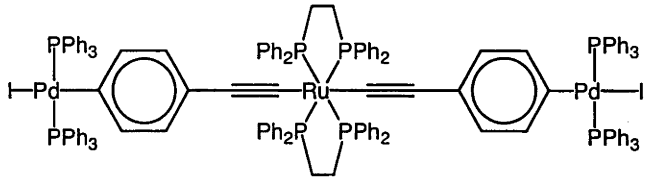

Figure 4.13. Suspected product of reaction between **24** and $Pd(PPh_3)_4$. Replacement with **25** gives analogous results

4.4.4. *Negishi Coupling*

Another reaction, conceptually similar to the Sonogashira reaction, is the Negishi coupling,[78,79] where an alkynyl species is reacted with zinc bromide to form BrZnC≡CR (this reactant can either be formed *in situ*, or added to the reaction). This species is then reacted with an aryl iodide in the presence of a Pd^0 catalyst to form the desired acetylide (Scheme 4.18.). Advantages of the Negishi reaction are that ethynyl groups can be added directly by use of reagents such as BrMgC≡CH (which is then converted *in situ* to BrZnC≡CH), and some variations of the reaction are experimentally simple (the need for magnesium and deoxygenated dry solvents can be eliminated). One disadvantage is that all of the literature examples use simple organic ligands as the acetylene.[80,81]

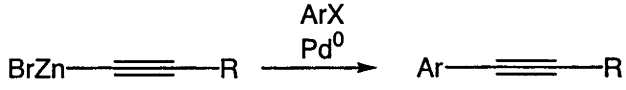

Scheme 4.18. Negishi Coupling

The complex 1,3-{*trans*-[(dppe)$_2$(PhC≡C)RuC≡C]}$_2$-5-(HC≡C)C$_6$H$_3$ (**20a**) was reacted with $ZnBr_2$ and $Pd(PPh_3)_4$, and then added to the reaction mixture **25**. After basic workup, ^1H and ^{31}P NMR showed unidentified decomposition products (Scheme 4.19.).

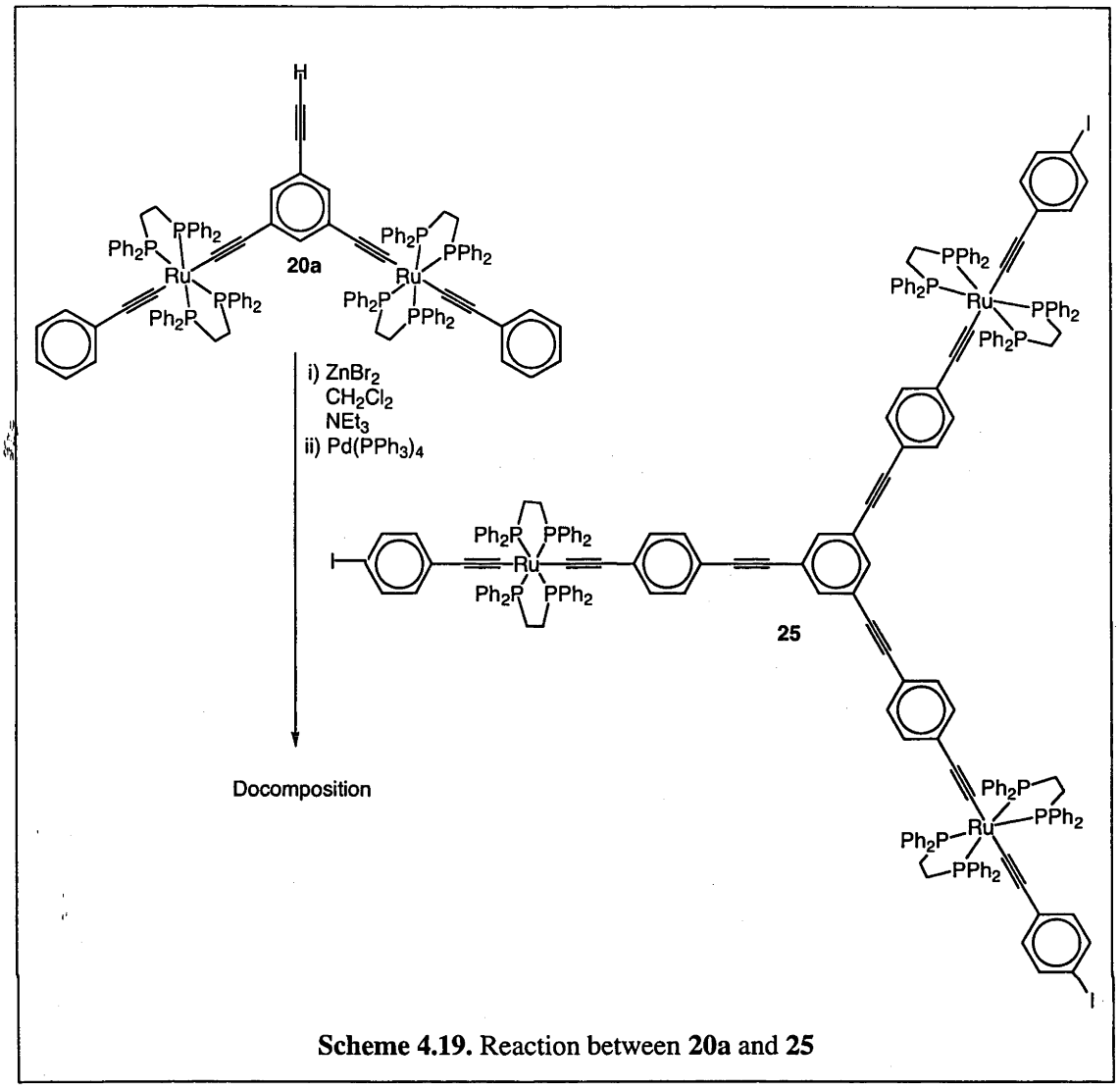

Scheme 4.19. Reaction between **20a** and **25**

4.4.5. *Acetonitrile Replacement*

One means of activating the reaction between the triruthenium organometallic core **9** and the wedge **20a** is the replacement of the chloro group on the core with a weaker leaving group. In order to test this, a model complex was synthesized. Scheme 4.20. shows the reaction between *trans*-[Ru(C≡CPh)Cl(dppe)$_2$] and acetonitrile with ammonium hexafluorophosphate to give the complex *trans*-[Ru(N≡CMe)(C≡CPh)(dppe)$_2$]PF_6 (**29**). The complex was characterized by ^1H and ^{31}P NMR, UV-vis, IR, FAB mass spectrometry and a satisfactory microanalysis. This complex was identifiable by examination of the ^1H and ^{31}P NMR spectral data: a peak at 1.35 ppm in the ^1H NMR was assigned to the methyl group on

the acetonitrile ligand, whereas the ^{31}P NMR possessed a singlet at 51 ppm, intermediate between 49 ppm and 54 ppm which is observed for mono- and bis-acetylides, respectively. The complex displayed multiplets at 2.64 and 6.6 - 8.1 ppm in the ^{1}H NMR, attributed to the bridging methylene protons of the dppe ligands and the phenyl protons, respectively.

Complex **29** was then heated with phenylacetylene in refluxing CH_2Cl_2 in an attempt to synthesize *trans*-[Ru(C≡CPh)$_2$(dppe)$_2$], but no reaction was observed. The analogous reaction in refluxing thf also led to no observable formation of the desired product. As this methodology was attempted in order to increase the rate of reaction, no further trial reactions were attempted.

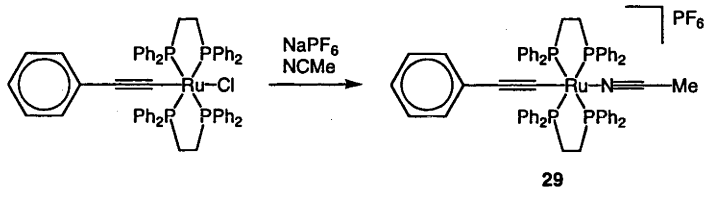

29

Scheme 4.20. Synthesis of *trans*-[Ru(C≡CPh)(N≡CMe)(dppe)$_2$]PF_6 (**29**)

Complex **29** was structurally characterized by an X-ray diffraction study. Two different views are displayed in ORTEP plots in Figures 4.14. and 4.15., and selected bond angles and lengths (Å) are listed in Table 4.1. Comparison with structural data for the related *trans*-[Ru(C≡CPh)Cl(dppe)$_2$][82] reveals that the Ru–C bond length is indistinguishable at three confidence intervals. in **29** (2.022(3) Å vs 2.007(5) Å), whereas the C≡C is indistinguishable.

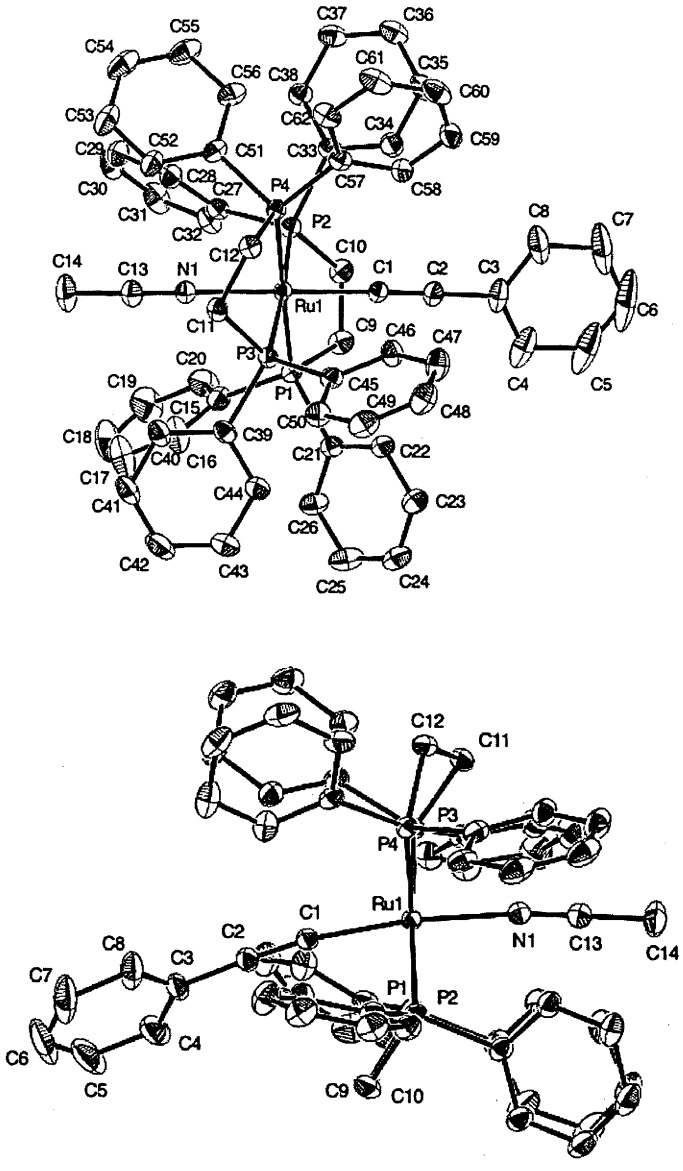

Figure 4.14. Thermal ellipsoid diagrams of the cation of *trans*-[Ru(C≡CPh)(N≡CMe)(dppe)$_2$]PF$_6$ (**29**) with labelling of selected atoms. Ellipsoids show 30% probability levels. Hydrogen atoms have been deleted for clarity. (by A. C. Willis)

Table 4.1. Selected bond distances (Å) and angles (deg.) for *trans*-[Ru(C≡CPh)(N≡CMe)(dppe)$_2$]PF$_6$ (**29**)			
Ru1–N1	2.072(2)	Ru1–C1	2.022(3)
Ru1–P1	2.3407(8)	Ru1–P2	2.3724(8)
Ru1–P3	2.3894(8)	Ru1–P4	2.3980(8)
N1–C13	1.152(4)	C13–C14	1.445(5)
C1–C2	1.212(4)	C2–C3	1.438(4)
P1–C9	1.844(3)	P2–C10	1.857(3)
P3–C11	1.845(3)	P4–C12	1.864(3)
C9–C10	1.515(5)	C11–C12	1.514(5)
N1–Ru1–C1	172.93(11)	P1–Ru1–N1	91.54(8)
P1–Ru1–P2	81.46(3)	P1–Ru1–P3	97.30(3)
P2–Ru1–P3	176.24(3)	P1–Ru1–P4	178.35(3)
Ru1–N1–C13	174.5(3)	N1–C13–C14	178.2(4)
Ru1–C1–C2	171.3(3)	C1–C2–C3	177.5(3)

4.4.6. *Wedge Activation by BuLi*

n-BuLi was used to abstract the proton from the ethynyl group, in order to activate the acetylide ligand to further reaction (Scheme 4.21.); both phenylacetylene and the wedge **22a** were reacted with *n*-BuLi to form a Li-acetylide complex, which was then reacted *in situ* with the octopolar triruthenium core, **9**. It was observed that an excess of *n*-BuLi caused ruthenium-acetylide complexes to turn green and decompose, so an excess of acetylene was added prior to reaction with 1,3,5-C_6H_3{C≡CC_6H_4-4-C≡C-*trans*-[RuCl(dppe)$_2$]}$_3$. These reactions were ultimately unsuccessful, returning the ruthenium acetylide starting materials only.

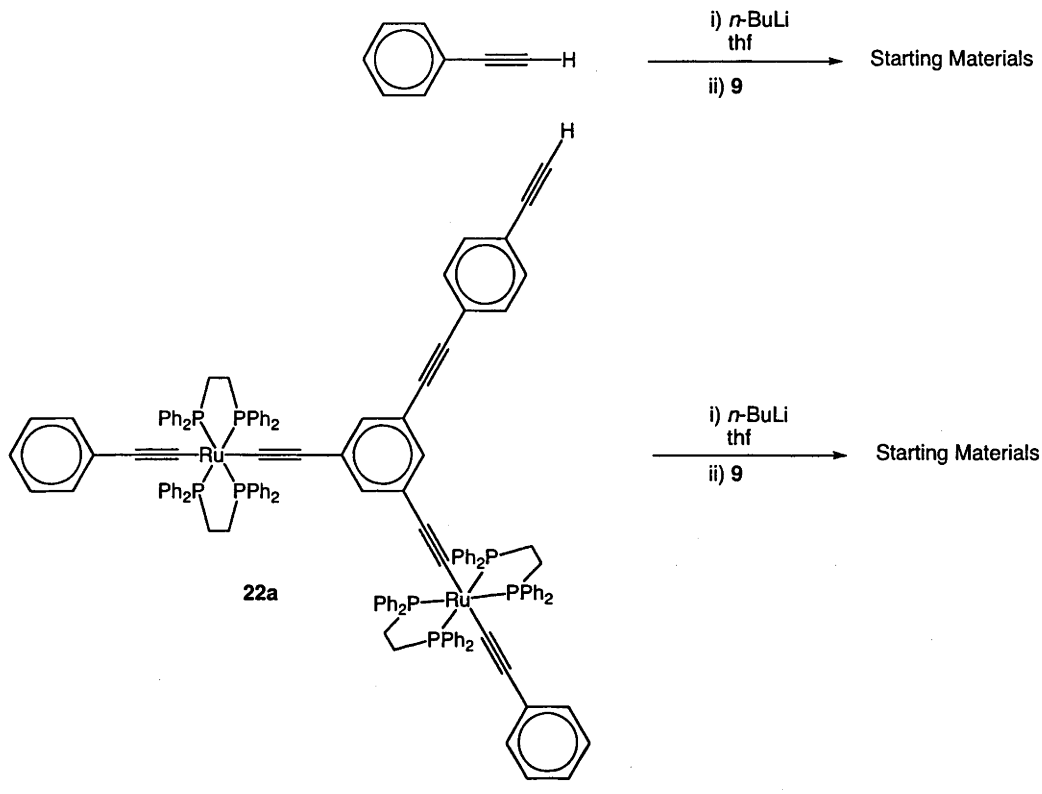

Scheme 4.21. Reactions involving acetylene activation using *n*-BuLi

4.4.7. *Acetylene Activation by $SnMe_3$*

The conversion of acetylenes into (trimethylstannyl)ethyne compounds prior to their reaction with a transition metal center is well known.[82-87] Of particular interest is the use of mild conditions in the synthesis of a number of complexes that normally require forcing conditions, such as the preparation of bis-acetylide osmium complexes, and bis-acetylide complexes incorporating the di-phosphine ligand dppm. Literature examples are, however, confined to relatively simple organic acetylenes, such as phenylacetylene; complex acetylenes containing transition-metal acetylides have not been reported. The dendrimer wedge **22a** could, in principle, be reacted with Me_3SnCl to give 1,3-{*trans*-$[(dppe)_2(PhC{\equiv}C)RuC{\equiv}C]\}_2$-5-$(Me_3SnC{\equiv}C\text{-}4\text{-}C_6H_4C{\equiv}C)C_6H_3$ (**30**), which could then in turn be reacted with a dendritic core **9** to give the desired product (Scheme 4.22.). The reaction was carried out between the dendrimer wedge **22a** and Me_3SnCl, but only decomposition products were observed by ^1H and ^{31}P NMR.

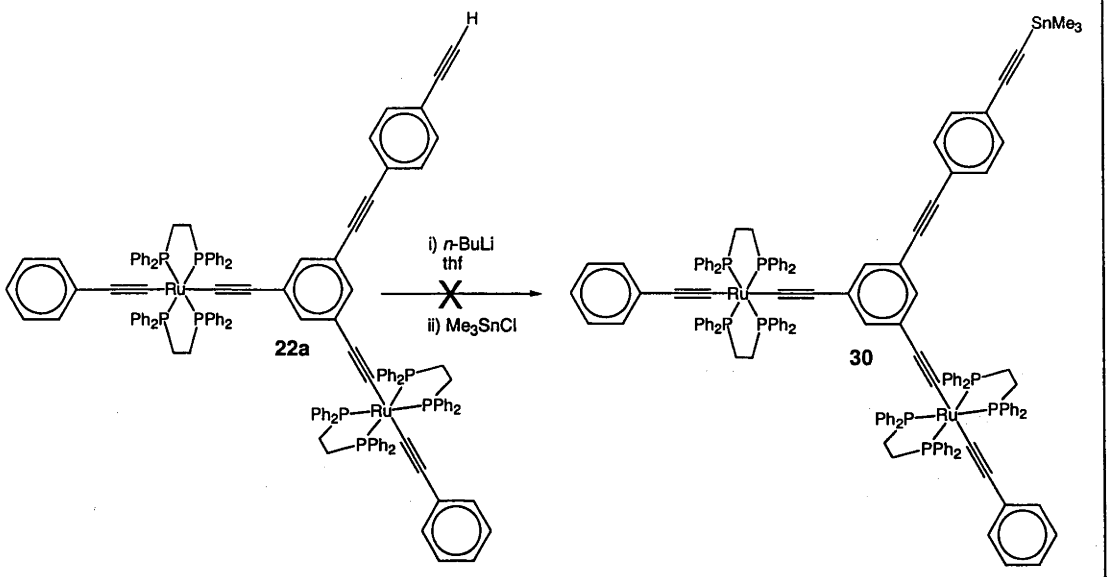

Scheme 4.22. Attempted synthesis of trimethyltin-containing wedge (**30**)

4.4.8. *Metal Replacement at Core*

In view of the lack of successful routes to the coupling of the synthetically simpler wedge, 1,3-{*trans*-[(dppe)$_2$(PhC≡C)RuC≡C]}$_2$-5-(HC≡C-4-C$_6$H$_4$C≡C)C$_6$H$_3$ (**2 2 a**), to the triruthenium core, 1,3,5-C$_6$H$_3${C≡C-4-C$_6$H$_4$C≡C-*trans*-[RuCl(dppe)$_2$]}$_3$ (**9**), a molecular modelling study was undertaken to investigate the steric differences between the two wedges **22a** and 1-(HC≡C)-C$_6$H$_3$-3,5-{C≡CC$_6$H$_4$-4-C≡C-*trans*-[Ru(C≡CPh)(dppe)$_2$]}$_2$ **22d**. Figure 4.15. displays the results of geometry optimization calculations on each complex, while Figure 4.16. displays the results of geometry optimization calculations on 1-{*trans*-[Ru(C≡CPh)(dppe)$_2$C≡CC$_6$H$_4$-4-C≡C}-C$_6$H$_3$-3,5-{C≡C-*trans*-[Ru(C≡CPh)(dppe)$_2$]}$_2$ and 1-{*trans*-[Ru(C≡CPh)(dppe)$_2$C≡C}-C$_6$H$_3$-3,5-{C≡CC$_6$H$_4$-4-C≡C-*trans*-[Ru(C≡CPh)(dppe)$_2$]}$_2$. These hypothetical complexes are the result of coupling a Ru(C≡CPh)(dppe)$_2$ moiety to wedges **22a** and **22d**, and serve as a model for the desired dendrimers produced from a successful coupling between each wedge and the core, **9**. Figure 4.16. shows that the three metal centers are separated roughly an equal distance from each other in 1-{*trans*-[Ru(C≡CPh)(dppe)$_2$C≡C}-C$_6$H$_3$-3,5-{C≡CC$_6$H$_4$-4-C≡C-*trans*-[Ru(C≡CPh)(dppe)$_2$]}$_2$, whereas in 1-{*trans*-[Ru(C≡CPh)(dppe)$_2$C≡CC$_6$H$_4$-4-C≡C}-C$_6$H$_3$-

3,5-{C≡C-*trans*-[Ru(C≡CPh)(dppe)$_2$]}$_2$ two of the three metal centers are considerably closer to one another, possibly preventing any changes in geometry required for a successful coupling. These calculations suggest that the steric bulk of the system needs to be reduced for a successful coupling between any of the above mentioned wedges and a core.

Replacement of the Ru(dppe)$_2$ moiety with Pt(PMe$_2$Ph)$_2$ in the core should lead to a large reduction in steric bulk at the reaction center. Figure 4.17. and Figure 4.18. present the results of a molecular modelling geometry optimization study of both the 1,3,5-C$_6$H$_3${C≡CC$_6$H$_4$-4-C≡C-*trans*-[PtCl(PMe$_2$Ph)$_2$]}$_3$ core **32** and the core **9**, respectively. It is immediately obvious that core **32** has considerably less steric bulk. For example, the orange chlorine atoms are clearly visible, whereas they are almost completely obscured in the core **9**.

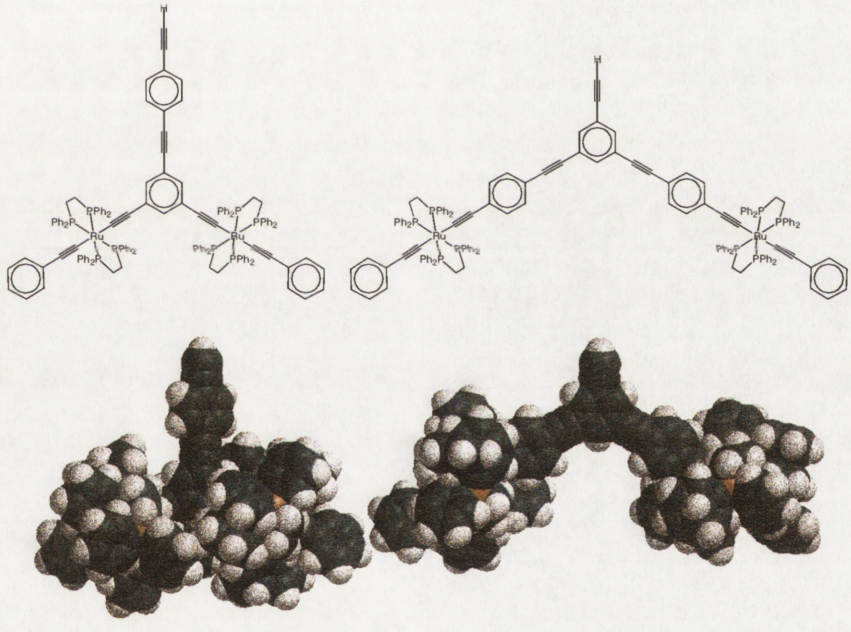

Figure 4.15. Molecular modelling-derived geometries of the dendritic wedges **22a** (left) and **22d** (right)

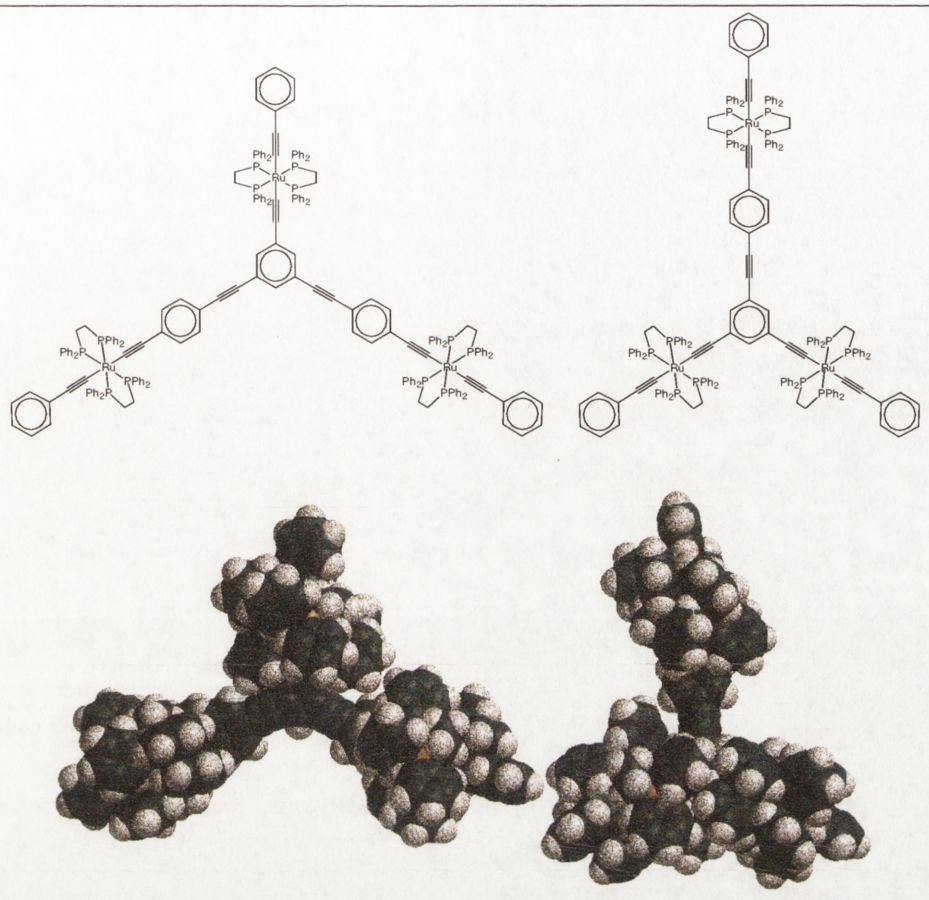

Figure 4.16. Molecular modelling-derived geometries of the hypothetical complexes 1-{*trans*-[Ru(C≡CPh)(dppe)$_2$C≡C}-C$_6$H$_3$-3,5-{C≡CC$_6$H$_4$-4-C≡C-*trans*-[Ru(C≡CPh)(dppe)$_2$]}$_2$ (left) and 1-{*trans*-[Ru(C≡CPh)(dppe)$_2$C≡CC$_6$H$_4$-4-C≡C}-C$_6$H$_3$-3,5-{C≡C-*trans*-[Ru(C≡CPh)(dppe)$_2$]}$_2$ (right)

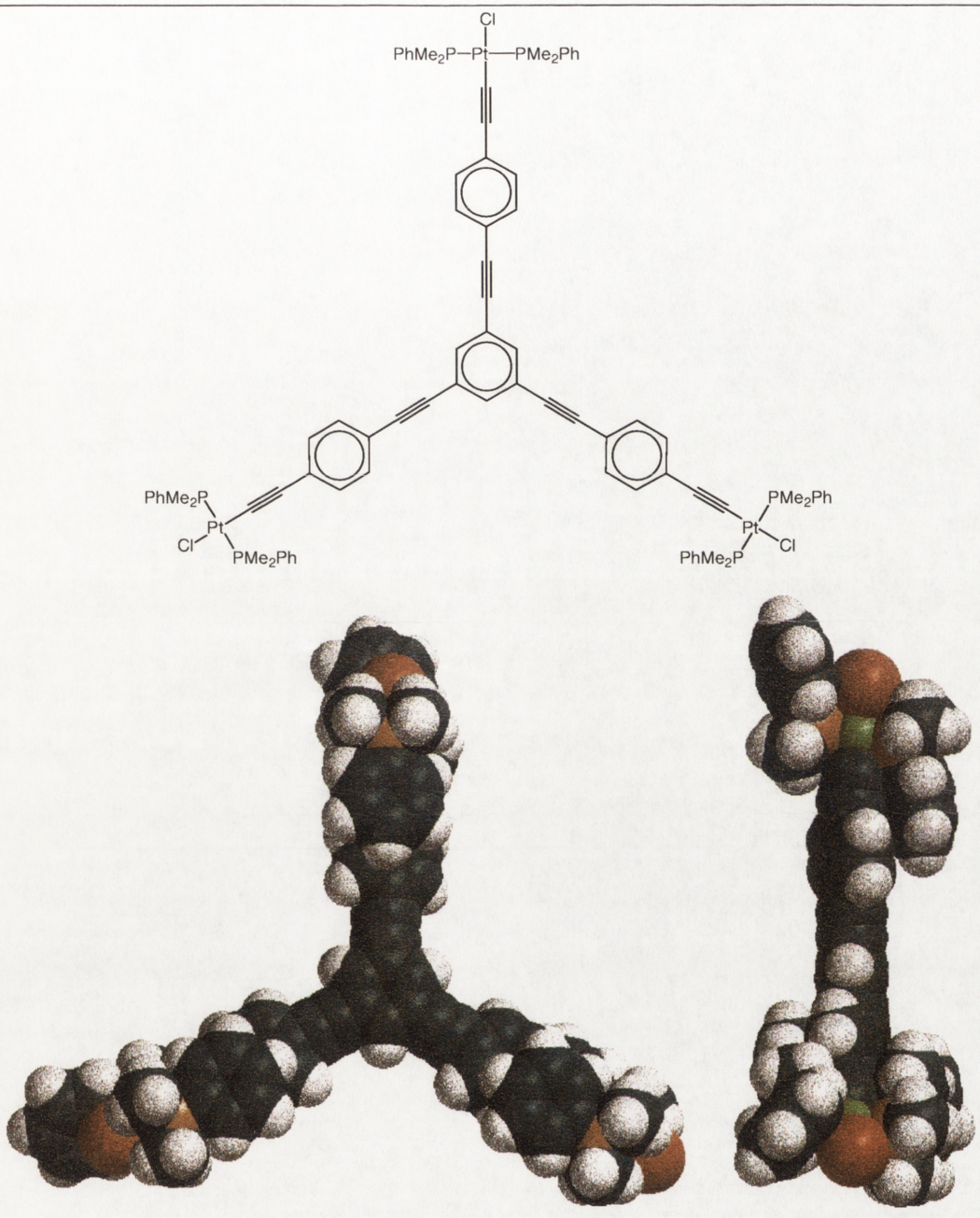

Figure 4.17. Front and profile of the geometry of 1,3,5-$C_6H_3\{C{\equiv}CC_6H_4$-4-$C{\equiv}C$-*trans*-$[PtCl(PMe_2Ph)_2]\}_3$ (**32**) derived from molecular modelling

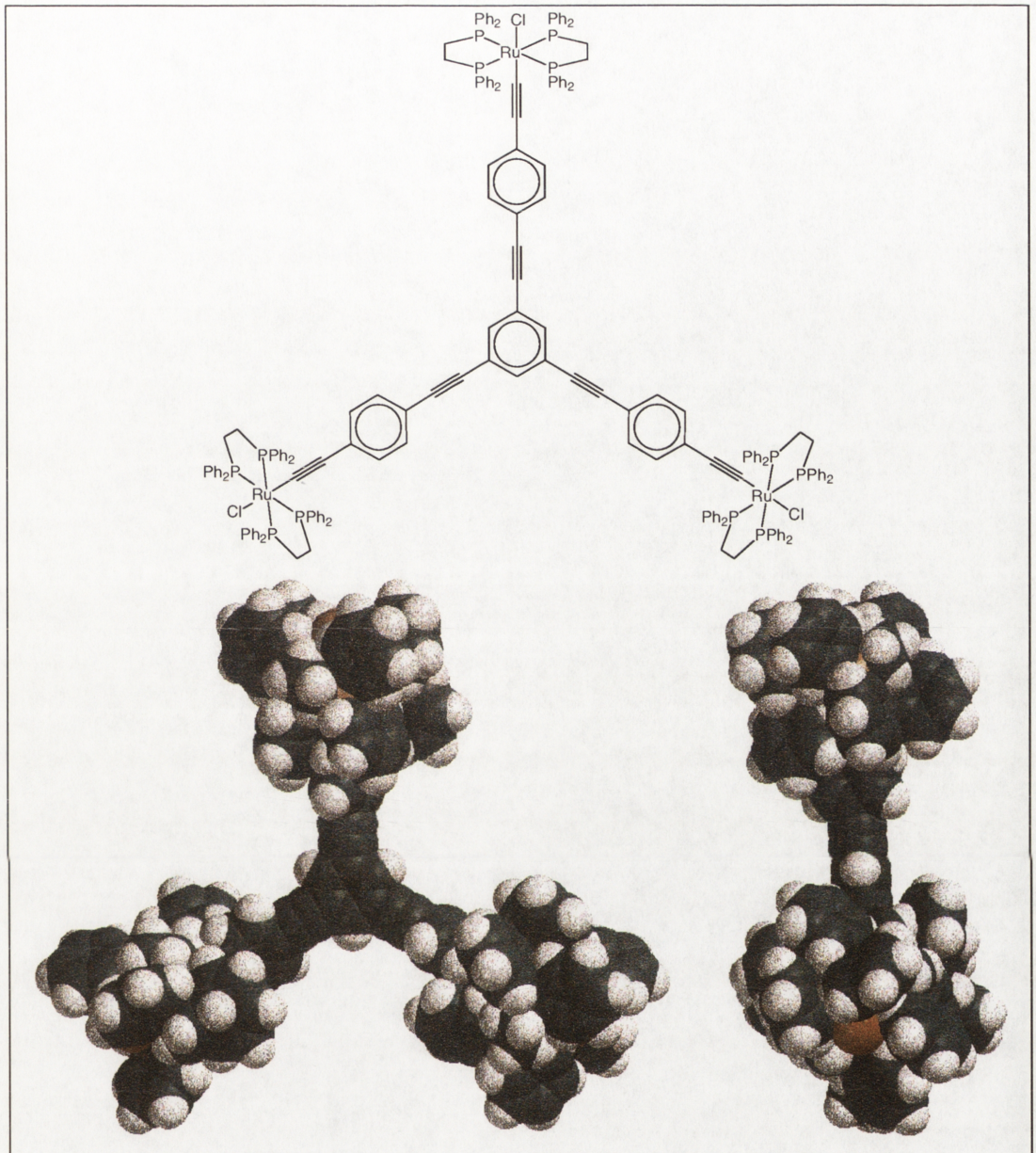

Figure 4.18. Front and profile of the geometry of 1,3,5-$C_6H_3\{C{\equiv}CC_6H_4$-4-$C{\equiv}C$-*trans*-$[RuCl(dppe)_2]\}_3$ **9** derived from molecular modelling

The bisphosphine-platinum-containing core and a linear analogue were synthesized by reaction of *cis*-$[PtCl_2(PMe_2Ph)_2]$ with the relevant alkynyl ligand and a CuCl catalyst (Scheme 4.23.). Because the reaction does not form a vinylidene complex *in situ*, there is no inherent means of avoiding generation of the bis-acetylide complex. To minimize formation

of the bis-acetylide complexes, an excess of *cis*-$[PtCl_2(PMe_2Ph)_2]$ was added, no trace of the bis-acetylide product being observed in the ^{31}P NMR spectrum. The products were characterized by ^{1}H and ^{31}P NMR, UV-vis, IR, FAB mass spectrometry and satisfactory microanalysis.

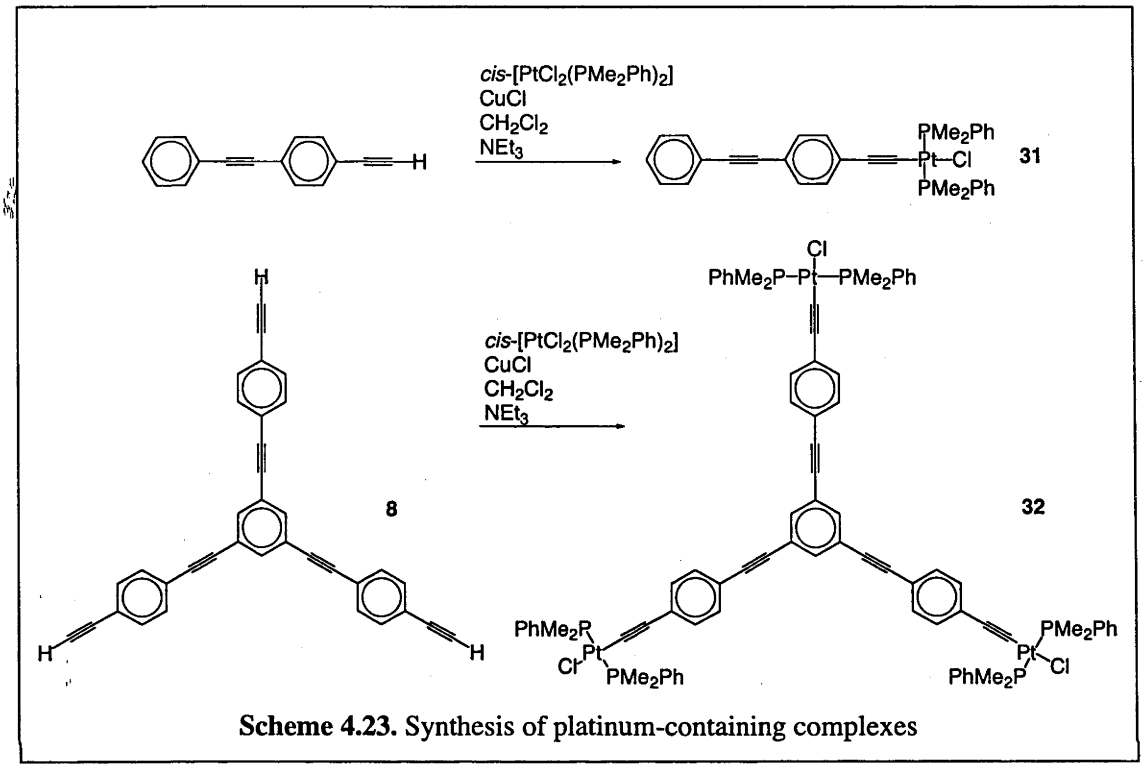

Scheme 4.23. Synthesis of platinum-containing complexes

A crystal of **31** was structurally characterized by X-ray diffraction. Selected bond distances and angles are listed in Table 4.2., and an ORTEP plot is displayed in Figure 4.19. The crystallographic asymmetric unit consists of one molecule of **31**. The complex shows square planar geometry around the metal center, with only small deviations from idealized geometries. An example of an octupolar platinum-acetylide complex incorporating a $C{\equiv}CC_6H_4$-4-$C{\equiv}CPh$ motif, 1,3,5-$[Cl(PEt_3)_2PtC{\equiv}CC_6H_4$-4-$C{\equiv}C]_3C_6H_3$, has been reported previously and structurally characterized.[88] Reported bond lengths, Pt–Cl: 2.358(6) Å, Pt–C: 1.95(2) Å, Pt–P: 2.276(9)-2.297(8) Å and C≡C: 1.14(3) Å, are similar to those observed with **31**.

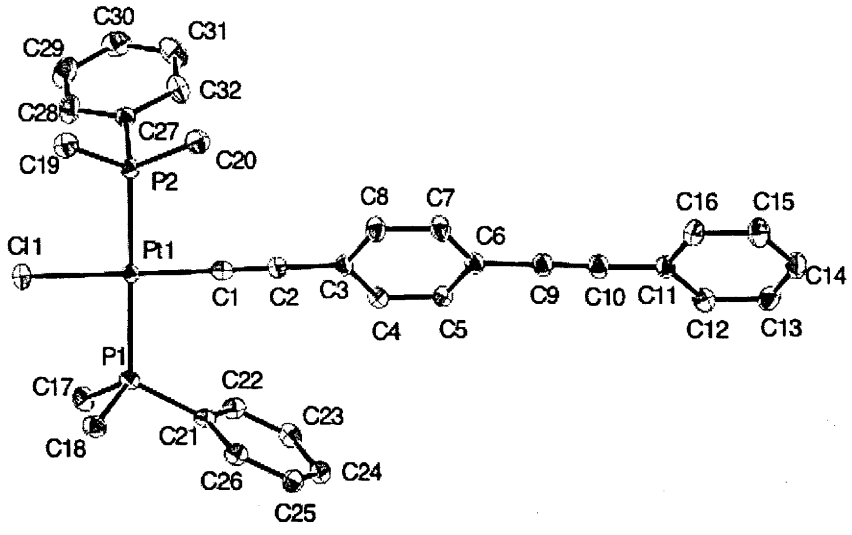

Figure 4.19. Thermal ellipsoid diagram of *trans*-[Pt(C≡CC$_6$H$_4$-4-C≡CPh)Cl(PMe$_2$Ph)$_2$] with labelling of selected atoms. Ellipsoids show 30% probability levels. H atoms have been deleted for clarity. (by A. C. Willis)

Table 4.2. Selected bond distances (Å) and angles (deg.) for **31**			
Pt1–C1	1.953(3)	Pt1–Cl1	2.3588(8)
Pt1–P1	2.3051(3)	Pt1–P2	2.3059(8)
C1–C2	1.200(4)	C9–C10	1.200(5)
C2–C3	1.392(4)	C10–C11	1.432(4)
P1–C17	1.813(3)	P1–C18	1.807(3)
P2–C19	1.810(3)	P2–C20	1.817(3)
P1–C21	1.819(3)	P2–C27	1.817(3)
Cl–Pt1–P1	87.70(3)	Cl1–Pt1–P2	91.52(3)
P1–Pt1–P2	177.16(3)	Cl1–Pt1–C1	177.25(9)
Pt1–C1–C2	178.7(3)	C1–C2–C3	177.4(3)
C6–C9–C10	178.7(4)	C9–C10–C11	177.7(4)

The platinum core, **32**, was reacted with the wedge, 1,3-{*trans*-[(dppe)$_2$(PhC≡C)RuC≡C]}$_2$-5-(HC≡C-4-C$_6$H$_4$C≡C)C$_6$H$_3$ (**22a**), in the presence of CuCl to give the desired mixed metal dendrimer complex, 1,3,5-C$_6$H$_3$(C≡CC$_6$H$_4$-4-C≡C-*trans*-[Pt(PMe$_2$Ph)$_2$]C≡CC$_6$H$_4$-4-C≡CC$_6$H$_3$-3,5-{C≡C-*trans*-[Ru(C≡CPh)(dppe)$_2$]}$_2$)$_3$ (**33**) (Scheme 4.24.). The geometry of the dendrimer was derived from molecular modelling, and is presented in Figure 4.20. The dendrimer was characterized by ^{1}H and ^{31}P NMR, UV-vis, IR, FAB mass spectrometry and satisfactory microanalysis.

The molecular modelling shows that all of the metal centers are well separated in space from each other. Many of the phenyl rings which make up the backbone of the molecule are twisted out of coplanarity.

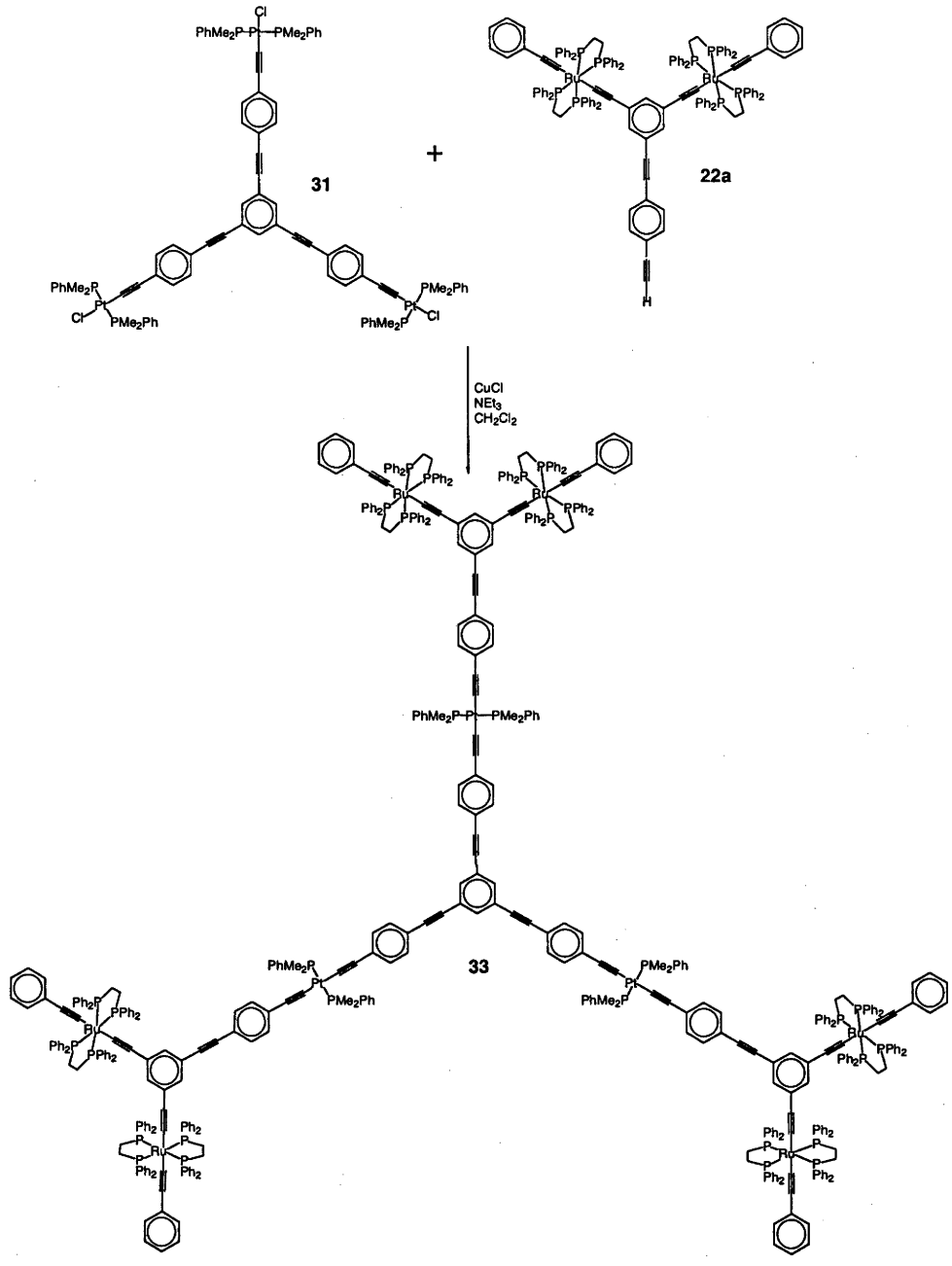

Scheme 4.24. Synthesis of 1,3,5-C_6H_3($C{\equiv}CC_6H_4$-4-$C{\equiv}C$-*trans*-[$PtCl(PMe_2Ph)_2$]$C{\equiv}CC_6H_4$-3,5-C_6H_3-{$C{\equiv}C$-*trans*-[$Ru(C{\equiv}CPh)(dppe)_2$]}$_2$)$_3$ (**33**)

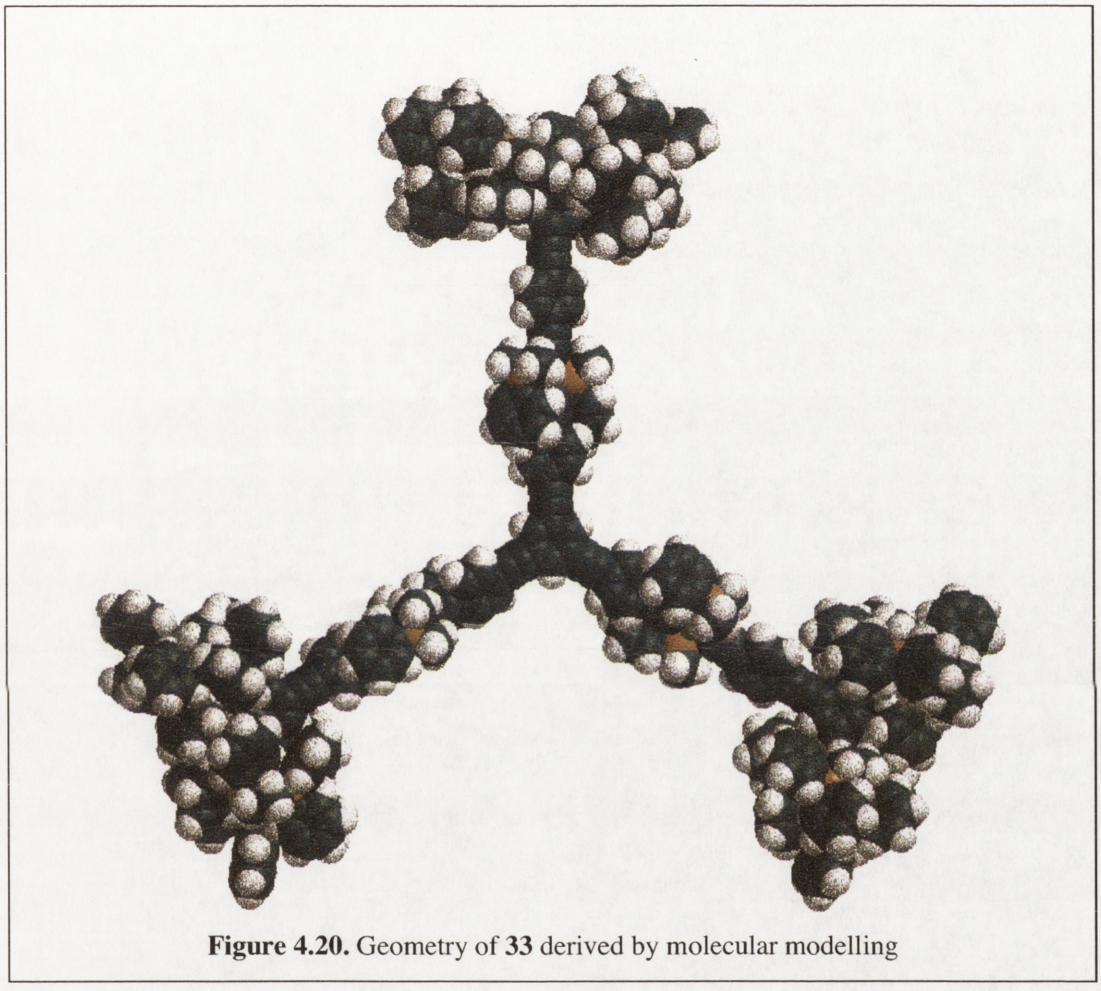

Figure 4.20. Geometry of **33** derived by molecular modelling

4.5. *Physical Properties*

^1H and ^{31}P NMR spectroscopy data are tabulated in Table 4.3., and UV-vis and IR data are listed in Table 4.4. The ^1H NMR spectra generally show two major features: a multiplet at approximately 2.6 ppm due to the protons in the dppe bridging unit, and a large number of resonances from approximately 6.8 to 7.5 ppm due to the phenyl groups. Complexes containing an C≡CSiMe$_3$ group, namely **18**, **21b** and **22c**, have a strong singlet at ~0.2 ppm. This resonance appears to be relatively insensitive to other parts of the molecule. The ethynyl proton in **20b** and **20c** occurs at approximately 3 ppm; in comparison, the ethynyl proton in **22b** and **22c** shows a shift in the ^1H NMR spectrum to approximately 3.1 ppm, due to the increased isolation of the ethynyl protons from the metal centers. Similar behaviour is observed in the analogues incorporating a phenyl ligand, **20a** and **22a**.[69]

The ^{31}P NMR is perhaps the most useful spectroscopic technique in characterizing the environment around the ruthenium core. Mono-acetylide complexes with a Ru–Cl bond, such as **27**, possess P atoms with a chemical shift in the range 49 – 50 ppm. In ruthenium bis-acetylide complexes, the ^{31}P NMR chemical shift increases to ~54 ppm. The nitro-containing complexes, **20b**, **21b**, **22b** and **22c**, all possess a ^{31}P chemical shifts of ca 0.1 ppm less than **20a**, **21a**, **22a** and **23a**. These figures are consistent with other examples found in the literature.[73,82,83] The complex *trans*-[Ru(C≡CPh)(N≡CMe)(dppe)$_2$]PF$_6$ (**29**) shows a ^{31}P NMR spectral shift of 51 ppm.

Examination of the ^{31}P NMR spectroscopic data for the platinum-containing complexes **31**, **32** and **33** reveals a chemical shift of –6.8 ppm in the case of complexes containing a chloro-ligand (**31** and **32**), which moves to –11.6 ppm upon replacement of the chloro ligand by an alkynyl group on conversion of **32** to **33**. These figures are consistent with literature values for *trans*-[Pt(C≡CPh)Cl(PMe$_2$Ph)$_2$] and *trans*-[Pt(C≡CPh)$_2$(PMe$_2$Ph)$_2$], which have ^{31}P NMR spectral shifts of –7.5 and –12.4 ppm, respectively.[89] **33** also contains a resonance at 54.4 ppm, consistent with a bis-acetylide ruthenium unit. The integral of these peaks is 1:2, as expected.

The C≡CRu stretching frequencies appear in the range 2055 – 2060 cm^{-1} for most acetylide complexes tabulated in Table 4.4., exceptions to this rule including the dendrimers and wedges incorporating a nitro group (**20b**, **21b**, **22b** and **23b**) and *trans*-[Ru(C≡CPh)(N≡CMe)(dppe)$_2$]PF_6 (**29**). Complexes incorporating nitro- substituents display C≡CRu stretching frequencies at ca 2045 cm^{-1}, whereas the mixed acetylide/nitrile complex, **29**, possesses two bands at 1967 and 2086 cm^{-1}, corresponding to the C≡CRu and N≡C vibrations. The IR spectra of the platinum-containing complexes **31** and **32** each show a band at approximately 2119 cm^{-1}, which is consistent with similar platinum complexes: *trans*-[Pt(C≡CPh)$_2$(PMe_2Ph)$_2$] 2106 cm^{-1},[90] *trans*-[Pt(C≡CCH_2OH)$_2$(PMe_2Ph)$_2$] 2120 cm^{-1},[91] *trans*-[Pt(C≡CCH_2CH_2OH)$_2$(PMe_2Ph)$_2$] 2110 cm^{-1} [91] and *trans*-[Pt(C≡CCH_2OPh)$_2$(PMe_2Ph)$_2$] 2115 cm^{-1}.[91] The mixed platinum/ruthenium dendrimer, **33**, contains two bands at 2060 and 2101 cm^{-1} assigned to the ruthenium- and platinum- bound acetylide groups, respectively.

Table 4.3. Selected ^{1}H and ^{31}P NMR data

Complex	Chemical Shift (ppm)				
	CH_2	Me	C≡CH	Phenyl	^{31}P
trans-[Ru(C≡CC_6H_4-4-C≡CPh)(C≡CC_6H_4-4-NEt_2)(dppe)$_2$] (**5**)	2.60			6.54-7.68	54.4
1,3,5-C_6H_3{C≡CC_6H_4-4-C≡C-*trans*-[Ru(C≡CC_6H_4-4-NEt_2)(dppe)$_2$]}$_3$ (**10**)	2.58			6.93-7.85	54.1
1,3-{*trans*-[(dppe)$_2$(Et_2N-4-C_6H_4C≡C)RuC≡C]}$_2$-5-Me_3SiC≡CC_6H_3 (**18**)	2.60	0.23		6.46-7.56	54.2
1,3-{*trans*-[(dppe)$_2$(O_2NC_6H_4-4-C≡C)RuC≡C]}$_2$-5-HC≡CC_6H_3 (**20b**)	2.60		3.06	6.47-7.96	54.0
1,3-{*trans*-[(dppe)$_2$(H_2NC_6H_4-4-C≡C)RuC≡C]}$_2$-5-HC≡CC_6H_3 (**20c**)	2.67		3.03	6.51-7.55	54.6
1,3-{*trans*-[(dppe)$_2$(O_2NC_6H_4-4-C≡C)RuC≡C]}$_2$-5-(Me_3SiC≡CC_6H_4-4-C≡C)C_6H_3 (**21b**)	2.60	0.26		6.48-7.96	53.9
1,3-{*trans*-[(dppe)$_2$(H_2NC_6H_4-4-C≡C)RuC≡C]}$_2$-5-(Me_3SiC≡CC_6H_4-4-C≡C)C_6H_3 (**21c**)	2.69	0.22		6.93-7.70	54.5
1,3-{*trans*-[(dppe)$_2$(O_2NC_6H_4-4-C≡C)RuC≡C]}$_2$-5-(HC≡CC_6H_4-4-C≡C)C_6H_3 (**22b**)	2.62		3.18	6.47-7.96	53.9
1,3-{*trans*-[(dppe)$_2$(H_2NC_6H_4-4-C≡C)RuC≡C]}$_2$-5-(HC≡CC_6H_4-4-C≡C)C_6H_3 (**22c**)	2.67		3.11	6.79-7.85	54.5
1,3,5-{3,5-(*trans*-[(dppe)$_2$(O_2NC_6H_4-4-C≡C)RuC≡C])$_2$$C_6H_3$-1-C≡C$C_6H_4$-4-C≡C}$_3$$C_6H_3$ (**23b**)	2.63			6.85-7.96	53.8
1,3,5-{3,5-(*trans*-[(dppe)$_2$(H_2NC_6H_4-4-C≡C)RuC≡C])$_2$$C_6H_3$-1-C≡C$C_6H_4$-4-C≡C}$_3$$C_6H_3$ (**23c**)	2.63			6.75-7.90	54.5
trans-[Ru(C≡CC_6H_4-4-I)$_2$(dppe)$_2$] (**24**)	2.66			6.41-8.14	53.9
1,3,5-C_6H_3{C≡CC_6H_4-4-C≡C-*trans*-[Ru(C≡CC_6H_4-4-I)(dppe)$_2$]}$_3$ (**25**)	2.61			6.42-7.66	54.2
{3,5-(*trans*-[(dppe)$_2$ClRuC≡C)$_2$$C_6H_3$-1-C≡C}$_2$ (**28**)	2.67			6.45-7.75	50.5

Table 4.3. continued Selected ^{1}H and ^{31}P NMR data

Complex	Chemical Shift (ppm)				
	CH_2	Me	C≡CH	Phenyl	^{31}P
trans-[Ru(C≡CPh)(N≡CMe)(dppe)$_2$]PF_6 (**29**)	2.64	1.35		6.58-808	51.2
trans-[Pt(C≡CC_6H_4-4-C≡CPh)Cl(PMe_2Ph)$_2$] (**31**)		1.96		6.98-7.81	-6.8
1,3,5-C_6H_3{C≡CC_6H_4-4-C≡C-*trans*-[PtCl(PMe_2Ph)$_2$]}$_3$ (**32**)		1.96		6.98-7.84	-6.8
1,3,5-C_6H_3(C≡CC_6H_4-4-C≡C-*trans*-[PtCl(PMe_2Ph)$_2$]C≡CC_6H_4-4-C_6H_3-3,5-{C≡C-*trans*-[Ru(C≡CPh)(dppe)$_2$]}$_2$)$_3$ (**33**)	2.68	2.10		6.67-7.90	-11.6, 54.4

Table 4.4. UV/vis and IR data

Compound	λ (nm)	ν(C≡C)
trans-[Ru(C≡CC_6H_4-4-NEt_2)(C≡CC_6H_4-4-C≡CPh)(dppe)$_2$] (**5**)	386	2054
1,3,5-C_6H_3{C≡CC_6H_4-4-C≡C-*trans*-[Ru(C≡CC_6H_4-4-NEt_2)(dppe)$_2$]}$_3$ (**10**)	410	2055
1,3-{*trans*-[(dppe)$_2$(Et_2N-4-C_6H_4C≡C)RuC≡C]}$_2$-5-Me_3SiC≡CC_6H_3 (**18**)		2053
1,3-{*trans*-[(dppe)$_2$(O_2NC_6H_4-4-C≡C)RuC≡C]}$_2$-5-HC≡CC_6H_3 (**20b**)	475	2045
1,3-{*trans*-[(dppe)$_2$(O_2NC_6H_4-4-C≡C)RuC≡C]}$_2$-5-(Me_3SiC≡CC_6H_4-4-C≡C)C_6H_3 (**21b**)	475	2153, 2045
1,3-{*trans*-[(dppe)$_2$(O_2NC_6H_4-4-C≡C)RuC≡C]}$_2$-5-(HC≡CC_6H_4-4-C≡C)C_6H_3 (**22b**)	474	2045
1,3,5-{3,5-(*trans*-[(dppe)$_2$(O_2NC_6H_4-4-C≡C)RuC≡C])$_2$$C_6H_3$-1-C≡C$C_6H_4$-4-C≡C}$_3$$C_6H_3$ (**23b**)	475	2045
1,3-{*trans*-[(dppe)$_2$(H_2NC_6H_4-4-C≡C)RuC≡C]}$_2$-5-HC≡CC_6H_3 (**20c**)	333	2055
1,3-{*trans*-[(dppe)$_2$(H_2NC_6H_4-4-C≡C)RuC≡C]}$_2$-5-(Me_3SiC≡CC_6H_4-4-C≡C)C_6H_3 (**21c**)	334	2154, 2053
1,3-{*trans*-[(dppe)$_2$(H_2NC_6H_4-4-C≡C)RuC≡C]}$_2$-5-(HC≡CC_6H_4-4-C≡C)C_6H_3 (**22c**)	328	2055
1,3,5-{3,5-(*trans*-[(dppe)$_2$(H_2NC_6H_4-4-C≡C)RuC≡C])$_2$$C_6H_3$-1-C≡C$C_6H_4$-4-C≡C}$_3$$C_6H_3$ (**23c**)	340	2052
{3,5-(*trans*-[(dppe)$_2$ClRuC≡C)$_2$$C_6H_3$-1-C≡C]}$_2$ (**28**)	335	2059
trans-[Ru(C≡CPh)(N≡CMe)(dppe)$_2$]PF_6 (**29**)	298	1967, 2086
trans-[Ru(C≡CC_6H_4-4-I)$_2$(dppe)$_2$] (**24**)	345	2060
1,3,5-C_6H_3{C≡CC_6H_4-4-C≡C-*trans*-[Ru(C≡CC_6H_4-4-I)(dppe)$_2$]}$_3$ (**25**)	345	2054
trans-[Pt(C≡CC_6H_4-4-C≡CPh)Cl(PMe_2Ph)$_2$] (**31**)	342	2119
1,3,5-C_6H_3{C≡CC_6H_4-4-C≡C-*trans*-[PtCl(PMe_2Ph)$_2$]}$_3$ (**32**)	345	2117

Table 4.4. continued UV/vis and IR data		
Compound	λ (nm)	ν(C≡C)
1,3,5-C_6H_3(C≡CC_6H_4-4-C≡C-*trans*-[Pt($PMe_2Ph)_2$]C≡CC_6H_4-3,5-C_6H_3-{C≡C-*trans*-[Ru(C≡CPh)$(dppe)_2$]}$_2$)$_3$ **(33)**	357, 421	2060, 2101

4.6. *Nonlinear Optical Properties*

4.6.1. *Z-Scan Studies*

Measurements of third-order molecular nonlinearities were performed using the Z-scan technique at 800 nm; results are presented in Table 4.5. When the nonlinearities of the diethylaminophenyl- complexes (**5**, **10** and **18**) are compared with those of their phenyl- and nitrophenyl- analogues, the complexes with electron-withdrawing ligands give indistinguishable results to those with electron-donating ligands, partly a result of the considerable uncertainties inherent in this technique. Complexes with both styles of ligands (donating or withdrawing, ie. polarizing) gave considerably higher nonlinearities than their corresponding phenyl-only equivalents. The dendrimer **23a** and its wedge constituents **20a**, **21a** and **22a** in most cases have nonlinearities with very large error margins, rendering comparision difficult. The species incorporating a nitro- group gave considerably higher nonlinearities. The nitro-containing dendrimer **23b**, in particular, exhibited surprising behaviour. It was expected to act as a two-photon absorber (ie. possess a positive γ_{imag}); rather, it acted as a saturable absorber, in contrast to the nitro- containing wedges (**20b**, **21b** and **22b**). Because of this, a study of the cubic nonlinearities of **23b** over a range of frequencies was undertaken. This study is detailed below. The dendrimer and associated wedges incorporating an $-NH_2$ group (**20c-23c**) exhibited higher nonlinearities than their phenyl containing analogues (**20a-23a**). Because of the high uncertainities associated with these complexes, the electron-donating wedges and dendrimer (**20c-23c**) are indistinguishable from their electron withdrawing analogues (**20b-23b**). The mixed metal dendrimer, **33**, posseses a γ_{800} of 7200 ± 2900 x 10^{-36} esu. This is substantially higher than the phenylacetylide containing dendrimer **23a** (1600 ± 2400 x 10^{-36} esu),[75] yet lower than 1,3,5-C_6H_3(C≡CC_6H_4-4-C≡C-*trans*-[Ru(dppe)$_2$]C≡C-3,5-C_6H_3-{C≡CC_6H_4-4-C≡C-*trans*-[Ru(C≡CPh)(dppe)$_2$]}$_2$)$_3$ (20 700 ± 700 x 10^{-36} esu).[27] Increasing the metal loading (proceeding from the Ru_6 to Ru_6M_3 dendrimers) and increasing electron richness (proceeding from Ru_6Pt_3, with a mixture of 18 and 16 valence electron metals to Ru_9, with 18 electron metal centres only) both result in an increase in γ_{800}.

Table 4.5. Cubic Nonlinearities at 800 nm

Complex	Re γ (10^{-36} esu)	Im γ (10^{-36} esu)	γ (10^{-36} esu)	Reference
trans-[Ru(C≡CC_6H_4-4-C≡CPh)(C≡CPh)(dppe)$_2$]	-670 ± 300	1300 ± 300	1500 ± 500	26
trans-[Ru(C≡CC_6H_4-4-C≡CPh)(C≡CC_6H_4-4-NEt_2)(dppe)$_2$] (**5**)	-1300 ± 1000	-3200 ± 500	3500 ± 1100	This work
1,3,5-C_6H_3{C≡CC_6H_4-4-C≡C-*trans*-[Ru(C≡CPh)(dppe)$_2$]}$_3$	-600 ± 200	2900 ± 500	3000 ± 600	26
1,3,5-C_6H_3{C≡CC_6H_4-4-C≡C-*trans*-[Ru(C≡CC_6H_4-4-NO_2)(dppe)$_2$]}$_3$	-5000 ± 1000	5600 ± 1000	7500 ± 1400	70
1,3,5-C_6H_3{C≡CC_6H_4-4-C≡C-*trans*-[Ru(C≡CC_6H_4-4-NEt_2)(dppe)$_2$]}$_3$ (**10**)	-8300 ± 3000	5300 ± 1000	9800 ± 3200	This work
1,3-{*trans*-[(dppe)$_2$(PhC≡C)RuC≡C]}$_2$-5-Me_3SiC≡CC_6H_3	-700 ± 100	2270 ± 300	2400 ± 300	27
1,3-{*trans*-[(dppe)$_2$(O_2N-4-C_6H_4C≡C)RuC≡C]}$_2$-5-Me_3SiC≡CC_6H_3	-5200 ± 1000	5200 ± 1000	7400 ± 1400	70
1,3-{*trans*-[(dppe)$_2$(Et_2N-4-C_6H_4C≡C)RuC≡C]}$_2$-5-Me_3SiC≡CC_6H_3 (**18**)	-3300 ± 1300	4600 ± 900	5700 ± 1600	This work
1,3-{*trans*-[(dppe)$_2$(PhC≡C)RuC≡C]}$_2$-5-HC≡CC_6H_3 (**20a**)	500 ± 400	200 ± 100	540 ± 100	75
1,3-{*trans*-[(dppe)$_2$(O_2NC_6H_4-4-C≡C)RuC≡C]}$_2$-5-HC≡CC_6H_3 (**20b**)	-1300 ± 1000	150 ± 40	1300 ± 1000	This work
1,3-{*trans*-[(dppe)$_2$(H_2NC_6H_4-4-C≡C)RuC≡C]}$_2$-5-HC≡CC_6H_3 (**20c**)	1000 ± 400	0 ± 100	1000 ± 400	This work
1,3-{*trans*-[(dppe)$_2$(PhC≡C)RuC≡C]}$_2$-5-(Me_3SiC≡CC_6H_4-4-C≡C)C_6H_3 (**21a**)	700 ± 1200	0 ± 0	700 ± 1200	75
1,3-{*trans*-[(dppe)$_2$(O_2NC_6H_4-4-C≡C)RuC≡C]}$_2$-5-(Me_3SiC≡CC_6H_4-4-C≡C)C_6H_3 (**21b**)	-1100 ± 220	310 ± 60	1100 230	This work
1,3-{*trans*-[(dppe)$_2$(H_2NC_6H_4-4-C≡C)RuC≡C]}$_2$-5-(Me_3SiC≡CC_6H_4-4-C≡C)C_6H_3 (**21c**)	-2200 ± 800	400 ± 200	2200 ± 800	This work

Table 4.5. continued Cubic Nonlinearities at 800 nm

Complex	Re γ (10^{-36} esu)	Im γ (10^{-36} esu)	γ (10^{-36} esu)	Reference
1,3-{*trans*-[(dppe)$_2$(PhC≡C)RuC≡C]}$_2$-5-(HC≡CC_6H_4-4-C≡C)C_6H_3 (**22a**)	1700 ± 500	0 ± 0	1700 ± 500	75
1,3-{*trans*-[(dppe)$_2$($O_2NC_6H_4$-4-C≡C])RuC≡C}$_2$-5-(HC≡CC_6H_4-4-C≡C)C_6H_3 (**22b**)	-5000 ± 1300	1320 ± 270	5200 ± 1300	This work
1,3-{*trans*-[(dppe)$_2$($H_2NC_6H_4$-4-C≡C)RuC≡C]}$_2$-5-(HC≡CC_6H_4-4-C≡C)C_6H_3 (**22c**)	-1400 ± 500	1300 ± 300	1900 ± 300	This work
1,3,5-{3,5-(*trans*-[(dppe)$_2$(PhC≡C)RuC≡C])$_2C_6H_3$C≡CC_6H_4-4-C≡C}$_3C_6H_3$ (**23a**)	-1600 ± 2400	0 ± 0	1600 ± 2400	75
1,3,5-{3,5-(*trans*-[(dppe)$_2$($O_2NC_6H_4$-4-C≡C)RuC≡C])$_2C_6H_3$C≡CC_6H_4-4-C≡C}$_3C_6H_3$ (**23b**)	-23000 ± 20000	-6200 ± 2800	24000 ± 20000	This work
1,3,5-{3,5-(*trans*-[(dppe)$_2$($H_2NC_6H_4$-4-C≡C)RuC≡C])$_2C_6H_3$C≡CC_6H_4-4-C≡C}$_3C_6H_3$ (**23c**)	-2900 ± 2300	4700 ± 1200	5500 ± 2600	This work
trans-[Ru(C≡CPh)(N≡CMe)(dppe)$_2$]PF_6 (**29**)	200 ± 40	10 ± 5	200 ± 40	This work
trans-[Ru(C≡CC_6H_4-4-I)$_2$(dppe)$_2$] (**24**)	-930 ± 340	120 ± 70	940 ± 350	This work
1,3,5-C_6H_3{C≡CC_6H_4-4-C≡C-*trans*-[Ru(C≡CC_6H_4-4-I)(dppe)$_2$]}$_3$ (**25**)	-850 ± 3000	800 ± 180	1200 ± 3000	This work
{3,5-(*trans*-[(dppe)$_2$ClRuC≡C)$_2C_6H_3$-1-C≡C}$_2$ (**28**)	950 ± 280	-60 ± 30	960 ± 280	This work
1,3,5-C_6H_3(C≡CC_6H_4-4-C≡C-*trans*-[PtCl(PMe_2Ph)$_2$]C≡CC_6H_4-3,5-C_6H_3-{C≡C-*trans*-[Ru(C≡CPh)(dppe)$_2$]}$_2$)$_3$ (**33**)	-6700 ± 2600	-2500 ± 1300	7200 ± 2900	This work

It was expected that, because of the red shift of the absorption spectrum of the nitrophenyl-containing dendrimer **23b** cf. the phenyl-containing dendrimer **23a**, the nonlinear properties of the molecule, including two-photon absorption (cf. Kamada *et al*[92]), should be enhanced. However, initial measurements at 800 nm showed no two-photon absorption effect, but, instead, a negative value of the nonlinear absorption coefficient β was determined (β is usually defined by the relation $\alpha_o = \alpha + \beta I$, thus a positive value of β indicates absorption coefficient, α, that increases with intensity I, as in the case of two-photon absorption and a negative value of β indicates saturable absorption). This prompted a more detailed investigation in which the nonlinear absorption characteristics over a range of wavelengths were evaluated, specifically the imaginary part of the hyperpolarizability γ_{imag}. Similar dispersion measurements have previously been carried out on a number of organic molecules,[25,93-99] polymers,[100,101] thin films,[102] nanoparticles,[103] fullerenes[104] and porphyrins,[105] but prior to the work presented here, no studies on molecular organometallic complexes had been reported. At the same time, the Z-scan results allowed the evaluation of the real part of the hyperpolarizability γ_{real}. It has to be cautioned that the accuracy of the results is lower for the real parts of γ compared to that for imaginary parts, because the nonlinear absorption of the solvent is negligible in the wavelength and intensity ranges used, whereas the refractive nonlinearity of the solute is always measured as an increment to the refractive nonlinearity of the solvent and glass walls of the cuvette.

Figure 4.21. shows the experimental results obtained in this study as well as a preliminary interpretation of the dispersion of the real and imaginary part of γ obtained using simplified dispersion formulae. It is confirmed that the nonlinear absorption shows a range (approximately 700 – 850 nm) where the sign of β is negative, corresponding to absorption saturation. Outside of this range, the sign of β is positive indicating two-photon absorption. At the same time, the real part of γ is negative in most of the range of the measurements, positive values being obtained around 1200 nm (two data points for γ_{real} around 1100 nm were omitted from the plot: there is a possibility that those data were unreliable).

Interpretation of the dispersion is challenging and cannot be accomplished in a comprehensive way until data on the structure of energetic levels of the investigated molecule are known in detail. To aid the interpretation of these results, a model is presented.[117] At this stage the interpretation is based on the results of the UV-Vis

spectroscopy, and it is assumed that the two transitions seen in the absorption spectrum, at 330 nm and 482 nm, are relevant for the nonlinear properties. Since absorption saturation effects are observed in a certain range of frequencies, the interpretation invokes an assumption that the Z-scan measurements provide results of competing processes: that of two-photon absorption and that of absorption bleaching.

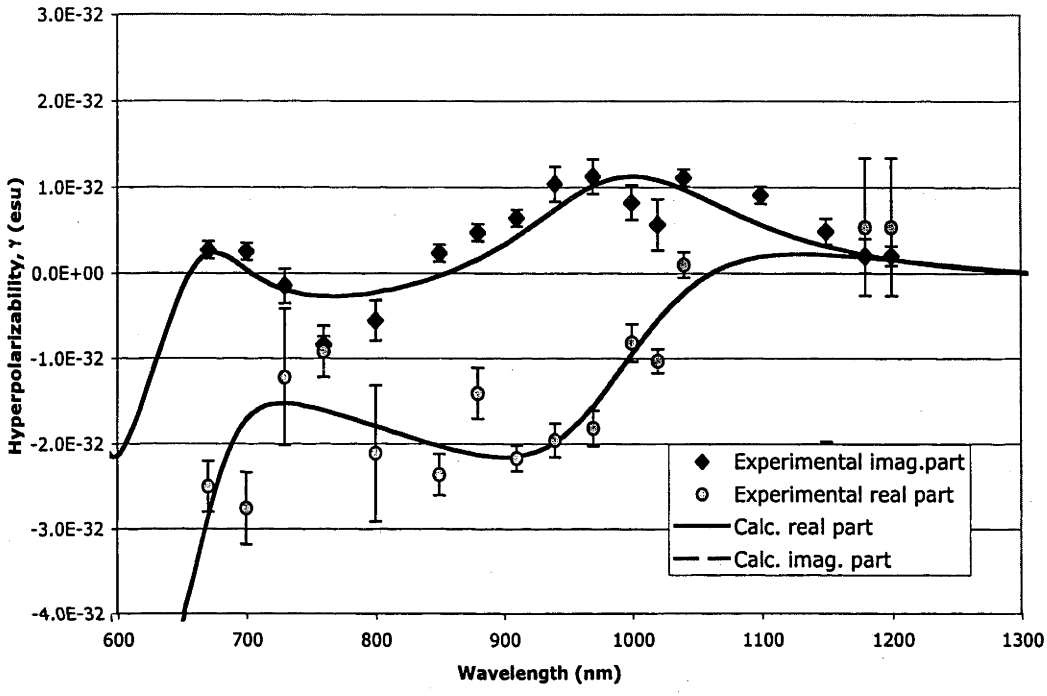

Figure 4.21. Experimental and calculated values of the real and imaginary parts of the second hyperpolarizability γ for the **23b**

The general sum-over-states expression for dispersion of the third-order polarizability is presented[106] as:

$$\gamma_{ijkl}(-\omega_\sigma;\omega_1,\omega_2,\omega_3) = \frac{1}{\hbar^3} P(i,j,k,l;-\omega_\sigma;\omega_1,\omega_2,\omega_3) \times$$

$$\left\{ \sum_{m\neq 0}\sum_{n\neq 0}\sum_{q\neq 0} \frac{\langle 0|\mu_i|m\rangle\langle m|\bar{\mu}_j|n\rangle\langle n|\bar{\mu}_k|q\rangle\langle q|\mu_l|0\rangle}{(\omega_{m0}-\omega_\sigma)(\omega_{n0}-\omega_2-\omega_3)(\omega_{q0}-\omega_3)} - \sum_{m\neq 0}\sum_{n\neq 0} \frac{\langle 0|\mu_i|m\rangle\langle m|\mu_j|0\rangle\langle 0|\mu_k|n\rangle\langle n|\mu_l|0\rangle}{(\omega_{m0}-\omega_\sigma)(\omega_{n0}-\omega_3)(\omega_{n0}+\omega_2)} \right\}$$

where 0 denotes the ground state, m, n and q denote excited states. This equation does not contain the damping factors, but they can be added where needed in the denominators to produce an expression suitable for calculations of the complex γ. The P operator in front of the curly brackets performs permutation on frequencies and indices, leading to 24 terms in each sum. This is in addition to the sums running over all excited states, so, with a huge number of terms, the dispersion of γ may in general be quite complicated. However, one can try to identify the leading terms of the sums presented above. Since the current interest is in the hyperpolarizability γ (-ω;ω,-ω,ω) at relatively low frequencies ω (below the first one-photon absorption peak), the most important terms in the expansion are likely those being close to resonance. In particular, one can expect that the leading terms will be those in which two-photon resonances are present, i.e. for two excited states at ω_a and ω_b these will be the terms containing frequency differences ω_a-2ω and ω_b-2ω. On the other hand, the absorption bleaching process can be modelled assuming that it is due to terms containing single-photon resonances.

Lines in Figure 4.21. were calculated taking the following simplified expression for γ:

$$\gamma \propto \left[\frac{A}{(\nu_a - 2\nu - i\Gamma_1)} + \frac{B}{(\nu_b - 2\nu - i\Gamma_2)} - \frac{C}{(\nu_a - \nu - i\Gamma_1)}\right] \times \frac{1}{(\nu_a - \nu)^2 + \Gamma_1^2}$$

where A , B and C were adjustable constants. This expression was roughly optimized to provide a fit to the experimental data resulting in the following parameters:

- The values of the damping constants Γ_1 and Γ_2 were 504 and 2252 cm^{-1}.
- The resonance frequencies taken for the calculations were ν_a = 20050 and cm^{-1} ν_b = 30030 cm^{-1}, corresponding to the wavelengths of 498 nm (a slight shift from the absorption spectrum peak wavelength of 482 nm provided a better match to the experimental data) and 333 nm.
- The values of the constants A, B and C were 8.6 x 10^{-24}, 7.6 x 10^{-24} and 2.4 x 10^{-23} in the case of the line fitting the real part of γ, and the constants were scaled 30% lower to provide the simultaneous fit for the imaginary part of γ.

Despite the obvious shortcomings of the expression used for the fitting, agreement of the observed dispersion of the nonlinear absorption (as represented by the imaginary part of γ) with that predicted on the basis of the above equation is quite reasonable. The coincidence of the peak of two-photon absorption with twice the wavelength of the lowest one-photon transition is intuitively expected, the second peak due to resonance with the excited state at 337 nm (thus the two-photon maximum being expected at 674 nm) is apparently distorted by the presence of a one-photon resonance leading to negative nonlinear absorption contribution.

4.6.2. *Optical-Limiting Studies*

Platinum-acetylide complexes have been known to possess a number of interesting optical properties.[88,107-109] Of interest is the complex *trans*-[Pt(C≡CC_6H_4-4-C≡CPh)$_2$(PBu_3)$_2$], which has been shown to act as a broadband optical limiter.[109] Because of the close structural similarities between the linear platinum complex *trans*-[Pt(C≡CC_6H_4-4-C≡CPh)Cl(PMe_2Ph)$_2$] **31**, and its octupolar analogue **32**, to *trans*-[Pt(C≡CC_6H_4-4-C≡CPh)$_2$(PBu_3)$_2$], it was decided to test their capacity to act as optical limiters at 532 nm.

Only poor optical limiting behaviour was exhibited by **31**. The effective absorption cross section at 523 nm was determined to be no larger than 4 x 10^{-20} cm^2. By comparison, the effective absorption cross section of *trans*-[Pt(C≡CC_6H_4-4-C≡CPh)$_2$(PBu_3)$_2$], was determined to be 7 x 10^{-17} cm^2.[109]

The octupolar platinum-acetylide complex **32** showed a considerably stronger effective absorption cross section than its linear analogue (7 x 10^{-19} cm^2). However, it is still significantly smaller than the effective absorption cross section of *trans*-[Pt(C≡CC_6H_4-4-C≡CPh)$_2$(PBu_3)$_2$]. Figure 4.22. displays a transmission vs. fluence plot for **32**, illustrating the drop-off in transmission as the fluence increases. A significant problem, however, exists in photodecomposition of the sample. The effective absorption cross section value quoted above applies to a fresh sample. Subsequent measurements on the same spot of the solution cell show considerable stronger changes of transmission, consistent with the formation of

absorbing species. Similar photodecomposition is observed for *trans*-[Pt(C≡CC_6H_4-4-C≡CPh)$_2$(PBu_3)$_2$].[109]

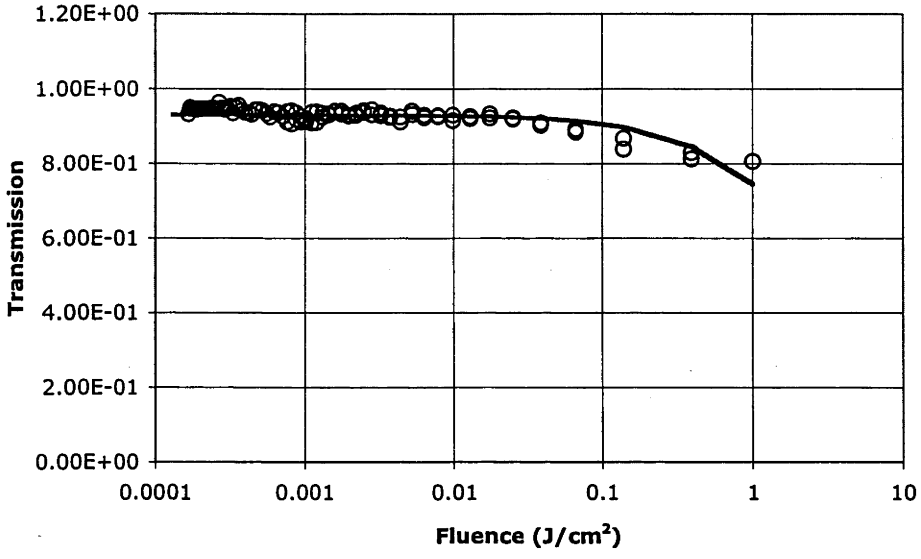

Figure 4.22. Transmission-fluence plot for **32**

4.7. *Conclusion*

Dendrimers have played a small but significant role as optical materials. Ruthenium-acetylide dendrimers have been examined as potential nonlinear optical materials. Cubic nonlinearities have ranged from modest to some of the highest observed values. This Chapter expands on the two existing design motifs and introduces a third based on a mixed platinum/ruthenium acetylide dendrimer.

A zero-generation dendrimer, linear analogue and a second-generation wedge precursor incorporating an electron-donating diethylamino- group on the periphery have been synthesized. Because of the instability of these complexes, this work wasn't taken to completion, but the large cubic nonlinearities indicated that this field is worth further investigation.

An existing dendrimer proved to be an excellent template for a more comprehensive investigation into electron-donating and electron-withdrawing ligands. In both cases, the cubic nonlinearities were increased considerably relative to the phenyl analogue. An in-depth investigation of the frequency dependence of the cubic nonlinearities was carried out on one of the dendrimers (**23b**). This study showed that the frequency dependence of the dendrimer can be explained by examining two competing phenomena: two-photon absorption and photo bleaching.

Existing transition-metal dendrimers with an organic core have modest third-order nonlinearities, whereas the synthetically more complex dendrimers containing metal-acetylide units in both the inner and outer generations have considerably larger nonlinearities. After many false leads, a synthetic route to mixed metal ruthenium/platinum acetylide dendrimers has been devised. This route is synthetically less demanding than pre-existing ruthenium-acetylide reaction schemes, but the third-order nonlinearities of the resultant dendrimer are smaller.

4.8. *Experimental*

4.8.1. *General Conditions*

All reactions were performed under a nitrogen atmosphere with the use of Schlenk techniques unless otherwise stated. Dichloromethane was dried by distilling over calcium hydride, and tetrahydrofuran and toluene were dried by distilling over sodium/benzophenone. Other solvents were used as received. The petroleum ether had a boiling range of 60-80 °C. Chromatography was performed on silica gel (230-400 mesh ASTM) or ungraded basic alumina.

Microanalysis were carried out at the Research School of Chemistry, Australian National University. UV-vis spectra of solutions in tetrahydrofuran in 1 cm cells were recorded using a Cary 5 spectrophotometer. Infrared spectra were recorded as dichloromethane solutions using a Perkin-Elmer System 2000 FT-IR. ^{1}H (300 MHz) and ^{31}P NMR (121 MHz) spectra were recorded using a Varian Gemini-300 FT NMR spectrometer and are referenced to residual chloroform (7.24 ppm) or external H_3PO_4 (0.0 ppm), respectively.

The synthesis of the nitro- containing dendrimers (**20b – 23b**) were performed with the assistance of a third year student, Ms Simone Ward.

4.8.2. *Reagents*

The following were prepared by literature procedures: 1,3,5-triethynylbenzene,[74] $Me_3SiC{\equiv}CC_6H_4$-4-I,[110] $HC{\equiv}C\ C_6H_4$-4-NO_2, $HC{\equiv}C\ C_6H_4$-4-NH_2,[110] $HC{\equiv}C\ C_6H_4$-4-$C{\equiv}CPh$,[111] *cis*-$[RuCl_2(dppe)_2]$,[112] 1,3,5-$C_6H_3(C{\equiv}CC_6H_4$-4-$C{\equiv}CSiMe_3)_3$ (**7**),[73] 1,3,5-$C_6H_3(C{\equiv}CC_6H_4$-4-$C{\equiv}CH)_3$ (**8**),[73] 1,3,5-$C_6H_3\{C{\equiv}CC_6H_4$-4-$C{\equiv}C$-*trans*-$[RuCl(dppe)_2]\}_3$ (**9**),[73] 1-$Me_3SiC{\equiv}C$)-C_6H_3-$\{C{\equiv}CC_6H_4$-4-$C{\equiv}C$-*trans*-$[RuCl(dppe)_2]\}_2$ (**17**),[73] 1,3-{*trans*-$[(dppe)_2(PhC{\equiv}C)RuC{\equiv}C]\}_2$-5-$(Me_3SiC{\equiv}C$-4-$C_6H_4)C_6H_3$ (**21a**)[69] and 1,3-{*trans*-$[(dppe)_2(PhC{\equiv}C)RuC{\equiv}C]\}_2$-5-$(HC{\equiv}C$-4-$C_6H_4)C_6H_3$ (**22a**).[69] The synthesis and characterization of *trans*-$[Ru(C{\equiv}CC_6H_4$-4-$C{\equiv}CPh)Cl(dppe)_2]$ (**4**) is described in Chapter 3.

Both *n*-butyllithium (Merck) and *t*-butyllithium (Aldrich) were titrated with diphenylacetic acid to determine their concentration prior to use.[113] Sodium hexafluorophosphate (Aldrich) was recrystallized from acetonitrile before use. Copper iodide (Unilab), ammonium hexafluorophosphate (Aldrich), tetrabutylammonium fluoride (Aldrich), 1,3,5-tribromobenzene (Aldrich), $[PdCl_2(PPh_3)_2]$ (PMO), CuCl (J. T. Baker), trimethylsilylacetylene (Aldrich), zinc bromide (Aldrich) and phenylacetylene (Aldrich) were used as received. $[Pd(PPh_3)_4]$ was a gift from Dr B. L. Flynn.

4.8.3. *Molecular Modeling*

Molecular modelling calculations were carried on a SGI IRIX workstation using the SYBYL forcefield[114] in the program SPARTAN 5.0.[115]

4.8.4. *Synthesis of Dendrimers with Electron-Donating Peripheral Substituents*

4.8.4.1. *Synthesis and characterization of $Et_2NC_6H_4$-4-C≡CSiMe$_3$ (2)*

4-Iodo-*N*,*N*-diethylaniline (3.73 g, 13.5 mmol), $PdCl_2(PPh_3)_2$ (95.2 mg, 0.136 mmol), CuI (27.6 mg, 0.145 mmol) and trimethylsilylacetylene (1.95 mL, 1.36 g, 13.8 mmol) were stirred in triethylamine (40 mL) at room temperature for 17 h. The solvent was removed under reduced pressure and the residue was washed through a silica plug with petroleum ether, to afford an orange oil (3.287 g, 98%). ^{1}H NMR: (δ, 300 MHz, $CDCl_3$); 0.20 (s, 9H, $SiMe_3$), 1.13 (t, 6H, 7 Hz, CH_3), 3.32 (4H, q, 7 Hz, CH_2), 6.52 (2H, AA'BB', 8 Hz, phenyl) 7.28 (2H, AA'BB', 8Hz, phenyl). EI HRMS: calc for $C_{15}H_{23}NSi$ 245.160, found 245.160.

4.8.4.2. *Synthesis and characterization of $Et_2NC_6H_4$-4-C≡CH (3)*

A solution of **2** (3.287 g, 13.39 mmol) and tetrabutylammonium fluoride (15 mL, 1.0 M in thf) were stirred in dichloromethane (50 mL) at room temperature for 30 min. The solvent was removed *in vacuo*, and the residue placed onto a silica column. A thick yellow oil was

removed with petroleum ether (1.644 g, 71%). Its identity was confirmed by comparison of ^{1}H NMR and EI MS data with literature data.[72]

4.8.4.3. *Synthesis and characterization of trans-[Ru(C≡CC$_6$H$_4$-4-C≡CPh)(C≡CC$_6$H$_4$-4-NEt$_2$)(dppe)$_2$] (5)*

Trans-[Ru(C≡CC$_6$H$_4$-4-C≡CPh)Cl(dppe)$_2$] **4** (55.5 mg, 0.049 mmol), HC≡CC$_6$H$_4$-4-Et$_2$ **3** (26.5 mg, 0.18 mmol), ammonium hexafluorophosphate (26.9 mg, 0.17 mmol) and triethylamine (2 mL) were heated at reflux in chloroform (40 mL) for 3 h. The solvent was removed under reduced pressure and the residue extracted into CH_2Cl_2. The solution was absorbed onto alumina and placed on an alumina column. The column was eluted with petroleum ether to remove excess acetylene, and then with 4:6 CH_2Cl_2:petroleum ether to remove the product as a yellow solid (19 mg, 31%). Anal. Calcd for $C_{80}H_{71}NP_4Ru$: C 75.58, H 5.63, N 1.10 %. Found: C 75.23, H 5.69, N 1.23%. IR: (CH_2Cl_2) ν(C≡C) 2054 cm^{-1}. UV-Vis: λ (thf) 386 nm, ε 22 700 M^{-1} cm^{-1}. ^{1}H NMR (δ, 300 MHz, $CDCl_3$); 1.13 (6H, t, 7 Hz, CH_3), 2.60 (8H, m, CH_2), 3.35 (4H, q, 7 Hz, CH_2), 6.54 – 7.68 (53H, m, phenyl). ^{31}P NMR: (δ, 121 MHz, $CDCl_3$); 54.39 (s). MS; *m/z* (fragment, relative intensity): 1273 ([M]$^+$, 7), 1100 ([M – $C_{12}H_{14}N$]$^+$, 45), 898 ([Ru(dppe)$_2$]$^+$, 100)

4.8.4.4. *Reaction between cis-[RuCl$_2$(dppe)$_2$] and 4-ethynyl-N,N-diethylaniline (3)*

A solution of **3** (125 mg, 0.721 mmol) and *cis*-[RuCl$_2$(dppe)$_2$] (129.0 mg, 0.133 mmol) and NH_4PF_6 (27.9 mg, 0.172 mmol) in CH_2Cl_2 (40 mL) was stirred for 15 h. NEt_3 (4 mL) was added and the solution taken to dryness under reduced pressure. The green residue was absorbed onto alumina and placed on a alumina column. The column was washed with petroleum ether (to remove excess acetylene) and CH_2Cl_2 to give a green solution. MeOH (40 mL) was added and the volume reduced to approximately 1 mL. An unidentified green powder (**6**) was collected by filtration (65.1 mg).

4.8.4.5. *Synthesis and characterization of 1,3,5-C_6H_3{C≡C-4-C_6H_4C≡C-trans-[Ru(C≡CC_6H_4-4-NEt_2)(dppe)$_2$]}$_3$ (**10**)*

1,3,5-C_6H_3{C≡CC_6H_4-4-C≡C-*trans*-[RuCl(dppe)$_2$]}$_3$ **9** (179 mg, 0.054 mmol), **3** (63.0 mg, 0.43 mmol), ammonium hexafluorophosphate (32.0 mg, 0.20 mmol) and triethylamine (2 mL) were heated in refluxing chloroform (40 mL) for 6 h. The solvent was removed *in vacuo*, and the residue placed onto an alumina column. The column was washed with 1:9 CH_2Cl_2: petroleum ether to remove excess acetylene, and then CH_2Cl_2 to remove a yellow solid (50 mg, 0.014 mmol, 26%). Anal. Calcd for $C_{228}H_{201}N_3P_{12}Ru_3$: C 74.86, H 5.54, N 1.15 %. Found: C 74.71, H 5.86, N 1.32%. IR: (CH_2Cl_2) ν(C≡C) 2055 cm^{-1}. UV-Vis: λ (thf) 410 nm, ε 153 000 M^{-1} cm^{-1}. ^1H NMR (δ, 300 MHz, $CDCl_3$); 1.13 (18H, t, 7 Hz, CH_3), 2.58 (24H, m, CH_2), 3.36 (12H, q, 7 Hz, NCH_2), 6.93 – 7.85 (147H, m, phenyl). ^{31}P NMR: (δ, 121 MHz, $CDCl_3$); 54.09 (s). MS; *m/z* (fragment, relative intensity): 898 (Ru(dppe)$_2$]$^+$, 100).

4.8.4.6. *Synthesis and characterization of 1,3-{trans-[(dppe)$_2$(4-$Et_2NC_6H_4$C≡C)RuC≡C]}$_2$-5-Me_3SiC≡CC_6H_3 (**18**)*

A solution of 1,3-{*trans*-[ClRu(dppe)$_2$RuC≡C]}$_2$-5-Me_3SiC≡CC_6H_3 **17** (59 mg, 0.026 mmol), HC≡CC_6H_4-4-NEt_2 **3** (40 mg, 0.23 mmol) and $NaPF_6$ (32 mg, 0.22 mmol) in chloroform (40 mL) and triethylamine (1 mL) was refluxed for 18 h. The reaction mixture was flashed through an alumina plug, and the solvent removed under reduced pressure. The product was washed with methanol to give a green-yellow powder (37 mg, 0.015 mmol, 57%). The products instability on alumina, prevented a definitive characterization. IR: (CH_2Cl_2) ν(C≡C) 2053 cm^{-1}. ^1H NMR (δ, 300 MHz, $CDCl_3$); 0.23 (9H, s, $SiMe_3$), 1.13 (12H, t, 7 Hz, CH_3), 2.60 (16H, m, CH_2), 3.35 (8H, q, 7 Hz, CH_2), 6.46 – 7.50 (99H, m, phenyl). ^{31}P NMR: (δ, 121 MHz, $CDCl_3$); 54.15 (s).

4.8.4.7. *Attempted Synthesis of 1,3-{trans-[(dppe)$_2$(4-Et$_2$NC$_6$H$_4$C≡C)RuC≡C]}$_2$-5-HC≡CC$_6$H$_3$*

A solution of **18** (14 mg, 5.5 μmol) and K_2CO_3 (12 mg, 86.8 μmol) in CH_2Cl_2 (5 mL) and MeOH (5 mL) was stirred for 2 h. The mixture was passed through an alumina plug with CH_2Cl_2. The yellow solution turned green on the alumina plug. ^1H and ^{31}P NMR spectroscopy indicated unidentified decomposition products.

4.8.5. *Synthesis of Peripherally-Metallated Dendrimers*

4.8.5.1. *Synthesis of 1,3-{trans-[(dppe)$_2$ClRuC≡C]}$_2$-5-HC≡CC$_6$H$_3$ (19)*

The synthesis of this product was achieved by a modification of the literature synthesis.[69] 1,3,5-Triethynylbenzene (135 mg, 0.899 mmol), *cis*-[$RuCl_2$(dppe)$_2$] (1.599 g, 1.65 mmol) and NH_4PF_6 (545 mg, 3.34 mmol) were heated in refluxing CH_2Cl_2 (25 mL) for 17 h. NEt_3 (1 mL) was added and the solution was immediately passed through an alumina plug, eluting with CH_2Cl_2. The solvent was removed under reduced pressure, and the remaining yellow powder triturated with diethyl ether to remove excess *trans*-[$RuCl_2$(dppe)$_2$]. The product was further purified by column chromatography on alumina using 4:1 CH_2Cl_2 : petroleum ether as eluent, to afford a yellow powder (1090 mg, 60 %). ^1H NMR (δ, 300 MHz, $CDCl_3$); 2.68 (16H, m, CH_2), 3.01 (1H, s, C≡CH), 6.41-7.70 (83H, m, phenyl). ^{31}P NMR: (δ, 121 MHz, $CDCl_3$); 50.5 (s).

4.8.5.2. *Synthesis and characterization of 1,3-{trans-[(dppe)$_2$(PhC≡C)RuC≡C]}$_2$-5-HC≡CC$_6$H$_3$ (20a)*

The synthesis of this product was achieved by a modification of the literature synthesis.[69] **19** (773 mg, 0.364 mmol), NH_4PF_6 (92 mg, 0.56 mmol), phenylaceylene (0.4 mL, 3.6 mmol) and triethylamine (2 mL) were stirred in refluxing dichloromethane (40 mL) for 17 h. The solution was allowed to cool and taken to dryness under reduced pressure. The yellow

powder was triturated with diethyl ether, and purified by column chromatography on alumina to afford a yellow solid (747 mg, 84 %), whose identity was confirmed by comparison of ^{1}H and ^{31}P NMR with literature values.[69] ^{1}H NMR (δ, 300 MHz, $CDCl_3$); 2.64 (16H, m, CH_2), 3.02 (1H, s, C≡CH), 6.41-7.70 (95H, m, phenyl). ^{31}P NMR: (δ, 121 MHz, $CDCl_3$); 54.4 (s).

4.8.5.3. *Synthesis and characterization of 1,3-{trans-[(dppe)$_2$($O_2NC_6H_4$-4-C≡C)Ru C≡C]}$_2$-5-HC≡CC_6H_3 (20b)*

1,3-{*trans*-[(dppe)$_2$(ClRuC≡C]}$_2$-5-HC≡CC_6H_3 **19** (512 mg, 0.254 mmol), NH_4PF_6 (55 mg, 0.337 mmol), $O_2NC_6H_4$-4-C≡CH (153 mg, 1.04 mmol) and triethylamine (1 mL) were stirred in refluxing dichloromethane (25 mL) for 22 h. The solution was filtered through an alumina plug and the solvent removed under reduced pressure. The red material was triturated with petroleum spirit and purified on an alumina column with dichloromethane and petroleum spirit (55:45) as eluent. The red solid was dried under vacuum (218 mg, 38%). Anal Calcd for $C_{132}H_{108}O_4N_2Ru_2P_8$: C 68.82, H 4.77, N, 1.20. Found C 69.18, H 4.66, N 1.54%. IR: (CH_2Cl_2) ν(C≡C) 2045 cm^{-1}. UV-Vis: λ (thf) 475 nm, ε 47 800 M^{-1} cm^{-1} ^{1}H NMR: (δ, 300 MHz, $CDCl_3$); 2.60 – 2.69 (16H, m, CH_2), 3.06 (1H, s, C≡CH), 6.47 – 7.96 (91H, m, Ph). ^{31}P NMR: (δ, 121 MHz, $CDCl_3$); 54.0 (s). FAB MS; *m/z* (fragment, relative intensity): 2237 ([M + H]$^+$, 20), 1044 ({*trans*-[(dppe)$_2$($O_2NC_6H_4$C≡C)Ru]}$^+$, 10), 898 ([Ru(dppe)$_2$]$^+$, 100)

4.8.5.4. *Synthesis and characterization of 1,3-{trans-[(dppe)$_2$($H_2NC_6H_4$-4-C≡C)Ru C≡C]}$_2$-5-HC≡CC_6H_3 (20c)*

A mixture of 1,3-{*trans*-[(dppe)$_2$ClRuC≡C]}$_2$-5-HC≡CC_6H_3 **19** (681 mg, 0.356 mmol), NH_4PF_6 (425 mg, 0.337 mmol), HC≡C_6H_4-4-NH_2 (420 mg, 3.59 mmol) and NEt_3 (2 mL) were stirred in refluxing CH_2Cl_2 (50 mL) for 18 h. The solution was allowed to cool and passed through an alumina plug with 55:45 CH_2Cl_2 : petroleum ether. The solvent was removed under reduced pressure, and the solid was triturated with petroleum ether. The

complex was further purified by column chromatography on alumina, eluting with a 1:1 solution of CH_2Cl_2 : petroleum ether, to afford a brown-yellow powder (340 mg, 44 %). Anal. Calcd for $C_{132}H_{112}N_2P_8Ru_2$: C 72.85, H 5.19, N 1.29. Found: C 71.97, H 5.02, N 1.27 %. IR: (CH_2Cl_2) ν(C≡C) 2054 cm^{-1}. UV-Vis: λ (thf) 333 nm, ε 23 000 M^{-1} cm^{-1}. ^1H NMR: (δ, 300 MHz, $CDCl_3$); 2.67 (16H, m, CH_2), 3.03 (1H, s, C≡CH), 6.51 – 7.55 (95H, m, phenyl). ^{31}P NMR: (δ, 121 MHz, $CDCl_3$); 54.6.

4.8.5.5. *Synthesis and characterization of 1,3-{trans-[(dppe)$_2$($O_2NC_6H_4$-4-C≡C)Ru C≡C]}$_2$-5-(Me_3SiC≡CC_6H_4-4-C≡C)C_6H_3 (21b)*

A mixture of 1,3-{*trans*-[(dppe)$_2$($O_2NC_6H_4$-4-C≡C)RuC≡C]}$_2$-5-HC≡CC_6H_3 (151 mg, 0.067 mmol) (**20b**), 4-Me_3SiC≡CC_6H_4-4-I (97 mg, 0.32 mmol) and $Pd(PPh_3)_4$ (23 mg, 0.020 mmol) was refluxed for 21 h in a 1:1 solution of CH_2Cl_2 : NEt_3 (20 mL). The solution was passed through an alumina plug and taken to dryness under reduced pressure. The product was purified by column chromatography on alumina with a 60:40 solution of CH_2Cl_2 : petroleum spirit as eluent, to give a red solid (82 mg, 50%). Anal. Calcd for $C_{143}H_{120}N_2O_4P_8Ru_2Si$: C 71.31, H 5.02, N 1.16. Found: C 71.24, H 5.41, N 1.19 %. IR: (CH_2Cl_2) ν(C≡C) 2045 cm^{-1}, ν(C≡C$SiMe_3$) 2153 cm^{-1}. UV-Vis: λ (thf) 475 nm, ε 46 830 M^{-1} cm^{-1} ^1H NMR: (δ, 300 MHz, $CDCl_3$); 0.26 (9H, s, Me), 2.60 – 2.69 (16H, m, CH_2), 6.48 – 7.96 (95H, m, Ph). ^{31}P NMR: (δ, 121 MHz, $CDCl_3$); 53.9 (s). FAB MS; *m/z* (fragment, relative intensity): 2409 ([M + H]$^+$, 10), 1044 ({*trans*-[(dppe)$_2$($O_2NC_6H_4C$≡C)Ru]}$^+$, 10), 898 ([Ru(dppe)$_2$]$^+$, 100)

4.8.5.6. *Synthesis and characterization of 1,3-{trans-[(dppe)$_2$($H_2NC_6H_4$-4-C≡C)Ru C≡C]}$_2$-5-(Me_3SiC≡CC_6H_4-4-C≡C)-C_6H_3 (21c)*

A solution of 1,3-{*trans*-[(dppe)$_2$($H_2NC_6H_4$-4-C≡C)RuC≡C]}$_2$-5-HC≡CC_6H_3 **20c** (285 mg, 0.138 mmol), Me_3SiC≡CC_6H_4-4-I (425 mg, 1.42 mmol) and $Pd(PPh_3)_4$ (6.0 mg, 6.7 μmol) in CH_2Cl_2 and NEt_3 (5 mL) was refluxed for 17 h. The solution was allowed to cool and passed through an alumina column with CH_2Cl_2 as eluent. The reaction mixture was taken

to dryness and triturated with petroleum ether. The residue was purified by liquid diffusion of MeOH into a solution in CH_2Cl_2 to afford a red-brown powder (130 mg, 41 %). Anal. Calcd for $C_{143}H_{124}N_2P_8Ru_2Si$: C 73.13, H 5.32, N 1.19. Found: C 72.91, H 5.22, N 1.13 %. IR: (CH_2Cl_2) ν(C≡CSiMe$_3$) 2154 cm^{-1} ν(C≡CRu) 2053 cm^{-1}. UV-Vis: λ (thf) 334 nm, ε 55 700 M^{-1} cm^{-1}. ^{1}H NMR: (δ, 300 MHz, $CDCl_3$); 0.22 (9H, s, Me), 2.69 (16H, m, CH_2), 3.66 (4H, m, NH_2), 6.93 – 7.70 (95H, m, Ph). ^{31}P NMR: (δ, 121 MHz, $CDCl_3$); 54.5 (s).

4.8.5.7. *Synthesis and characterization of 1,3-{trans-[(dppe)$_2$(O$_2$NC$_6$H$_4$-4-C≡C)Ru C≡C]}$_2$-5-(HC≡CC$_6$H$_4$-4-C≡C)C$_6$H$_3$ (22b)*

A mixture of 1,3-{*trans*-[(dppe)$_2$(O$_2$NC$_6$H$_4$-4-C≡C)RuC≡C]}$_2$-5-(Me$_3$SiC≡C-4-C$_6$H$_4$)C$_6$H$_3$ **21b** (51 mg, 0.021 mmol) and NBu$^n_4$F (0.5 mL, 1 M in thf) in CH_2Cl_2 (10 mL) was stirred for 1 h. The resultant solution was passed through an alumina plug and taken to dryness under reduced pressure to yield a red powder (38 mg, 77%). Anal. Calcd for $C_{140}H_{112}N_2O_4P_8Ru_2$: C 71.97, H 4.83, N 1.20. Found: C 71.77, H 5.16, N 1.15 %. IR: (CH_2Cl_2) ν(C≡C) 2045 cm^{-1}. UV-Vis: λ (thf) 474 nm, ε 40 790 M^{-1} cm^{-1}. ^{1}H NMR: (δ, 300 MHz, $CDCl_3$); 2.62 – 2.66 (16H, m, CH_2), 3.18 (1H, s, C≡CH), 6.47 – 7.96 (95H, m, Ph). ^{31}P NMR: (δ, 121 MHz, $CDCl_3$); 53.9 (s). FAB MS; *m/z* (fragment, relative intensity): 898 ([Ru(dppe)$_2$]$^+$, 8).

4.8.5.8. *Synthesis and characterization of 1,3-{trans-[(dppe)$_2$(H$_2$NC$_6$H$_4$-4-C≡C)Ru C≡C]}$_2$-5-(HC≡CC$_6$H$_4$-4-C≡C)C$_6$H$_3$ (22c)*

A mixture of 1,3-{*trans*-[(dppe)$_2$(H$_2$NC$_6$H$_4$-4-C≡C)RuC≡C]}$_2$-5-(Me$_3$SiC≡C-4-C$_6$H$_4$)C$_6$H$_3$ **21c** (110 mg, 0.047 mmol) and NBu$^n_4$F (1.0 mL, 1 M in thf) in CH_2Cl_2 (40 mL) was stirred for 1 h. The resultant solution was passed through an alumina plug and taken to dryness under reduced pressure to yield a red powder. This was further purified by liquid diffusion of MeOH into a solution in CH_2Cl_2 (95 mg, 89 %). Anal. Calcd for $C_{140}H_{116}N_2P_8Ru_2$: C 73.87, H 5.14, N 1.23. Found: C 72.81, H 5.10, N 1.17 %. IR: (CH_2Cl_2) ν(C≡C) 2055 cm^{-1}. UV-Vis: λ (thf) 328 nm, ε 93 200 M^{-1} cm^{-1}. ^{1}H NMR: (δ, 300 MHz, $CDCl_3$); 2.67 (16H, m,

CH_2), 3.11 (1H, s, C≡CH), 3.72 (4H, m, NH_2), 6.79 – 7.85 (95H, m, Ph). ^{31}P NMR: (δ, 121 MHz, $CDCl_3$); 54.5.

4.8.5.9. *Synthesis and characterization of 1,3,5-(3,5-{trans-[(dppe)$_2$($O_2NC_6H_4$-4-C≡C)RuC≡C]}$_2$$C_6H_3$-1-C≡C$C_6H_4$-4-C≡C]$_3$$C_6H_3$ (23b)*

A mixture of 1,3-{*trans*-[(dppe)$_2$($O_2NC_6H_4$-4-C≡C)RuC≡C]}$_2$-5-(HC≡C-4-C_6H_4)C_6H_3 **22b** (26 mg, 0.011 mmol), 1,3,5-triiodobenzene (1.9 mg, 0.004 mmol) and $Pd(PPh_3)_4$ (25 mg, 0.022 mmol) was refluxed for 22 h in a 1:1 solution of dichloromethane:triethylamine (30 mL). The solution was passed through an alumina plug and the solvent removed under reduced pressure to yield a red powder (25 mg, 82 %). Anal. Calcd for $C_{426}H_{336}N_6O_{12}P_{24}Ru_6$: C 72.26, H 4.78, N 1.19. Found: C 72.05, H 4.67, N 1.18 %. IR: (CH_2Cl_2) ν(C≡C) 2045 cm^{-1}. UV-Vis: λ (thf) 475 nm, ε 108 660 M^{-1} cm^{-1}. ^1H NMR: (δ, 300 MHz, $CDCl_3$); 2.63 – 2.66 (48H, m, CH_2), 6.85 – 7.96 (288H, m, Ph). ^{31}P NMR: (δ, 121 MHz, $CDCl_3$); 53.8 (s). FAB MS; *m/z* (fragment, relative intensity): 898 ([Ru(dppe)$_2$]$^+$, 3).

4.8.5.10. *Synthesis and characterization of 1,3,5-(3,5-{trans-[(dppe)$_2$($H_2NC_6H_4$-4-C≡C)RuC≡C]}$_2$$C_6H_3$-1-C≡C$C_6H_4$-4-C≡C]$_3$$C_6H_3$ (23c)*

A mixture of 1,3-{*trans*-[(dppe)$_2$($H_2NC_6H_4$-4-C≡C)RuC≡C]}$_2$-5-(HC≡C-4-C_6H_4)C_6H_3 **22c** (88 mg, 0.039 mmol), 1,3,5-triiodobenzene (5.9 mg, 0.013 mmol) and $Pd(PPh_3)_4$ (47 mg, 0.053 mmol) was refluxed for 17 h in a 1:1 solution of dichloromethane:triethylamine (40 mL). The solution was passed through an alumina plug and the solvent removed under reduced pressure to yield a red powder (57 mg, 64 %). Anal. Calcd for $C_{426}H_{348}N_6P_{24}Ru_3$: C 74.14, H 5.08, N 1.22. Found: C 73.96, H 5.22, N 1.20 %. IR: (CH_2Cl_2) ν(C≡C) 2052 cm^{-1}. UV-Vis: λ (thf) 340 nm, ε 342 000 M^{-1} cm^{-1}. ^1H NMR: (δ, 300 MHz, $CDCl_3$); 2.63 (48H, m, CH_2), 3.74 (12H, m, NH_2), 6.75 – 7.90 (288H, m, Ph). ^{31}P NMR: (δ, 121 MHz, $CDCl_3$); 54.5 (s).

4.8.6. *Improved Methods of Dendrimer Synthesis*

4.8.6.1. *Reaction between 1,3-{trans-[(dppe)$_2$(PhC≡C)RuC≡C]}$_2$-5-(HC≡C-4-C$_6$H$_4$)C$_6$H$_3$ and 1,3,5-C$_6$H$_3${C≡CC$_6$H$_4$-4-C≡C-trans-[RuCl(dppe)$_2$]}$_3$*

A solution of 1,3,5-C_6H_3{C≡CC_6H_4-4-C≡C-*trans*-[RuCl(dppe)$_2$]}$_3$ **9** (21 mg, 6.5 μmol), 1,3-{*trans*-[(dppe)$_2$(PhC≡C)RuC≡C]}$_2$-5-(HC≡C-4-C_6H_4)C_6H_3 **22a** (44 mg, 0.020 mmol) and NH_4PF_6 (17 mg, 0.10 mmol) in CH_2Cl_2 (15 mL) and NEt_3 (1 mL) was stirred for 89 h. The solution was passed through an alumina plug with CH_2Cl_2, and taken to dryness on a rotary evaporator to afford a yellow powder. ^1H and ^{31}P NMR indicate no reaction. The powder was redissolved in CH_2Cl_2 (45 mL) and NEt_3 (2 mL). NH_4PF_6 (60 mg, 0.37 mmol) was added and the solution was refluxed for 24 h. The solution was passed through an alumina plug with CH_2Cl_2, and taken to dryness on a rotary evaporator to afford a yellow powder. ^1H and ^{31}P NMR indicate either no reaction or slight decomposition of the wedge **22a**. A small sample of the yellow powder (9 mg) was taken and dissolved in $CHCl_3$ (40 mL) and NEt_3 (1 mL). NH_4PF_6 (30 mg, 0.18 mmol) was added and the solution refluxed for 15 h. The solution was allowed to cool, passed through an alumina column with CH_2Cl_2 as eluent and taken to dryness. ^1H and ^{31}P NMR indicated decomposition of the wedge **22a**.

4.8.6.2. *Songashira Coupling*

4.8.6.2.1. *Synthesis and characterization of trans-[Ru(C≡CC_6H_4-4-I)$_2$(dppe)$_2$] (24)*

A solution of *cis*-[$RuCl_2$(dppe)$_2$] (155 mg, 0.160 mmol), 4-iodoethynylbenzene (90 mg, 0.395 mmol) and NH_4PF_6 (132 mg, 0.810 mmol) was stirred in CH_2Cl_2 (50 mL) for 11 h. NEt_3 (3 mL) was added and the solution stirred for 9 h. The reaction mixture was passed through an alumina column with CH_2Cl_2 as eluent and taken to dryness under reduced pressure. The residue was triturated with Et_2O to afford a yellow powder (182 mg, 84 %). Anal. Calcd for $C_{68}H_{56}I_2P_4Ru$: C 60.41, H 4.18. Found: C 59.95, H 4.15 %. IR: (CH_2Cl_2) ν(C≡C) 2060 cm^{-1}. UV-Vis: λ (thf) 345 nm, ε 5400 M^{-1} cm^{-1}. ^1H NMR: (δ, 300 MHz, $CDCl_3$); 2.66 (8H, m, CH_2), 6.41 – 8.14 (48H, m, Ph). ^{31}P NMR: (δ, 121 MHz, $CDCl_3$);

53.9 (s). FAB MS; *m/z* (fragment, relative intensity): 1351 ([M]+, 15), 1125 ([M – I]+, 20), 898 ([Ru(dppe)$_2$]+, 40).

4.8.6.2.2. *Reaction between trans-[Ru(C≡CC$_6$H$_4$-4-I)$_2$(dppe)$_2$] and phenylacetylene*

A solution of *trans*-[Ru(C≡CC$_6$H$_4$-4-I)$_2$(dppe)$_2$] **24** (35 mg, 0.026 mmol), Pd(PPh)$_3$)$_4$ (24 mg, 0.027 mmol) and phenylacetylene (0.1 mL, 0.98 mmol) in CH_2Cl_2 (10 mL) and NEt_3 (10 mL) was stirred for 19 h. The reaction mixture was passed through an alumina plug and taken to dryness under reduced pressure. ^{1}H and ^{31}P NMR indicated unidentified decomposition products.

4.8.6.2.3. *Reaction between trans-[Ru(C≡CC$_6$H$_4$-4-I)$_2$(dppe)$_2$] and 1,3-{trans-[(dppe)$_2$(PhC≡C)RuC≡C]}$_2$-5-HC≡CC$_6$H$_3$*

A solution of *trans*-[Ru(C≡CC$_6$H$_4$-4-I)$_2$(dppe)$_2$] **24** (49 mg, 0.036 mmol), 1,3-{*trans*-[(dppe)$_2$(PhC≡C)RuC≡C]}$_2$-5-HC≡CC$_6$H$_3$ **20a** (158 mg, 0.074 mmol) and Pd(PPh$_3$)$_4$ (30 mg, 0.033 mmol) in CH_2Cl_2 (15 mL) and NEt_3 (15 mL) was stirred for 18 h. The reaction mixture was passed through an alumina plug and taken to dryness under reduced pressure. ^{1}H and ^{31}P NMR indicate the presence of unreacted wedge **20a** and unidentified decomposition products.

4.8.6.2.4. *Synthesis and characterization of 1,3,5-C$_6$H$_3${C≡CC$_6$H$_4$-4-C≡C-trans-[Ru(C≡CC$_6$H$_4$-4-I)(dppe)$_2$]}$_3$ (25)*

A solution of 1,3,5-C$_6$H$_3${C≡CC$_6$H$_4$-4-C≡C-*trans*-[RuCl(dppe)$_2$]}$_3$ **9** (272 mg, 0.084 mmol), $NaPF_6$ (120 mg, 0.74 mmol) and 4-iodophenylaceylene (171 mg, 0.75 mmol) in CH_2Cl_2 (40 mL) and NEt_3 (2 mL) was refluxed for 48 h. The solution was allowed to cool and was then passed through an alumina column with CH_2Cl_2 as eluent. The solvent was removed and the residue was triturated with petroleum ether. The residue was dissolved in a

minium volume of CH_2Cl_2. MeOH was added and a yellow powder collected by filtration (351 mg, 91 %) Anal. Calcd for $C_{216}H_{171}I_3P_{12}Ru_3$: C 67.87, H 4.51. Found: C 67.51, H 4.23 %. IR: (CH_2Cl_2) ν(C≡C) 2054 cm^{-1}. UV-Vis: λ (thf) 345 (sh) nm, ε 8500 M^{-1} cm^{-1}. ^1H NMR: (δ, 300 MHz, $CDCl_3$); 2.61 (24H, m, CH_2), 6.42 – 7.66 (135H, m, Ph). ^{31}P NMR: (δ, 121 MHz, $CDCl_3$); 54.2.

4.8.6.2.5. *Attempted Synthesis of 1,3,5-C_6H_3(CC≡C_6H_4-4-C≡C-trans-[Ru(dppe)$_2$]C≡CC_6H_4-4-C≡CC_6H_3-3,5-{C≡C-trans-[Ru(C≡CPh)(dppe)$_2$]}$_2$)$_3$ (**26**) from 1,3,5-C_6H_3{C≡CC_6H_4-4-C≡C-trans-[Ru(C≡CC_6H_4-4-I)(dppe)$_2$]}$_3$ and 1,3-{trans-[(dppe)$_2$(PhC≡C)RuC≡C]}$_2$-5-HC≡CC_6H_3*

A solution of 1,3,5-C_6H_3{C≡CC_6H_4-4-C≡C-*trans*-[Ru(C≡CC_6H_4-4-I)(dppe)$_2$]}$_3$ (13 mg, 3.4 μmol) (**25**), 1,3-{*trans*-[(dppe)$_2$(PhC≡C)RuC≡C]}$_2$-5-HC≡CC_6H_3 (22 mg, 0.010 mmol) (**20a**), $PdCl_2(PPh_3)_2$ (4.0 mg, 5.7 μmol) and CuI (4 mg, 0.02 mmol) in CH_2Cl_2 (10 mL) and NEt_3 (10 mL) was stirred for 15 h. The reaction mixture was passed through an alumina column with CH_2Cl_2, and taken to dryness under reduced pressure. ^1H and ^{31}P NMR indicated the presence of unreacted **25** and {3,5-(*trans*-[(dppe)$_2$(PhC≡C)RuC≡C)$_2$$C_6H_3$C≡C}$_2$. Attempts to separate the mixture by column chromatography were unsuccessful.

4.8.6.2.6. *Attempted synthesis of trans-[Ru(dppe)$_2$]{C≡CC_6H_4-4-C≡C-1-C_6H_3-3,5-(C≡C-trans-[RuCl(dppe)$_2$])$_2$}$_2$ (27)*

A solution of *trans*-[Ru(C≡CC_6H_4-4-I)$_2$(dppe)$_2$] **24** (10 mg, 7.4 μmol), 1,3-{*trans*-[(dppe)$_2$ClRuC≡C]}$_2$-5-HC≡CC_6H_3 **19** (30 mg, 0.015 mmol), $PdCl_2(PPh_3)_2$ (2 mg, 3 μmol) and CuI (9.0 mg, 4.7 mmol) in CH_2Cl_2 (25 mL) and NEt_3 (2 mL) was stirred for 17 h. The reaction mixture was passed through an alumina column with CH_2Cl_2 as eluent and taken to dryness. ^1H and ^{31}P NMR indicated the presence of **24** and the homo-coupled product **28**. Attempts to separate the two components with alumina column chromatography were unsuccessfully.

4.8.6.2.7. *Rational synthesis and characterization of {3,5-(trans-[(dppe)$_2$ClRuC≡C)$_2$C$_6$H$_3$C≡C}$_2$ (28)*

A solution of 1,3-{*trans*-[(dppe)$_2$ClRuC≡C]}$_2$-5-HC≡CC$_6$H$_3$ **19** (39 mg, 0.019 mmol), PdCl$_2$(PPh$_3$)$_2$ (2 mg, 3 μmol) and CuI (2.0 mg, 11 μmol) in CH_2Cl_2 (30 mL) and NEt_3 (1 mL) was stirred for 48 h. The reaction mixture was passed through an alumina column with CH_2Cl_2 as eluent and taken to dryness. Recrystallized from CH_2Cl_2 and MeOH afforded a yellow powder (36 mg, 92%). Anal. Calcd for $C_{232}H_{198}Cl_4P_{16}Ru_2$: C 69.18 H 4.95. Found: C 68.88 H 4.45 %. IR: (CH_2Cl_2) ν(C≡C) 2059 cm^{-1}. UV-Vis: λ (thf) 335 nm, ε 139 000 M^{-1} cm^{-1}. ^{1}H NMR: (δ, 300 MHz, $CDCl_3$); 2.67 (32H, m, CH_2), 6.45 – 7.75 (166H, m, Ph). ^{31}P NMR: (δ, 121 MHz, $CDCl_3$); 50.5 (s).

4.8.6.2.8. *Reaction between 1,3,5-C$_6$H$_3${C≡CC$_6$H$_4$-4-C≡C-trans-[Ru(C≡CC$_6$H$_4$-4-I)(dppe)$_2$]}$_3$ and phenylacetylene*

A solution of 1,3-{*trans*-[(dppe)$_2$(PhC≡C)RuC≡C]}$_2$-5-HC≡CC$_6$H$_3$ **20a** (40 mg, 0.019 mmol), *trans*-[Ru(C≡CC$_6$H$_4$-4-I)$_2$(dppe)$_2$] **24** (50 mg, 0.037 mmol), phenylacetylene (0.1 mL, 0.091 mmol) and Pd(PPh$_3$)$_4$ (10 mg, 0.011 mmol) in CH_2Cl_2 (15 mL) and NEt_3 (15 mL) was stirred for 17 h. The reaction mixture was taken to dryness under reduced pressure, and a yellow-brown residue extracted with petroleum ether. The remaining yellow residue was passed through an alumina column with CH_2Cl_2 and the solution taken to dryness under reduced pressure. ^{1}H and ^{31}P NMR indicated unreacted **24** and **20a** only.

4.8.6.2.9. *Reaction between 1,3,5-C$_6$H$_3${C≡CC$_6$H$_4$-4-C≡C-trans-[Ru(C≡CC$_6$H$_4$-4-I)(dppe)$_2$]}$_3$ and phenylacetylene*

A solution of 1,3,5-C$_6$H$_3${C≡CC$_6$H$_4$-4-C≡C-*trans*-[Ru(C≡CC$_6$H$_4$-4-I)(dppe)$_2$]}$_3$ **25** (35 mg, 9.2 μmol), phenylacetylene (0.03 mL, 0.3 mmol) and Pd(PPh$_3$)$_4$ (14 mg, 0.016 mmol) in CH_2Cl_2 (15 mL) and NEt_3 (15 mL) was stirred for 17 h. The reaction mixture was taken to dryness under reduced pressure, and a yellow-brown residue extracted with petroleum ether. The remaining yellow residue was passed through an alumina column with CH_2Cl_2 and the

solution taken to dryness under reduced pressure. ^{1}H and ^{31}P NMR indicated unreacted **25** only.

4.8.6.3. *Negishi Coupling*

4.8.6.3.1. *Attempted Synthesis of trans-[Ru(C≡CC$_6$H$_4$-4-C≡CPh)$_2$(dppe)$_2$]*

A solution of ZnBr (5.2 mg, 0.045 mmol) in thf (10 mL) and NEt_3 (0.3 mL) was stirred for 1 h. *trans*-[Ru(C≡CC$_6$H$_4$-4-I)$_2$(dppe)$_2$] **24** (22 mg, 0.016 mmol) was added and the solution was stirred for 5 min. Phenylacetylene (0.1 mL, 0.91 mmol) was added and the solution was stirred for 5 min. $PdCl_2(PPh_3)_2$ (2.8 mg, 4.0 μmol) was added and the solution was stirred for 15 h. The reaction mixture was passed through an alumina plug with CH_2Cl_2 and the solvent volume reduced to ~5 mL under reduced pressure. Petroleum ether was added, and a yellow powder collected by filtration. ^{1}H and ^{31}P NMR indicated decomposition.

4.8.6.3.2. *Attempted Synthesis of 1,3,5-C$_6$H$_3$(CC≡C$_6$H$_4$-4-C≡C-trans-[Ru(dppe)$_2$]C≡CC$_6$H$_4$-4-C≡CC$_6$H$_3$-3,5-{C≡C-trans-[RuCl(dppe)$_2$]}$_2$)$_3$*

A solution of 1,3,5-C$_6$H$_3${C≡CC$_6$H$_4$-4-C≡C-*trans*-[Ru(C≡CC$_6$H$_4$-4-I)(dppe)$_2$]}$_3$ **25** (20 mg, 0.0052 mol), 1,3-{*trans*-[(dppe)$_2$ClRuC≡C]}$_2$-5-C$_6$H$_3$ **19** (32 mg, 0.0099 mol), ZnBr (20 mg, 0.17 mmol) and $PdCl_2(PPh_3)_2$ (1.7 mg, 2.4 μmol) in CH_2Cl_2 (10 mL) and NEt_3 (10 mL) was refluxed for 12 h. The reaction mixture was passed through an alumina column with CH_2Cl_2. ^{1}H and ^{31}P NMR indicated decomposition.

4.8.6.3.3. *Attempted Synthesis of 1,3,3-C$_6$H$_3$(CC≡C$_6$H$_4$-4-C≡C-trans-[Ru(dppe)$_2$]C≡CC$_6$H$_4$-4-C≡CC$_6$H$_3$-3,5-{C≡C-trans-[Ru(C≡CPh)(dppe)$_2$]}$_2$)$_3$ (26)*

A solution of 1,3-{*trans*-[(dppe)$_2$(PhC≡C)RuC≡C]}$_2$-5-HC≡CC$_6$H$_3$ **20a** (43 mg, 0.020 mmol), ZnBr (30 mg, 0.15 mmol) and $Pd(PPh_3)_4$ (2.5 mg, 2.8 μmol) in CH_2Cl_2 (30 mL)

and NEt_3 (25 mL) was stirred for 5 min. 1,3,5-C_6H_3{C≡CC_6H_4-4-C≡C-*trans*-[Ru(C≡CC_6H_4-4-I)(dppe)$_2$]}$_3$ **25** (26 mg, 6.8 μmol) was added, and the solution was refluxed for 18 h. The reaction mixture was passed through an alumina column with CH_2Cl_2. ^{1}H and ^{31}P NMR indicated decomposition.

4.8.6.4. *Wedge Activation by BuLi*

4.8.6.4.1. *Attempted Synthesis of 1,3,3-C_6H_3(CC≡C_6H_4-4-C≡C-trans-[Ru(dppe)$_2$]C≡CC_6H_4-4-C≡CC_6H_3-3,5-{C≡C-trans-[Ru(C≡CPh)(dppe)$_2$]}$_2$)$_3$*

A solution of 1,3-{*trans*-[(dppe)$_2$(PhC≡C)RuC≡C]}$_2$-5-(HC≡C-4-C_6H_4)C_6H_3 **22a** (159 mg, 71 μmol) in thf (30 mL) was cooled in a dry-ice/acetone bath. *n*-BuLi (0.04 mL, 1.5 M) was added and the solution stirred for 45 min. 1,3,5-C_6H_3{C≡CC_6H_4-4-C≡C-*trans*-[RuCl(dppe)$_2$]}$_3$ **9** (67 mg, 0.021 mmol) was added and the solution was allowed to warm to room temperature over 17 h. The reaction mixture was passed through an alumina plug with CH_2Cl_2 and the eluate taken to dryness under reduced pressure. ^{1}H and ^{31}P NMR indicated **22a**[69] and **9**.[26]

4.8.6.4.2. *Attempted Synthesis of 1,3,5-C_6H_3{C≡CC_6H_4-4-C≡C-trans-[Ru(C≡CPh)(dppe)$_2$]}$_3$*

A solution of phenylacetylene (0.2 mL, 1.84 mmol) in thf (15 mL) was cooled in a dry-ice/acetone bath. *n*-BuLi (1 mL, 1.5 M) was added and solution stirred for 1 h. 1,3,5-C_6H_3{C≡CC_6H_4-4-C≡C-*trans*-[RuCl(dppe)$_2$]}$_3$ **9** (14 mg, 4.3 μmol) was added, and the solution was allowed to return to room temperature over 17 h. The reaction mixture was passed through an alumina plug with CH_2Cl_2 as eluent and the solvent removed under reduced pressure. The yellow residue was triturated with petroleum ether. ^{1}H and ^{31}P NMR indicated of **9** only.[26]

4.8.6.4.3. *Reaction between 1,3,5-(3,5-{trans-[(dppe)$_2$(PhC≡C)RuC≡C]}$_2$C$_6$H$_3$C≡CC$_6$H$_4$C≡C]$_3$C$_6$H$_3$ and 1,3,5-C$_6$H$_3${C≡C-4-C$_6$H$_4$C≡C-trans-[RuCl(dppe)$_2$]}$_3$ with BuLi*

To a solution of 1,3-{*trans*-[(dppe)$_2$(PhC≡C)RuC≡C]}$_2$-5-(HC≡C-4-C$_6$H$_4$)C$_6$H$_3$ **22a** (160 mg, 0.071 mmol) in thf (30 mL) in a dry ice/acetone bath was slowly added *n*-BuLi (0.04 mL, 1.5 mol L^{-1}) and the solution stirred for 45 min. 1,3,5-C$_6$H$_3${C≡CC$_6$H$_4$-4-C≡C-*trans*-[RuCl(dppe)$_2$]}$_3$ **9** (74 mg, 0.023 mmol) was added and the solution was allowed to warm to room temperature over 17 h. The reaction mixture was passed through an alumina column with CH_2Cl_2 as eluent and taken to dryness under reduced pressure. ^{1}H and ^{31}P NMR indicated starting materials only.

4.8.6.5. *Acetonitrile Replacement*

4.8.6.5.1. *Synthesis and Characterization of trans-[Ru(C≡CPh)(N≡CCH$_3$)(dppe)$_2$]PF$_6$ (29)*

Trans-[Ru(C≡CPh)Cl(dppe)$_2$] (200 mg, 0.193 mmol) and sodium hexafluorophosphate (65 mg, 0.40 mmol) were refluxed in acetonitrile (15 mL) for 30 min and the solution allowed to cool. The solution was filtered and taken to dryness under reduced pressure. The residue was then extracted with CH_2Cl_2 and taken to dryness to give a very light yellow solid (228 mg, 99%). Anal Calcd for $C_{62}H_{56}F_6NP_5Ru$: C 62.84, H 4.76, N 1.18. Found: C 62.89, H 4.67, N 1.15 %. IR: (CH_2Cl_2) ν(N≡C) 1967 cm^{-1}, ν(C≡C) 2086 cm^{-1}. UV-Vis: λ (thf) 298 nm, ε 12 400 M^{-1} cm^{-1}. ^{1}H NMR: (δ, 300 MHz, $CDCl_3$); 1.35 (3H, s, CH_3), 2.64 – 2.75 (8H, m, CH_2), 6.58 – 8.08 (45H, m, Ph). ^{31}P NMR: (δ, 121 MHz, $CDCl_3$); 51.22 (s). FAB MS *m/z* (fragment, relative intensity): 1040 ([M]$^+$, 10), 999 ([M – NC_2H_3]$^+$, 45), 878 ([Ru(dppe)$_2$]$^+$, 80).

4.8.6.5.2. *Reaction between trans-[Ru(N≡CCH$_3$)(C≡CPh)(dppe)$_2$]PF$_6$ and phenylacetylene*

A solution of *trans*-[Ru(N≡CCH$_3$)(C≡CPh)(dppe)$_2$]PF$_6$ (**29**) (65 mg, 0.055 mmol) and phenylacetylene (0.01 mL, 0.91 mmol) in CH_2Cl_2 (10 mL) was stirred for 2 h. The reaction was taken to dryness under reduced pressure, ^{1}H and ^{31}P NMR indicating no reaction. The residue was redissolved in CH_2Cl_2 (10 mL) and phenylacetylene (0.01 mL, 0.91 mmol) was added. The solution was refluxed for 2 h, and taken to dryness under reduced pressure. ^{1}H and ^{31}P NMR indicated no reaction.

4.8.6.6. *Acetylene Activation by SnMe$_3$*

4.8.6.6.1. *Attempted synthesis of 1,3-{trans-[(dppe)$_2$(PhC$_6$H$_4$C≡C)RuC≡C]}$_2$-5-(Me$_3$SnC≡C-4-C$_6$H$_4$)-C$_6$H$_3$ (30)*

A solution of 1,3-{*trans*-[(dppe)$_2$(PhC≡C)RuC≡C]}$_2$-5-(HC≡C-4-C$_6$H$_4$)C$_6$H$_3$ **22a** (64 mg, 0.028 mmol) in thf (50 mL) was cooled in a dry ice/acetone bath. *n*-BuLi (0.04 mL, 1.5 mol L^{-1}, mmol) was slowly added, and the solution was stirred for 45 min. Me_3SnCl (0.3 mL, mmol) was added and the solution was stirred for a further 90 min. The solution was allowed to warm to RT with stirring for 15 h. The reaction mixture was passed through an alumina plug with CH_2Cl_2, and the eluate was taken to dryness under reduced pressure. A yellow powder was purified by liquid diffusion of Et_2O into a CH_2Cl_2 solution. ^{1}H and ^{31}P NMR showed only decomposition products.

4.8.6.7. *Metal Replacement at Core*

4.8.6.7.1. *Synthesis and Characterization of trans-[Pt(C≡C C_6H_4-4-C≡CPh)Cl(PMe_2Ph)$_2$] (31)*

A solution of *cis*-[$PtCl_2(PMe_2Ph)_2$] (45 mg, 68 μmol), HC≡CC_6H_4-4-C≡CPh (8.8 mg, 44 μmol) and CuCl (6.6 mg, 67 μmol) in CH_2Cl_2 (10 mL) and NEt_3 (10 mL) was stirred for 17 h. The reaction mixture was passed through an alumina plug with CH_2Cl_2, and the eluate was taken to dryness under reduced pressure. Pale yellow needle crystals were grown by diffusion of MeOH into a solution in CH_2Cl_2 (28 mg, 90%). Anal. Calcd for $C_{32}H_{31}ClP_2Pt$: C 54.28, H 4.41. Found: C 54.21, H 3.82 %. IR: (CH_2Cl_2) ν(C≡C) 2119 cm^{-1}. UV-Vis: λ (thf) 342 nm, ε 33 600 M^{-1} cm^{-1}. ^1H NMR: (δ, 300 MHz, $CDCl_3$); 1.93 (12H, t, 4 Hz, Me), 6.98 – 7.81 (19H, m, phenyl). ^{31}P NMR: (δ, 121 MHz, $CDCl_3$); -6.84 (s, J_{PtP}: 2396 Hz).

4.8.6.7.2. *Synthesis and Characterization of 1,3,5-C_6H_3{C≡CC_6H_4-4-C≡C-trans-[PtCl(PMe_2Ph)$_2$]}$_3$ (32)*

A solution of *cis*-[$PtCl_2(PMe_2Ph)_2$] (48 mg, 72 μmol), 1,3,5-C_6H_3(C≡CC_6H_4-4-C≡CH)$_3$ (7.4 mg, 17 μmol) (**8**) and CuCl (15 mg, 0.15 mmol) in CH_2Cl_2 (15 mL) and NEt_3 (10 mL) was stirred for 17 h. The reaction mixture was passed through an alumina plug with CH_2Cl_2 as eluent, and the eluate was taken to dryness under reduced pressure. The residue was purified by solvent diffusion of MeOH into CH_2Cl_2 solution to afford a very pale yellow powder (27 mg, 83%). Anal. Calcd for $C_{84}H_{81}Cl_3P_6Pt_3$: C 51.27, H 4.15. Found: C 51.01, H 4.23 %. IR: (CH_2Cl_2) ν(C≡C) 2117 cm^{-1}. UV-Vis: λ (thf) 345 nm, ε 123 000 M^{-1} cm^{-1}. ^1H NMR: (δ, 300 MHz, $CDCl_3$); 1.94 (48H, t, 4 Hz, Me), 6.98 – 7.84 (45H, m, phenyl). ^{31}P NMR: (δ, 121 MHz, $CDCl_3$); -6.84 (s, J_{PtP}: 2400 Hz). FAB MS; *m/z* (fragment, relative intensity): 1970 ([M]$^+$, 2), 471 ([Pt(PMe_2Ph)]$^+$, 40).

4.8.6.7.3. *Synthesis and Characterization of 1,3,5-C_6H_3($C{\equiv}CC_6H_4$-4-$C{\equiv}C$-trans-[$PtCl(PMe_2Ph)_2$]$C{\equiv}CC_6H_4$-3,5-C_6H_3-{$C{\equiv}C$-trans-[$Ru(C{\equiv}CPh)(dppe)_2$]}$_2$)$_3$ (33)*

A solution of 1,3,5-C_6H_3{$C{\equiv}CC_6H_4$-4-$C{\equiv}C$-*trans*-[$PtCl(PMe_2Ph)_2$]}$_3$ **32** (21 mg, 11 μmol), 1,3-{*trans*-[$(dppe)_2(PhC{\equiv}C)RuC{\equiv}C$]}$_2$-5-($HC{\equiv}C$-4-$C_6H_4$)$C_6H_3$ **22a** (73 mg, 34 μmol) and CuCl (15 mg, 0.15 mmol) in CH_2Cl_2 (20 mL) and NEt_3 (5 mL) was stirred for 19 h. The reaction mixture was passed through an alumina plug with CH_2Cl_2 as eluent, and the eluate was taken to dryness under reduced pressure. The residue was purified by vapour diffusion of MeOH in a solution in CH_2Cl_2 to afford a yellow powder (53 mg, 56 %). Anal. Calcd for $C_{504}H_{420}P_{30}Pt_3Ru_6$: C 70.41, H 4.92. Found: C 69.51, H 5.02 %. IR: (CH_2Cl_2) ν(C≡CPt) 2101 cm^{-1}, ν(C≡CRu) 2060 cm^{-1}. UV-Vis: λ (thf) 357 nm, ε 52 300 M^{-1} cm^{-1}. ^1H NMR: (δ, 300 MHz, $CDCl_3$); 2.13 (48H, t, 4 Hz, Me), 2.68 (48H, m, CH_2), 6.67 – 7.90 (**X**H, m, phenyl). ^{31}P NMR: (δ, 121 MHz, $CDCl_3$); -11.62 (6P, s, J_{PtP}: 2380 Hz), 54.25 (24P, s). FAB MS; *m/z* (fragment, relative intensity): 898 ($[Ru(dppe)_2]^+$, 55), 471 ($[Pt(PMe_2Ph)_2]^+$, 35).

4.8.7. *Z-Scan Measurements*

Z-scan measurements were performed using two amplified femtosecond laser systems. The first system was based on a Coherent Mira-900D Ti-sapphire oscillator and included a chirped pulse Ti-sapphire amplifier operating at a repetition rate of 30 Hz. This system was used at wavelength 800 nm and provided ca 150 fs FWHM pulses. The second system was a Clark-MXR CPA-2001 regenerative amplifier pumping a Light Conversion TOPAS optical parametric amplifier. This system was operated at a repetition rate of 250 Hz (reduced from the usual default rate of 1 kHz to minimize potential problems with thermal effects and sample photodecomposition). The output of the optical parametric amplifier was tuned in the range 650 nm to 1300 nm using the second harmonic of the signal, the second harmonic of the idler, or the signal, respectively, in three wavelength ranges for tuning the system. The pulse duration was ca 150 fs.

The Z-scan set-ups used lenses with the focal lengths suitable for creating focal spots with the $1/e^2$ radius, w_0, being in the range 40 – 65 μm. This resulted in the Rayleigh lengths, $z_R = \frac{\pi w_0^2}{\lambda}$, being greater than 3 mm; the measurements of solutions in 1 mm thick glass cells with ca 1 mm thick glass walls could therefore be treated in the thin sample approximation. Due to the deviations from Gaussian character of the beam from the OPA, it was necessary to perform some spatial filtering of the beam. This resulted in the beam approximating the truncated Airy pattern case discussed by Rhee *et al.*[116] All measurements were calibrated against Z-scans taken on the pure solvent and on silica and glass plates of thicknesses in the range 1 - 2.5 mm. It was assumed that the dispersion of the nonlinear refractive index of silica can be neglected in the range of wavelengths investigated, and so the value $n_2 = 3 \times 10^{-16}$ cm^2 W^{-1} was adopted throughout the range. The light intensities used in the three different wavelength ranges differed somewhat, but as a rule the intensities were adjusted to obtain nonlinear phase shifts for the measured samples in the range 0.5 – 1.0 rd, corresponding to peak intensities of the order of 100 GW cm^{-1}.

4.8.8. *Optical Limiting Measurements*

The measurements were performed using the Z-scan technique at 523 nm, with about 5 microjoules, 40 ns pulses from a frequency-doubled Q-switched Nd:YLF diode-pumped laser. Solutions of both compounds were placed in 1 mm path length glass cells. The open-aperture Z-scans were converted into transmission-fluence plots using an assumption of Gaussian beam propagation and the spot size determination made on the basis of numerical fitting of the closed-aperture Z-scan obtained simultaneously with the open-aperture measurement (the signal in the closed-aperture Z-scan was due to thermal nonlinearity of the solutions). The data was analysed in the way similar to that described in 4.8.7., assuming that excited state absorption is responsible for the effect.

4.9. *References*

(1) Dhenaut, C.; Ledoux, I.; Samuel, I. D. W.; Zyss, J.; Bourgault, M.; Bozec, H. Le. *Nature* **1995**, *374*, 339.

(2) Stadler, S.; Feiner, F.; Brauchle, C.; Brandl, S.; Gompper, R. *Chem. Phys. Lett.* **1995**, *245*, 292.

(3) Stadler, S.; Brauchle, C.; Brandl, S.; Gompper, R. *Chem. Mater.* **1996**, *8*, 676.

(4) Stadler, S.; Dietrich, R.; Bourhill, G.; Brauchle, C. *Opt. Lett.* **1996**, *21*, 251.

(5) Verbiest, T.; Clays, K.; Persoons, A.; Meyers, F.; Brédas, J.-L. *Opt. Lett.* **1993**, *18*, 525.

(6) Verbiest, T.; Clays, K.; Samyn, C.; Wolff, J.; Reinhoudt, D.; Persoons, A. *J. Am. Chem. Soc.* **1994**, *116*, 9320.

(7) Verbiest, T.; Houbrechts, S.; Kauranen, M.; Clays, K.; Persoons, A. *J. Mater. Chem.* **1997**, *7*, 2175.

(8) Sastre, A.; Torres, T.; Diaz-Garcia, M. A.; Agulló-López, F.; Dhenaut, C.; Brasselet, S.; Ledoux, I.; Zyss, J. *J. Am. Chem. Soc.* **1996**, *118*, 2746.

(9) Lambert, C.; Nöll, G.; Schmälzlin, E.; Meerholz, K.; Bräuchle, C. *Chem. Eur. J.* **1998**, *4*, 2129.

(10) Ray, P. C.; Das, P. K. *Chem. Phys. Lett.* **1995**, *244*, 153.

(11) Zyss, J.; Dhenaut, C.; Chauvan, T.; Ledoux, I. *Chem. Phys. Lett.* **1993**, *206*, 409.

(12) Chui, T. W.; Wong, K. Y. *J. Chem. Phys.* **1998**, *109*, 1391.

(13) Boas, U.; Heegaard, P. M. H. *Chem. Soc. Rev.* **2004**, *33*, 43.

(14) Sakthivel, T.; Florence, A. T. *Drug Delivery Technology* **2003**, *3*, 52.

(15) Aulenta, F.; Hayes, W.; Rannard, S. *European Polymer Journal* **2003**, *39*, 1741.

(16) Kakkar, A. K. *Macromol. Symp.* **2003**, *196*, 145.

(17) Trévisiol, E.; Le Berre-Anton, V.; Leclaire, J.; Pratviel, G.; Caminade, A.-M.; Majoral, J.-P.; François, J. M.; Meuinier, B. *New J. Chem.* **2003**, *27*, 1713.

(18) Adronov, A.; Fréchet, J. M. J. *Chem. Commun.* **2000**, 1701.

(19) Sato, T.; Jiang, D.-L.; Aida, T. *J. Am. Chem. Soc.* **1999**, *121*, 10658.

(20) Peng, Z.; Pan, Y.; Xu, B.; Zhang, J. *J. Am. Chem. Soc.* **2000**, *122*, 6619.

(21) Devadoss, C.; Bharathi, P.; Moore, J. S. *J. Am. Chem. Soc.* **1996**, *118*, 9635.

(22) Denti, G.; Campagna, S.; Serroni, S.; Ciano, M.; Balzani, V. *J. Am. Chem. Soc.* **1992**, *114*, 2944.

(23) Adronov, A.; Gilat, S. L.; Fréchet, J. M. J.; Ohta, K.; Neuwahl, F. V. R.; Fleming, G. R. *J. Am. Chem. Soc.* **2000**, *122*, 1175.

(24) Balzani, V.; Ceroni, P.; Maestri, M.; Vicinelli, V. *Current Opinion in Chemical Biology* **2003**, *7*, 657.

(25) Drobizhev, M.; Karotki, A.; Rebane, A.; Spangler, C. W. *Opt. Lett.* **2001**, *26*, 1081.

(26) McDonagh, A. M.; Humphrey, M. G.; Samoc, M.; Luther-Davies, B.; Houbrechts, S.; Wada, T.; Sasabe, H.; Persoons, A. *J. Am. Chem. Soc.* **1999**, *121*, 1405.

(27) McDonagh, A. M.; Humphrey, M. G.; Samoc, M.; Luther-Davies, B. *Organometallics* **1999**, *18*, 5195.

(28) Kang, S. H.; Luo, J.; Ma, H.; Barto, R. R.; Frank, C. W. *Macromolecules* **2003**, *36*, 4355.

(29) Ma, H.; Liu, S.; Luo, J.; Suresh, S.; Liu, L.; Kang, S. H.; Haller, M.; Sassa, T.; Dalton, L. R.; Jen, A. K.-Y. *Adv. Funct. Mater.* **2002**, *12*, 565.

(30) Hobson, L. J.; Harrison, R. M. *Current Opinion in Solid State & Materials Science* **1997**, *2*, 683.

(31) Leclaire, J.; Coppel, Y.; Caminade, A.-M.; Majoral, J.-P. *J. Am. Chem. Soc.* **2004**, *126*, 2304.

(32) Frechet, J. M. J. *J. Polymer Science A.* **2003**, *41*, 3713.

(33) Smith, D. K. *Tetrahedron* **2003**, *59*, 3797.

(34) Albrecht, M.; Hovestad, N. J.; Boersma, J.; van Koten, G. *Chem.--Eur. J.* **2001**, *7*, 1289.

(35) Albrecht, M.; Gossage, R. A.; Lutz, M.; Spek, A. L.; van Koten, G. *Chem. Eur. J.* **2000**, *6*, 1431.

(36) Alonso, B.; Morán, M.; Casado, C. M.; Lobete, F.; Losada, J.; Cuadrado, I. *Chem. Mater.* **1995**, *7*, 1440.

(37) Alonso, B.; Blais, J.-C.; Astruc, D. *Organometallics* **2002**, *21*, 1001.

(38) Casado, C. M.; González, B.; Cuadrado, I.; Alonso, B.; Morán, M.; Losada, J. *Angew. Chem. Int. Ed.* **2000**, *39*, 2135.

(39) van de Covering, R.; Kuil, M.; Gebbink, R. J. M. K.; van Koten, G. *Chem. Commun.* **2002**, 1636.

(40) Cuadrado, I.; Morán, M.; Moya, A.; Casado, C. M.; Barranco, M.; Alonso, B. *Inorg. Chim. Acta.* **1996**, *251*, 5.

(41) Cuadrado, I.; Casado, C. M.; Alonso, B.; Morán, M.; Losada, J.; Belsky, V. *J. Am. Chem. Soc.* **1997**, *119*, 7613.

(42) Cuadrado, I.; Morán, M.; Casado, C. M.; Alonso, B.; Losada, J. *Coord. Chem. Rev.* **1999**, *193-195*, 395.

(43) Dani, P.; Karlen, T.; Gossage, R. A.; Smeets, W. J. J.; Spek, A. L.; van Koten, G. *J. Am. Chem. Soc.* **1997**, *119*, 11317.

(44) Dijkstra, H. P.; Kruithof, C. A.; Ronde, N.; van de Covering, R.; Ramón, D. J.; Vogt, D.; van Klink, G. P. M.; van Koten, G. *J. Org. Chem.* **2003**, *68*, 675.

(45) Gossage, R. A.; Jastrzebski, J. T. B. H.; van Ameijde, J.; Mulders, S. J. E.; Brouwer, A. J.; Liskamp, R. M. J.; van Koten, G. *Tetrahedron Letters* **1999**, *40*, 1413.

(46) Hurley, A. L.; Mohler, D. L. *Org. Lett.* **2000**, *2*, 2745.

(47) Kriesel, J. W.; König, S.; Freitas, M. A.; Marshall, A. G.; Leary, J. A.; Tilley, T. D. *J. Am. Chem. Soc.* **1998**, *120*, 12207.

(48) Larré, C.; Donnadieu, B.; Caminade, A.-M.; Majoral, J.-P. *Chem. Eur. J.* **1998**, *4*, 2031.

(49) Liao, Y.-H.; Moss, J. R. *Organometallics* **1995**, *14*, 2130.

(50) Liao, Y.-H.; Moss, J. R. *Organometallics* **1996**, *15*, 4307.

(51) Liu, G.-X.; Puddephatt, R. J. *Inorg. Chim. Acta.* **1996**, *251*, 319.

(52) Mavunkal, I. J.; Moss, J. R.; Bacsa, J. *J. Organomet. Chem.* **2000**, *593-594*, 361.

(53) Meijer, M. D.; Kleij, A. W.; Williams, B. S.; Ellis, D. E.; Lutz, M.; Spek, A. L.; van Klink, G. P. M.; van Koten, G. *Organometallics* **2002**, *21*, 264.

(54) Müller, C.; Vos, D.; Jutzi *J. Organomet. Chem.* **2000**, *600*, 127.

(55) Miller, L. L.; Zinger, B.; Schlechte, J. S. *Chem. Mater.* **1999**, *11*, 2313.

(56) Petrucci-Samija, M.; Guillemette, V.; Dasgupta, M.; Kakkar, A. K. *J. Am. Chem. Soc.* **1999**, *121*, 1968.

(57) Rodriguez, G.; Albrecht, M.; Schoenmaker, J.; Ford, A.; Lutz, M.; Spek, A. L.; van Koten, G. *J. Am. Chem. Soc.* **2002**, *124*, 5127.

(58) Shu, C.-F.; Shen, H.-M. *J. Mater. Chem.* **1997**, *7*, 47.

(59) Turriin, C.-O.; Chiffre, J.; de Montauzon, D.; Balavoine, G.; Manoury, E.; Caminade, A.-M.; Majoral, J.-P. *Organometallics* **2002**, *21*, 1891.

(60) Valentini, M.; Pregosin, P. S.; Rüegger, H. *Organometallics* **2000**, *19*, 2551.

(61) Waybright, S. M.; McAlpine, K.; Laskoski, M.; Smith, M. D.; Bunz, U. H. F. *J. Am. Chem. Soc.* **2002**, *124*, 8661.

(62) Leininger, S.; Stang, P. J.; Huang, S. *Organometallics* **1998**, *17*, 3981.

(63) Onitsuka, K.; Iuchi, A.; Fujimoto, M.; Takahashi, S. *Chem. Commun.* **2001**, 741.

(64) Ohshiro, N.; Takei, F.; Onitsuka, K.; Takahashi, S. *J. Organomet. Chem.* **1998**, *569*, 195.

(65) Onitsuka, K.; Fujimoto, M.; Ohshiro, N.; Takahashi, S. *Angew. Chem. Int. Ed.* **1999**, *38*, 689.

(66) Onitsuka, K.; Kitajima, H.; Fujimoto, M.; Iuchi, A.; Takei, F.; Takahashi, S. *Chem. Commun.* **2002**, 2576.

(67) Onitsuka, K.; Shimizu, A.; Takahashi, S. *Chem. Commun.* **2003**, 280.

(68) Hearshaw, M. A.; Moss, J. R. *Chem. Commun.* **1998**, 1.

(69) Hurst, S.; Cifuentes, M. P.; Humphrey, M. G. *Organometallics* **2002**, *21*, 2353.

(70) McDonagh, A. M. Transition Metal Acetylide Complexes for Nonlinear Optics. PhD Thesis. Department of Chemistry, Australian National University, 1999.

(71) Banwell, M. G.; Flynn, B. L.; Willis, A. C.; Hamel, E. *Aust. J. Chem.* **1999**, *52*, 767.

(72) Akiyama, S.; Nakatsuji, S.; Yoshida, K.; Nakashima, K.; Hagiwara, T.; Tsuruta, H.; Yoshida, T. *Bull. Chem. Soc. Jpn* **1983**, *56*, 361.

(73) McDonagh, A. M.; Powell, C. E.; Morrall, J. P.; Cifuentes, M. P.; Humphrey, M. G. *Organometallics* **2003**, *22*, 1402.

(74) Trumbo, D. L.; Marvel, C. S. *J. Polym. Sci.: Part A: Polym. Chem.* **1986**, *24*, 2311.

(75) Hurst, S. Transition Metal Vinylidene and Acetylide Complexes for Nonlinear Optics. PhD Thesis Department of Chemistry, Australian National University, 2001.

(76) Sonogashira, K.; Tohda, Y.; Hagihara, N. *Tetrahedron Lett.* **1975**, 4467.

(77) Elangovan, A.; Wang, Y.-H.; Ho, T.-I. *Org. Lett.* **2003**, *5*, 1841.

(78) Negishi, E.-i.; Kotora, M.; Xu, C. *J. Org. Chem.* **1997**, *62*, 8957.

(79) Anastasia, L.; Negishi, E.-i. *Org. Lett.* **2001**, *3*, 3111.

(80) Negishi, E.-i.; Qian, M.; Zeng, F.; Anastasia, L.; Babinski, D. *Org. Lett.* **2003**, *5*, 1597.

(81) Negishi, E.-i.; Anastasia, L. *Chem. Rev.* **2003**, *103*, 1979.

(82) Faulkner, C. W.; Ingham, S. L.; Khan, M. S.; Lewis, J.; Long, N. J.; Raithby, P. R. *J. Organomet. Chem.* **1994**, *482*, 139.

(83) Atherton, Z.; Faulkner, C. W.; Ingham, S. L.; Kakkar, A. K.; Khan, M. S.; Lewis, J.; Long, N. J.; Raithby, P. R. *J. Organomet. Chem.* **1993**, *462*, 265.

(84) Davies, S. J.; Johnson, B. F. G.; Lewis, J.; Raithby, P. R. *J. Organomet. Chem.* **1991**, *414*, C51.

(85) Khan, M. S.; Davies, S. J.; Kakkar, A. K.; Schwartz, D.; Lin, B.; Johnson, B. F. G.; Lewis, J. *J. Organomet. Chem.* **1992**, *424*, 87.

(86) Lewis, J.; Khan, M. S.; Kakkar, A. K.; Johnson, B. F. G. *J. Organomet. Chem.* **1992**, *425*, 165.

(87) Khan, M. S.; Kakkar, A. K.; Ingham, S. L.; Raithby, P. R.; Lewis, J.; Spencer, B.; Wittmann, F.; Friend, R. H. *J. Organomet. Chem.* **1994**, *472*, 247.

(88) Yam, V. W.-W.; Tao, C.-H.; Zhang, L.; Wong, K. M.-C.; Cheung, K.-K. *Organometallics* **2001**, *20*, 453.

(89) Cross, R. J.; Davidson, M. F. *J. Chem. Soc., Dalton Trans.* **1986**, 1987.

(90) Yamazaki, S. *Polyhedron* **1992**, *11*, 1983.

(91) Empsall, H. D.; Shaw, B. L.; Stringer, A. J. *J. Organomet. Chem.* **1975**, *94*, 131.

(92) Kamada, K.; Ohta, K.; Iwase, Y.; Kondo, K. *Chem. Phys. Lett.* **2003**, *372*, 386.

(93) Amano, M.; Kaino, T. *J. Appl. Phys.* **1990**, *68*, 6024.

(94) Keuren, E. V.; Wakebe, T.; Andreaus, R.; Möhwald, H.; Schrof, W.; Belov, V.; Matsuda, H.; Rangel-Rojo, R. *Appl. Phys. Lett.* **1999**, *75*, 3312.

(95) Hsu, C.-C.; Liu, S.; Wang, C. C.; Wang, C. H. *J. Chem. Phys.* **2001**, *114*, 7103.

(96) Ziegler, L. D. *J. Phys. Chem. A* **2003**, *107*, 8282.

(97) Belfield, K. D.; Hagan, D. J.; van Stryland, E. W.; Schafer, K. J.; Negres, R. A. *Org. Lett.* **1999**, *1*, 1575.

(98) Woodford, J. N.; Wang, C. H.; Jen, A. K.-Y. *Chem. Phys.* **2001**, *271*, 137.

(99) Wang, C. H.; Lin, Y. C.; Tai, O. Y.; Jen, A. K.-Y. *J. Chem. Phys.* **2003**, *119*, 6237.

(100) Nahata, A.; Shan, J.; Yardley, J. T.; Wu, C. *J. Opt. Soc. Am. B* **1993**, *10*, 1553.

(101) Rebane, A.; Drobizhev, M.; Karotki, A. *Journal of Luminescence* **2002**, *98*, 341.

(102) Geisler, T.; Pedersen, K.; Underhill, A. E.; Dhindsa, A. S.; Greve, D. R.; Bjørnholm, T.; Petersen, J. C. *J. Phys. Chem. B* **1997**, *101*, 10625.

(103) Pan, X. Y.; Chigarev, N. V.; Jiang, H. B.; Huang, W. T.; Gong, Q.; Liu, C. L.; Kobryanskii, V. M.; Paraschuk, D. Y. *Chem. Phys. Lett.* **2002**, *365*, 117

(104) Couris, S.; Koudoumas, E.; Ruth, A. A.; Leach, S. *J. Phys. Chem. B.* **1995**, *28*, 4537.

(105) Uyeda, H. T.; Zhao, Y.; Wostyn, K.; Asselberghs, I.; Clays, K.; Therien, M. J. *J. Am. Chem. Soc.* **2002**, *124*, 13806.

(106) Willetts, A.; Rice, J. E.; Burland, D. M.; Shelton, D. P. *J. Chem. Phys* **1992**, *10*, 7590.

(107) McKay, T. J.; Bolger, J. A.; Staromlynska, J.; Davy, J. R. *J. Chem. Phys.* **1998**, *108*, 5537.

(108) McKay, T. J.; Staromlynska, J.; Wilson, P.; Davy, J. R. *J. Appl. Phys.* **1999**, *85*, 1337.

(109) Staromlynska, J.; McKay, T. J.; Wilson, P. *J. Appl. Phys.* **2000**, *88*, 1726.

(110) Takahashi, S.; Kuroyama, Y.; Sonogashira, K.; Hagihara, N. *Synthesis* **1980**, 627.

(111) Lavastre, O.; Cabioch, S.; Dixneuf, P. H.; Vohlidal, J. *Tetrahedron* **1997**, *53*, 7595.

(112) Chaudret, B.; Commenges, G.; Poilblanc, R. *J. Chem. Soc., Dalton Trans.* **1984**, 1635.

(113) Kofron, W. G.; Baclowski, L. M. *J. Org. Chem.* **1976**, *41*, 1879.

(114) Clark, M.; Cramer, R. D. I.; van Opdensch, N. *J. Comput. Chem.* **1989**, *10*, 982.

(115) *Spartan version 5.0*, Wavefunction, Inc: Irvine, CA, 1997.

(116) Rhee, B. K.; Byun, J. S.; van Stryland, E. W. *J. Opt. Soc. Am. B* **1996**, *13*, 2720.

(117) Samoc, M. Personal Communication.